THES JRB-599

FAILURE ANALYSIS OF THE WORLD TRADE CENTER 5 BUILDING

A Thesis

in partial fulfillment of the requirements for the

Degree of Master of Science

By

Kevin J. LaMalva

Date: May 1, 2007

Approved:

Professor Jonathan R. Barnett, Advisor
(Fire Protection Engineering and Mechanical Engineering, WPI)

Donald Dusenberry, Co-Advisor
(Senior Principal, SGH)

Abstract

This project involves a failure analysis of the internal structural collapse that occurred in World Trade Center 5 (WTC 5) due to fire exposure alone on September 11, 2001. It is hypothesized that the steel column-tree assembly failed during the heating phase of the fire. The results of this research have serious and far-reaching implications, for this method of construction is utilized in approximately 20,000 existing buildings and continues to be very popular. Catastrophic failure during the heating phase of a fire would endanger the lives of firefighters and building occupants undergoing extended egress times (e.g., high-rise buildings), or relying upon defend-in-place strategies (e.g., hospitals). Computer software was used to reconstruct the fire event and predict the structural performance of the assembly when exposed to the fire. Results from a finite element, thermal-stress model confirms this hypothesis, for it is concluded that the catastrophic, progressive structural collapse occurred approximately 2 hours into the fire exposure.

Acknowledgements

This thesis project would not have been possible without the support of the many people involved. Dr. Jonathan Barnett is a Professor of Fire Protection Engineering and Mechanical Engineering at Worcester Polytechnic Institute (WPI) and was also a member of the Building Performance Study (BPS) Team. The BPS Team compiled observations and preliminary analyses of the performance of WTC 5; Professor Barnett was the primary author of this report chapter within the Federal Emergency Management Agency's World Trade Center Building Performance Study (2002). This work is the foundation of this research. For instance, the forensic evidence collected by Professor Barnett has proved to be absolutely critical to the feasibility of this research. Professor Barnett is the main advisor of this project and has provided guidance from its inception to its completion.

The mission of the Society of Fire Protection Engineers (SFPE) Educational and Scientific Foundation is "to advance the science of practice of Fire Protection Engineering internationally, by advocating and supporting engineering research." This foundation is funded solely by volunteer contributions by SFPE members, the SFPE Chapter, and corporate supporters. The SFPE Educational and Scientific Foundation has embraced this research and awarded a full grant to support it. In other words, this project was made possible by generosity of this foundation.

Simpson Gumpertz & Heger Inc. (SGH) is a consulting engineering firm headquartered in Boston, MA that specializes in advanced engineering for buildings, infrastructure, and special structures. SGH has provided tremendous support of this project from its inception, from professional advice to technical support (e.g., ABAQUS support). Donald Dusenberry is a Senior Principal at SGH who has provided ongoing support as the co-advisor of this project. Mr. Dusenberry has provided very interesting insights relating to structural engineering and construction practices. Ronald Hamburger is a Principal and Region Head at SGH, and also member of the BPS Team for the WTC investigation. Mr. Hamburger has provided insights concerning the investigation of the WTC site. Frank Kan is a Principal at SGH who has provided solutions to complex finite element modeling challenges (ABAQUS) and has also shared advice concerning advanced mechanics. Gunjeet Juneja is a Senior Engineer at SGH who has complimented the advice of Mr. Kan in terms of troubleshooting the ABAQUS models created for this project.

Gilsanz Murray Steficek (GMS) is a consulting engineering firm headquartered in New York City, NY that provides full-service structural engineering. Ramon Gilsanz is a Partner of GMS and also was part of the BPS Team for the WTC investigation. Mr. Gilsanz has provided critical information pertaining to the historical structural practices of New York City. Mr. Gilsanz also helped to make arrangements for the release of sensitive documents related to WTC 5 (e.g., structural plans) which proved to be essential for the project. The Port Authority of NY & NJ assisted with the process of obtaining these sensitive documents.

The National Institute of Standards and Technology (NIST) is a federal organization that conducts research in many specialized areas (e.g., Fire Protection Engineering). Dr. John Gross is an Engineer at NIST that provided forensic evidence from WTC 5 which complimented those collected by Professor Barnett. Dr. Gross also recorded the dimensions of key specimens for use in this project.

The WPI Computing and Communications Center (CCC) has provided ongoing technical support for this project. Adriana Hera is an Academic Computer Application Scientist at the CCC who provided ABAQUS training over a three-month period. Siamak Najafi is Director of Research Computing and Randolph Robinson is an Academic Computer Application Scientist at WPI; both have provided ongoing technical support relating to computational performance.

This project was truly a product of the talent and insight from all of the people involved. The professionals described above deserve a great amount of gratitude for their selfless generosity of time and monetary support. In closing, *I extent my greatest thanks to all those talented people involved in this project*.

Table of Contents

List of Figures

List of Tables

1 Executive Summary

1.1 Introduction

World Trade Center 5 (WTC 5) was a 9-story building with standard office and retail space located in New York City, NY. On September 11, 2001, flaming debris from WTC 1 ignited fires in WTC 5 which burned unchecked and caused a localized collapse from the 8th floor through the 5th floor in the eastern section of the building. More precisely, the eastern portion of WTC 5 experienced an internal progressive collapse due to the fire, not structural impact. This project focuses on this particular failure.

The scope of this project involves the determination of the temperature history of the steel beams of WTC 5 and then using that information to predict the structural behavior of the column-tree and shear connection assembly. Finite element analysis software is used for this task. The purpose of this analysis is to determine whether the failure of the steel assembly occurred during the heating phase of the fire or when the building cooled down. Common knowledge suggests that the failure would have been during the cooling phase in which excessive thermal contraction of the members induces large stresses at the connections.

The symmetrical nature of the local collapse strongly suggests that the failures were due to the uncontrolled fires. Moreover, it is hypothesized that the failure occurred during the heating phase of the fire because the columns remained straight and freestanding after the collapse. Furthermore, the shear connections were located a significant distance away from the columns, thereby weakening their ability to transfer heat energy to a cooler sink (i.e., the columns). If the expected failure mechanism had occurred during the cooling phase, the columns would most likely have been deformed to some extent due to the tensile forces that would have developed in the girders.

Failure of the steel assembly in WTC 5 during the heating phase of the fire would represent a clear risk to firefighters attempting to extinguish fires in buildings utilizing structural column-tree assemblies (also known as the Gerber beam design). Moreover, occupants residing in hospitals or high-rise buildings of this type of construction could be at risk due to extended egress times (e.g., high-rise buildings only allow a limited amount of people to egress at once via relatively narrow stairways). Firefighters will continue to be privy to this type of steel construction because approximately 20,000 existing buildings utilize the Gerber beam design and this construction type is still very popular today. Therefore, it is imperative to understand the atypical localized failure within WTC 5.

1.2 Evidence Pertaining to the Research

Forensic evidence is a key component to understanding the internal structural collapse that occurred in WTC 5 due to fire alone. Forensic evidence serves as a baseline for the research and serves to reinforce specific findings derived from numerical methods. Once the WTC site was changed from a rescue to a recovery operation following the events of September 11, 2001, the Federal Emergency Management Agency (FEMA) formed a Building Performance Study (BPS) team consisting of many specialists. The BPS team surveyed the WTC 5 site and collected photographic evidence, as well as specimen samples to make a preliminary performance assessment of the building, as well as supplement future study. This photographic evidence was analyzed to form the hypothesis that the internal, progressive structural collapse of WTC 5 occurred during the heating phase of the fire exposure. Moreover, this forensic evidence could serve to validate any conclusions drawn from the research contained in this project.

The structural plans and details of WTC 5 were obtained from the Port Authority of NY & NJ. Due to the extensive litigation surrounding the WTC site, the Freedom of Information Act was utilized to legally obtain these sensitive documents. These construction documents are essential to this project because they describe the size of the structural elements and the detailed dimensions of the connections. This information is crucial to the development of an accurate model of the structural assembly using the finite element software ABAQUS.

1.3 Fire Event Reconstruction

By referencing the 2005 National Institute of Standards and Technology (NIST) report on WTC 1 and 2, the effective heat of combustion and the peak heat release rate of the fire that occurred within WTC 5 were estimated. More precisely, a series of calorimeter tests and a full-scale Fire Dynamics Simulator (FDS) analysis were used to derive appropriate values for the effective heat of combustion and the peak heat release rate, respectively. Results from the 2005 NIST reports were able to be extrapolated, for WTC 5 had a similar office configuration as compared to that for WTC 1 and 2. Lastly, a 1995 NIST report involving a survey of office buildings was used to derive an appropriate fuel load for WTC 5.

Using the information derived from the NIST reports, heat release rate versus time curves for a medium, fast, and ultra-fast growing fire were derived. The growth phase of the fire was assumed to follow a time-squared regime. Moreover, the 1994 Eurocode (EC1) provided a method to determine the extent of the fire decay phase. Finally, a comparison of the fuel load to the fuel burned over time resulted in the final set of heat release rate curves. Using these curves as input, the Consolidated Fire and Smoke Transport Model (CFAST) from NIST was used to derive temperature history scenarios of the reconstructed fire.

CFAST is one of the most versatile and widely used zone models. Moreover, this software performs well for fuel-controlled fires, which was the case of the fire in WTC 5 due to the large impact holes in the roof of the western portion of the building. The temperature history scenarios were derived from CFAST and then compared to parametric curves in the Eurocode, which are meant to represent real fire exposures. There is reasonable agreement between the reconstructed WTC 5 fire and the parametric curves.

1.4 Finite Element Model Development

In order to model the shear connection assembly of WTC 5 accurately using ABAQUS, the nonlinear, temperature-dependent properties of A36 steel must be known. Using experimental data from Harmathy, temperature-dependent stress-strain curves for A36 steel were derived. These curves for nominal stress and strain were converted to true stress and true plastic strain for input into ABAQUS. The following temperature-dependent thermal properties of A36 steel were also derived from the literature: specific heat, conductivity, and the instantaneous coefficient of thermal expansion.

The connection failures as a result of fire exposure in WTC 5 were due to shear rupture of the web portion of the beam stems. This type of failure occurs when the bolts bear against the weak side (i.e., acting toward the free end of the member) of the bolt holes. Moreover, this bearing stress causes shear planes to form in the web steel. Finally, cracks along the shear planes cause catastrophic failure of the shear connection. The goal of this project is to predict when the shear connections of WTC 5 experienced catastrophic failure as described above. In order to accomplish this goal, the time at which cracks along the shear planes begin to form must be derived. ABAQUS does not have the capabilities to predict the formation of cracks within a deformable body explicitly. Therefore, an indirect technique was derived to predict the time at which connection failure occurred.

A failure criterion determination model created in ABAQUS includes a single bolt and hole. Using the AISC Steel Manual (LRFD), a failure load was derived and applied to this model. The plastic shear strain at failure was then derived to serve as the failure criterion for shear rupture at a bolt hole. This failure criterion is important, for the stress distribution in the vicinity of the bolt hole has limited application at elevated temperatures in terms of predicting failure.

ABAQUS was used to create a mechanical model that encompasses the stress behavior of the four structural bays of interest on the 8th floor (hypothesized as the initial region of failure). This model serves as the foundation for the final model: a sequentially-coupled, thermal stress analysis of the four structural bays of interest. This model utilizes symmetry boundary conditions to capture the behavior of several structural bays. The gravity load was derived by referencing the 1970 New York City Building Code and accounting for the self-weight of the assembly. A 10% reduction in the live load was included to account for the fact that occupants were not in the building during the fire.

The mechanical model was tested at ambient conditions to ensure the results are realistic. The behavior of any steel assembly under ambient, service conditions is well understood and easily discernable from experience. The maximum deflection of the floor girder was found to be generally consistent with structural engineering standards. Thus, the behavior of the mechanical model was validated for normal ambient conditions.

ABAQUS was used to create a thermal model that encompasses the heat transfer behavior of the four structural bays of interest on the 8th floor of WTC 5 when exposed to the reconstructed fire. Results from the thermal model serve as input into the final

thermal-stress model. The temperature distribution of the steel assembly in three-dimensional space and time is integral for understanding of the thermal-stress behavior, since steel strength is highly temperature-dependent. Moreover, the geometric complexity of the structural assembly makes reliance upon hand calculations impossible if accurate results are to be derived. It is assumed that turbulent natural convection is the heating mode of the structural assembly via the upper gas layer temperature history derived using CFAST.

In order to fully understand the performance of the WTC 5 assembly during its fire exposure on September 11, 2001, the thermal model must be combined with the mechanical model: the result is a sequentially-coupled, thermal stress model. Since the stress behavior depends upon the temperature, but not vice versa (frictional heating is negligible), a sequentially-coupled model yields accurate results; a fully-coupled, thermal-stress analysis was not required. It was also assumed that the steel insulation stays completely attached during the entire fire exposure. The thermal-stress model is essentially a copy of the mechanical model with critical changes: temperature-dependent properties were used and the nodal temperature history from the thermal model served as input.

1.5 Finite Element Modeling Results

ABAQUS was used to create a thermal model that encompasses the heat transfer behavior of the four structural bays of interest on the 8th floor of WTC 5 when exposed to the reconstructed fire. The temperature distribution of the steel in space and time was derived from the analysis. It is hypothesized that the Gerber beam design utilized for WTC 5 isolates the shear connections from their heat sinks (i.e., the columns). As a result, a shear connection would experience a significant heat build-up during a fire exposure. The results of the thermal model support this hypothesis fully.

It was determined that the temperature gradient between the end of the beam stem welded to the column and its other end at the shear connection is approximately 450 ºC after one hour of fire exposure. Moreover, the interface between the beam stem and column is kept relatively cool. Since heat at the shear connection must travel across the entire length of the beam stem (4 feet) before it reaches the heat sink, heat builds up quickly in the vicinity of the bolt holes. This effect is exacerbated by the fact that the beam stem itself is being heated which reduces the thermal flow from the connection.

It is observed that the insulation functions as predicted: it delays the transmission of heat to the steel during the fire exposure. Moreover, it can be observed that the top of the assembly remains relatively cool due to the heat sink effect of the concrete slab above it. Lastly, the average temperature of the steel agrees with estimates from hand calculations.

ABAQUS was used to create a sequentially-coupled, thermal-stress model that encompasses the global behavior of the four structural bays of interest on the 8th floor of WTC 5 when exposed to the reconstructed fire. This model serves as an accurate reconstruction of the quasi-dynamic thermal-stress behaviors that occurred and led to progressive structural collapse. This model integrates a vast amount of research and is capable of representing highly-nonlinear thermal and mechanical behaviors.

The structural assembly is initially at ambient temperature (20 °C) carrying the specified gravity loads with minimal deflection. As the compartment heats up in the first hour of fire exposure, the steel assembly slowly increases in temperature. As the steel heats up, it undergoes thermal expansion which causes the floor girder to elongate significantly and close the gap between it and the beam stem. This elongation causes relatively harmless compressive stress concentrations to form on the strong side (toward the beam stem span) of the bolt holes

As the temperature of the steel assembly increases, its rigidity decreases steadily and the floor girder begins to undergo significant deflection. This deflection causes the lower flange of the floor girder to contact and penetrate the beam stem web. This phenomenon shall be referred to as the formation of a *fulcrum point*. After 2 hours of fire exposure, the loss of rigidity in the steel "outpaces" its thermal expansion and the top bolt of the shear connection undergoes a stress reversal and begins to bear against the weak side of the bolt hole.

The stress reversal described above can be attributed to the fulcrum mechanism which has fully formed at this point in time during the fire exposure. The fulcrum mechanism fully forms because tensile stresses surrounding the lower flange's penetration into the beam stem web arrests further penetration in this region. According to the failure criterion established, the shear connection experiences "runaway" failure at this point in time. More precisely, the model shows that the plastic shear strain reaches values that are triple and quadruple the failure limit over the course of only minutes. Once the top bolt has failed, the failure of the remaining two bolts would happen almost instantaneously; this can be referred to as an "un-zipping" effect.

It is observed that the failure identified in the finite element model is very similar to that observed in a collected WTC 5 structural specimen that underwent failure. More precisely, the angles at which the bolts pried against the bolt holes are similar in the model and the specimen. Moreover, photographs of failed beam stems show evidence of fulcrum point penetrations. The sequentially-coupled, thermal-stress model has estimated the time (i.e., 2 hours) in which catastrophic structural collapse occurred within WTC 5.

1.6 Conclusions

The fire that occurred within WTC 5 was estimated using relevant data and computer modeling. The official construction documents of WTC 5 were referenced to determine the dimensions of the steel assembly accurately. Using this information, finite element models were created. It has been determined that WTC 5 experienced a catastrophic, progressive structural collapse during the heating phase of its fire exposure. More precisely, the thermal-stress model predicts a "runaway" bolt rupture failure at approximately 2 hours of exposure to the building fire.

It is not the precise time of failure which is paramount, but the fact that the structure failed during the fire's heating phase, as opposed to its cooling phase, which would have been expected based upon current knowledge and experience of structural fire performance. In a general sense, this early failure is very surprising, but in view of the construction details of WTC 5, this failure is physically reasonable. More precisely, the Gerber beam design used for floors 5 through 8 of WTC 5 possesses certain details which make it inherently weak in terms of fire endurance.

The Gerber beam design isolates the shear connections from their heat sinks to the rest of the "cooler" structure via the columns. The results of the thermal model demonstrate how this isolation causes a shear connection to become 450 °C hotter than the interface at the column after one hour of fire exposure; this gradient reduces to 400 °C after two hours. This heating phenomenon is exacerbated by the fact that the shear connection has a relatively-high surface area to volume ratio, which allows for efficient heating via turbulent convection from the hot upper layer gases. Moreover, the beam stem itself was heated by the fire exposure which reduces the thermal flow from the shear connection toward the column.

The initial structural collapse on the 8th floor of WTC 5 due to fire exposure alone led to the progressive collapse down through the 5th floor below it. These collapses were due to the kinetic energy of the falling debris from the 8th floor and subsequent floors below it. This collapse may have progressed all of the way down to the ground level, if it had not been for the moment-type connections utilized for the 4th floor, which has special architectural features. The 9th floor of the building experienced a similar fire exposure as the 8th floor, but it did not collapse. In fact, forensic evidence demonstrates that the beams reached the catenary phase and remained stable. The only difference between the structural assembly on the 8th floor and that on the 9th floor is the location of the shear connections; on the 9th floor, the connections were made at the columns.

WTC 5 utilized the Gerber beam design which represents a common type of steel construction. Since it is possible for people to be inside in a building utilizing the Gerber beam design after 2 hours of a fire exposure (the time these analyses show it would take for the system to fail), there is cause for concern. WTC 5 experienced *progressive* collapse, so a fire many floors above occupants may still represent a danger if the fire is not controlled by the active suppression systems for any number of reasons. The structure itself is the last line of defense against fire and must be designed to resist a collapse due to a fire event. In terms of structural fire protection engineering, WTC 5 did not represent

an engineering failure, but rather a failure to engineer (for fire exposure). The solutions to structural fire protection engineering problems do not necessarily need to be elaborate (e.g., designing a "fortress"), but rather well-engineered. Whereas structural design for seismic and wind considerations is performance-based, structural fire protection is still primarily prescriptive and/or proprietary. This fact has the unfortunate effect of preventing engineers from fully understanding and designing for building performance during fires.

In general, there has been limited research into the fire performance of bolted connections in structural assemblies. It is recommended that full-scale experiments be conducted to verify the results of this research. More precisely, a typical structural bay from the 8th floor of WTC 5 should be reconstructed and exposed to fire. If it is indeed confirmed that the Gerber beam design is susceptible to collapse during the heating phase of a fire, more research is required to ensure public safety in these types of buildings. In the case of the Gerber beam design, certain hypersensitive structural details which contribute to the formation of a fulcrum point failure mechanism may be identified. The most apparent hypersensitive details include: the geometry of the bolt holes at the shear connection, the construction clearance distance between the beam stem and the floor girder at the shear connection, and the location of the shear connection itself with respect to its heat sink (i.e., the column).

The finite element models created for this project could be further researched and used to devise pre-engineered solutions to the building codes. By addressing the influence of the hypersensitive structural details identified above, updated methods of using the Gerber beam design could be engineered. It may be discovered that using slotted-type bolt holes significantly increases the fire endurance of the structural assembly by allowing large rotations with limited bearing stresses. If this is the case, then provisions may be made to the building code using this pre-engineered solution. Therefore, increased fire endurance may be incorporated into routine structural work that involves the Gerber beam design.

It has been mentioned that approximately 20,000 existing steel structures in the U.S. utilize the Gerber beam design. Since it has been demonstrated that this type of design may be prone to failure during the heating phase of a fire, fire department incident commanders should be made aware of this risk. Certain incident commanders may wish to survey those buildings which utilize the Gerber beam design in their respective districts so that they can make better informed decisions during a fire event.

2 Introduction

2.1 Project Overview

2.1.1 Background

The Federal Emergency Management Agency (FEMA) World Trade Center Building Performance Study provides preliminary observations of World Trade Center 5 (WTC 5) after the events of September 11, 2001. WTC 5 was a 9-story building with standard office and retail space (120,000 sq. ft. per floor) located in New York City, NY (see Figure 1 below). On September 11, 2001, debris damage from WTC 1 caused localized collapses from the roof to the 3rd floor of WTC 5 toward the western portion of the building. Furthermore, the ensuing fires that burned unchecked in WTC 5 caused a localized collapse from the 8th floor to the 4th floor in the eastern section. More precisely, the eastern portion of WTC 5 experienced an internal progressive collapse due to the fire, not structural impact. This project focuses on this particular failure.

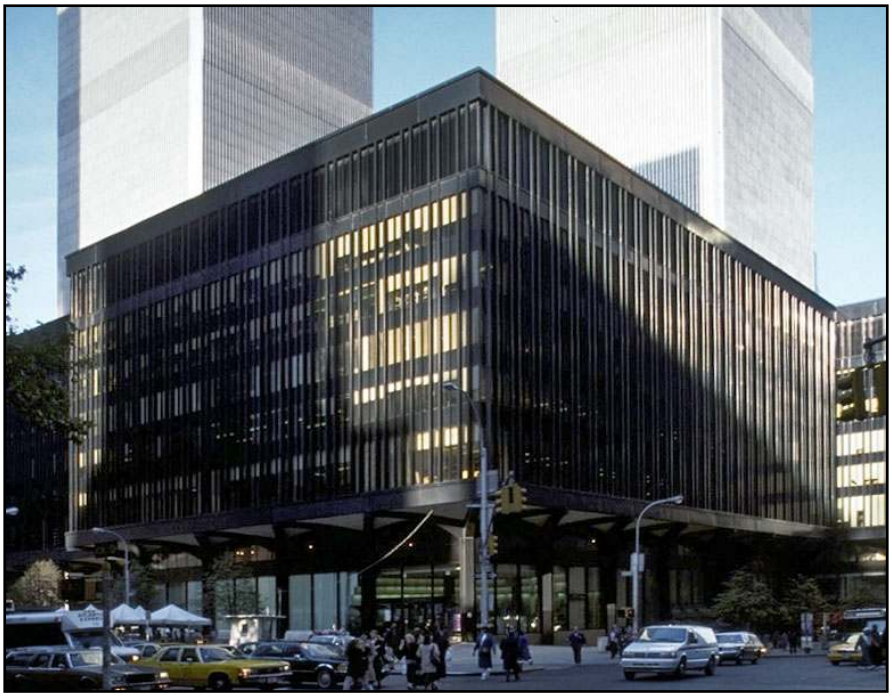

Figure 1: World Trade Center 5 (Prior to 9/11/2001)

The scope of this project involves the determination of the temperature history of the steel beams of WTC 5 and then using that information to predict the structural behavior of the column-tree and shear connection assembly. The purpose of this analysis is to determine whether the failure of the steel assembly occurred during the heating phase of the fire or when the building cooled down.

2.1.2 The Structure

The floors of WTC 5 were constructed of 4 inch-thick lightweight concrete fill on metal decking. Floors 5 through 8 utilized a column-tree system (Gerber beam design) at interior column lines in which a 4-foot-long beam stem was shop-welded to the column on each side, and the floor girder was simply-connected with shear tabs to the beam stems (see Figure 2 and Figure 3 below). The 9th floor and the roof utilized a more conventional bay system as shown in Figure 4 below. The differences between these two structural systems is peculiar since floors 5 through 8 experienced progressive collapse, while the 9th floor and roof stayed intact in the eastern portion of the building.

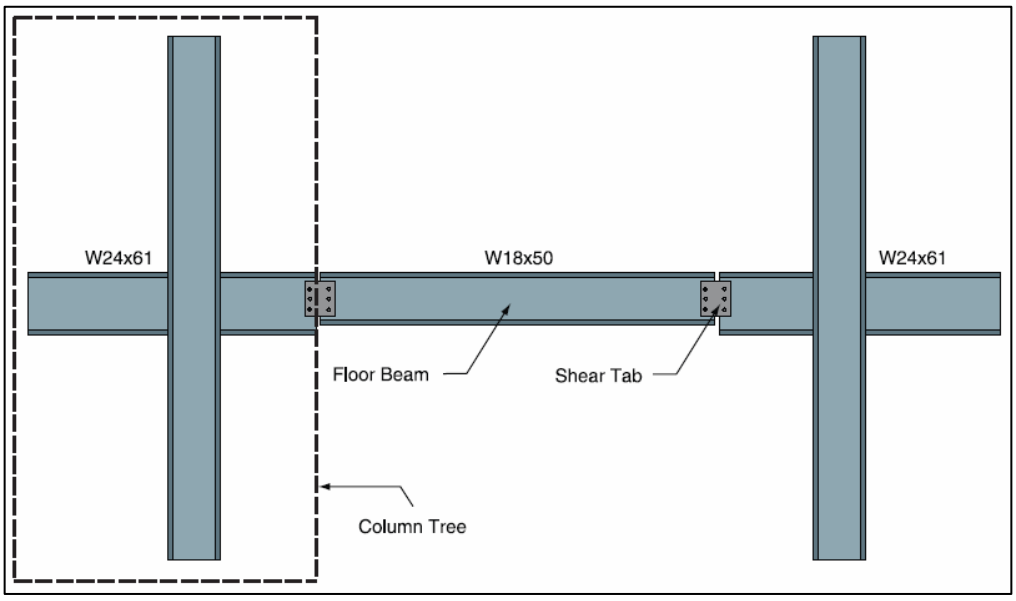

Figure 2: Typical Column-Tree System (Not to Scale)

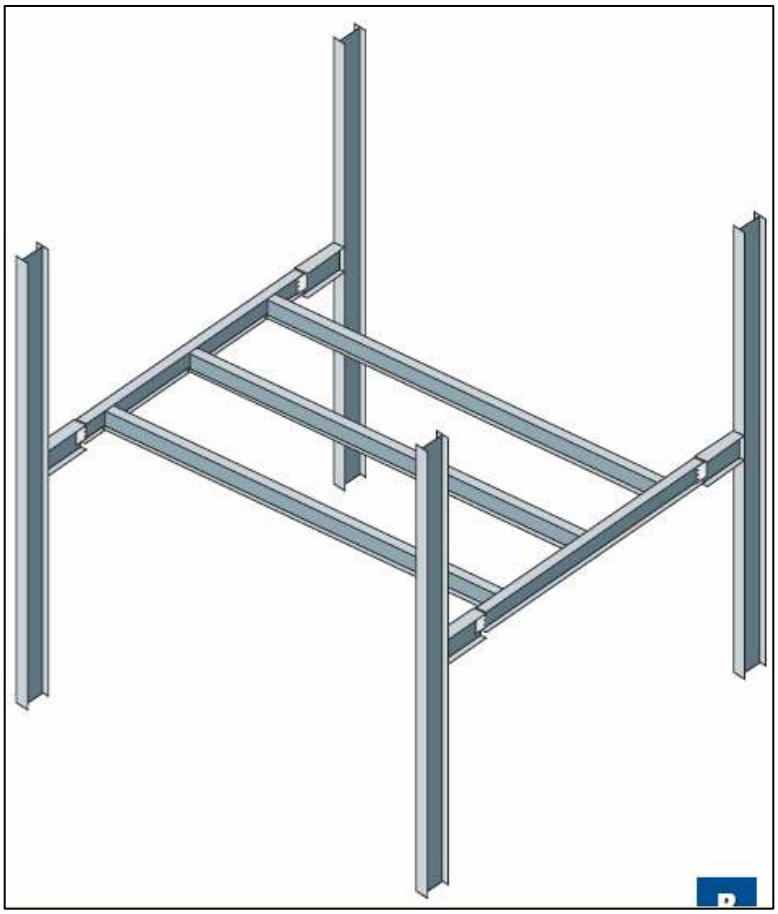

Figure 3: Typical Interior Bay Framing in WTC 5 (Floors 5, 6, 7, and 8)

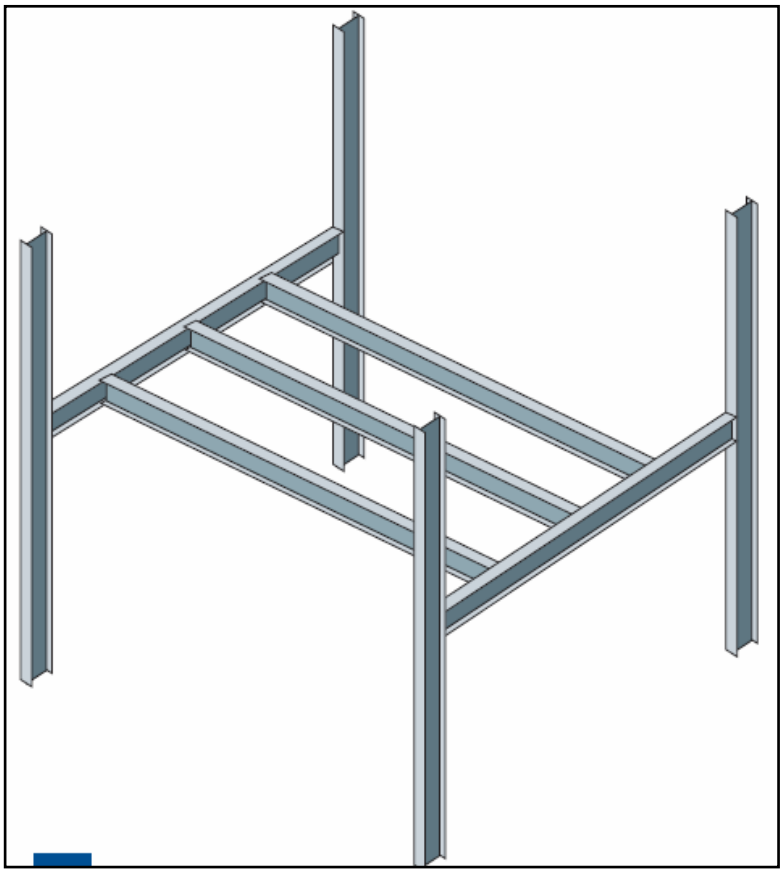

Figure 4: Typical Interior Bay Framing in WTC 5 (Floor 9 and Roof)

Generally in a fire the beam and the underside of the concrete slab are heated, causing thermal bowing. As the beam deflects downward, it also undergoes thermal expansion, causing compressive axial restraint forces to develop in the surrounding structure. In time, the yield strength and modulus of elasticity of the steel decreases steadily and the deflection increases, alleviating these restraint forces. The beam then becomes a catenary and tensile forces develop in the beam to resist the dead load on the structure. As the fire reaches its decay stage, the temperature of the compartment decreases and the beam undergoes thermal contraction, which increases the tensile forces within the beam and on the bolted connections. Therefore, steel beam failure can be expected during the cooling phase of a fire if it were to happen. There were instances in WTC 5 which followed this expected mechanism: Figure 5 below shows the 9th floor after the fire had burned out. The exception is the internal structural collapse under an intact portion of the roof from the 8th floor down to through the 5th floor.

Figure 5: 9th Floor of WTC 5 After Fire Burnout

2.1.3 Observation of the Damage

The local collapse of WTC 5 was the first documented case in which a protected steel structure had collapsed entirely due to fire. The symmetrical nature of the local collapse strongly suggests that the failures were due to the uncontrolled fires. This is supported by the observation that the columns in this area remained straight and freestanding (see Figure 6 below) and the roof was not penetrated in this region of the building. Therefore, impact damage by debris from WTC 1 or WTC 2 can be ruled out. This local collapse appeared to have begun at the shear connections where girders were connected to shop-fabricated beam stems and column assemblies. Figure 7 below provides an aerial view of the internal collapse area of WTC 5, which has a footprint of 11,000 square feet.

The fire-induced failure that led to the progressive collapse of WTC 5 was atypical for steel buildings in general. As observed on the ninth floor, the steel beams were expected to deflect significantly, yet carry the load (see Figure 5 above). It is hypothesized that the failure occurred during the heating phase of the fire because the columns remained straight and freestanding after the collapse. Furthermore, the shear connections were located a significant distance away from the columns, thereby weakening their ability to transfer heat energy to a cooler sink (i.e., the columns). If the expected failure mechanism had occurred during the cooling phase, the columns most likely would have been deformed to some extent due to the tensile forces that would have developed in the beams.

Figure 6: Internal Collapse Area in WTC 5

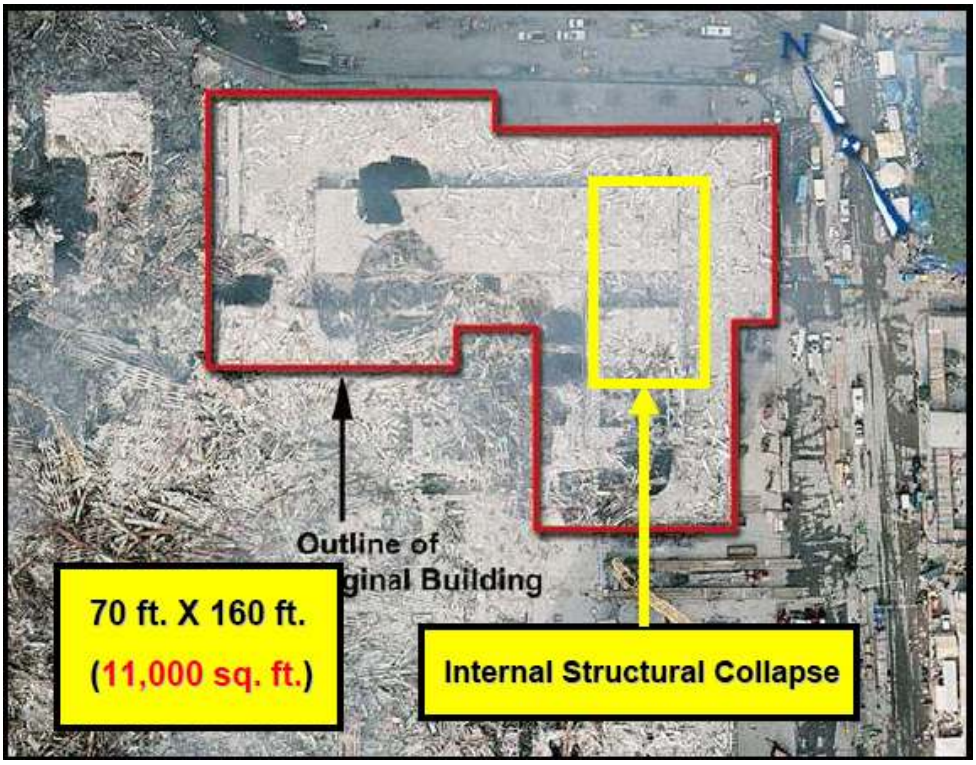

Figure 7: Internal Collapse Area of WTC 5 (Arial View)

2.1.4 Importance of this Research

During the late 20th century, analyses of the fire performance of steel gusset plate connections have alerted firefighters to the inherent dangers of fighting a fire in a residential occupancy with lightweight wooden roof trusses. During the heating phase of a fire, the destruction of the fibers holding the gusset plate to the wooden truss often releases causing failure (Brannigan 83). The economy of this type of truss construction is apparent, yet the danger it poses to firefighters has been proven. This project has a similar life safety objective as those prior analyses of steel shear plate connections for wooden roof trusses. Failure of the steel assembly in WTC 5 during the heating phase of the fire would represent a clear risk to firefighters attempting to extinguish fires in buildings utilizing the Gerber beam design. Moreover, occupants residing in hospitals or high rise buildings of this design type may be at risk due to extended egress times (e.g., occupants in high-rise buildings often are directed -via a voice communication system- to evacuate in phases so that a limited amount of people egress at once).

If the shear connections of WTC 5 failed during the heating phase of the fire, then fire department incident commanders must be informed of this hazard associated with this type of column-tree assembly (Gerber beam design). Firefighters will continue to be privy to this type of construction because approximately 20,000 existing buildings are comprised of column-tree assemblies and the Gerber beam design is still very popular today. Therefore, it is imperative to understand the early local failure within WTC 5.

2.1.5 Modeling the Fire Incident

There was a complete burnout of all combustibles above the 5th floor of WTC 5, and the sprinkler system did not operate at all due to a drained water supply (see Figure 8 below). The computer model CFAST can predict the effect of a specified fire on gas temperatures, various gas concentrations, and smoke layer heights within a compartment. This software is used to approximate the temperature history of a typical compartment in WTC 5.

Figure 8: WTC 5 Involved in Fire

2.1.6 Finite Element Modeling

The finite element software ABAQUS is used to determine the thermal and mechanical responses of the column-tree assembly in WTC 5 to the elevated temperature history derived from CFAST. ABAQUS is able to model non-linear material properties (e.g., the variation of steel's thermal conductivity with elevated temperatures) and represent large deflection theory.

The analyses using ABAQUS are sectioned into two primary steps. First, a thermal analysis is conducted to determine the transient temperature distribution of the steel assembly in three-dimensional space and time. This information is then incorporated into a thermal-stress analysis in which the structural response is analyzed. It is anticipated that these analyses will demonstrate whether the local failure of WTC 5 occurred during the heating or cooling phase of the fire exposure.

2.2 Hypothesized Failure Mode

Figure 2 above provides a schematic of the column-tree and floor girder assembly contained in WTC 5. Figure 6 above shows the observed failure of this assembly. It is observed that the columns did not experience any permanent deformation; the steel remained elastic. Figure 6 above suggests that the girders did not undergo the typical failure mechanism sequence that simply-connected beams usually do when subjected to elevated temperatures from fire. It is hypothesized that the girders failed during the heating phase of the fire, which would explain why the columns were found to be straight and freestanding.

The figures shown below are schematics that present a comparison between the common failure mechanism sequence and that which is hypothesized in the case of the local collapse of WTC 5. More precisely, the expected failure mechanisms for both a girder that is connected directly to the columns and a girder which connects to shop-welded beam stems (WTC 5) are analyzed. The girders on the 9th floor of WTC 5 (directly above the local collapse area) underwent the common failure mechanism, for their connections were made at the columns.

The conditions shown in Figure 10 occur prior to fire exposure, when the girder is under normal service conditions. For both cases, the girder resists the distributed loading with compressive stress above the centroid of the beam's cross-section, and tension below it (both are relatively equal).

The conditions shown in Figure 11 occur as the fire begins to heat the compartment. In both cases, the girder undergoes thermal expansion. This expansion causes compressive axial restraint forces to develop which cause the compressive stress block to extend below the centroid of the girder cross-section.

The conditions shown in Figure 12 occur as the fire becomes fully-developed. For both cases, the yield strength and elastic modulus decrease as a result of the elevated temperatures. As the rigidity of the girder decreases, the axial restraint forces are alleviated and the girder begins to sag under the gravity load.

The conditions shown in Figure 13 occur during a later stage of the fully-developed fire. In the case of the girder connected directly to the columns, the girder becomes a catenary. Essentially, the girder becomes a "cable" in which the entire cross-section experiences tensile stress. In the case of the column-tree assembly from WTC 5, it is hypothesized that failure occurs during the fire prior to the development of this catenary action. More precisely, the high-strength steel bolts tear through the webs of the beam stems prior to the girder reaching the catenary phase.

The conditions shown in Figure 14 occur during the cooling phase of the fire. Since the members are insulated, it takes a significant amount of time after the fire has burned out for the steel to begin to cool. In the case of the girder connected directly to the columns, the girder eventually undergoes thermal contraction. This thermal contraction causes significant axial tensile forces to develop and the columns are usually deformed

permanently as a result. It is hypothesized that the column-tree assembly from WTC 5 never reached this mechanism prior to its failure. The web tear out failure of a collected WTC 5 beam stem specimen is shown in Figure 9 below.

Figure 9: Recovered Beam Stem Sample from WTC 5

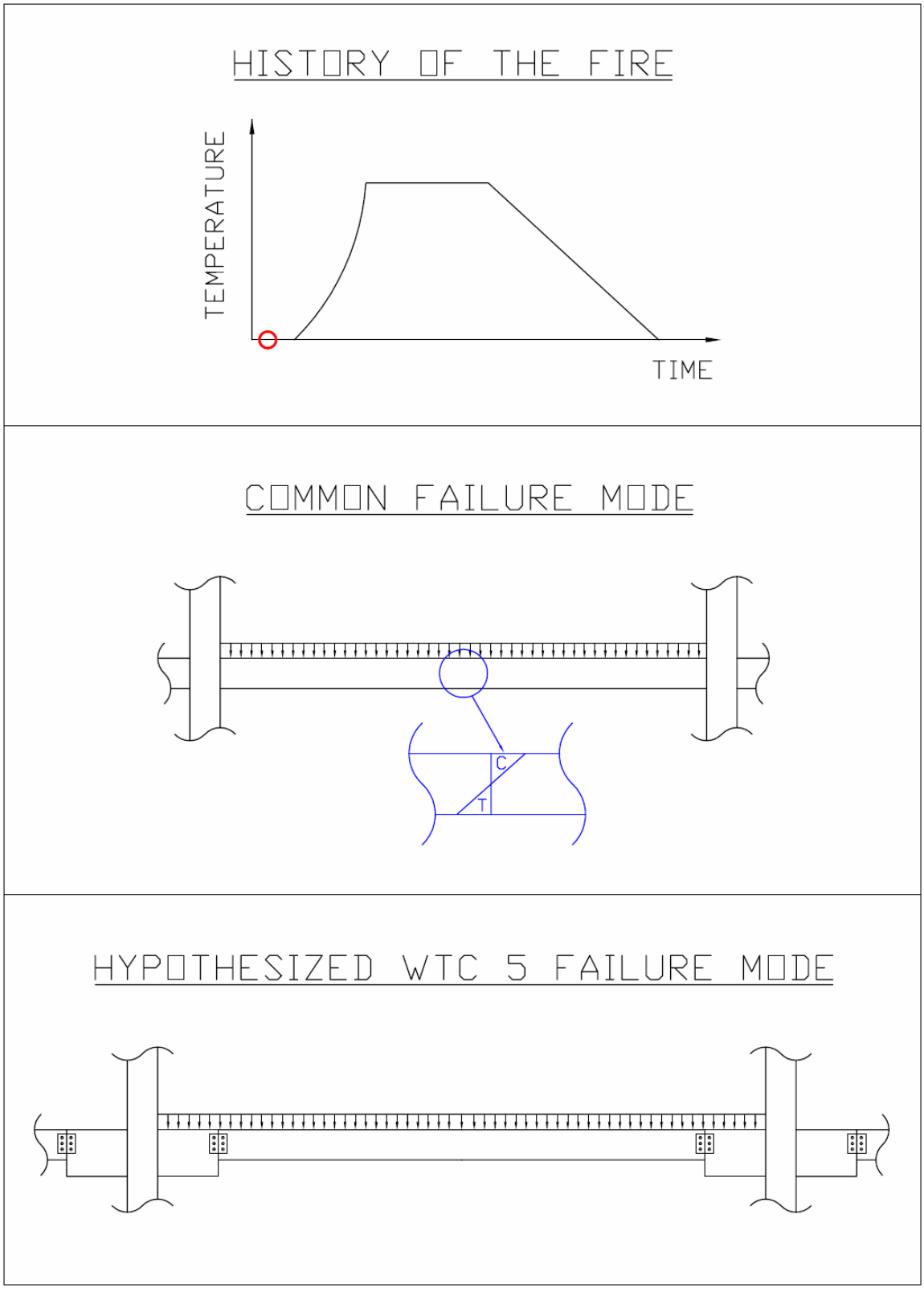

Figure 10: Failure Mechanism Comparison (Phase I)

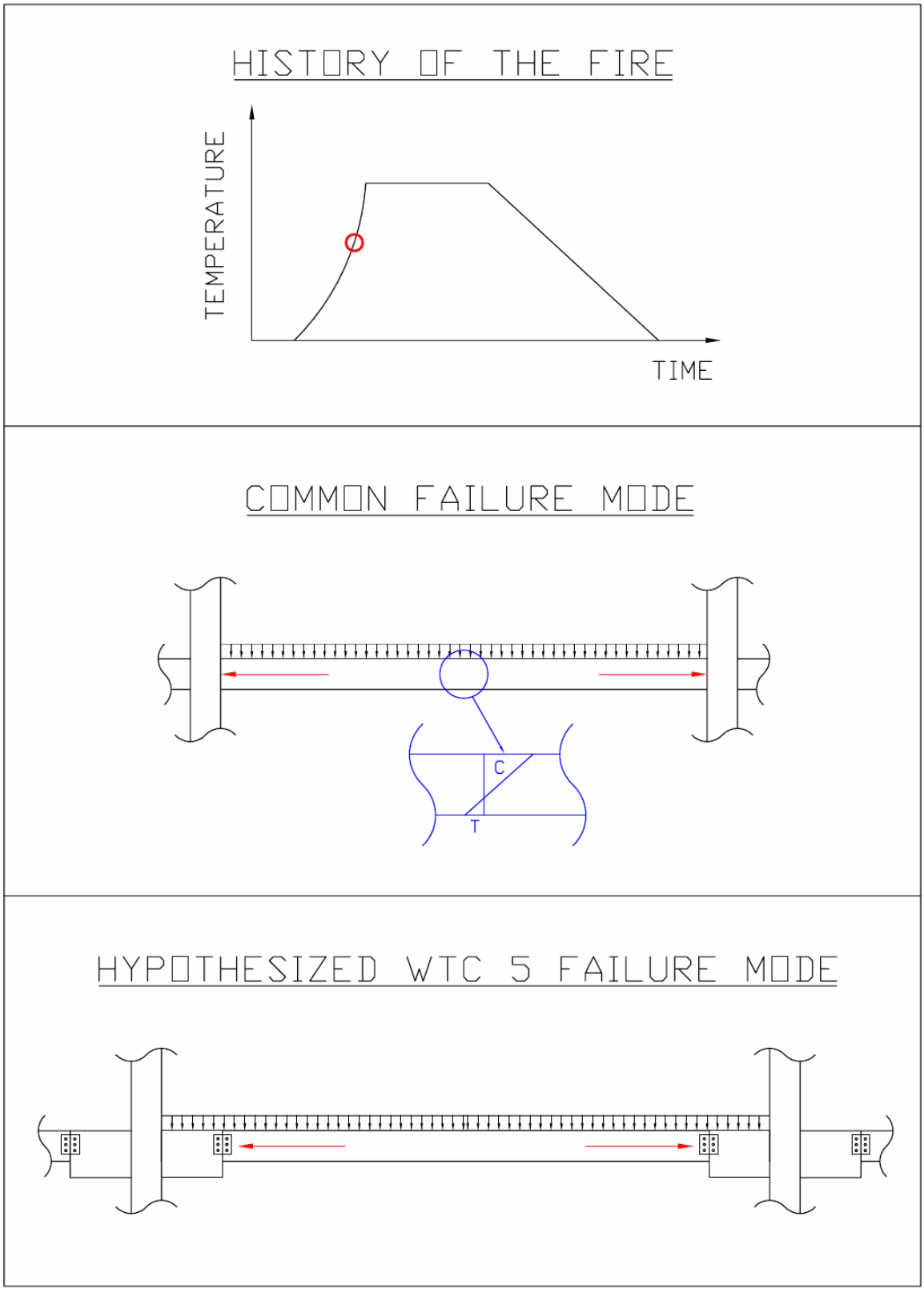

Figure 11: Failure Mechanism Comparison (Phase II)

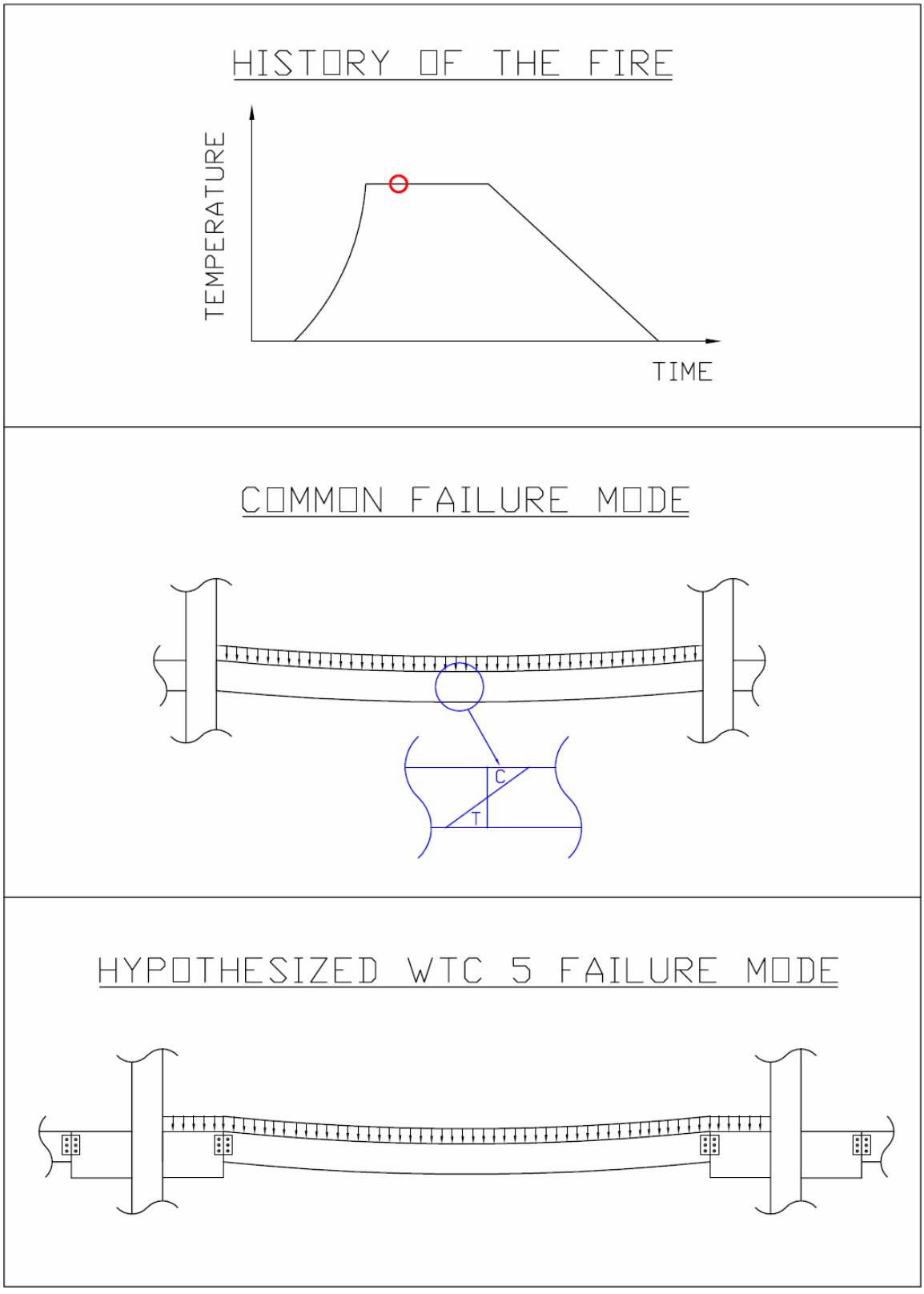

Figure 12: Failure Mechanism Comparison (Phase III)

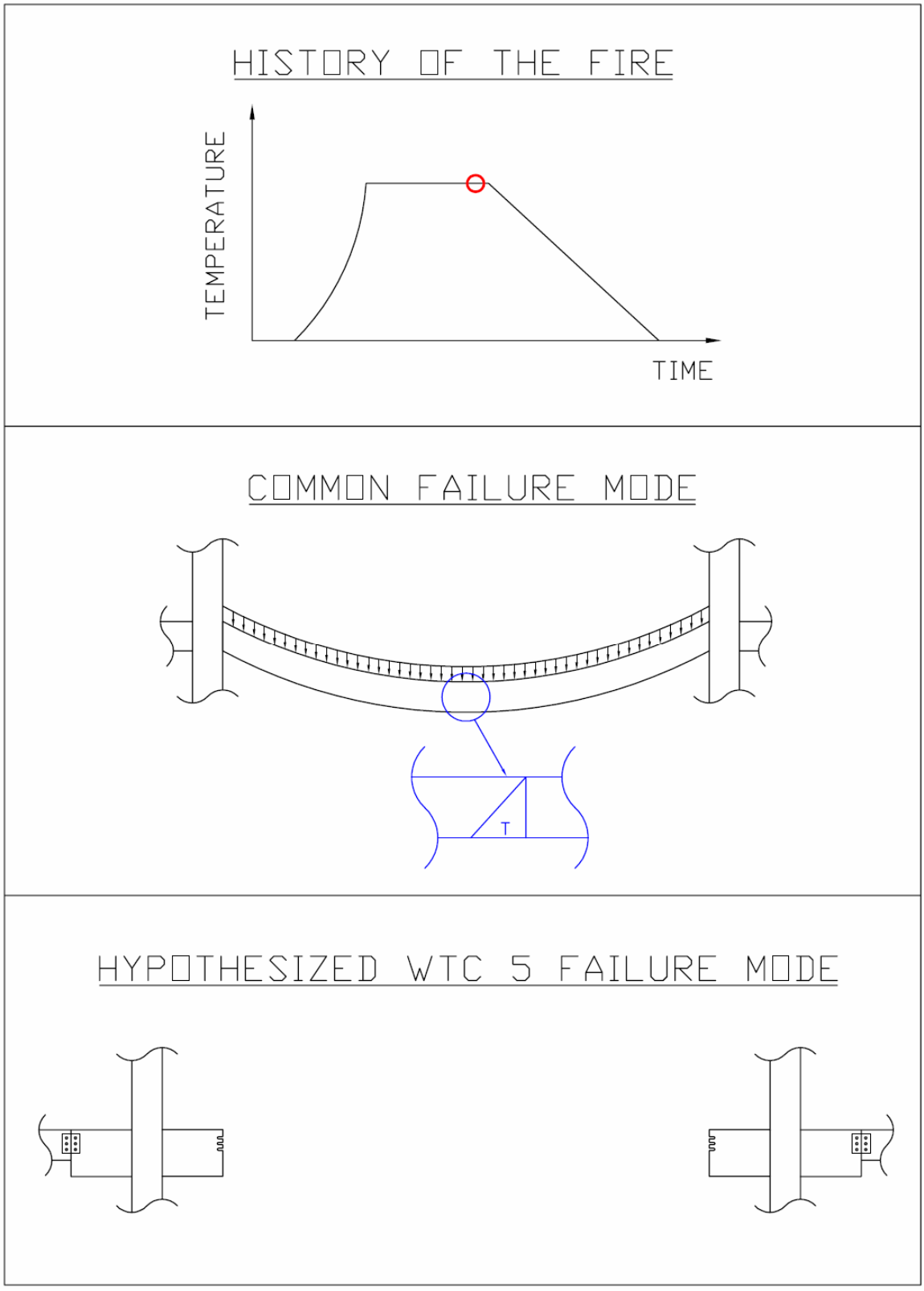

Figure 13: Failure Mechanism Comparison (Phase IV)

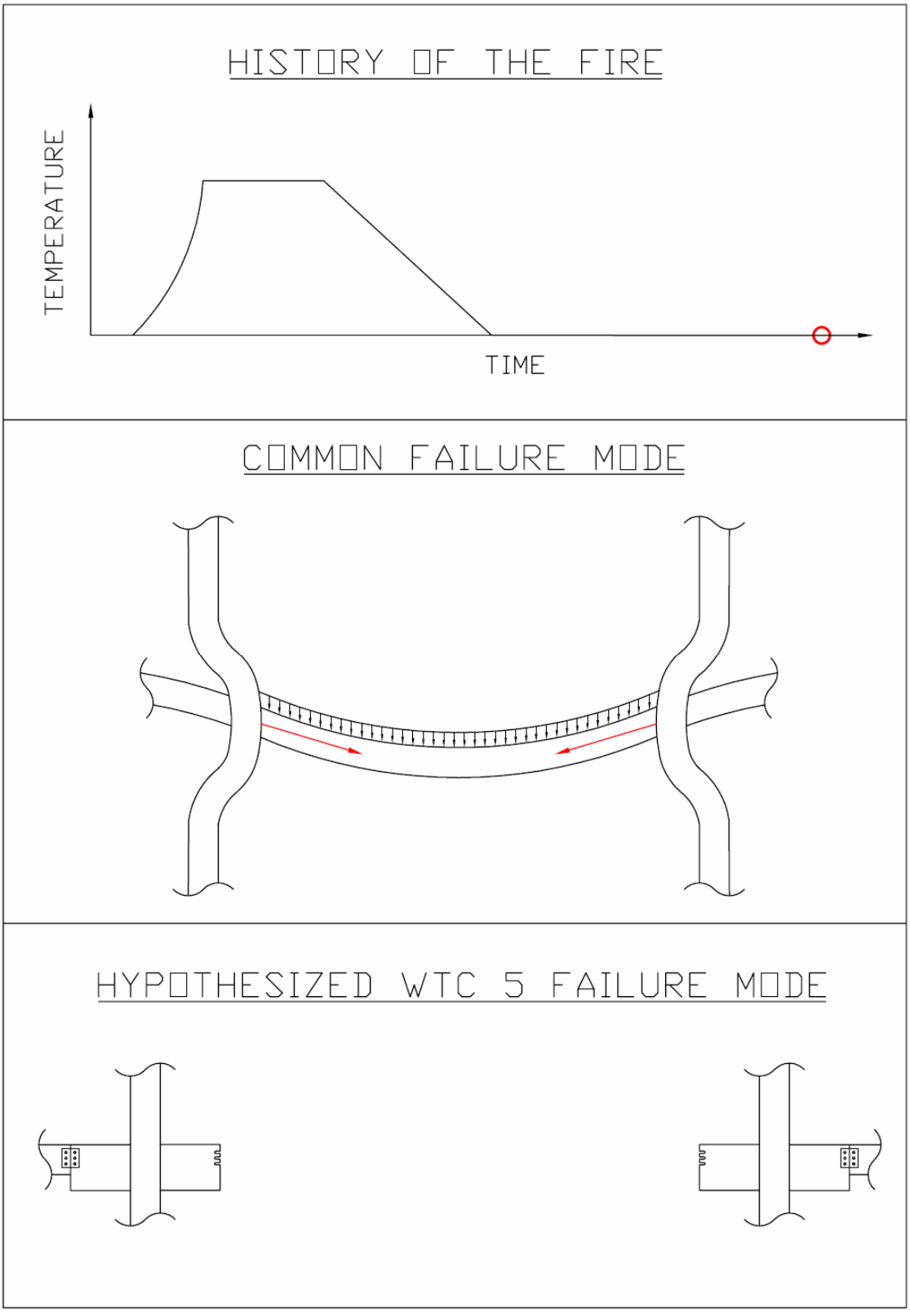

Figure 14: Failure Mechanism Comparison (Phase V)

2.3 Gerber Beam Design

The Gerber beam design method (also known as the cantilever-splice construction method), which was extensively used in the construction of WTC 5, was invented in the 19th Century by Professor Gerber in Germany. Gerber's design was in response to railroad bridge failures caused by uneven support settlements during this time. The Gerber beam design locates hinges at inflection points to allow settlement without an increase in the maximum bending stress (Schierle). Figure 15 below shows common configurations for the Gerber beam design applied to railroad construction.

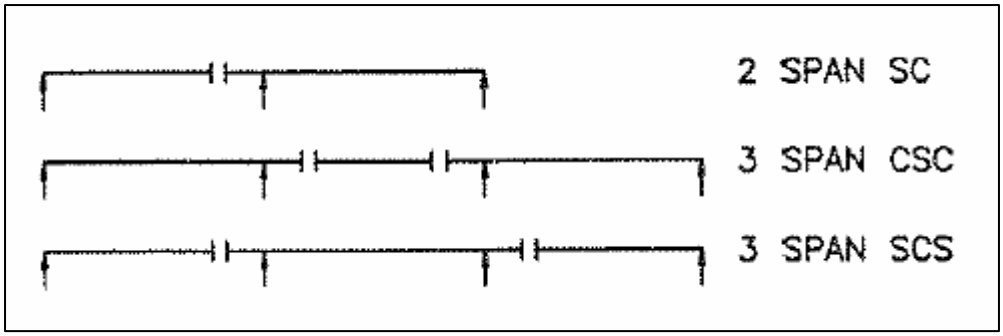

Figure 15: Common Gerber Beam Design Configurations

Following its application to railroads, structural engineers realized the benefits of applying the Gerber beam design to building construction. The primary advantage of this application of the Gerber beam design is economy. The structural design of a member in a building is most often governed by its allowable deflection under service loads. The maximum deflection of a member is a highly-nonlinear function of its span (L) as shown in Equation 1 below.

$$\Delta_{max} = \frac{5\varpi L^4}{384EI} \qquad (1)$$

Equation 1 above demonstrates the tremendous influence the span length has upon the required size of the steel beam to resist an allowable deflection threshold. The Gerber beam design allows structural engineers to use different sized members toward the midspan and at the supports which dramatically reduces the amount of steel required to carry the loads effectively under service conditions. Compared to simple beam framing, the use of the Gerber beam design may result in 15% to 30% savings in steel, on the order of $0.15 to $0.30 per square foot of floor area. Larger bays and longer spans tend to increase this savings in steel costs (Hemstad 129). Figure 2 and Figure 3 above show the use of the Gerber beam design in typical structural bays of WTC 5.

The erection of a structure utilizing the Gerber beam design is no more difficult than simple framing. Moreover, the Gerber beam design avoids the complexity and high cost of field-connected moment splices needed for continuous beam construction, which is

often used to limit beam deflection. Since Gerber beam systems are statically determinate, small errors in length of support columns are easily accommodated. The most common application of the Gerber beam design is light industrial, warehouse, school, and office construction (129, 130-134).

A major disadvantage common to both the Gerber beam design and simple framing techniques is the lack of structural redundancy and reserve strength that are inherent in continuous framing. The ratio of lengths of the cantilever to the main span is selected by designers to optimize the size of the beam required. Reasonably simple equations available to the designer yield the optimum cantilever lengths for a given beam layout (134).

While more demanding analytically than simple framing techniques, in buildings with large bays, the Gerber beam design typically is the most economical system. In large buildings with regular repetitive layouts (e.g., WTC 5), this additional design effort is often offset by the construction savings realized. Therefore, the Gerber beam design is considered by many structural engineers to be viable for many routine building designs (137).

3 Evidence Pertinent to the Research

3.1 Analysis of Forensic Evidence

Forensic evidence is a key component to understanding the internal structural collapse that occurred in WTC 5 due to fire alone. Forensic evidence is the baseline of the research and serves to reinforce specific findings derived from numerical methods. Once the WTC site was changed from a rescue to a recovery operation following the events of September 11, 2001, FEMA formed a Building Performance Study (BPS) team consisting of specialists in tall building design, steel and connection technology, fire and blast engineering, and structural investigation and analysis. The BPS team surveyed the WTC 5 site and collected photographic evidence and specimen samples to make a preliminary performance assessment of the building, as well as supplement future study. This section shall analyze relevant evidence as originally described in Chapter 4 of the World Trade Center Building Performance Study: *Data Collection, Preliminary Observations, and Recommendations*.

WTC 5 was damaged by impact of flaming debris from WTC 1 and the subsequent fires. The impact damage areas in western section of WTC 5 are shown in Figure 16 below. Ensuing fires that burned unchecked in the building caused a localized collapse from the 8th through the 5th floors in the eastern section of the building. Figure 17, Figure 18, Figure 19, and Figure 20 below show diagrammatically the collapsed areas of WTC 5 due to impact, as well as due to fire alone.

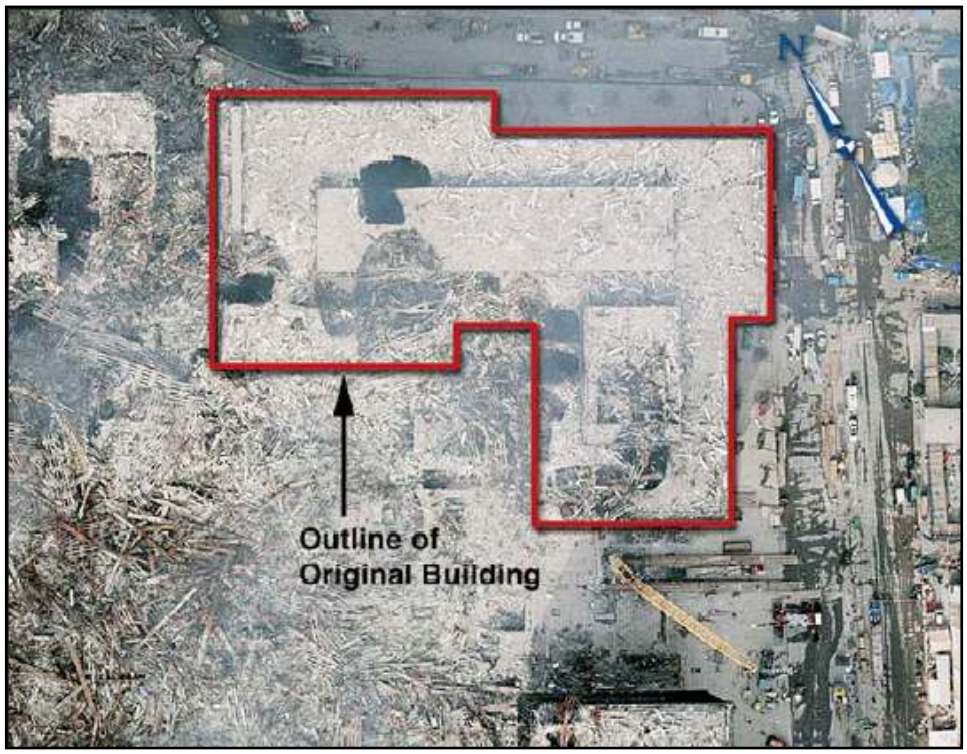

Figure 16: Aerial View of WTC 5 Damage

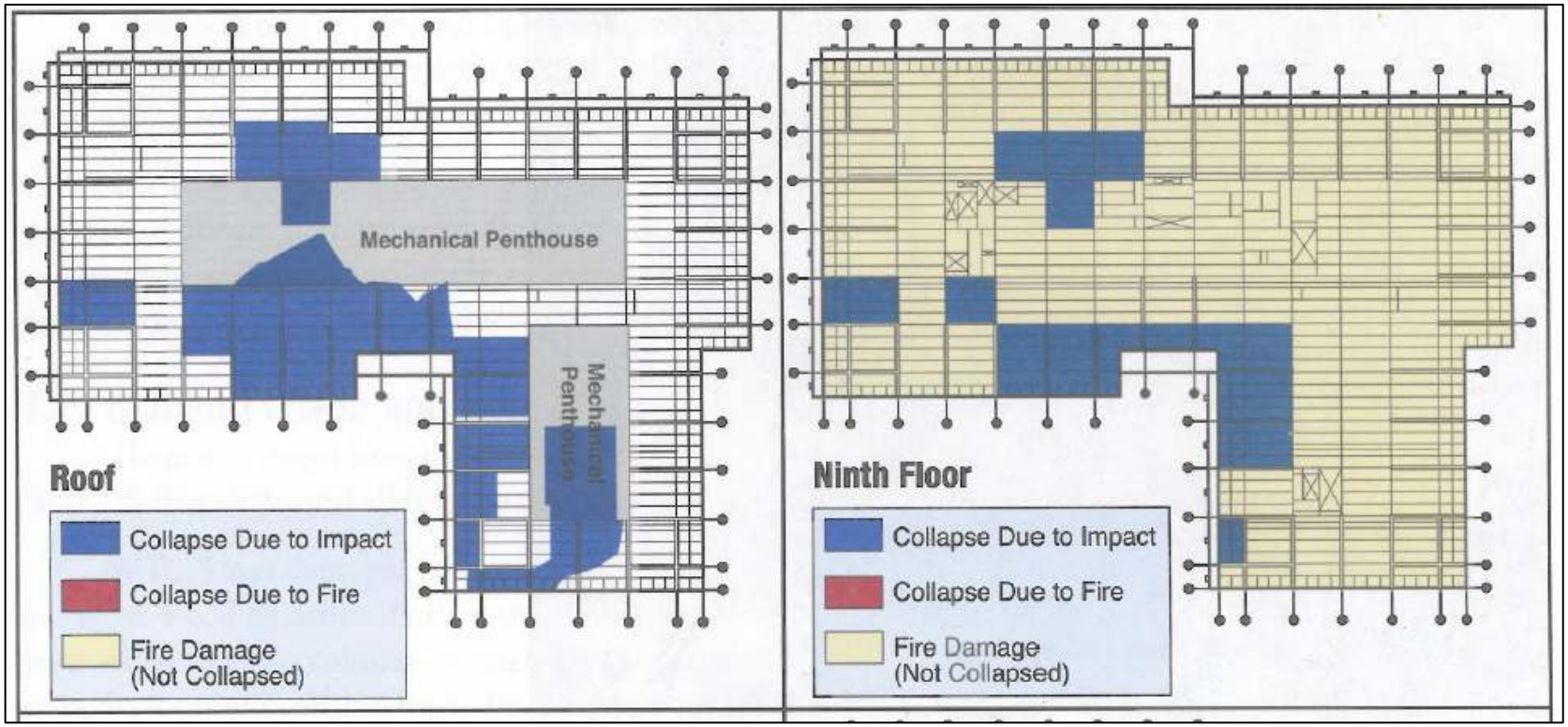

Figure 17: Approximate Locations of Failed Floor Sections in WTC 5 (Roof and 9th Floor)

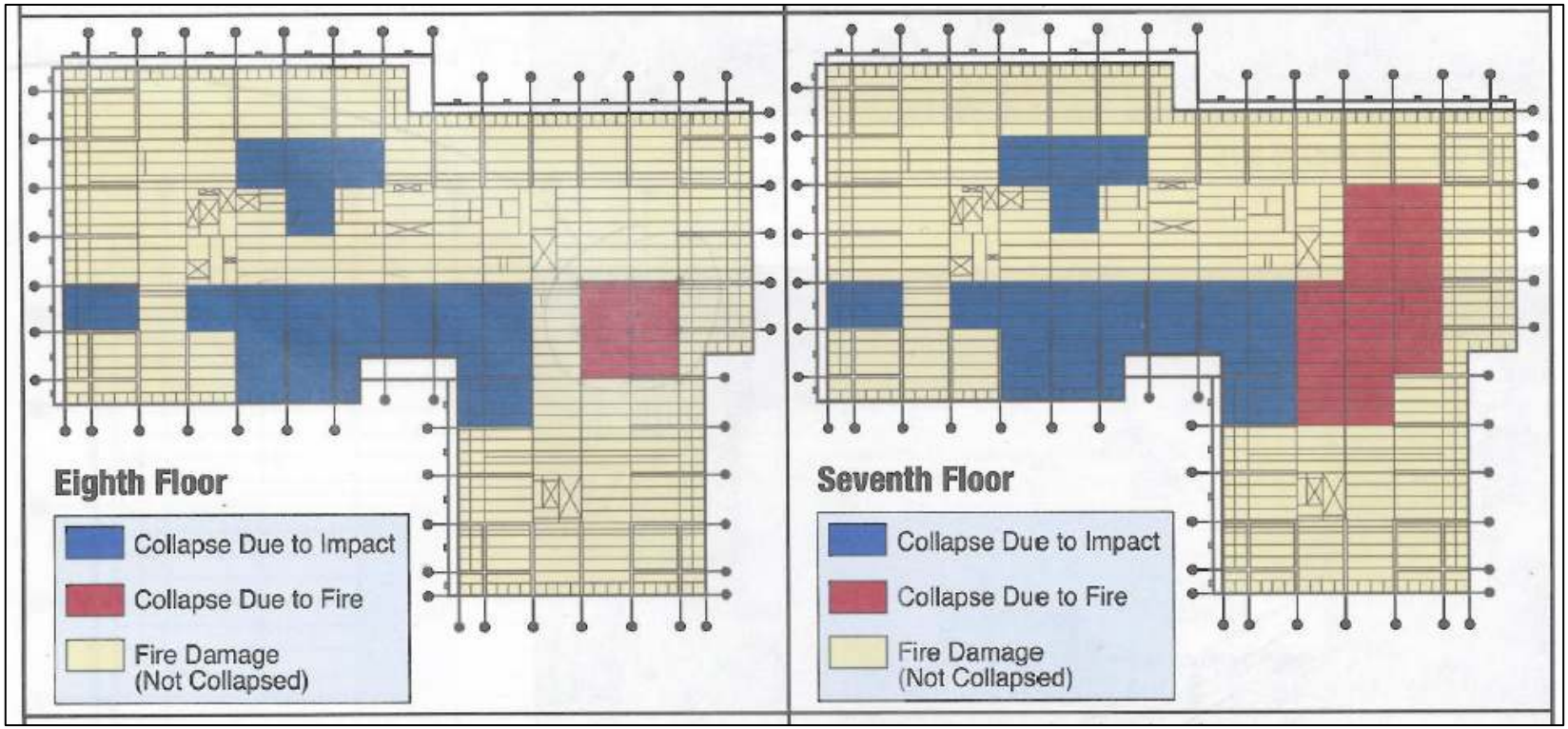

Figure 18: Approximate Locations of Failed Floor Sections in WTC 5 (8th and 7th Floors)

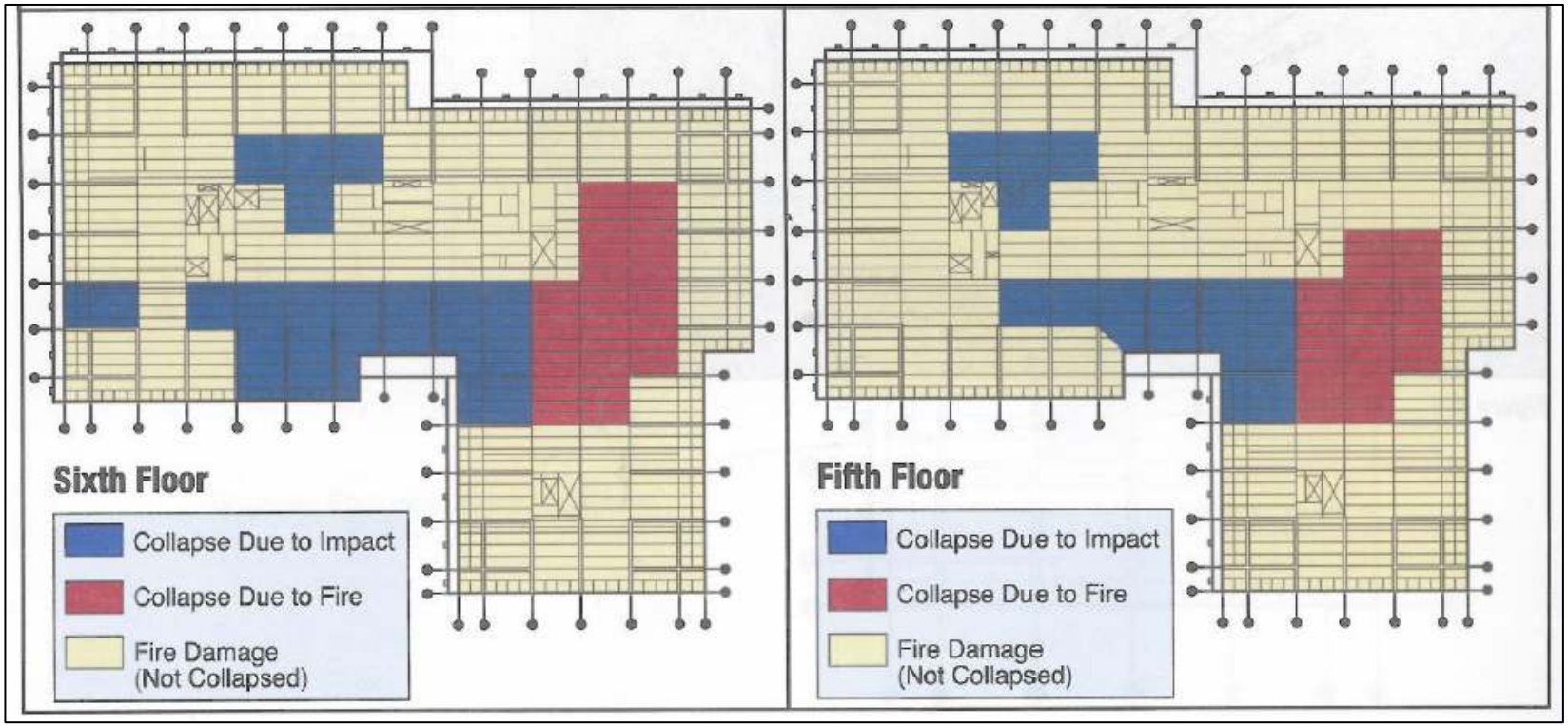

Figure 19: Approximate Locations of Failed Floor Sections in WTC 5 (6th and 5th Floors)

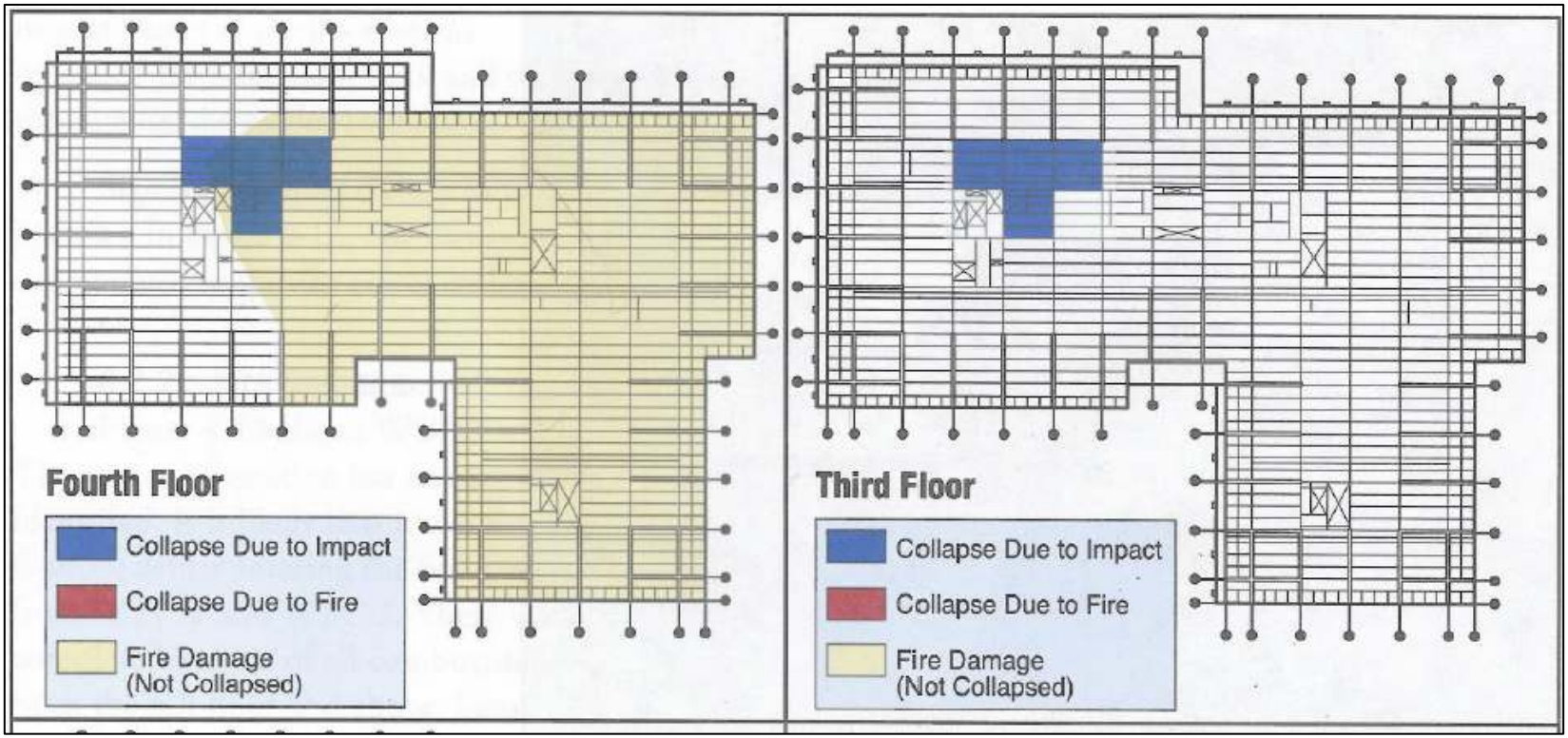

Figure 20: Approximate Locations of Failed Floor Sections in WTC 5 (4th and 3rd Floors)

Figure 21 and Figure 22 below show the deformed beams on the 9th floor of WTC 5. It is observed that the beams reached the catenary phase in which they no longer behave as typical beams, but more like tensile cables.

Figure 21: Deformed Beams in WTC 5 (9th Floor) (View 1)

Figure 22: Deformed Beams in WTC 5 (9th Floor) (View 2)

Figure 24, Figure 25, Figure 26, and Figure 27 below show different perspectives of the internal structural collapse from the 8th through the 5th floors of WTC 5. The sole focus of the project is this particular collapse, which was due to fire alone.

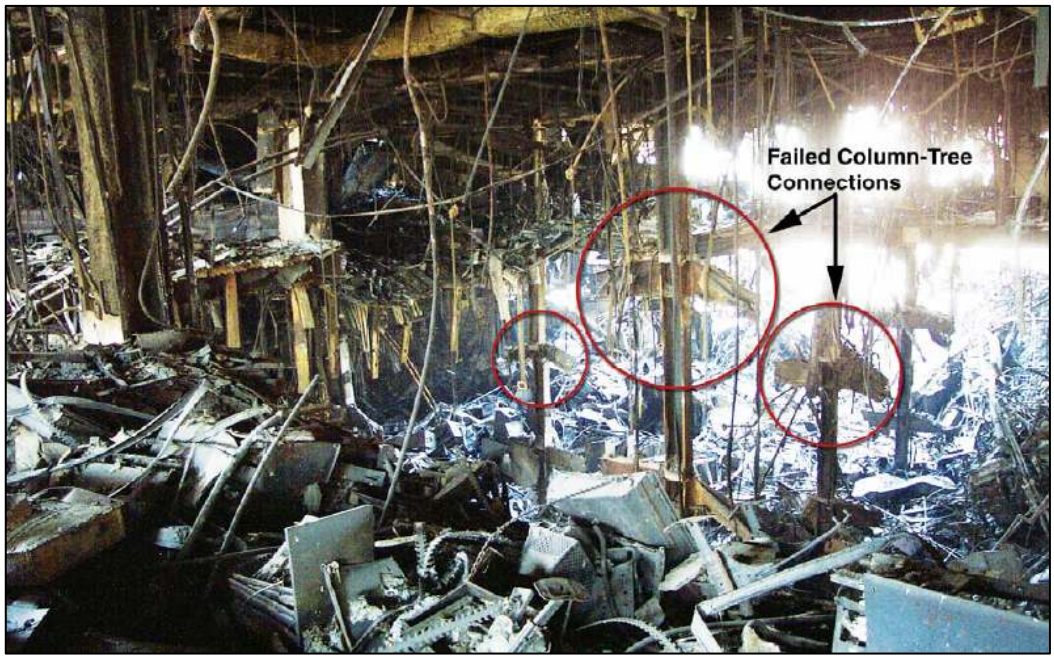

Figure 23: Localized Structural Collapse of WTC 5 (Perspective 1)

Figure 24: Localized Structural Collapse of WTC 5 (Perspective 2)

Figure 25: Localized Structural Collapse of WTC 5 (Perspective 3)

Figure 26: Localized Structural Collapse of WTC 5 (Perspective 4)

Figure 27: Localized Structural Collapse of WTC 5 (Perspective 5)

Figure 28 below is a photograph of a typical shear connection between a beam stem and a floor girder. The upper floors of the building used three bolts at the shear connections; the lower floors used four bolts. Figure 29 and Figure 30 below is a shear connection specimen and its associated drawing detail, respectively (Figure 31 and Figure 32 show a second shear connection specimen and its detail). It is observed that there is a nominal gap distance of ½ in. between the beam stem and the floor girder. Figure 33 below is a web stem specimen collected from WTC 5. This specimen experienced web rupture from what appears to be a moment force. Shear connections of this type are not designed to resist moment forces.

Figure 28: Typical Shear Connection in WTC 5

Figure 29: Shear Connection Specimen from WTC 5 (1 of 2)

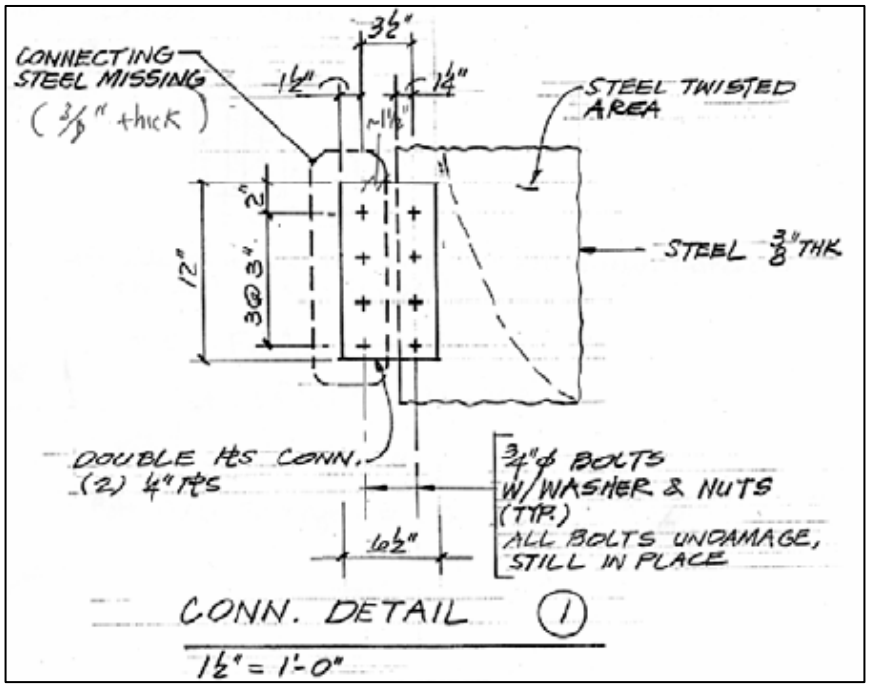

Figure 30: Drawing Detail of Shear Connection Specimen from WTC 5 (1 of 2)

Figure 31: Shear Connection Specimen from WTC 5 (2 of 2)

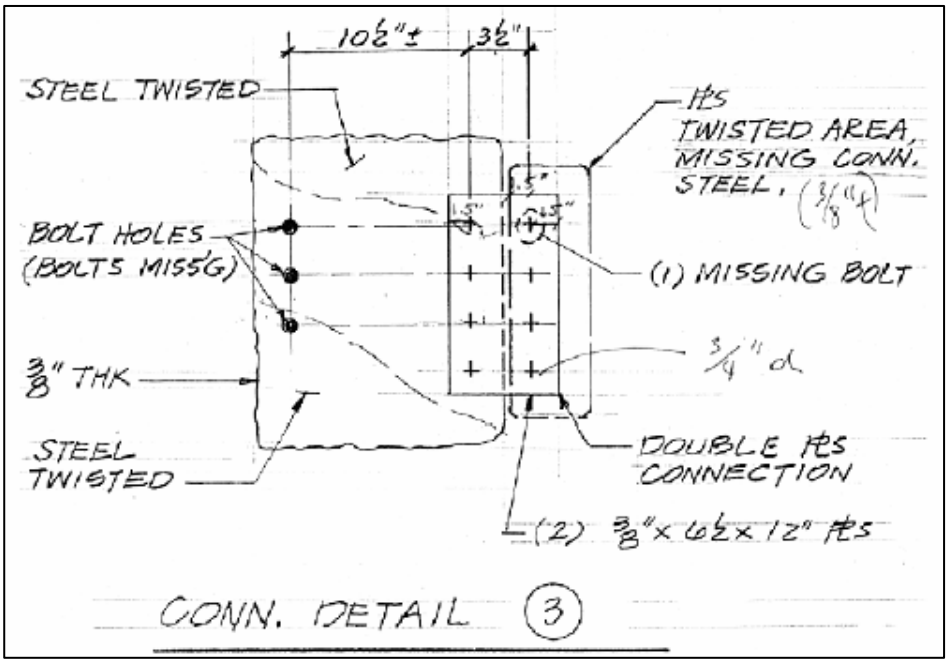

Figure 32: Drawing Detail of Shear Connection Specimen from WTC 5 (2 of 2)

Figure 33: Failed Beam Stem Web Specimen from WTC 5

Figure 33 above is clearly part of a beam stem because Figure 27 above shows a failed beam stem still attached to a column, and the observed bolt hole failure appears very similar between the collected specimen and the beam stem still intact.

Figure 34 below shows the exterior of WTC 5 during its demolition. It is observed that in addition to their specified 1-3/8 in. (3-hour), spray-applied insulation, mostly all of the building columns were either located behind walls or fully boxed in with wall material during their service. This would suggest that mostly all of the columns were fully shielded during the fire and probably never reached very high temperatures relative to the beams and girders, which were not shielded and had 1-in. (2-hour) insulation. Therefore, the columns would have acted as heat sinks for the beams and girders to the rest of the "cooler" structure.

Figure 34: Exterior View of WTC 5 (Shielded Columns)

3.2 Review of the Structural Plans and Details

The structural plans and details of WTC 5 were obtained from the Port Authority of NY & NJ. Due to the extensive litigation surrounding the WTC site, the Freedom of Information Act was utilized to legally obtain these sensitive documents. These construction documents are essential to this project because they describe the size of the structural elements and the detailed dimensions of the connections. This information is crucial to the development of an accurate finite element model of the structural assembly using ABAQUS.

Figure 35 below is the title block of the structural plans for the 6th, 7th, and 8th floors of WTC 5. The initial collapse due solely to fire exposure was on the 8th floor of WTC 5; the initial four structural bays to collapse are shown in Figure 36 below.

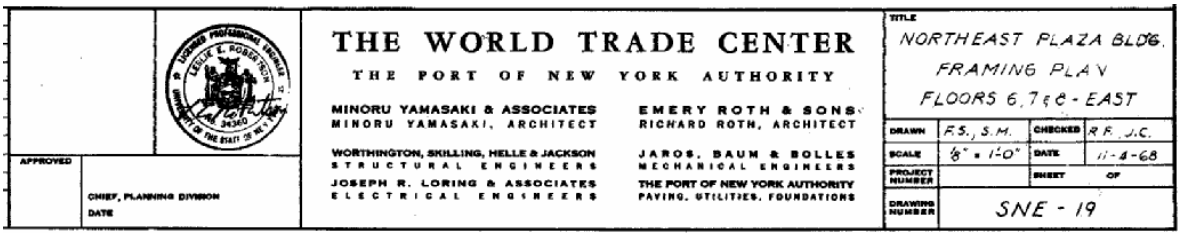

Figure 35: Title Block for WTC 5 Structural Plans (6th, 7th, and 8th Floors)

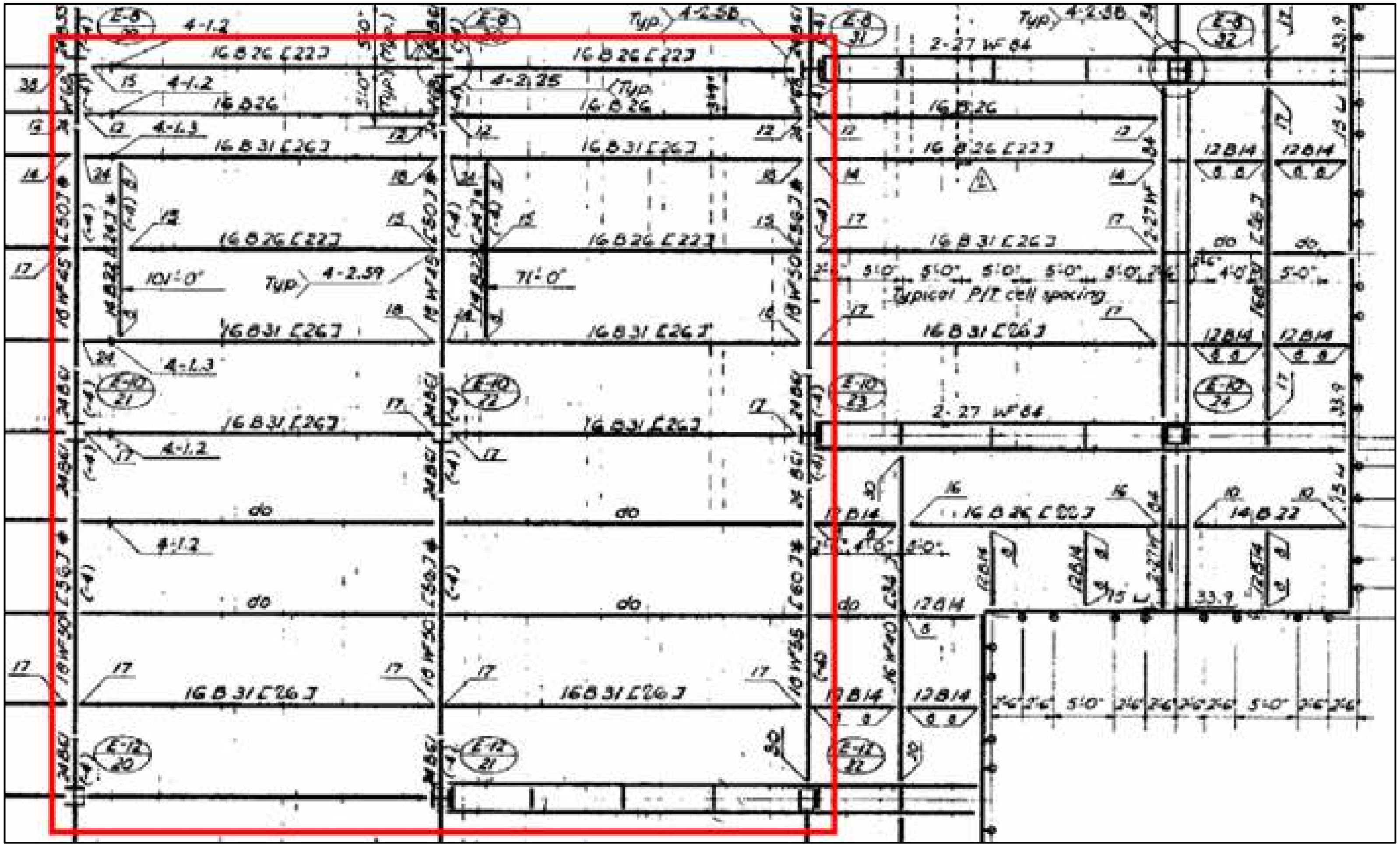

Figure 36: Four Structural Bays that Initially Collapsed Due to Fire (8th Floor)

The structural drawings of WTC 5 reference details contained in the *Drawing Book NE*. The *Drawing Book NE* contains many structural details, ranging from column schedules to connection dimensions. The *Drawing Book NE* specifies that A36 steel is used for structural members and A325 steel is used for bolts. Referencing the column schedule, the typical column size on the 8th floor in the area of collapse was stated to be W14X103.

According to the *Drawing Book NE*, the shear connections in WTC 5 are friction-type. More precisely, a pretension force of 39 kips was applied to each bolt. Currently, friction-type connections are implemented to resist stress reversals due to lateral loads, but this type of connection was commonly specified for structures built in the 1970s. The standard bolt and hole diameter at the shear connections is 7/8 in. and 15/16 in., respectively. Figure 37 and Figure 38 below show the elevation and plan views of the shear connections in WTC 5 above the 4th floor, respectively. Figure 38 shows that strip shims are required between the shear tabs and the web of the floor girder.

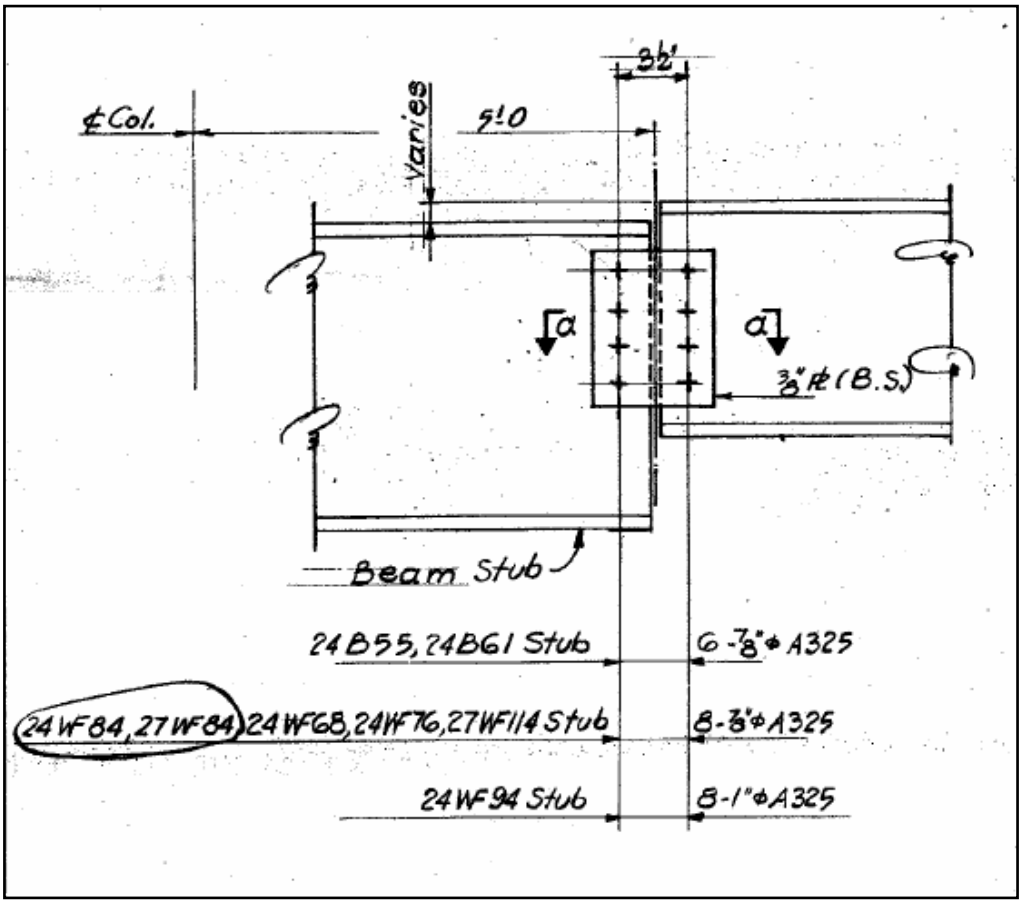

Figure 37: Elevation View of the Shear Connections in WTC 5

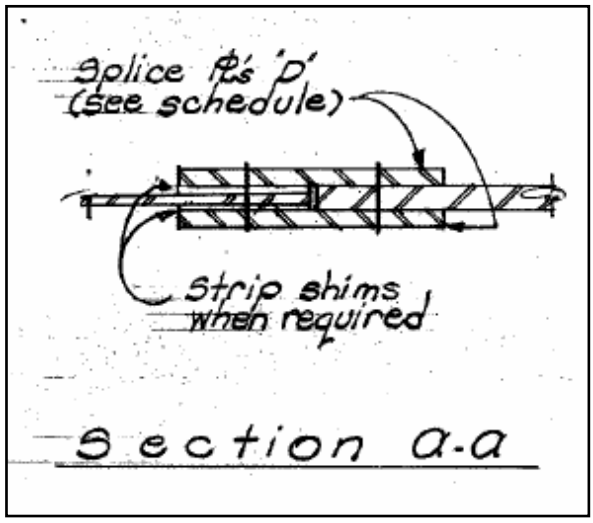

Figure 38: Plan View of the Shear Connections in WTC 5

The girder-to-beam stem connections on the 4th floor are different from those shown in Figure 37 above. Figure 39 below shows that these connections were moment-resisting.

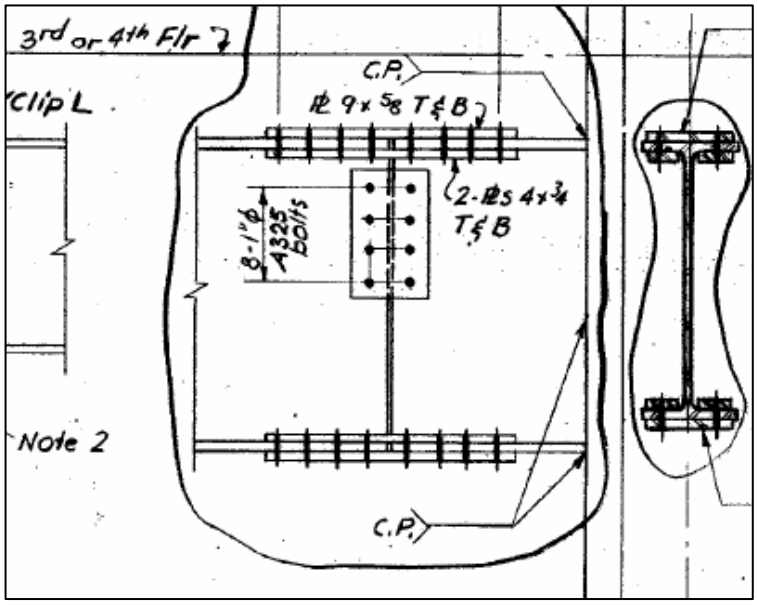

Figure 39: Typical Connection on the 4th Floor of WTC 5

The *Drawing Book NE* specifies that the lightweight concrete slab (110 pcf) is supported by a 22 gage metal deck. Moreover, shear studs are specified along the lengths of the supporting beams. The concrete slab does not contain any bar reinforcement, but rather utilizes welded wire fabric to help prevent cracking. The welded wire fabric conforms to ASTM A185. The *Drawing Book NE* also specifies that column stiffeners are not required.

4 Fire Event Reconstruction

It is important to estimate the fire exposure which occurred in WTC 5 on September 11, 2001. This information is required to determine the fire performance of the WTC 5 structure.

4.1 Estimation of the Effective Heat of Combustion

The National Institute of Standards and Technology (NIST) released a report in 2005 (by Ohlemiller et al.) which describes a series of six fire tests of single office cubicles, the dominant combustibles in the WTC 1 building. For each test, the entire assembly was placed beneath the hood of a NIST 10 MW calorimeter and the effective heat of combustion was derived. Figure 40 and Figure 41 below show the office cubicle testing assembly prior to and during fire exposure for one of the six tests conducted.

Figure 40: Office Cubicle Testing Assembly

Figure 41: Office Cubicle Assembly During Fire Exposure

Table 1: Measurements of the Effective Heat of Combustion

	Test					
	1	*2*	*3*	*4*	*5*	*6*
Effective Heat of Combustion [MJ/kg]	17.4	19.8	19.3	16.9	18	18.2

Table 1 above presents the effective heat of combustion for each of the six fire tests, which are based upon the cone calorimeter readings. The average value is used to develop the reconstruction of the fire that occurred in a compartment of WTC 5. This assumption is reasonable because WTC 5 had a similar office configuration as WTC 1.

Effective Heat of Combustion = 18.3 MJ/kg (average)

4.2 Estimation of the Fuel Load

In 1995, NIST released a report (by Caro el al.) which describes fuel load surveys of office buildings located in Washington, D.C. This report considered fuel load as the ratio of the total equivalent weight of the fuel commodities to the floor area of the space. A total of six offices were inventoried, three compartment-type designs and three open plan workstations.

Two survey strategies were utilized to conduct the fuel load surveys. The first strategy targeted offices in the process of being relocated or remodeled. This allowed for a simplified weighing process since office contents were packaged in boxes. The second strategy involved conducting surveys in offices in operation. In this case, combustibles were weighed individually.

Figure 42 below presents the results of the fuel load survey. The 80th percentile fuel load is approximately 20 lb. per square foot (98 kg. per square meter). Therefore, the total fuel load contained within a 9.14 m. by 9.14 m. compartment of WTC 5 may be estimated as follows:

$$\textbf{Fuel Load} = \left(98\,{}^{kg}\!/_{m^2}\right)\left[(9.14m)(9.14m)\right] = \textbf{8,187 kg.}$$

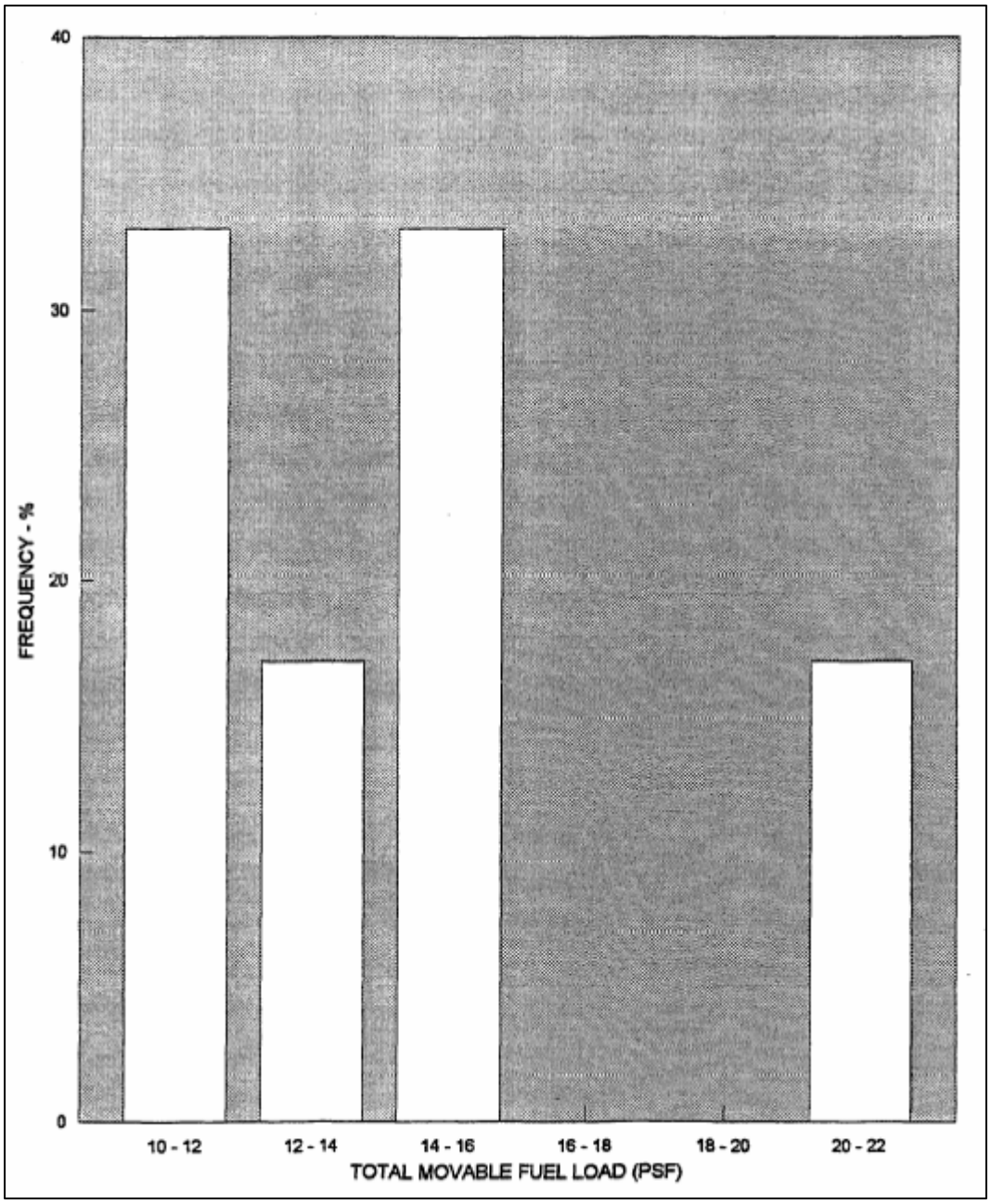

Figure 42: Frequency Distribution of Fuel Load

4.3 Estimation of the Peak Heat Release Rate

A 2005 NIST report (by McGrattan el al.) presents the results of numerical simulations of the fires that occurred in WTC 1. The calculations were performed with the NIST Fire Dynamics Simulator (FDS) 4.0, a computational fluid dynamics model that describes the flow of smoke and hot gases from a fire. The thousands of photographs and videotapes taken by eyewitnesses from around the exterior of the buildings served as an assessment of the fidelity of the fire model. Figure 43 below shows a model of WTC 1 (floors 92 through 99) that was used to represent the compartmentalization of the building and the combustibles contained.

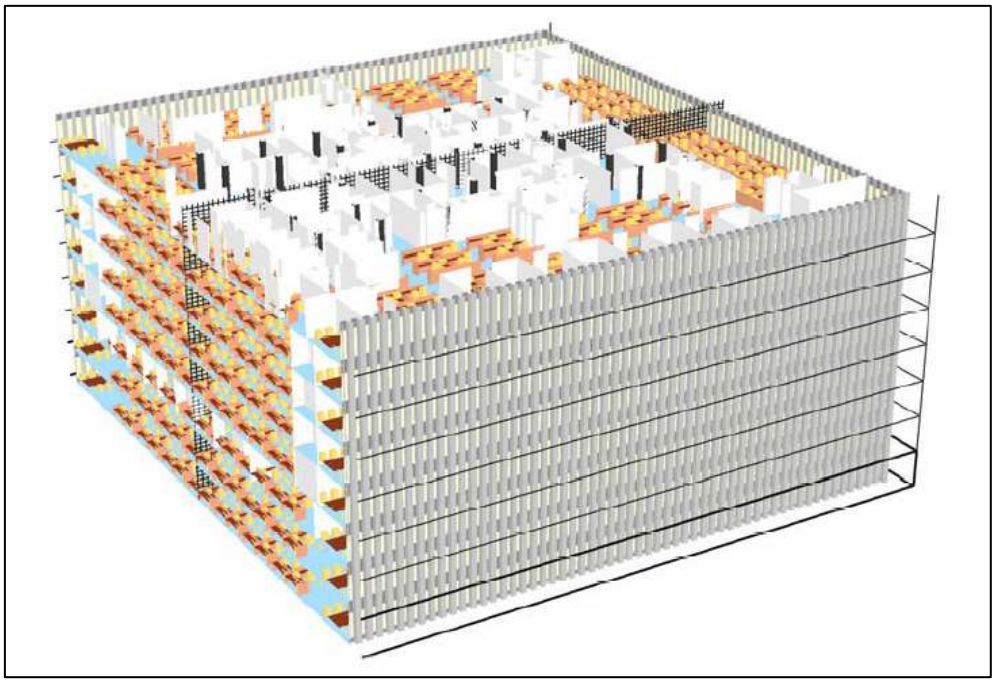

Figure 43: 8-Floor FDS Model of WTC 1

The computer simulations conducted for WTC 1 estimate the peak heat release rate to be between 1 GW and 1.5 GW for fires that occurred on multiple floors. The upper bound of 1.5 GW was considered for this case. Figure 44 below provides evidence that approximately one quarter of the floor area on a given story of WTC 1 was involved in fire at any given time. More precisely, Figure 44 shows the upper layer temperatures for six times during the fire exposure; at each location the temperature peaked at about 1000 °C. Each floor of WTC 1 was approximately 4,000 square meters in area. Therefore, the heat release rate per square meter of floor area can be derived as follows:

$$HRR/_{m^2} = \frac{1500 MW}{(8\,floors)\left[\left(1/_4\,floor\right)\left(4{,}000\,m^2/_{floor}\right)\right]} = 0.1875\,MW/_{m^2}$$

As mentioned, WTC 5 had a similar office configuration as compared to WTC 1. Therefore, the results of the rigorous numerical analyses conducted for WTC 1 can be extrapolated to derive a peak heat release rate for WTC 5. It is known that a typical compartment in WTC 5 was 9.14 m. by 9.14 m. Therefore, an appropriate peak heat release rate for the reconstructed fire can be derived as follows:

$$\textbf{Peak HRR} = \left(0.1875\,MW/_{m^2}\right)\left[(9.14m)(9.14m)\right] \approx \textbf{16 MW}$$

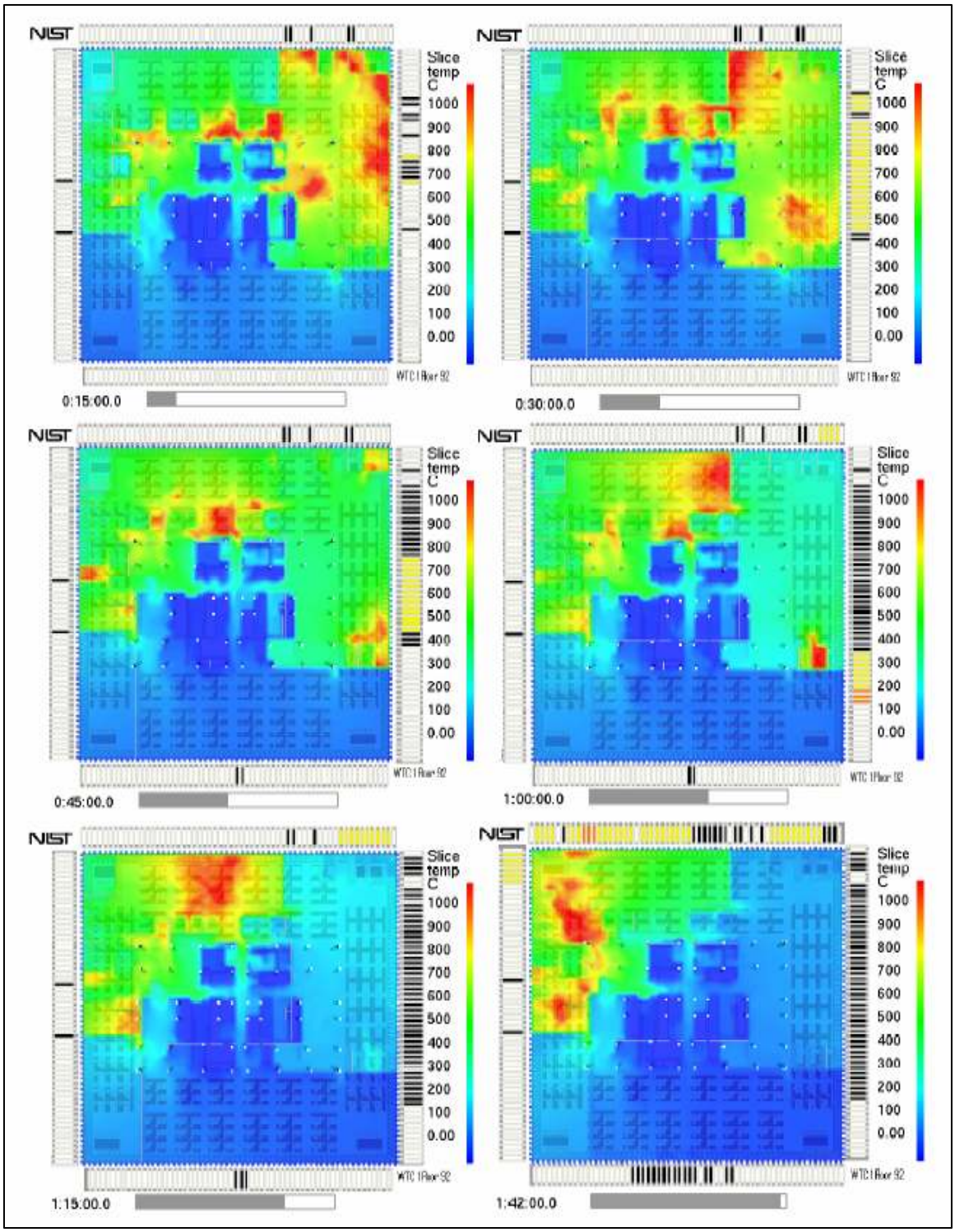

Figure 44: Upper Layer Temperatures of WTC 1, Floor 92

4.4 Development of the Temperature History

The effective heat of combustion of the fuel contained within WTC 5 was estimated to be 18.3 MJ/kg. Furthermore, the fuel load contained within the WTC 5 compartment of interest and the peak heat release rate of the fire was estimated to be 8,187 kg and 16 MW, respectively. These parameters were derived from two 2005 NIST reports that study WTC 1, as well as a 1995 NIST report. Using this information as a starting point, the reconstructed fire temperature history was developed to serve as input to the finite element model of the structural assembly.

The growth of a fire may be represented using Equation 2 below:

$$Q = \alpha t^2 \qquad (2)$$

Q is the rate of heat release [kW]

α is the fire intensity coefficient [kW/s^2]

The SFPE Handbook provides standard values for the fire intensity coefficient, as shown below.

Medium Growing Fire: $\alpha = 0.0117\, kW/s^2$

Fast Growing Fire: $\alpha = 0.0469\, kW/s^2$

Ultra-fast Growing Fire: $\alpha = 0.1876\, kW/s^2$

The 1994 Eurocode (EC1) provides a method to determine the decay period of a design fire. If the heat release rate is constant during the fully-involved (post-flashover) period with a linear decay rate, the implied curve of heat release rate versus time should be such that one-third of the fuel load (energy) is consumed during the decay phase of the fire.

The fuel flow rate is defined by Equation 3 below:

$$\dot{m}_f = \frac{Q}{\Delta H_{ch}} \qquad (3)$$

ΔH_{ch} is the effective heat of combustion

Using Equation 3, the total fuel burned over the course of the fire exposure may be calculated. Since the effective heat of combustion, fuel load, peak heat release rate, and the fire growth and decay characteristics are known, the medium, fast, and ultra-fast growing scenarios of the heat release rate history of the reconstructed fire may be defined as shown in Figure 45, Figure 46, and Figure 47, respectively. For each of these cases, approximately 8,187 kg of fuel is burned (2,729 kg during the decay phase).

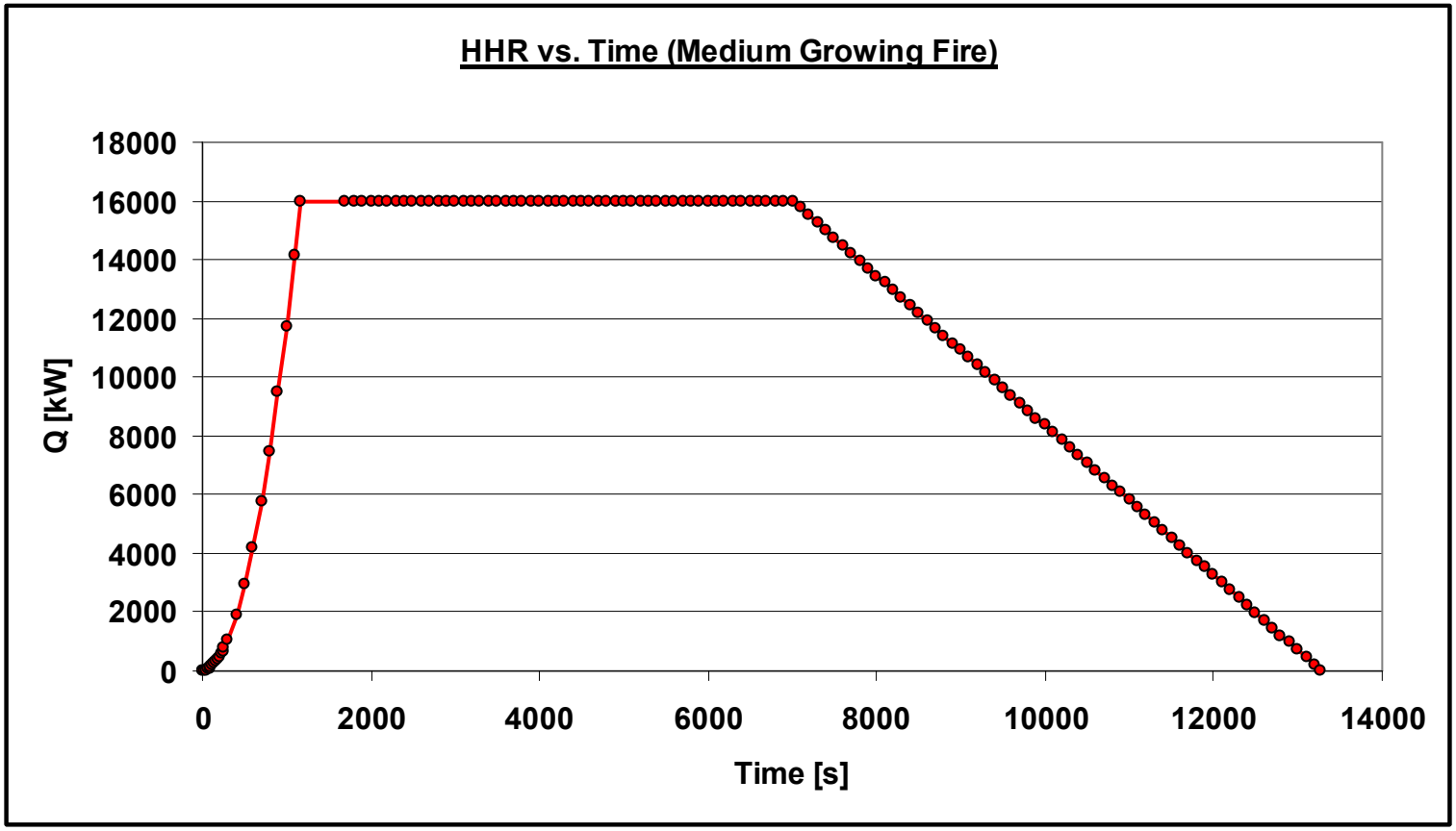

Figure 45: Heat Release Versus Time (Medium Growing Fire)

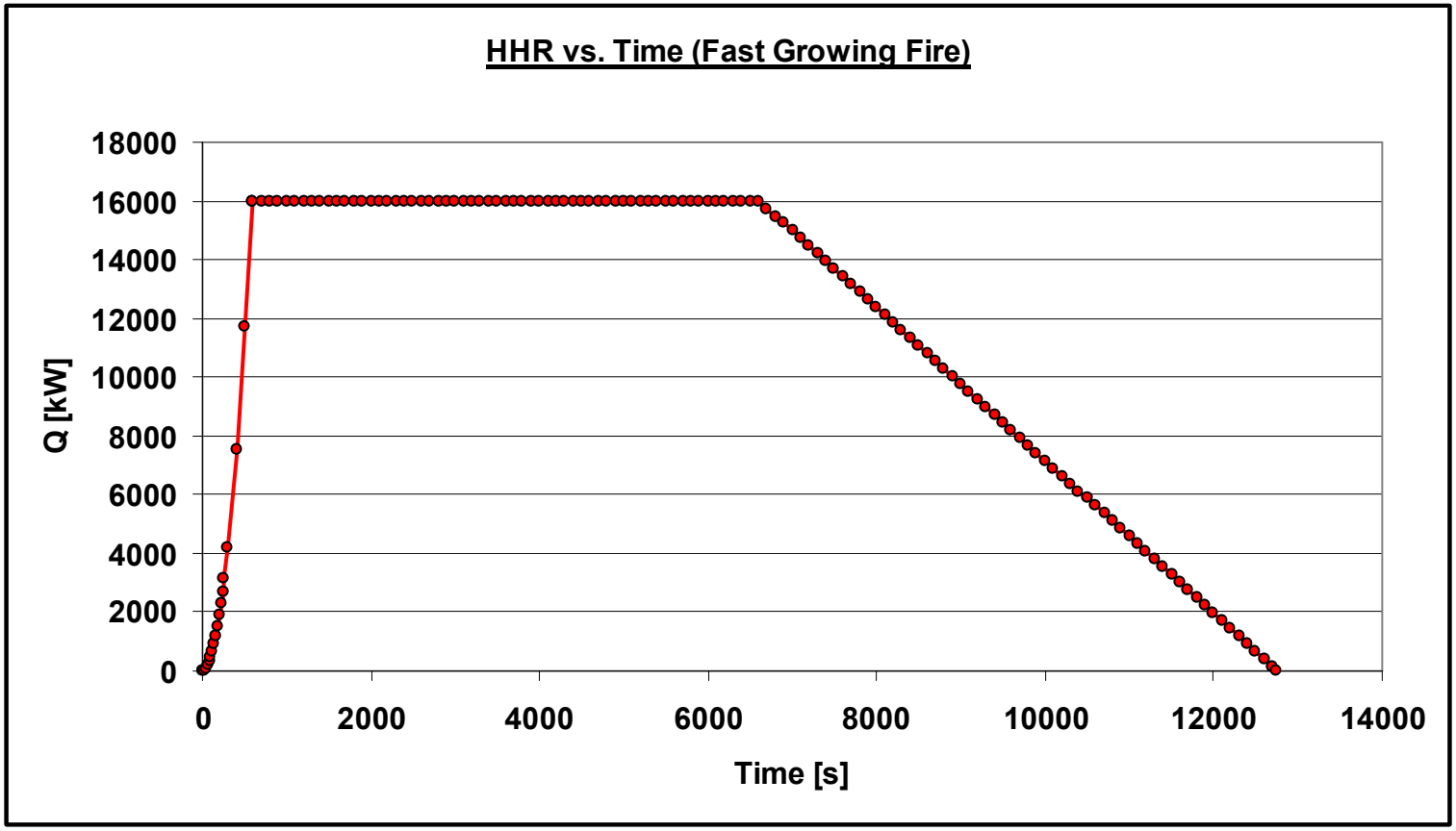

Figure 46: Heat Release Versus Time (Fast Growing Fire)

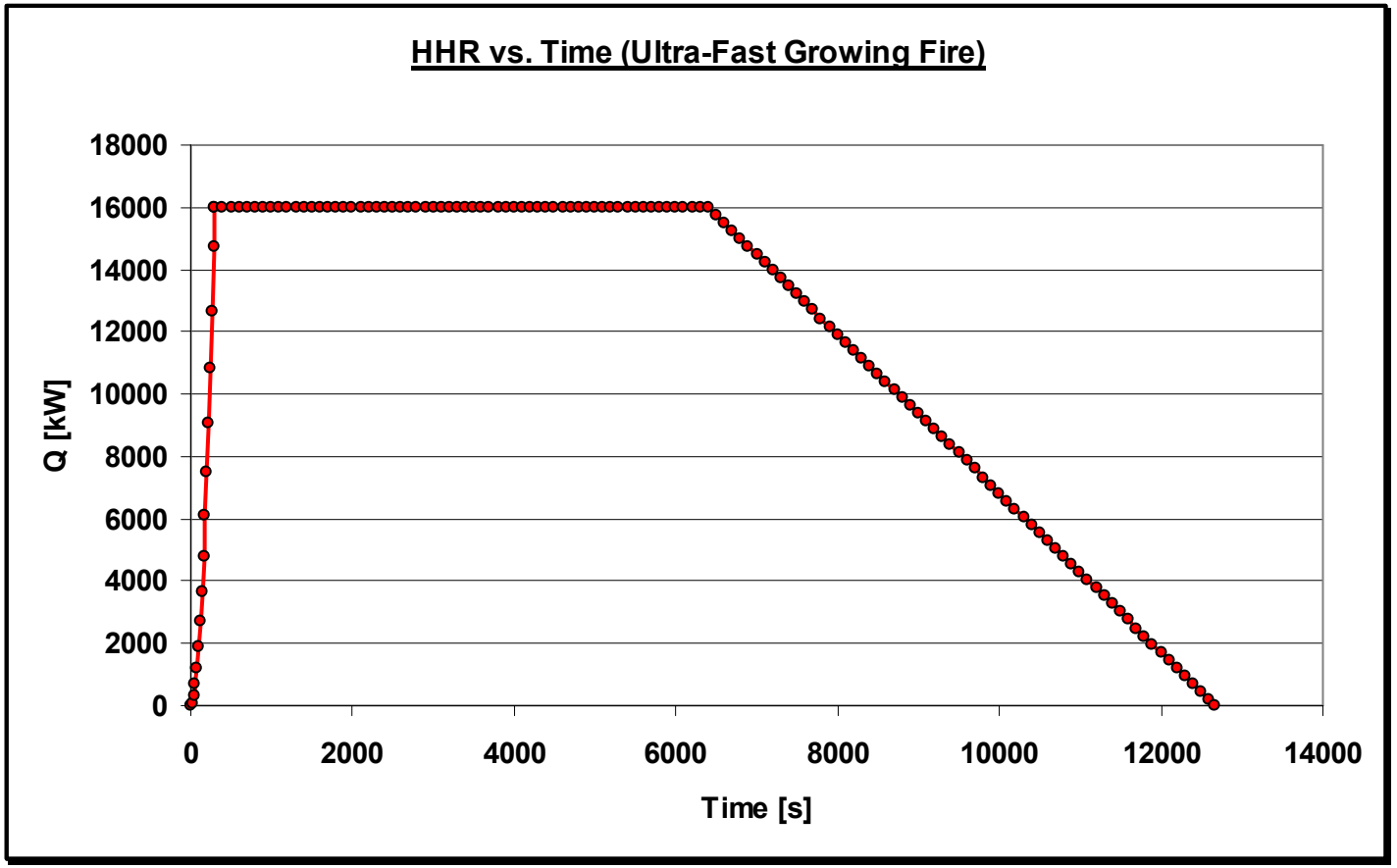

Figure 47: Heat Release Versus Time (Ultra-fast Growing Fire)

The Consolidated Fire and Smoke Transport Model (CFAST) from NIST was used to derive temperature history scenarios of the reconstructed fire based upon the heat release rate curves shown above and the geometry of a typical WTC 5 compartment. NIST has also developed the Fire Dynamics Simulator (FDS), which involves the use of computational fluid dynamics (CFD). The FDS software was not used because the longest feasible fire duration for a CFD model is about 1 hour, in terms of computational time; the reconstructed fire is expected to be about 4 hours. Moreover, FDS cannot be readily applied to post-flashover fires because of the excessive turbulence. CFAST can handle much longer fire exposure histories, and it provides reasonably accurate results except for the very early development of the fire (prior to the formation of two distinct gas layers). The effect of the very early fire development on the protected steel is negligible, thus the use of CFAST is logical. The fire within WTC 5 was also estimated to be fuel-controlled: a condition which CFAST handles very well.

In typical compartments, post-flashover fires are ventilation controlled. In the case of WTC 5, large holes in the roof of the western portion of the building were present during the fire exposure which allowed for smoke venting from the eastern portion (see Figure 48 below). Therefore, a fuel-controlled fire was simulated using CFAST by providing five flow vents from the compartment (see Figure 49 and Figure 50 below). The high ventilation conditions may provide the fire with an abundance of oxygen, but it also serves to vent heat from the upper gas layer from the compartment. Therefore, a fire that does not produce a very high peak temperature would be expected.

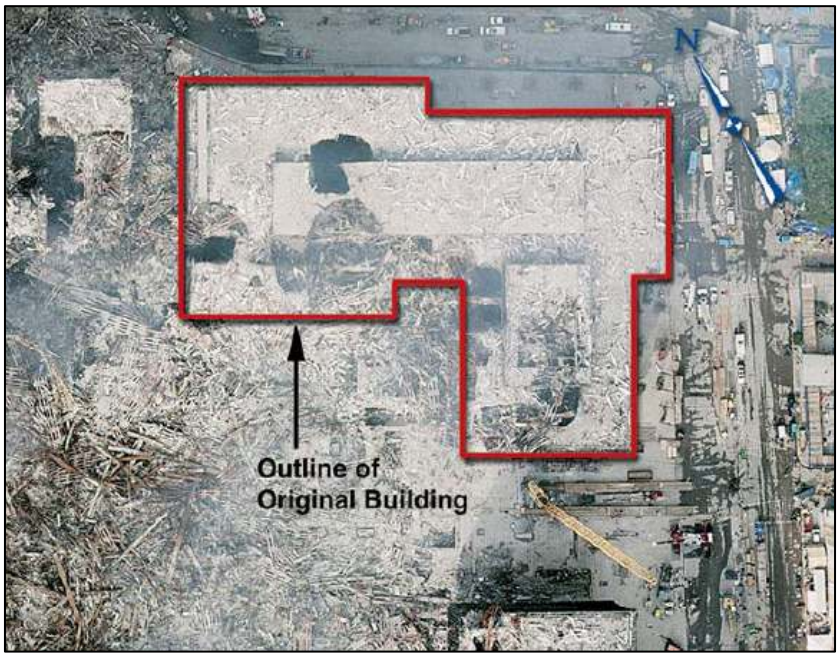

Figure 48: Roof Damage to WTC 5

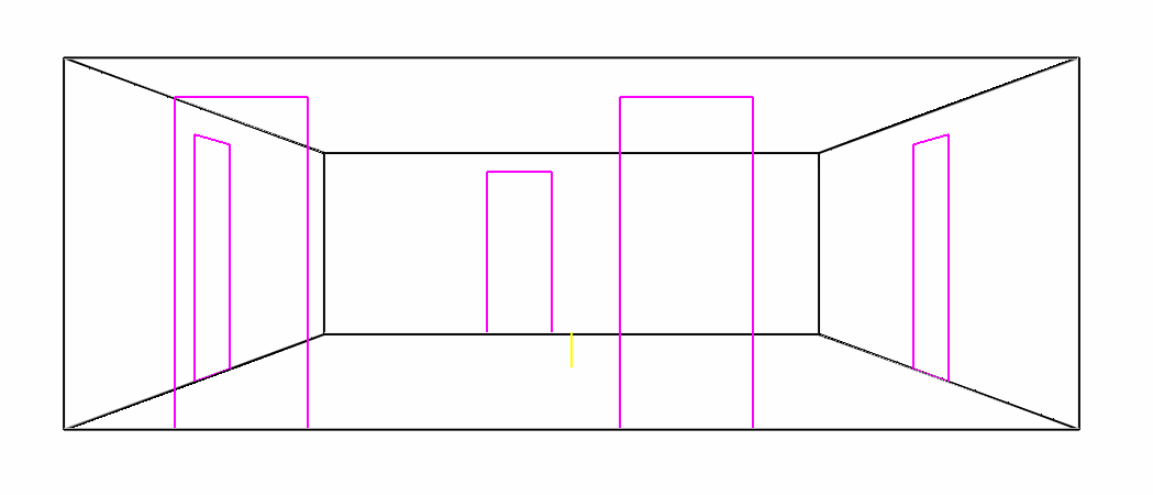

Figure 49: WTC 5 Compartment Model in CFAST (Elevation View)

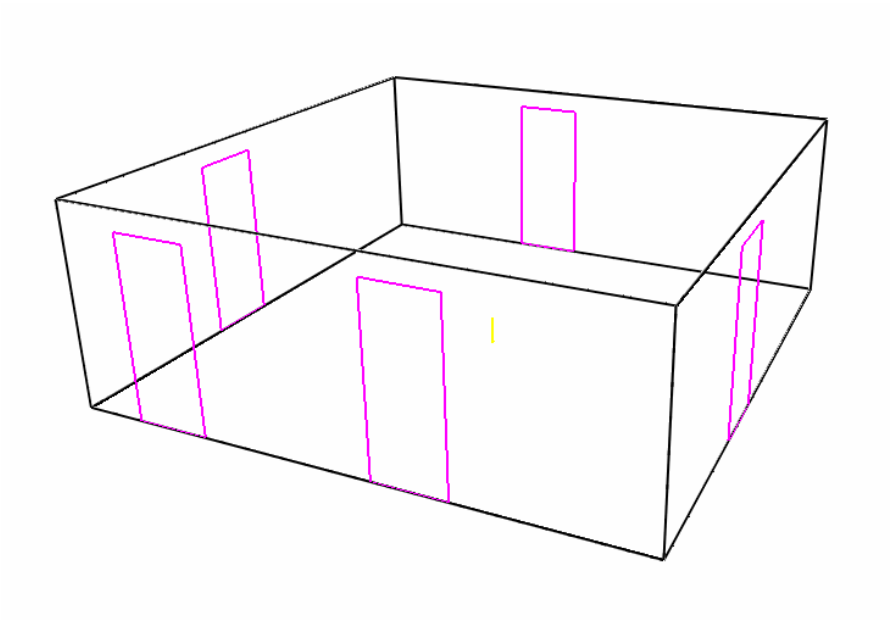

Figure 50: WTC 5 Compartment Model in CFAST (Isometric View)

The temperature histories of the medium, fast, and ultra-fast fire scenarios that were derived from CFAST are shown in Figure 51, Figure 52, and Figure 53, respectively. By comparing the heat release rate versus time plots from the results of CFAST to those manually inputted at the start of the simulation, it was confirmed that all three of the design fires are indeed fuel-controlled. More precisely, the heat release rate peaked at 16 MW for each of the design fires; the ventilation conditions did not affect the combustion process. Figure 54 below shows a comparison of the three temperature history scenarios of the reconstructed fire to that for the ASTM E-119 furnace test.

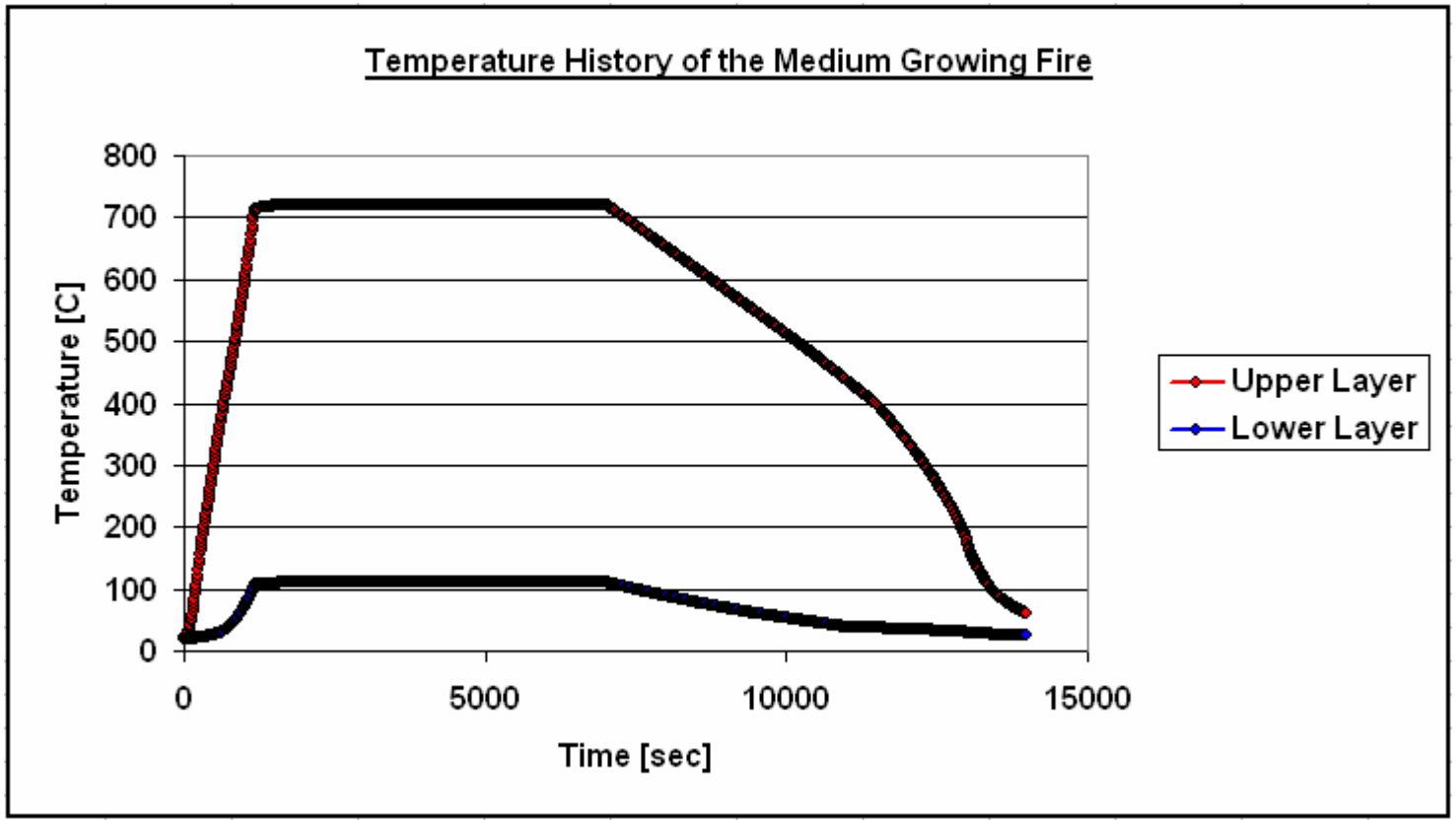

Figure 51: Temperature History of the Medium Growing Fire Scenario

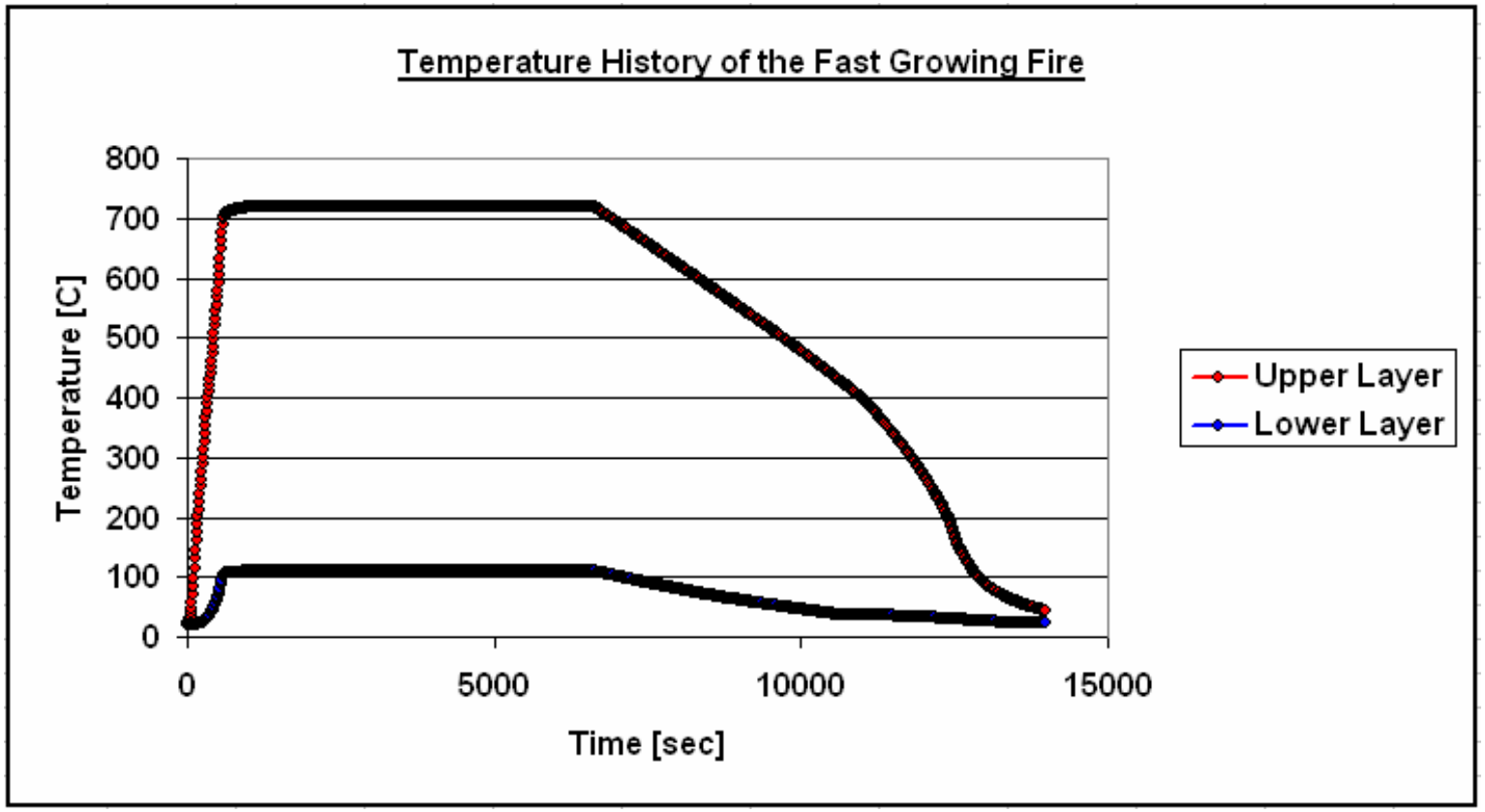

Figure 52: Temperature History of the Fast Growing Fire Scenario

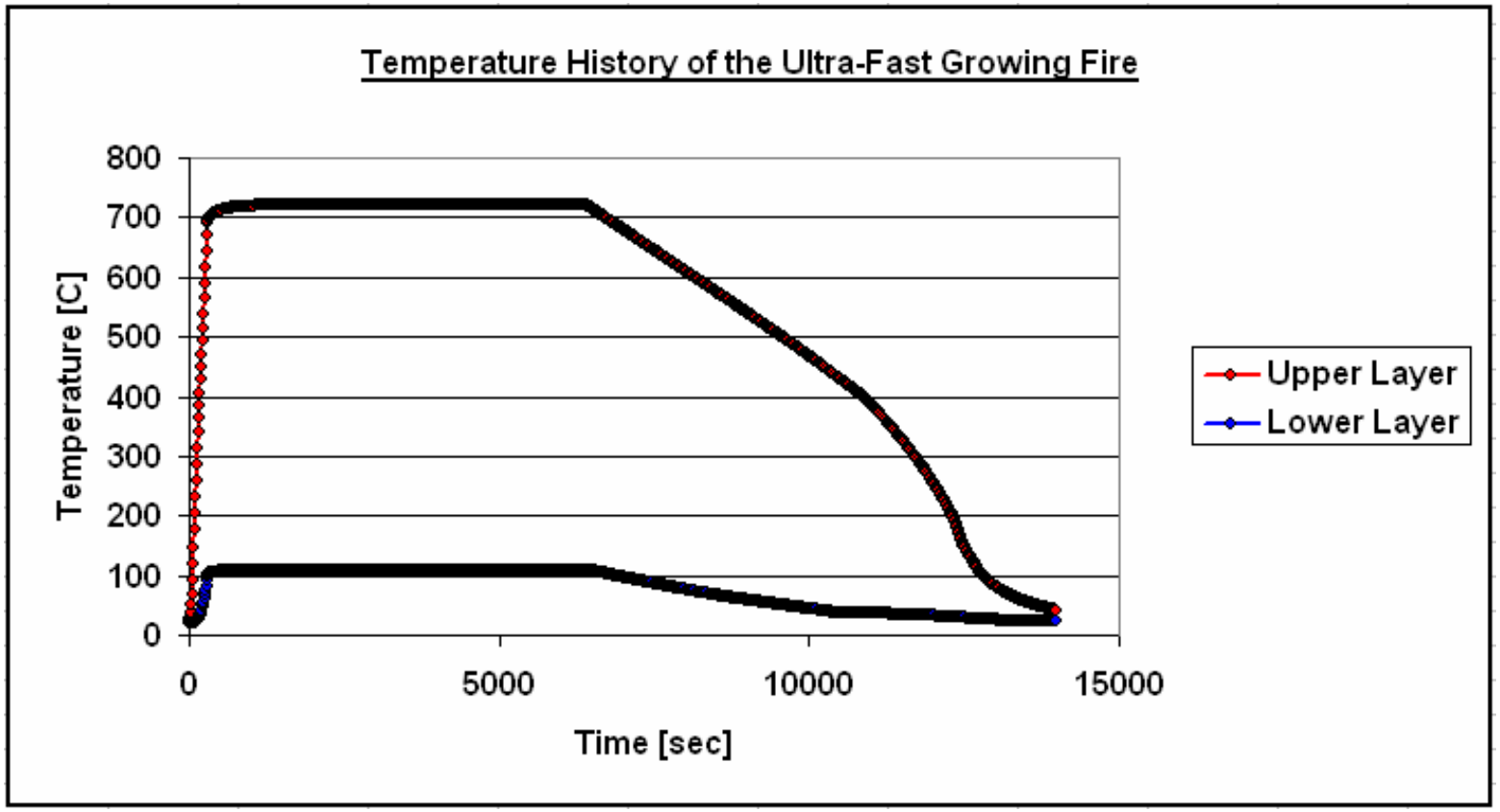

Figure 53: Temperature History of the Ultra-Fast Growing Fire Scenario

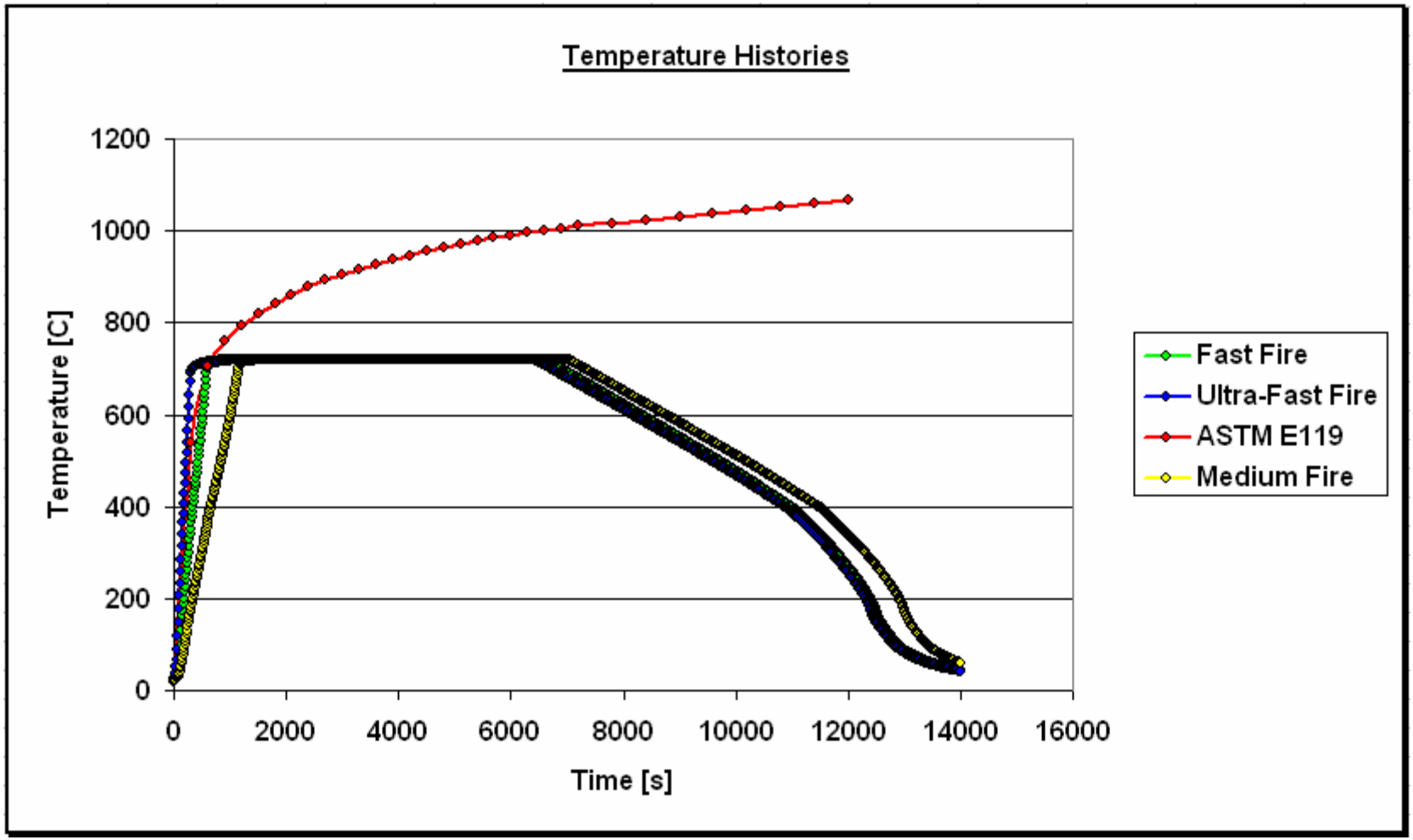

Figure 54: Comparison of the Temperature History Scenarios of the Reconstructed Fire

The most widely referenced time-temperature curves for real fire exposure are those of Magnusson and Thelandersson. These curves are derived from heat balance calculations for the burning rate of ventilation controlled fires. Figure 55 below shows the effect of varying the fuel load for a constant size of ventilation opening. It can be observed that these temperature history curves last about 4 hours and are relatively comparable to those derived for the reconstructed fire in WTC 5 (as shown in Figure 54 above). The fire in WTC 5 was fuel controlled, as opposed to ventilation controlled, thus the differences between the two curves is expected. It can therefore be stated that the reconstructed fire of WTC 5 is physically reasonable.

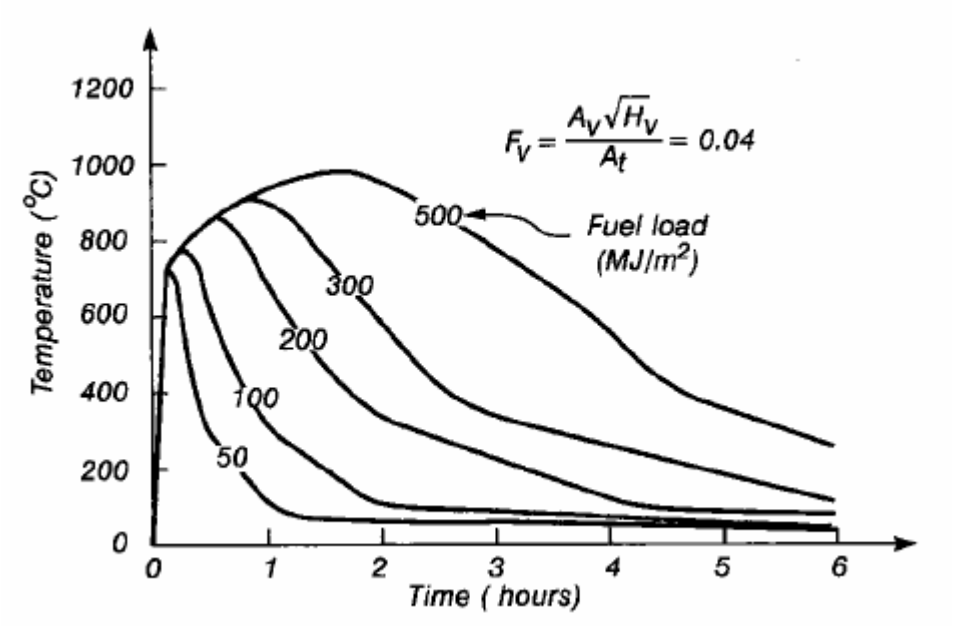

Figure 55: Time-Temperature Curves for Real Fire Exposure (EC1)

5 Finite Element Modeling Development

5.1 Nonlinear Temperature-Dependent Steel Properties

In order to model the shear connection assembly of WTC 5 accurately using ABAQUS, the nonlinear, temperature-dependent properties of A36 steel were determined. The strength of steel is best represented using a stress versus strain graph. At ambient temperature, the strength of steel can be divided into three distinct regimes: the elastic regime, the creep strain regime, and the strain hardening regime.

During the elastic regime, the stress on a test specimen can be increased up to the steel's inherent yield point without permanent deformation occurring. Once the yield point of the steel has been surpassed, the steel begins to undergo permanent deformation continuously under constant stress. After a significant amount of strain has occurred, the molecular structure of the steel begins to realign and the strain hardening regime begins, in which a gain in strength is realized. The strain hardening regime continues until the steel specimen completely ruptures.

Harmathy performed A36 steel strength tests at a wide range of elevated temperatures. The results of this work are shown in Figure 56 below. As this figure shows, most normal construction steels have very well-defined yield strength at normal temperatures, but this disappears at elevated temperatures. The 2005 NIST report concerning WTC 1 and 2 references this data from Harmathy. For added clarity, the results shown in Figure 56 are represented in Figure 57 below.

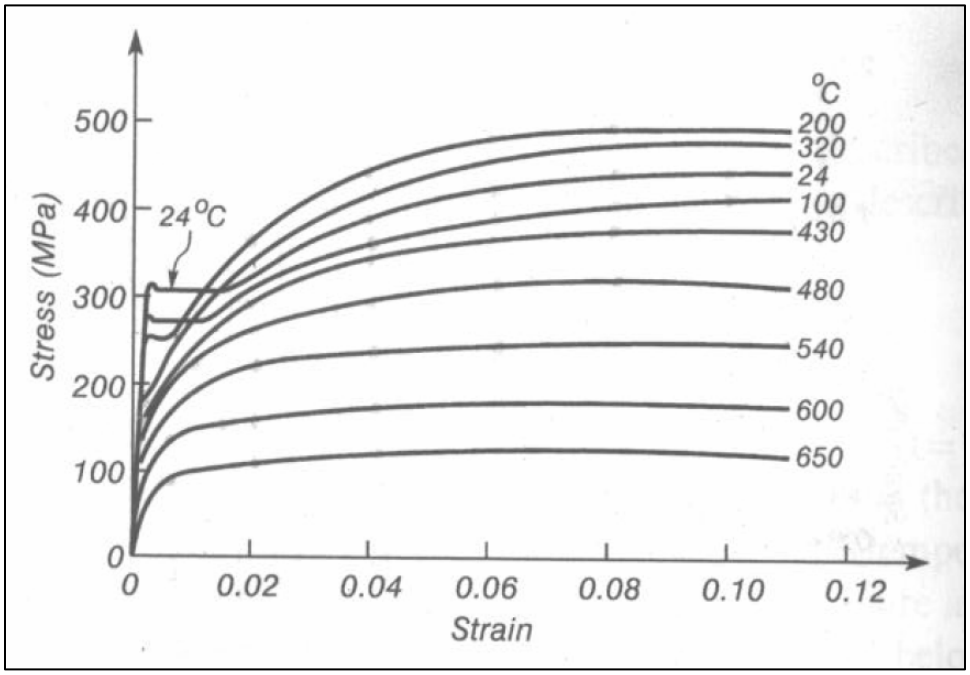

Figure 56: Stress-Strain Test Results (Harmathy)

The data represented in Figure 57 below can not be directly transferred to the ABAQUS model. ABAQUS only interprets steel strength properties represented as true stress and true plastic strain. The data points in Figure 57 below represent nominal stress and nominal total strain. Equations 4 through 6 were used to convert the data points from Figure 57 into true stress and true plastic strain.

$$\sigma_{true} = \sigma_{nom}\left(1 + \varepsilon_{nom}\right) \text{ (true stress)} \qquad (4)$$

$$\varepsilon_{true} = \ln\left(1 + \varepsilon_{nom}\right) \text{ (true strain)} \qquad (5)$$

$$\varepsilon_{true}^{pl} = \varepsilon_{true}^{total} - \varepsilon_{true}^{elastic} \text{ (true plastic strain)} \qquad (6)$$

Using the stress-strain curves shown in Figure 57 in conjunction with Equations 4 through 6, the nonlinear, temperature-dependent strength properties of A36 steel were accurately incorporated into ABAQUS.

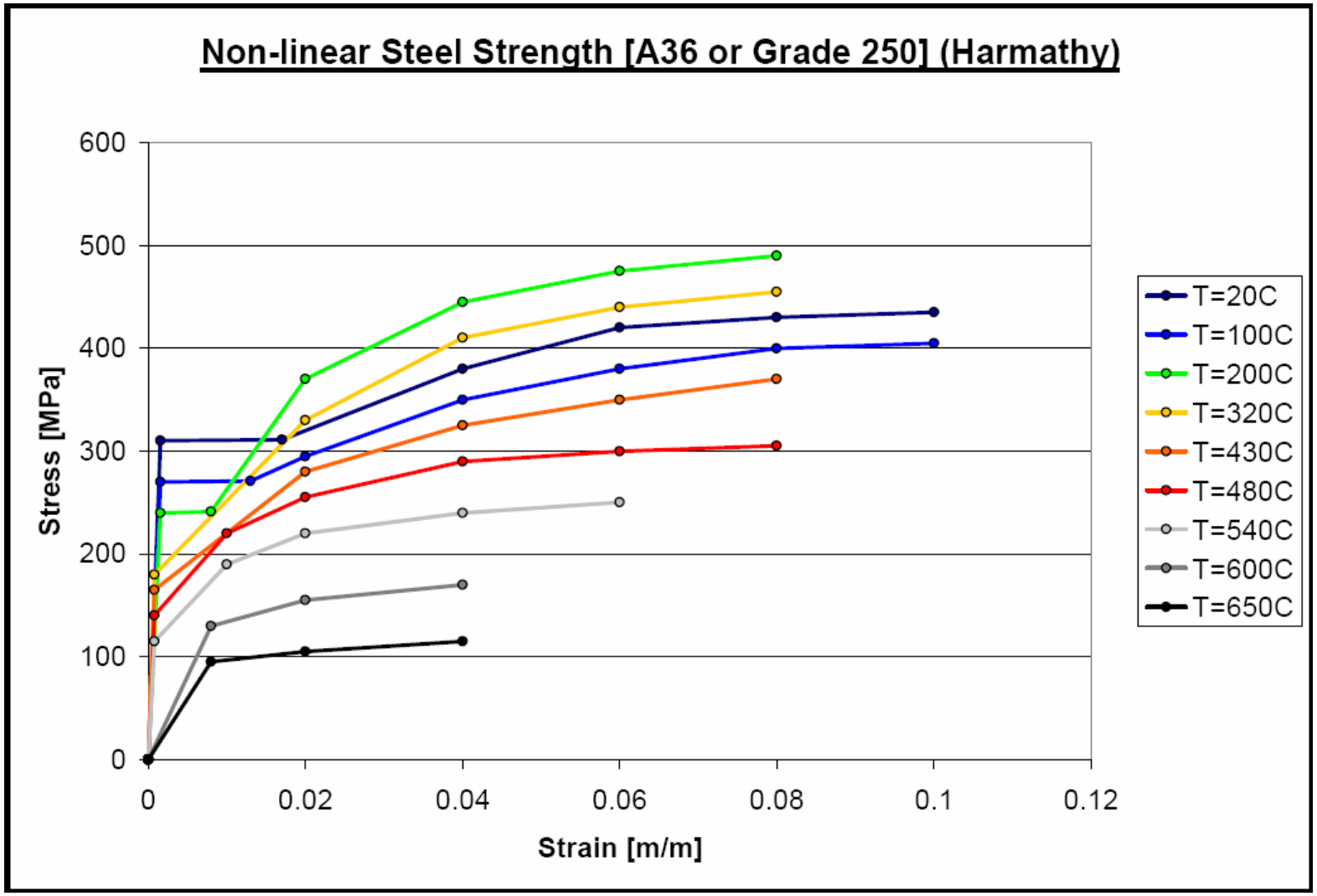

Figure 57: Nonlinear, Temperature-Dependent A36 Steel Strength Properties

In addition to the strength properties described above, the temperature-dependent thermal properties of A36 steel were also characterized. The density of steel is shown below and remains essentially constant with temperature.

$$\rho = 7850 \, {kg}/{m^3} \quad \text{(density of steel)}$$

The specific heat of steel is highly temperature-dependent and can be characterized using Equations 7 and 8 (Buchanan 176).

$$C_p = 425 + 0.773T - \left(1.69x10^{-3}\right)T^2 + \left(2.22x10^{-6}\right)T^3 \qquad (7) \qquad 20^o C \le T \le 600^o C$$

$$Cp = 666 + \frac{13002}{\left(738 - T\right)} \qquad (8) \qquad 600^o C \le T \le 735^o C$$

Using Equations 7 and 8, the specific heat can be derived for various steel temperatures (see Table 2 below). Table 2 below serves as input to the finite element software.

Table 2: Temperature-Dependent Specific Heat of Steel

Steel Temperature [ºC]	Specific Heat [J/(kg*K)]
20	440
100	488
200	530
300	565
400	606
500	667
600	760
700	1009

The conductivity of steel is also highly temperature-dependent and can be characterized using Equation 9 (177).

$$k = 54 - 0.0333T \qquad (9) \qquad 20^o C \le T \le 800^o C$$

Using Equation 9, the conductivity can be derived for various steel temperatures (see Table 3 below). Table 3 below serves as input to the finite element software.

Table 3: Temperature-Dependent Conductivity of Steel

Steel Temperature [ºC]	Conductivity [W/(m*K)]
20	53
100	51
200	47
300	44
400	41
500	37
600	34
700	31

The 2005 NIST report on WTC 1 and WTC 2 referenced Figure 58 below to derive the instantaneous coefficient of thermal expansion as a function of the temperature of the steel. Table 4 below presents the data in tabular form, which serves as input to the finite element software.

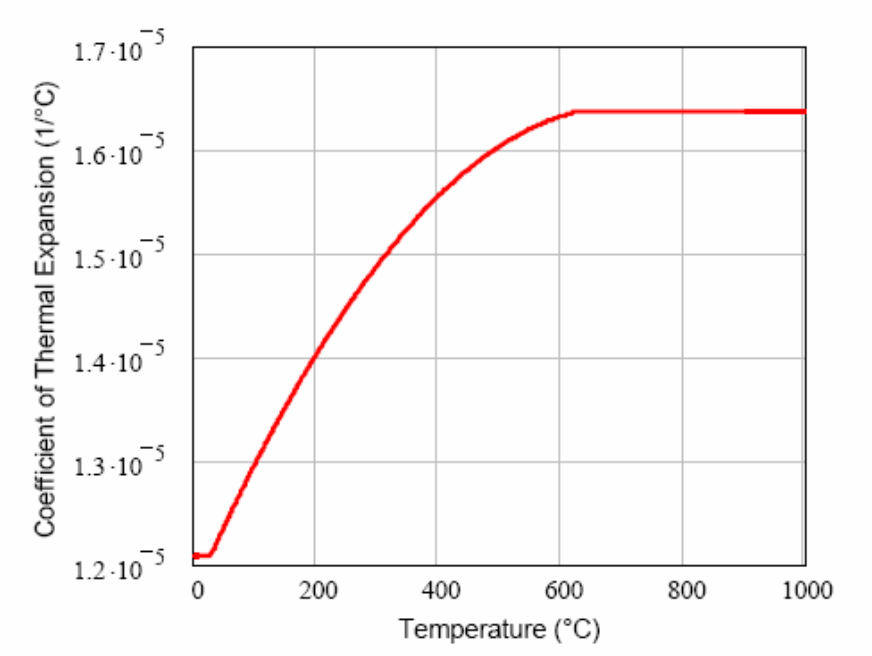

Figure 58: Temperature-Dependent Coefficient of Thermal Expansion

Table 4: Temperature-Dependent Coefficient of Thermal Expansion

Steel Temperature [ºC]	Expansion Coefficient [1/ ºC]
20	1.20x10^-5
100	1.30x10^-5
200	1.40x10^-5
300	1.50x10^-5
400	1.55x10^-5
500	1.60x10^-5
600	1.62x10^-5
700	1.63x10^-5

5.2 Failure Criterion for Web Rupture Failure

The WTC 5 connection failures not influenced by debris impact were due to shear rupture of the web portion of the beam stems. Figure 59 below is forensic evidence that demonstrates this shear rupture failure. This type of failure occurs when the bolts bear against the weak side (i.e., acting toward the free end of the member) of the bolt holes. Moreover, this bearing stress causes shear planes to form in the web steel. Finally, cracks along the shear planes cause catastrophic failure of the shear connection.

Figure 59: Web Tear Out of a Beam Stem Web from WTC 5

The goal of this project is to predict when the shear connections of WTC 5 experienced catastrophic failure as described above. In order to accomplish this goal, the time at which cracks along the shear planes begin to form must be derived. ABAQUS does not have the capabilities to predict the formation of cracks within a deformable body explicitly. Therefore, an indirect technique was derived to predict the time at which connection failure will occur.

The 3rd edition of the AISC Steel Manual (LRFD) provides an equation for ultimate shear strength of bolted connections (Equation 10). This equation yields the maximum tensile force at failure due to web tear out (shear rupture) of a bolted connection. Equation 10 has been determined from extensive experimental research of bolted connections. The stress intensity factor (1.2) is an empirical coefficient that accounts for the tensile resistance of steel surrounding the bolt hole. In typical design practice, a safety factor of 0.75 would be multiplied by Equation 10 to derive a conservative limiting load value.

$$R_{failure} = 1.2 L_c t_w F_u \qquad (10)$$

L_c = clear distance, in the direction of load, between the edge of the hole and the edge of the material [in]

t_w = thickness of the web of the beam [in]

F_u = ultimate strength of the material [ksi]

If Equation 10 is used without a safety factor, the load at failure can be derived for a simple case. A one-bolt model was created in ABAQUS to resemble to the shear connections of WTC 5 in a small-scale form (see Figure 60 below). This simple connection has the same clear distance, web thickness, and steel ultimate strength as the shear connections in WTC 5. The load required to cause shear rupture failure of the simple connection model was calculated as shown below.

$$R_{failure} = (1.2)(01.03125in)(0.4375in)(58ksi)$$
$$R_{failure} = 31.4kips$$

The failure criterion determination model has two distinct parts: a steel section and a high-strength (A325) bolt. These two parts are composed of 3D stress, linear, hexahedral, reduced-integration (C3D8R) elements. A36 and A325 steels are used for the steel section and bolt, respectively. The A36 steel has strength properties as defined in Section 5.1; the yield and ultimate strengths for the A325 steel were also specified. The assembly is composed of four instances: three steel sections and a bolt. 12 surfaces were defined for use with contact interactions. The analysis is composed of three steps: Contact, Pretension, and Load. The Contact and Pretension steps apply 1% and 100% of the required bolt pretension force, respectively. Figure 62 shows the application of the pretension force to the bolt. The Load step applies 100% of the failure load (31.4 kips) to the connection assembly.

Seven contact interactions which are assumed to be frictionless (e.g., contact between the steel plates) were specified. This is a reasonable assumption because at failure the bolts would be fully in bearing. Furthermore, at elevated temperatures (when failure would have occurred), thermal expansion of the bolts would most likely render friction to be negligible. However, in the final thermal-stress model, friction will be accounted for in order to capture pre-failure behaviors accurately. In terms of its application to the thermal-stress model, it is conservative to assume that this failure criterion determination model is frictionless, for it will yield the highest possible strain for the given failure load.

The failure criterion determination model has three boundary conditions which include a fixed end constraint and two conditions to constrain the steel sections and bolt during the

Contact and Pretension steps. A full analysis was performed on a single-processor of a Sunfire X4100 machine with a FP rating of 117 and 4 GB of RAM. The memory policy of the job run was set to the default (moderate). The job took approximately 3 hours to complete. Figure 63 below shows the stress distribution of the shear connection as a result of the pretension force in the bolt. Figure 64, Figure 65, and Figure 66 show the stress distribution, equivalent strain, and shear stress at failure, respectively.

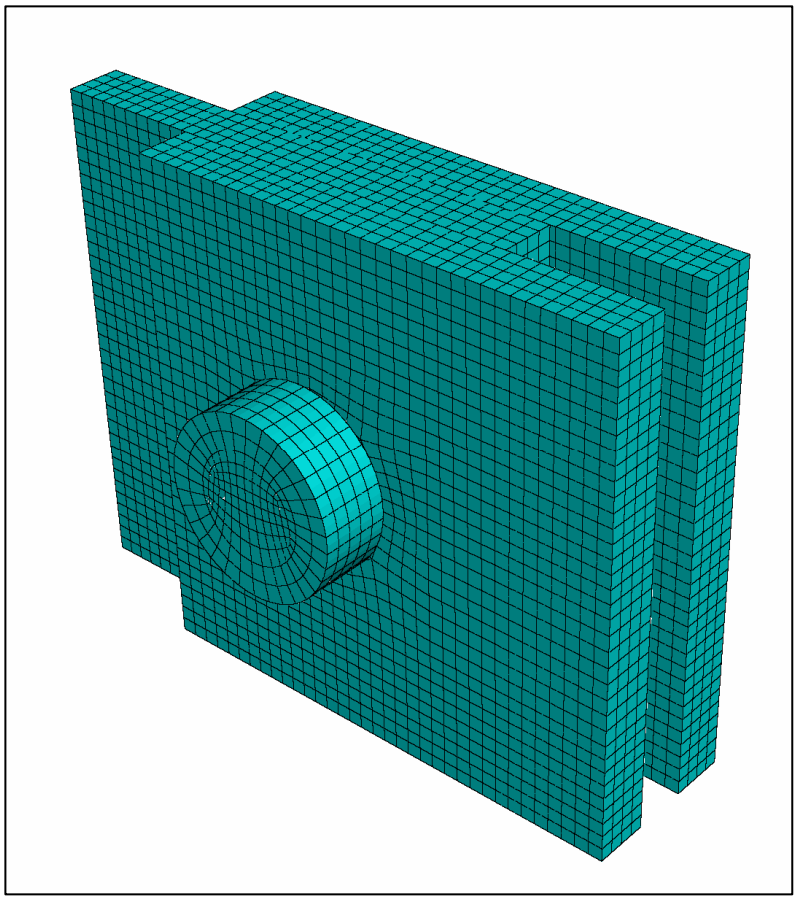

Figure 60: Failure Criterion Determination Model Mesh

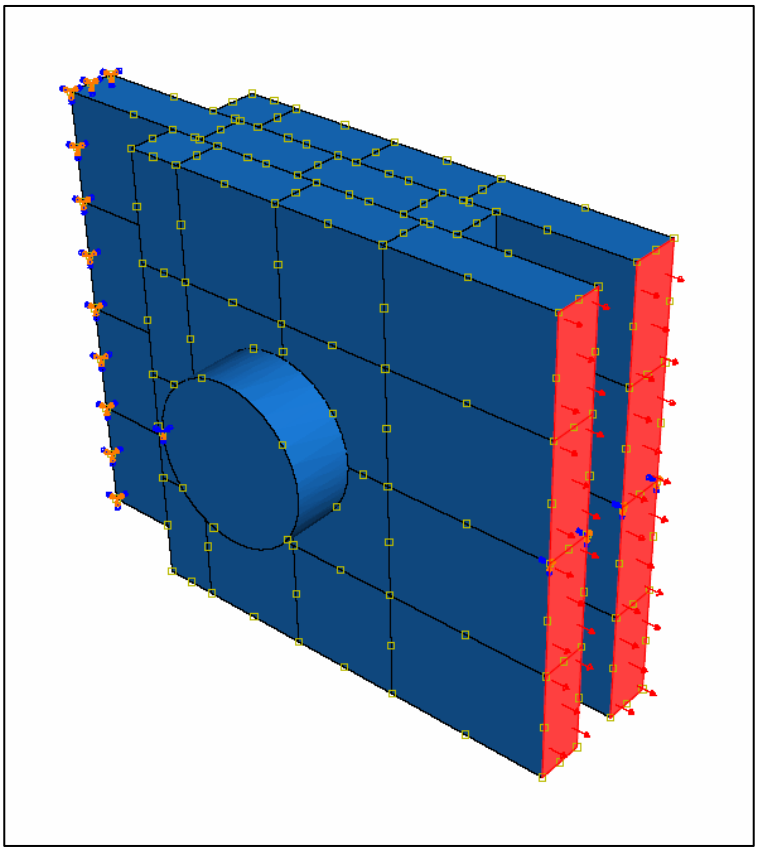

Figure 61: Failure Load Application

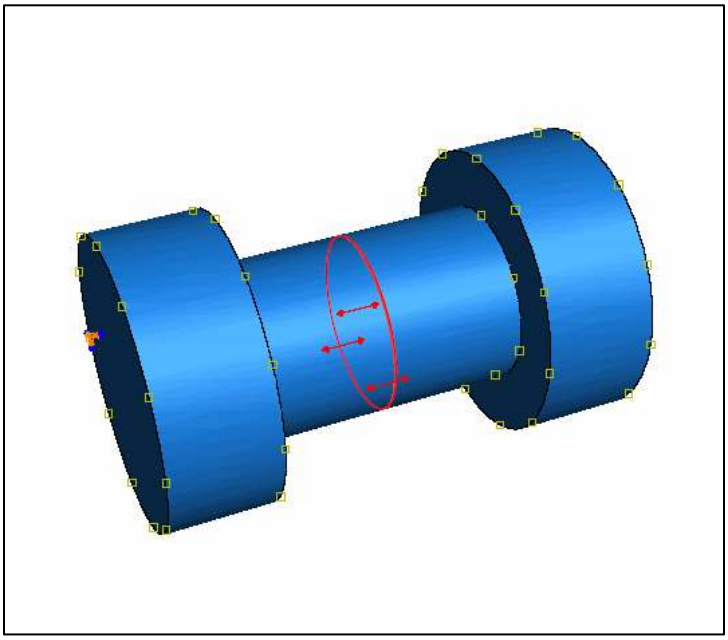

Figure 62: Bolt Pretension Force Application

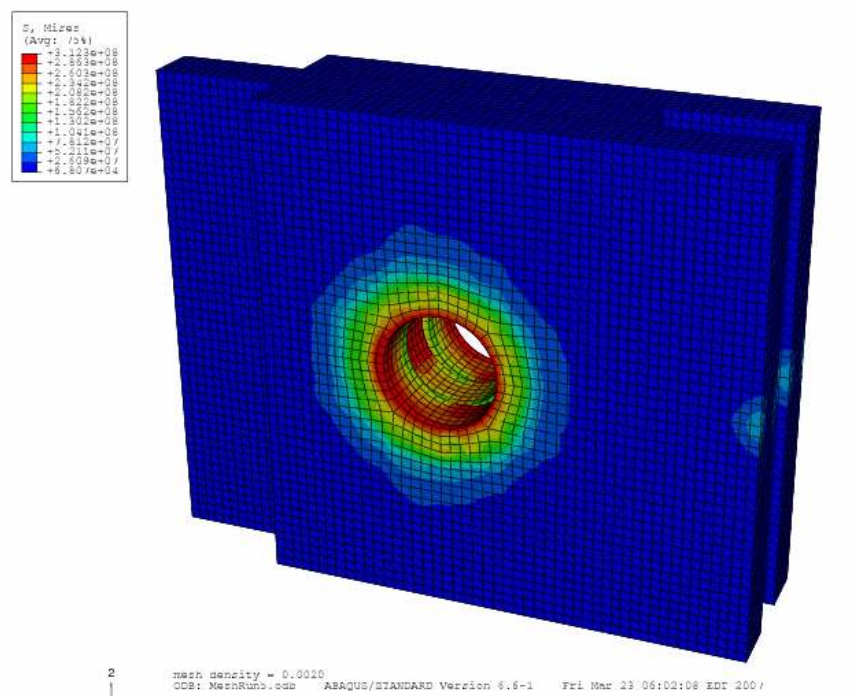

Figure 63: Stress Distribution Caused by Bolt Pretension

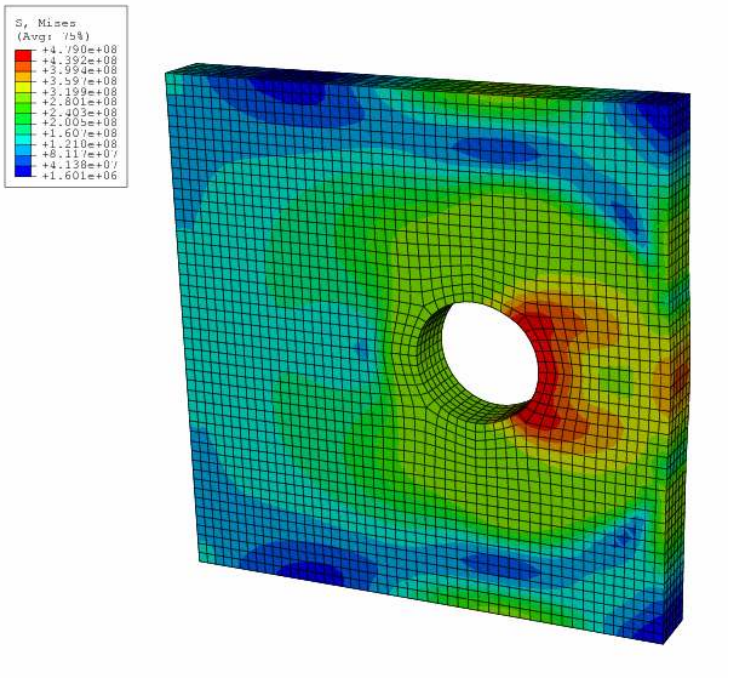

Figure 64: Stress Distribution (Failure Load Application)

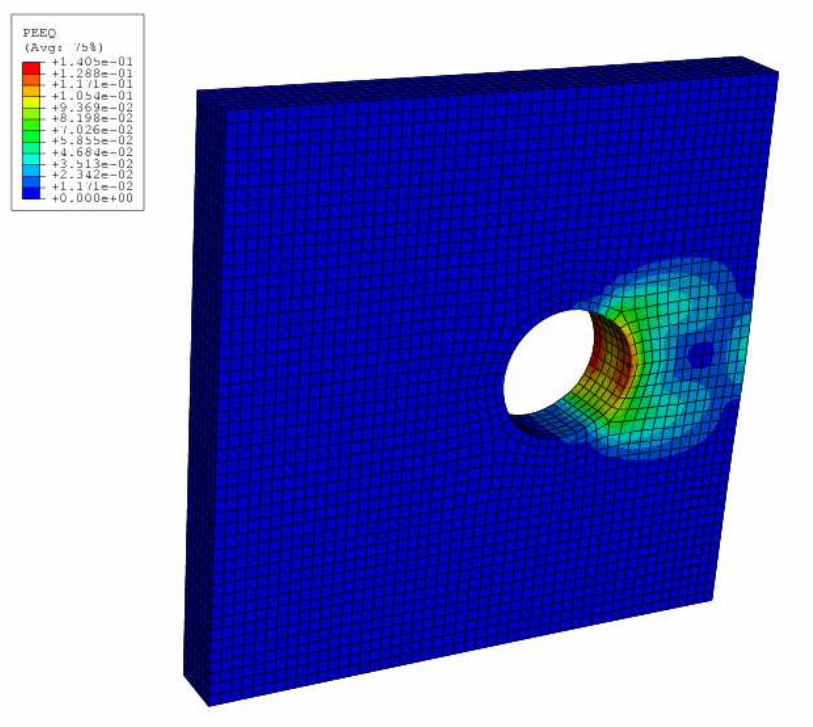

Figure 65: Equivalent Strain Distribution (Failure Load Application)

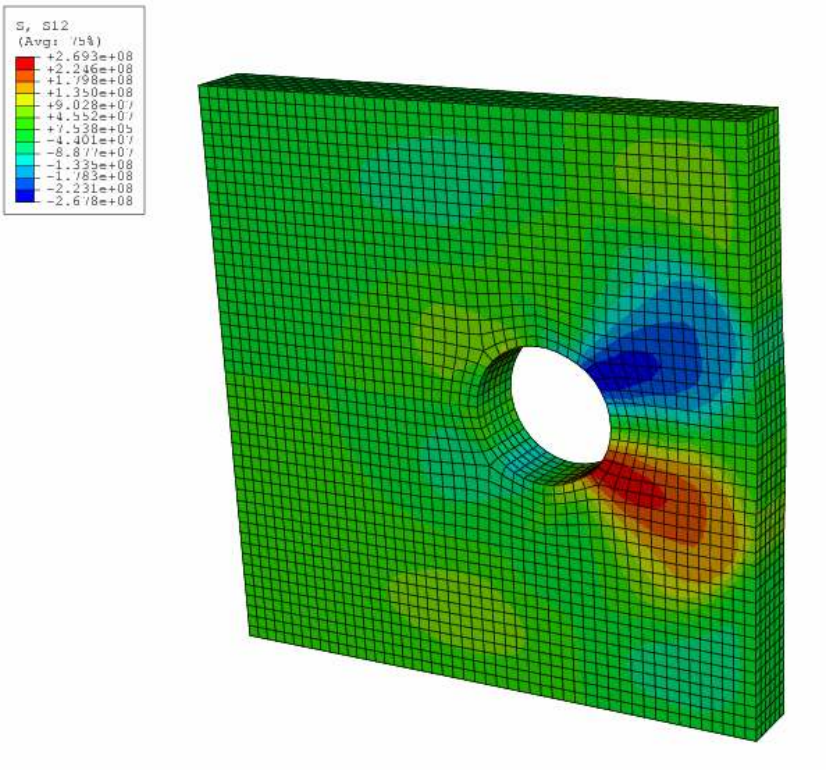

Figure 66: Shear Stress Distribution (Failure Load Application)

The stress distribution in the vicinity of the bolt hole is not helpful in the determination of failure of the steel at elevated temperatures. As steel heats up, its strength and rigidity are constantly changing in three-dimensional space and time. Under constant loading, steel at a higher temperature is expected to have lower stresses, yet higher deformation. This is because steel, as it weakens under the influence of elevated temperatures, also softens: it does not need as much stress to deform permanently. Therefore, it is not feasible to use the stress distribution as the criterion for failure, for it would require constant iteration in space and time.

It is the opinion of various structural engineering professionals at Simpson Gumpertz & Heger Inc. (SGH) that the plastic shear strain in the vicinity of the bolt hole is the best indicator of shear rupture failure at elevated temperatures. Strain can be assessed consistently at elevated temperatures, and forensic evidence suggests that shear was the mode of failure in WTC 5.

Shear strain is the deformation of a solid body in which a plane in the body is displaced parallel to itself relative to parallel planes in the body. Quantitatively, shear strain is the displacement of any plane relative to a second plane divided by the perpendicular distance between the planes. Therefore, by applying the failure load, the shear strain at failure can be derived and used as the main criterion for catastrophic shear rupture failure in the final thermal-stress model of WTC 5.

The shear strain of the steel in the vicinity of the bolt hole was observed under the failure loading (see Figure 67 below). Furthermore, a mesh refinement analysis was conducted in order to ensure that the result is mesh-independent. Table 5 below summarizes the mesh refinement analysis and shows that the failure criterion for the WTC 5 thermal-stress model is a shear strain of approximately 0.16 (or 16%) at the weak side of a bolt hole.

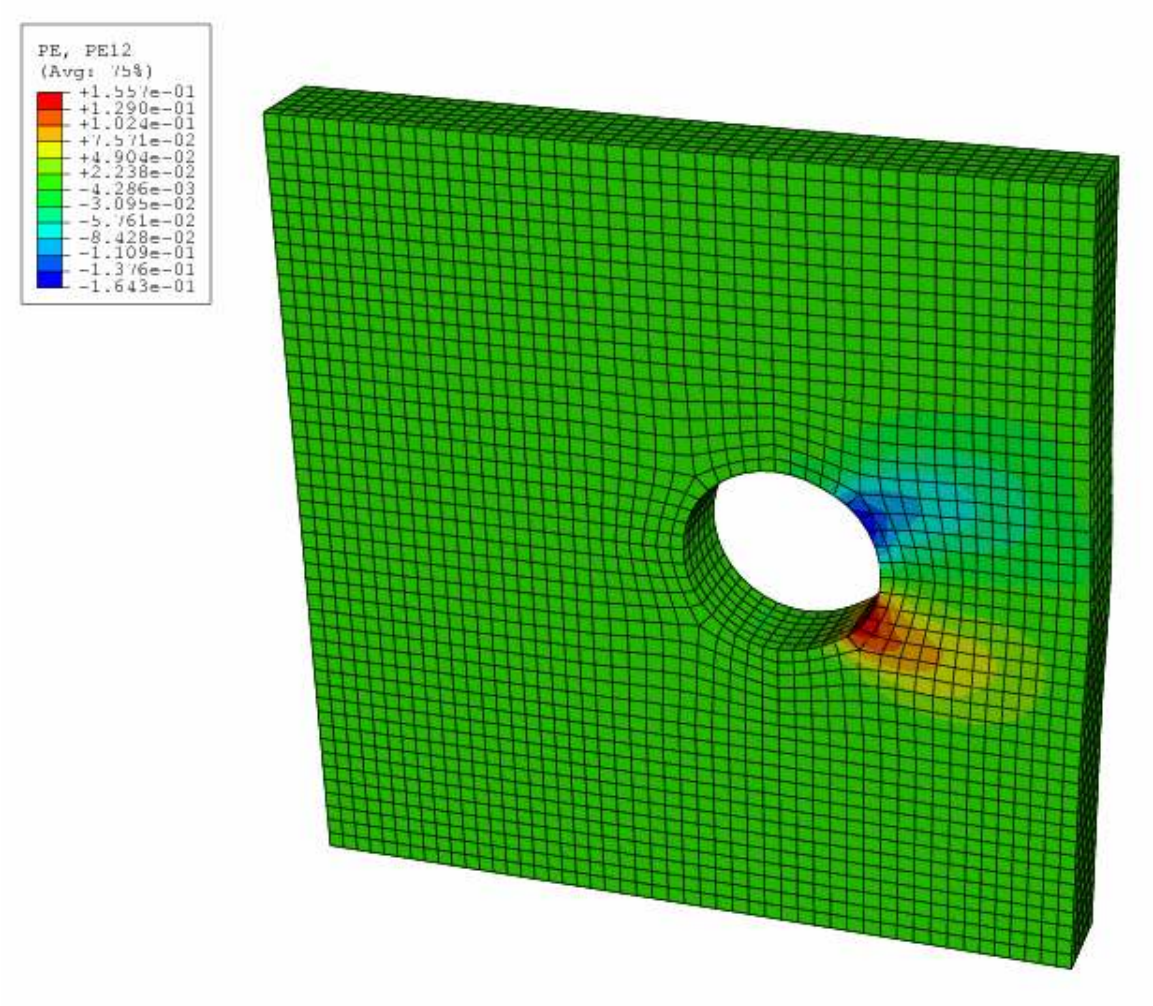

Figure 67: Shear Strain Distribution (Failure Load Application)

Table 5: Mesh Refinement Analysis (Failure Criterion Model)

Number of Hexahedral Mesh Elements	Maximum Shear Strain (PE12)
5,146	0.093
8,626	0.126
15,748	0.145
21,700	0.156
44,140	0.156

$$PE12_{failure} = 0.156$$

5.3 Development of the Mechanical Model

ABAQUS was used to create a mechanical model that encompasses the stress behavior of the four structural bays of interest on the 8th floor (initial region of collapse). Unlike the thermal model (see Section 5.4 below), the floor beams are not included because their stress behavior is not a concern for this project; they are required in the thermal model to account for their heat transfer influence on the floor girders. Moreover, the modeling of connections between the floor beams and the floor girders is not in the scope of this project. The mechanical model shall serve as the foundation for the final model: a sequentially-coupled, thermal-stress analysis of the four structural bays of interest.

The mechanical model consists of 10 separate parts in ABAQUS. Some of these parts are referenced multiple times as assembly instances. Each part utilizes hexahedral, structured, linear, 3D stress elements for its meshing. The fine mesh parts use reduced integration elements (C3D8R) and the intermediate and coarse mesh parts use incompatible mode elements (C3D8I). The incompatible modes elements prevent "hour-glassing" (i.e., added stiffness due to bending effects). If incompatible mode elements are not used, the software will enforce hour-glassing controls, which detract energy from realistic plasticity of the material under stress. Table 6 below summarizes the number of elements used to mesh each part. The regions of most interest are in the vicinity of the bolt holes; these areas utilize the finest meshes in the model in order to derive very accurate results in these regions.

Table 6: Number of Elements Used for Each Model Part (Meshing)

Model Part	Number of Elements
Beam Stem (Fine Mesh Section)	16,626
Beam Stem (Intermediate Mesh Section)	198
Beam Stem (Coarse Mesh Section)	244
Bolt	964
Column	304
Shear Tab	2,688
Steel Shim	2,184
Floor Girder (Fine Mesh Section)	14,706
Floor Girder (Intermediate Mesh Section)	168
Floor Girder (Coarse Mesh Section)	800
Total:	**38,882**

The mechanical model contains two types of steel: A36 and A325. The A36 steel is assigned to every part except the high-strength bolts, which is composed of A325 steel. Forensic evidence proves that the bolts themselves did not fail, but rather the beam stem web, which is composed of A36 steel. Therefore, only the A36 steel was assigned the temperature-dependent strength properties as described in Section 5.1. The density of both types of steel is 7850 [kg/(m^3)] and their Poisson's ratio is 0.32. The A325 steel has a modulus of elasticity of 29,000 ksi and yield strength of 325 ksi.

The mechanical model is composed of 17 assembly instances and 52 defined surfaces. According to the specifications of WTC 5, the bolts were installed with 39 kips of pretension. It should be noted that North American practice prior to 1985 required all high-strength bolts to provide pretension, regardless of whether it was needed.

The analysis of the model is divided into three steps: Contact, Pretension, and Load. The Contact step applies 1% of the bolt pretension load and the Pretension applies 100% of the pretension load. The Load step applies the gravity load to the top of the structural assembly. For each step, the Full Newton (Direct) solution technique is utilized.

The gravity load was derived by referencing the 1970 New York City Building Code and accounting for the self-weight of the assembly (including the concrete slab which is not explicitly modeled). The self-weight of the assembly is as follows: 4 in. thick lightweight concrete slab: 38.3 psf; W18X50 girder: 50 plf. The building code specifies the live loads as follows: office load: 50 psf; partition load: 15 psf. No safety factors were used in the calculations to account for the fact that the live load during a fire situation is lower than when the structure is in service. More precisely, the live load from occupants is not present during a fire, but all other office materials (e.g., desks) remain in place. The Eurocode specifies a 10% reduction in live load from that calculated for design. The tributary area of the beam stem and floor girder span is shown in Figure 68 below.

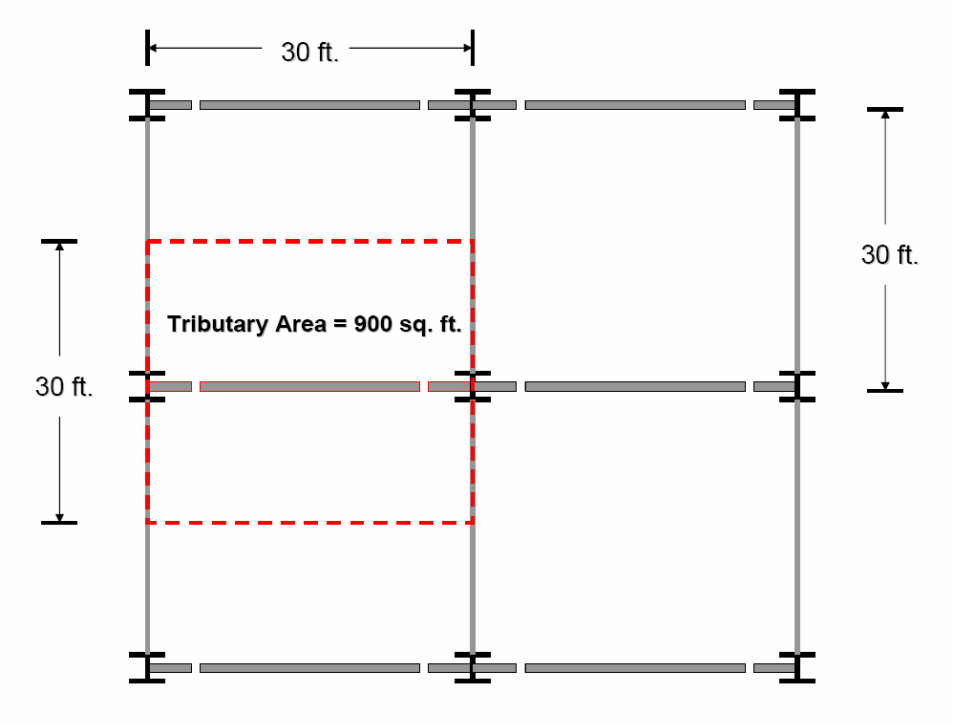

Figure 68: Tributary Area of the Beam Stem/Girder Span

The total resultant load acting on the tributary area is calculated as follows:

$$P = \left[(50\,psf + 15\,psf + 38.3\,psf)(900\,ft^2)\right] + \left[(50\,plf)(30\,ft)\right] = 94470\,lbs$$

The load calculated above would translate into a distributed load across the span of the beam stems and floor girder of about 3 kips per foot, which is reasonable. The total surface area of the tops of the beam stems and the floor girder may be calculated as follows:

$$A = 2\left[(48in)(7in)\right] + \left[(264in)(7.5in)\right] = 2652in^2$$

Therefore, the pressure load that should be specified in the software is as follows:

$$\text{Service Load (Pressure)} = {}^{94470\,lbs}\!\!\diagup\!\!_{2652\,in^2} = 35.6\,psi \;\; (245453 \text{ Pa})$$

The mechanical model relies upon 35 contact interactions to reconstruct the behavior of the assembly under loading. Hard contact is used with automatic adjustment for overclosures (i.e., unrealistic penetration of surfaces). Moreover, automatic stabilization via viscous damping is set during the Contact step for every interaction involving contact within each of the bolt holes. Static-kinetic exponential decay friction is specified (tangential behavior) for each of the contact interactions. The coefficients of friction were specified as follows: static coefficient: 0.15; kinetic coefficient: 0.08; and decay coefficient: 0.1. These values are typical for untreated steel at the interface between bolts and the clamped surface. The exact values of the friction coefficients are not critical for this model because the shear connections of WTC 5 were most likely in bearing at the time the bolts were tightened due to the dead load of the assembly. Moreover, once the bolts have slipped due to thermal expansion prior to failure, the frictional resistance becomes negligible.

Seven constraints using the Tie feature are used in the model to fuse various instances together. For example, a constraint was used to represent the full-penetration shop weld connecting the beam stem to the column. As mentioned, a pretension force of 39 kips is applied to each of the six bolts in the model. The model utilizes 8 boundary conditions to achieve realistic behavior. The floor girders are prevented from undergoing lateral torsional buckling because the WTC 5 assembly included shear studs that prevented this failure mode (plus the floor beams added to the buckling resistance).

Symmetry conditions were specified at the symmetry lines of the column and floor girder to capture multi-bay behavior in the model. The column is assumed to be pin-ended; applicable boundary conditions were used. Lastly, the floor girder, shear tabs, and bolts were constrained during the Contact and Pretension steps to simulate stability during its construction.

A single predefined field that encompasses the entire assembly was used to specify the initial temperature of the steel. The mechanical model was tested at ambient conditions to

ensure the model behaves realistically. The behavior of any steel assembly under ambient, service conditions is well understood and easily discernable from experience. A full analysis was performed on a single-processor of a Sunfire X4100 machine with a FP rating of 117 and 4 GB of RAM. The memory policy of the job run was set to the default (moderate). The job took approximately 7 hours to complete.

Figure 69 below shows a contour representation of the deflection of the floor girder under the gravity loading. The maximum deflection is 0.87 in., which makes physical sense. The deflection of a beam is typically the governing factor in a common structural design. The structural engineer usually selects a beam size that limits the maximum deflection to (1/360) of its span. If the floor girder can be assumed to be pin-ended at the beam stem connections, then the maximum allowable deflection according to structural engineering standards is 22 ft. (264 in.) divided by 360, or 0.73 in. It makes sense that the software predicts a slightly larger deflection since the bolts were not positioned at the bottom of the bolt holes at the start of the analysis. In other words, the gravity loading caused the bolts (and thus the floor girder) to translate (rigid body motion) downward slightly.

Figure 70 and Figure 71 below show the stress distribution in the vicinity of the shear connection. The upper limit (red) of the contour plot was set to the ultimate strength of the A36 steel (58 ksi). Figure 72 below shows a plot of the equivalent strain; no permanent deformation is observed. This makes physical sense, for permanent deformation would not be expected under ambient conditions. It can be concluded that the mechanical model represents the structural behavior of the assembly accurately under ambient conditions. Therefore, this model will serve as a proper foundation for the sequentially-coupled, thermal-stress model.

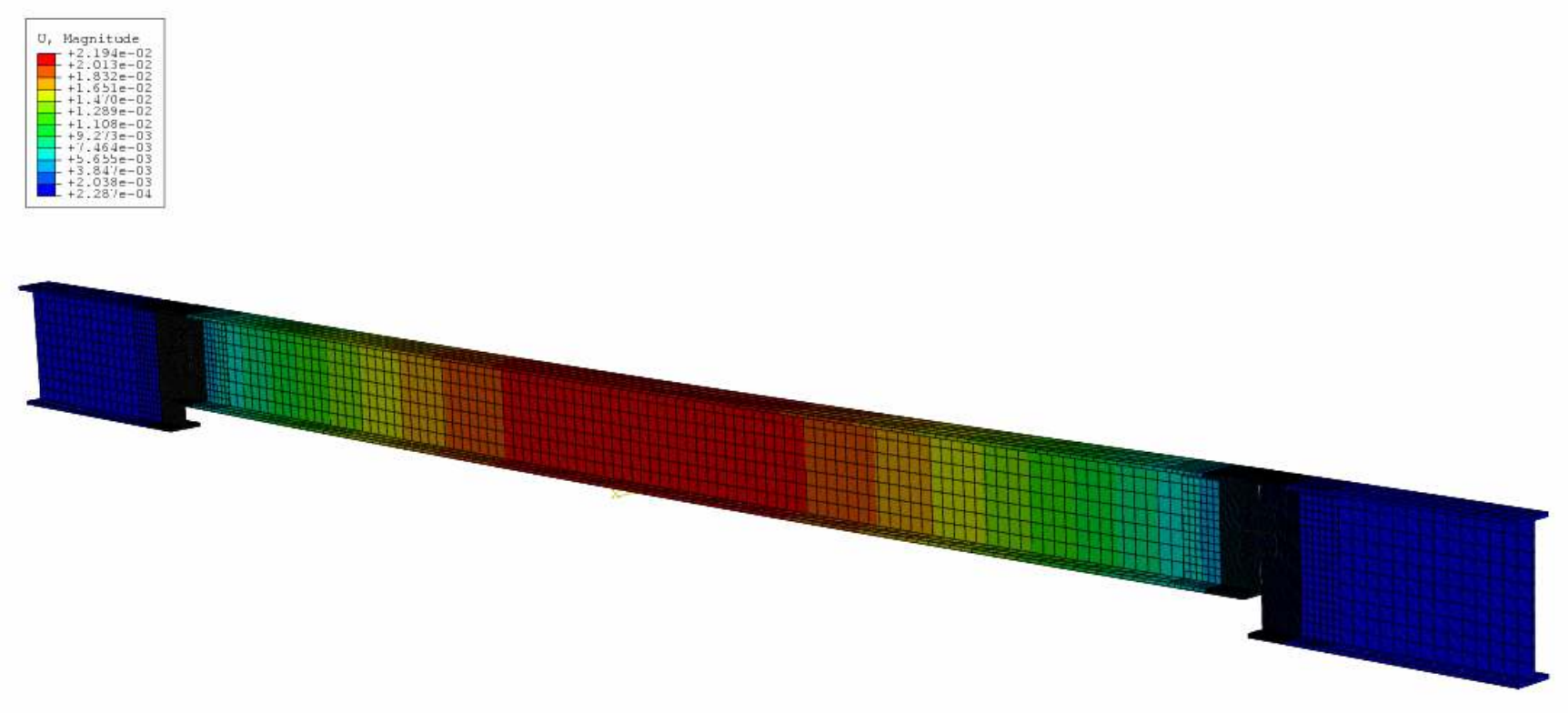

Figure 69: Deflection of the Floor Girder

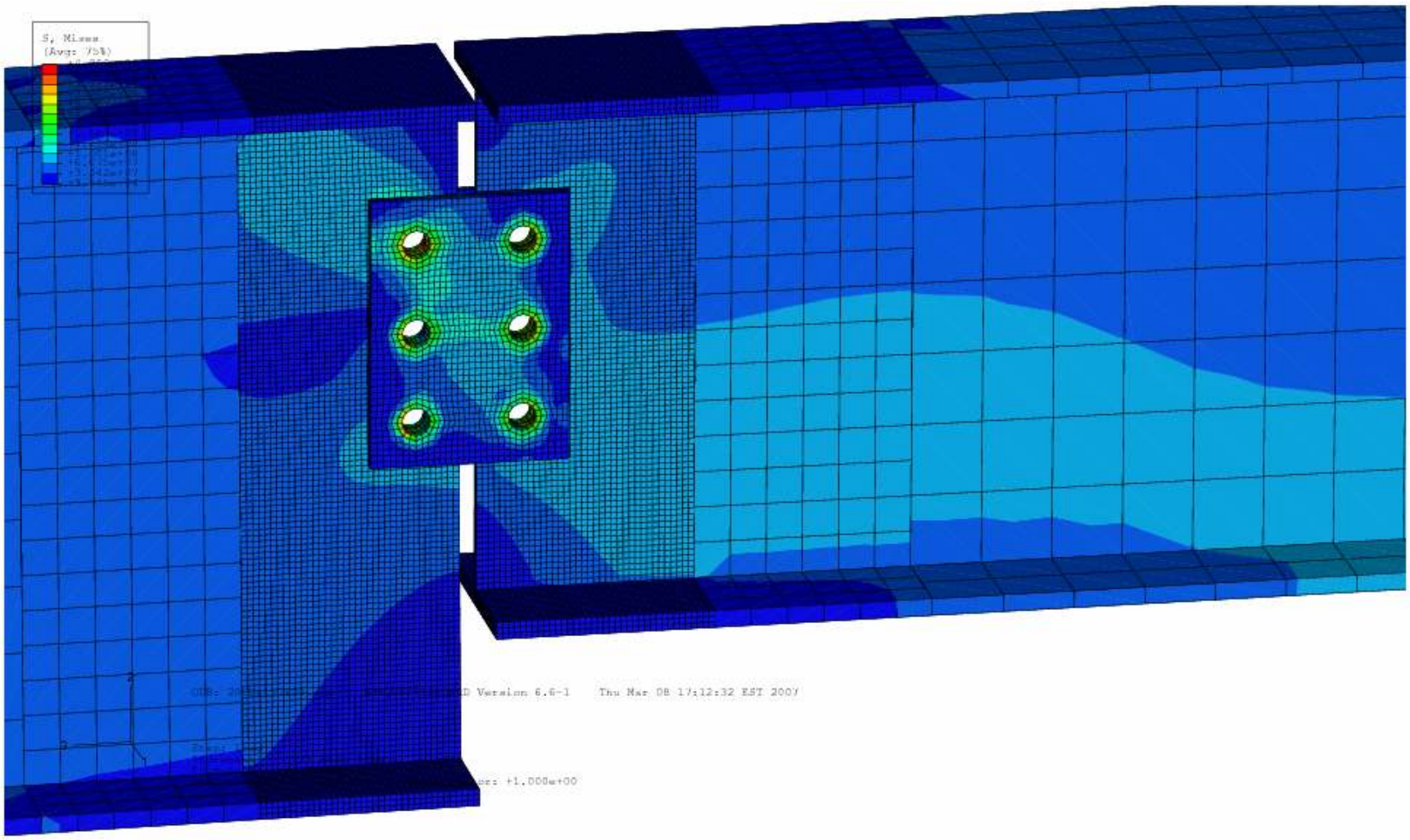

Figure 70: Von Mises Stress Distribution (Shear Tabs Included)

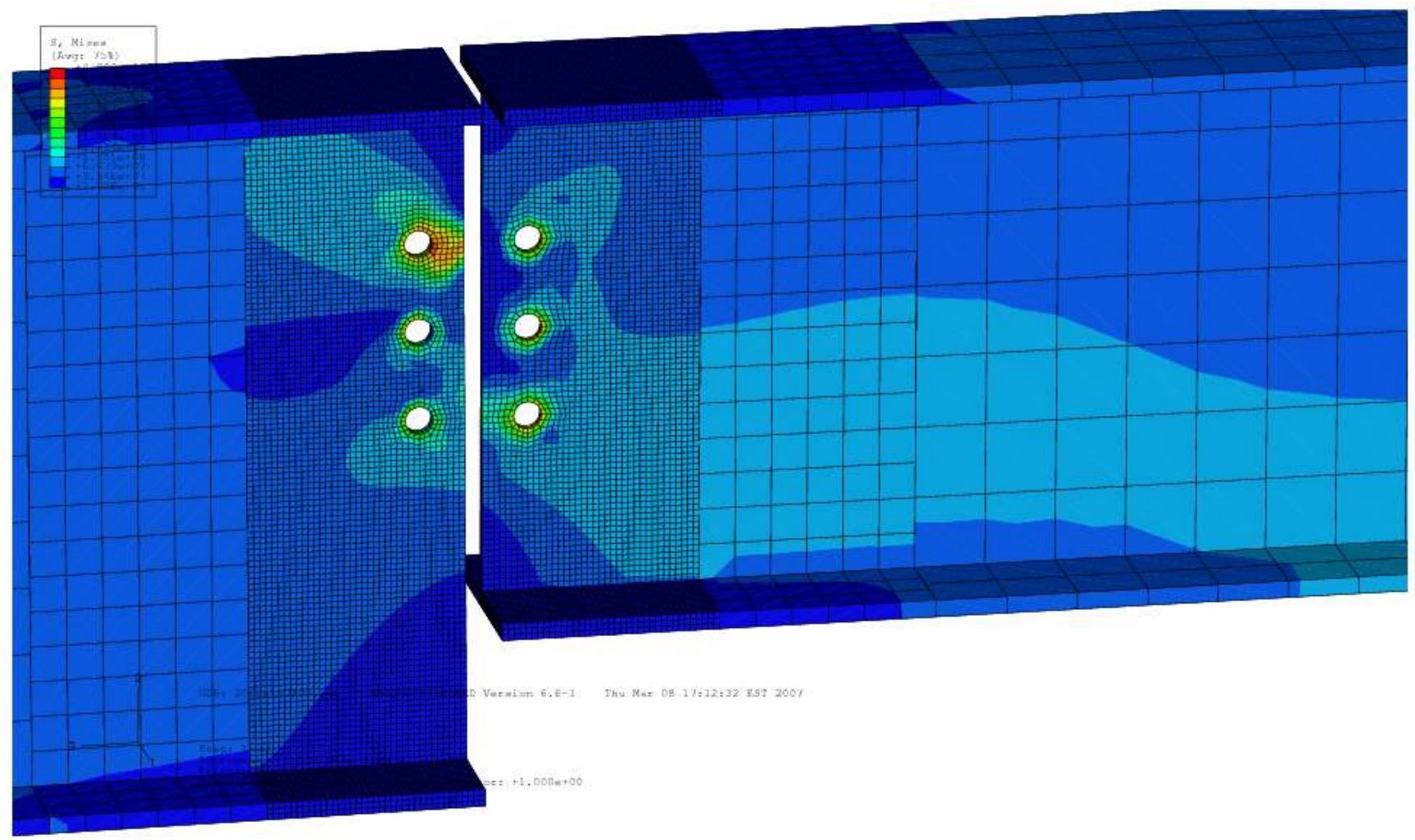

Figure 71: Von Mises Stress Distribution (Shear Tabs Excluded)

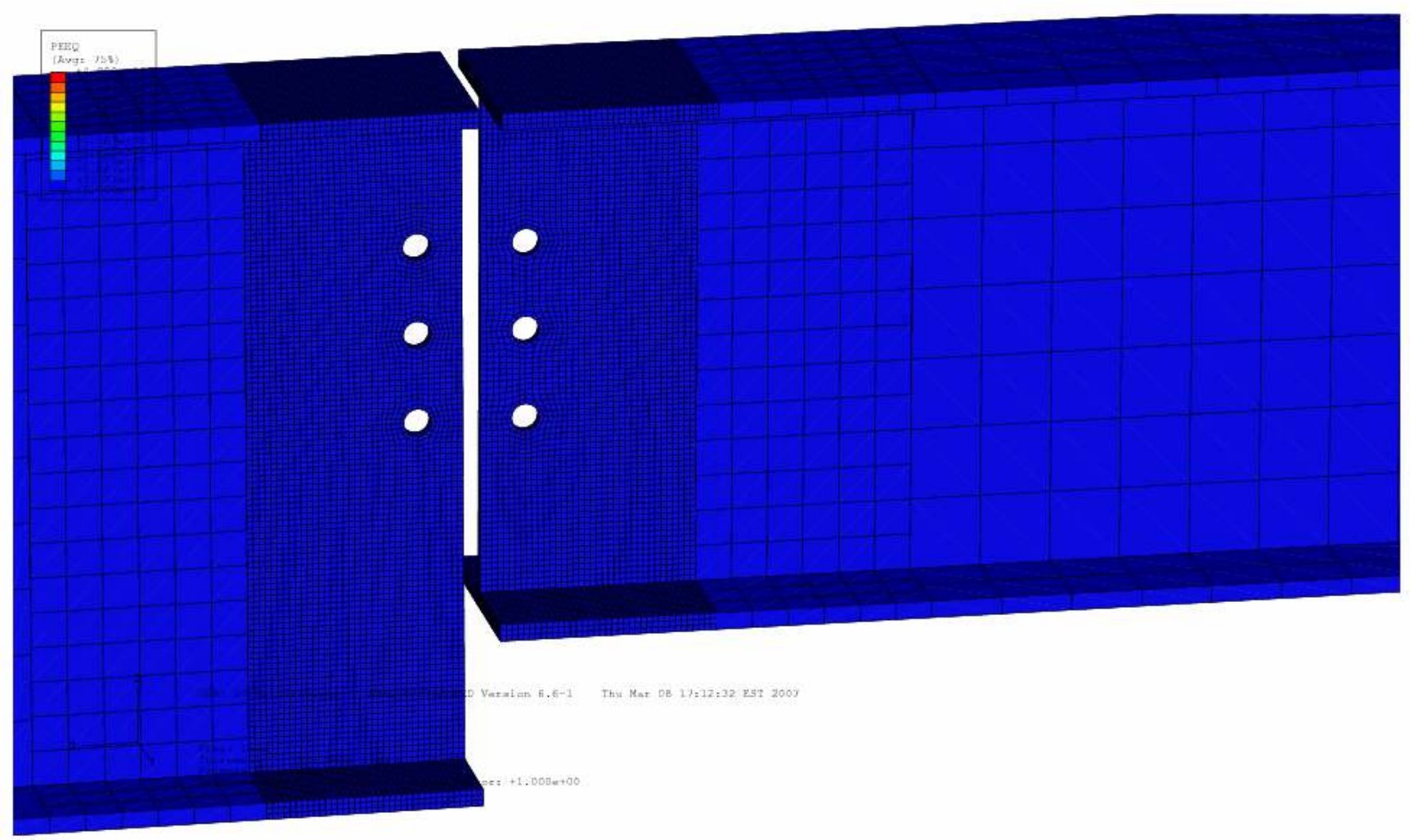

Figure 72: Equivalent Strain Distribution (No Permanent Deformation Observed)

5.4 Development of the Thermal Model

ABAQUS was used to create a thermal model that encompasses the heat transfer behavior of the four structural bays of interest on the 8th floor of WTC 5 when exposed to the reconstructed fire. Results from this model shall serve as input into the final model: a sequentially-coupled, thermal stress analysis of the four structural bays of interest. The temperature distribution of the steel assembly in three-dimensional space and time is integral for understanding of the thermal-stress behavior, since steel strength is highly temperature-dependent. Moreover, the geometric complexity of the structural assembly makes reliance upon hand calculations impossible if accurate results are to be derived.

The thermal model consists of 20 separate parts in ABAQUS. Some of these parts are referenced multiple times as assembly instances. Each part utilizes hexahedral, structured, linear, heat transfer elements for its meshing (DCC3D8: an 8-node convection/diffusion brick). The exception to this convention is the bolt part, which uses a sweep-type meshing scheme (the rest of the mesh properties are the same as described above). Table 7 below summarizes the number of elements used to mesh each part. The areas of most interest are in the vicinity of the bolt holes; these areas utilized the finest meshes in the model in order to derive very accurate results.

Table 7: Number of Elements Used for Each Model Part (Meshing)

Model Part	Number of Elements
Beam Stem (Fine Mesh Section)	16,626
Beam Stem (Intermediate Mesh Section)	198
Beam Stem (Coarse Mesh Section)	244
Bolt	964
Column	304
Concrete Slab	3,867
Floor Beam (Full Geometry)	912
Floor Beam (Half Geometry)	760
Shear Tab	2,688
Steel Shim	2,184
Floor Girder (Fine Mesh Section)	14,706
Floor Girder (Intermediate Mesh Section)	168
Floor Girder (Fine Mesh Section)	800
Beam Stem Insulation	22,332
Floor Beam Insulation (Full Geometry)	7,600
Floor Beam Insulation (Half Geometry)	4.560
Floor Girder Insulation	14,360
Shear Tab Insulation	710
Total:	**93,983**

The thermal model contains four types of material: A36 steel; A325 steel; mineral fiber, spray-applied insulation (also known as "fireproofing"); and lightweight concrete. The A36 and A325 steels have temperature-dependent thermal properties. It was assumed that the lightweight concrete and insulation have thermal properties that are a constant function of temperature. This is a reasonable assumption because the change in thermal properties of insulation and concrete is negligible in comparison to that of steel. Moreover, the thermal-stress behavior of these materials is not a concern for this research. The thermal properties defined in the model for the insulation and lightweight concrete are summarized in Table 8 below. The temperature-dependent thermal properties of steel (same for A36 and A325 types) are discussed at length in Section 5.1.

Table 8: Thermal Properties of Insulation and Concrete

Thermal Property	Mineral Fiber Insulation	Lightweight Concrete
Conductivity	0.12 [W/(m*K)]	0.80 [W/(m*K)]
Density	350 [kg/(m^3)]	1,534 [kg/(m^3)]
Specific Heat	1,200 [J/(Kg*K)]	840 [J/(Kg*K)]

The thermal model is composed of 42 assembly instances. Figure 73 and Figure 74 below are screenshots of the thermal model assembly. There are also 96 defined surfaces for use with interaction properties. The beam stems, floor girder, and floor beams are protected by "2-hour" insulation that is 1-in. thick. During the fire exposure in WTC 5, the columns were shielded behind walls and were also protected by "3-hour" insulation that is 1-3/8 in. thick (see Figure 34 above). It is assumed that the columns were not significantly heated by the fire and acted as heat sinks for the structural assembly which resides directly above the fire. The thermal model consists of a single transient thermal analysis step with a duration lasting 28,000 seconds (about 8 hours). The Thermal step is segmented into 80-second increments and uses the Full Newton (Direct) solution technique.

The thermal model relies upon 59 defined interactions to reconstruct the thermal behavior that occurred on the 8th floor of WTC 5 during its fire exposure. These interactions consist of 56 contact definitions, 2 natural convection definitions, and 1 radiation specification. The contact definitions are used to simulate the heat transfer between the various instances contained in the global model. It is assumed that perfect contact is achieved between the insulation and the steel parts. Therefore, any microscopic air gaps at the contact interfaces are neglected in this analysis.

It is assumed that turbulent natural convection is the heating mode of the structural assembly. Moreover, the convection heat transfer coefficient is specified as 20 [W/(m^2*K)] and the sink temperature amplitude is derived from the CFAST results. More precisely, the upper layer gas temperature history derived from the reconstructed fire is specified to heat the structural assembly over the course of 4 hours (the following 4 hours represent the time after burnout of the 8th floor compartment). Radiation of the

heated structure to the ambient is represented in the thermal model. Since radiation feedback from the compartment is neglected, the model is conservative (i.e., the steel temperatures during the heating phase would be slightly higher than what the results suggest). The emissivity is specified as 0.9 and the sink temperature amplitude is equal to the upper layer gas temperature history from the CFAST results.

In addition to interaction properties, the thermal model also imposes 33 separate constraints. Each of these constraints utilizes the Tie method to fuse model instances together. The thermal model contains a single predefined field which specifies the initial temperature of the steel (20 ºC). A full analysis was performed on a single-processor of a Sunfire X4100 machine with a FP rating of 117 and 4 GB of RAM. The memory policy of the job run was set to the default (moderate). The job lasted approximately 17 hours and underwent 350 increments of analysis. The results of this thermal analysis are discussed in Section 6.1.

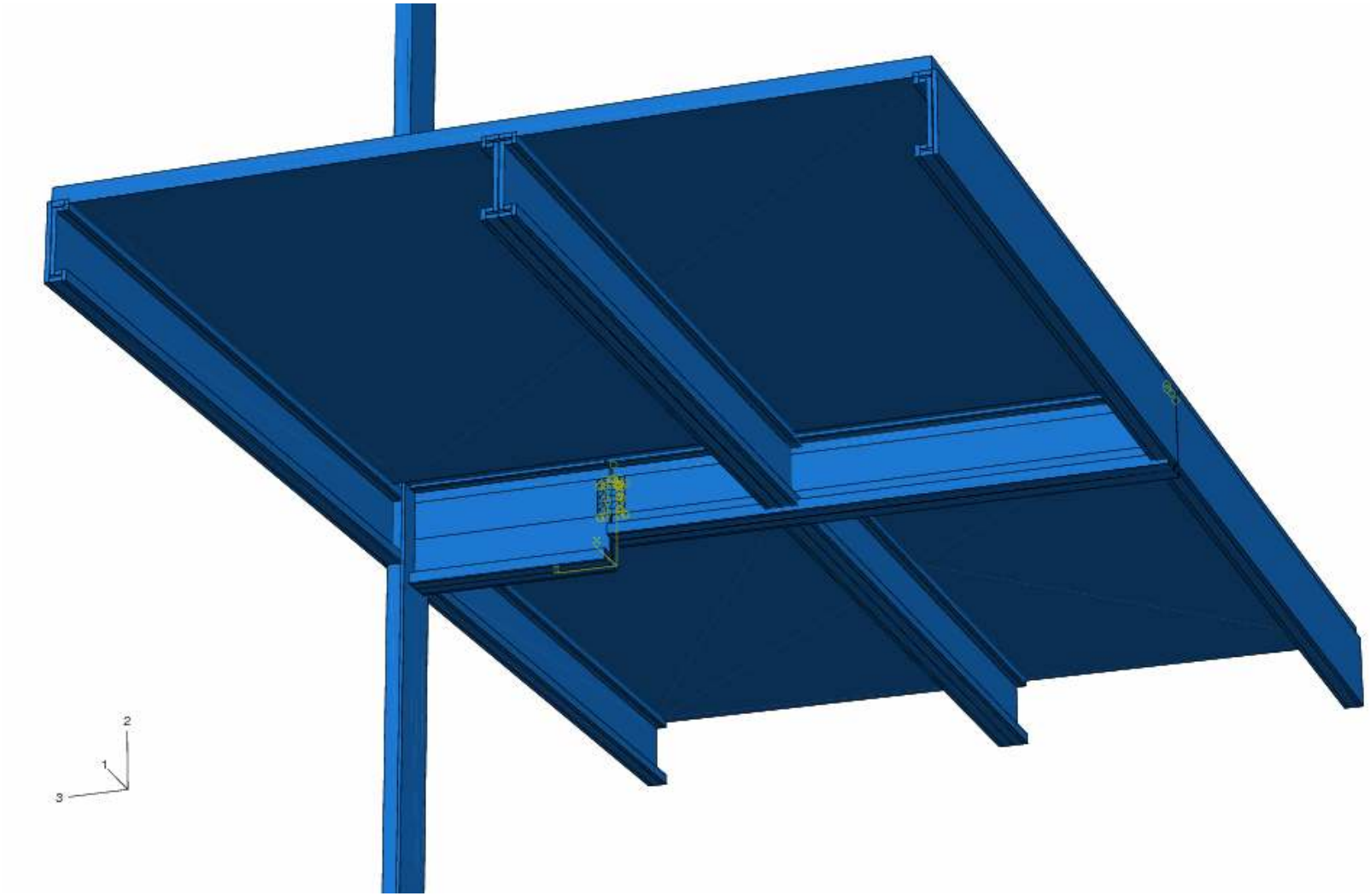

Figure 73: Thermal Model Assembly

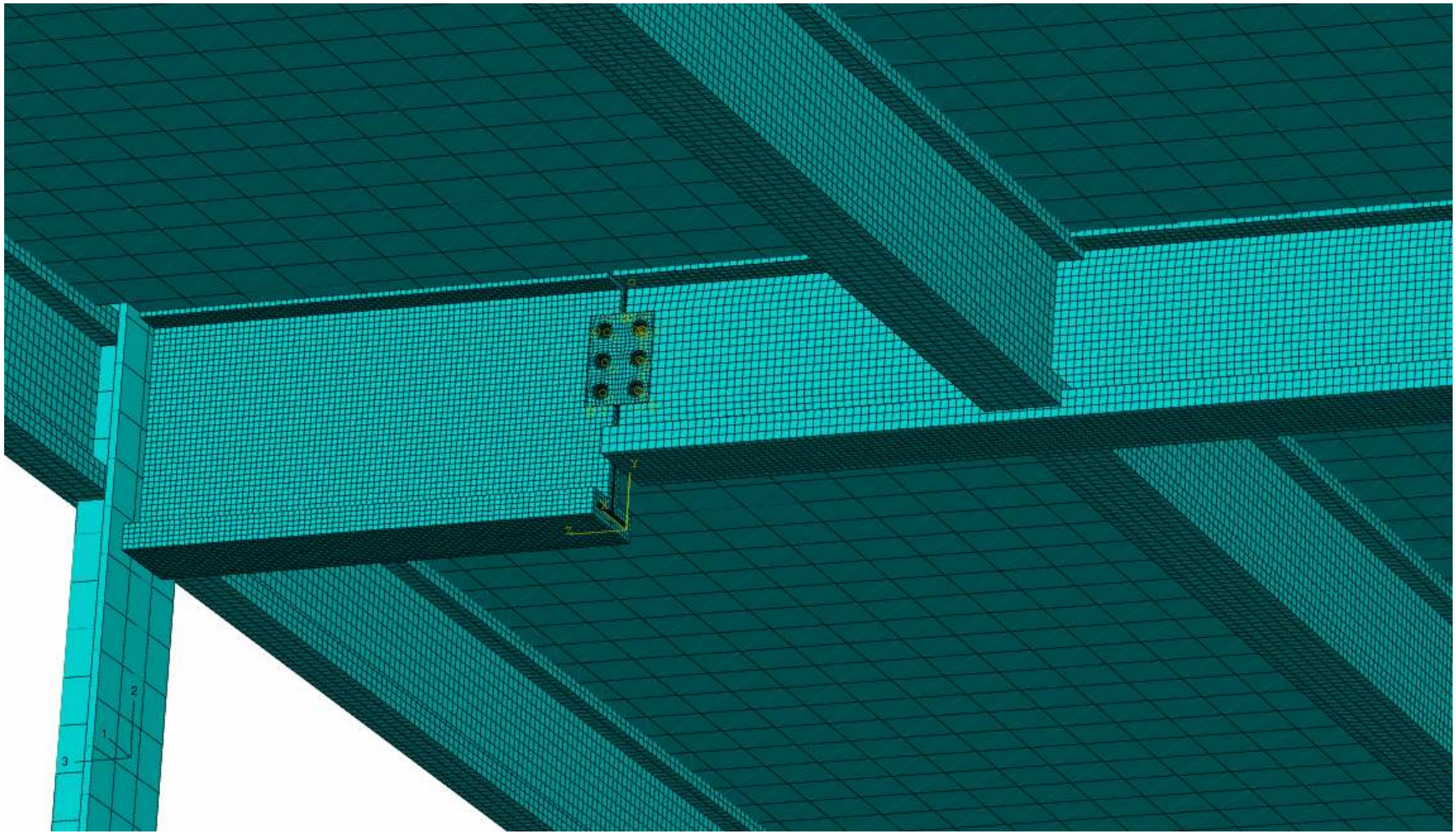

Figure 74: Meshing of the Thermal Model Assembly

5.5 Development of the Thermal-Stress Model

ABAQUS has been used to create both a mechanical and thermal model of the four structural bays of interest in WTC 5. The thermal model captures the heat transfer behavior of the structure when it is exposed to the reconstructed fire event. More precisely, the thermal model provides the temperature distribution of the structural assembly in both three-dimensional space and time. The mechanical model captures the stress behavior of the structure when subjected to its service load.

In order to fully understand the performance of the WTC 5 assembly during its fire exposure on September 11, 2001, the thermal model must be combined with the mechanical model: the result is a sequentially-coupled, thermal stress model. Since the stress behavior depends upon the temperature, but not vice versa (frictional heating is negligible), a sequentially-coupled model yields accurate results; a fully-coupled, thermal-stress analysis was not required. It was also assumed that the steel insulation stays completely attached during the fire exposure.

The sequentially-coupled, thermal-stress model is essentially a copy of the mechanical model with critical changes. The thermal-stress model has the same parts, mesh elements, interactions (friction included), constraints, loads (service load and bolt pretension), and boundary conditions (e.g., prevention of lateral torsional buckling) as the mechanical model (see Section 5.3 for a detailed description of these model features). In the thermal-stress model, the use of temperature-dependent steel properties is crucial. Figure 57 above is the test data from Harmathy that captures the stress-strain behavior of A36 steel at elevated temperatures; this data was used as input into the model. Additionally, the instantaneous coefficient of thermal expansion changes with elevated temperatures (as described in Section 5.1).

The mechanical model is composed of three analysis steps: Contact, Pretension, and Load. A fourth analysis step was added for the thermal-stress model: the Thermal step. This fourth step has a time period of 28,000 seconds (approximately 8 hours), which encompasses the heating and cooling phases of the fire event. The specified maximum increment size for this step is 80 seconds in order to maintain a reasonable time resolution. The solution technique for this step is the same as that for the previous steps (Full Newton (Direct)). A predefined field was applied to the entire model: the distribution of this field is derived from the results of the thermal model. The meshes of this model and the thermal model are compatible, and interpolation of midside nodes was specified. Essentially, the Thermal step maintains the gravity load applied during the Load step, and then applies the temperature history of the steel which is variable in three-dimensional space and time.

For this analysis, a field output request was specified as an addition to the default stress analysis result variables: nodal temperature (NT) was requested for the results. This allows for viewing of the steel temperature and deformation performance simultaneously. A full analysis was performed on four parallel processors of a Sunfire X4100 (quad-core) machine with a FP rating of 117 and 4 GB of RAM (per processor). The memory policy

of the job run was set to the maximum for fully-devoted processing power. The job lasted approximately 48 hours and underwent 530 increments of analysis (501 increments in the Thermal step). The results of the sequentially-couple, thermal-stress analysis are discussed in Section 6.2.

6 Finite Element Modeling Results

6.1 Results of the Thermal Analysis

ABAQUS was used to create a thermal model that encompasses the heat transfer behavior of the four structural bays of interest on the 8th floor of WTC 5 when exposed to the reconstructed fire. Results from this model serve as input into the final model: a sequentially-coupled, thermal-stress analysis of the four structural bays of interest. The temperature distribution of the steel in space and time is derived from the analysis.

Figure 75 below shows the temperature distribution of the steel assembly after 1 hour of fire exposure (the insulation has been removed from the results rendering for illustrative purposes). The limits of the contour plot are as follows: upper limit is 720 ºC (maximum temperature the upper layer gas temperature reaches) and the lower limit is 20 ºC (ambient temperature). It is observed that the concrete slab acts as a heat sink for the steel assembly. This is illustrated in Figure 75 below, for the steel temperature is lower at higher elevations (near the concrete slab).

Using the "probe" capability of the software, it was determined that the temperature gradient between the end of the beam stem welded to the column and its other end at the shear connection is approximately 450 ºC after one hour of fire exposure. This clearly proves one of the hypotheses of this project: the Gerber beam design thermally isolates the shear connections from their heat sinks (the columns). More precisely, since heat at the shear connection must travel across the entire length of the beam stem (4 feet) before it reaches the heat sink, heat builds up quickly in the vicinity of the bolt holes. The interface of the beam stem and the column is kept relatively cool during the fire exposure. This can be attributed to the efficient dissipation of heat at this location, for heat is transmitted through the steel faster than the heat from the fire is conducted through the insulation. Table 9 below summarizes the thermal results at future points in time, which includes the heating and cooling of the structural assembly.

Table 9: Summary of Thermal Analysis Results

Reference	Duration of Analysis (Fire: t < 4 hours) (Burnout: t > 4 hours)	Temperature Gradient (Across Beam Stem) (Left-to-Right)
Figure 75	1 hour	450 ºC
Figure 76	2 hours	400 ºC
Figure 77	3 hours	250 ºC
Figure 78	4 hours	Negligible
Figure 79	5 hours	-150 ºC
Figure 80	6 hours	-150 ºC
Figure 81	7 hours	-150 ºC
Figure 82	8 hours	-50 ºC

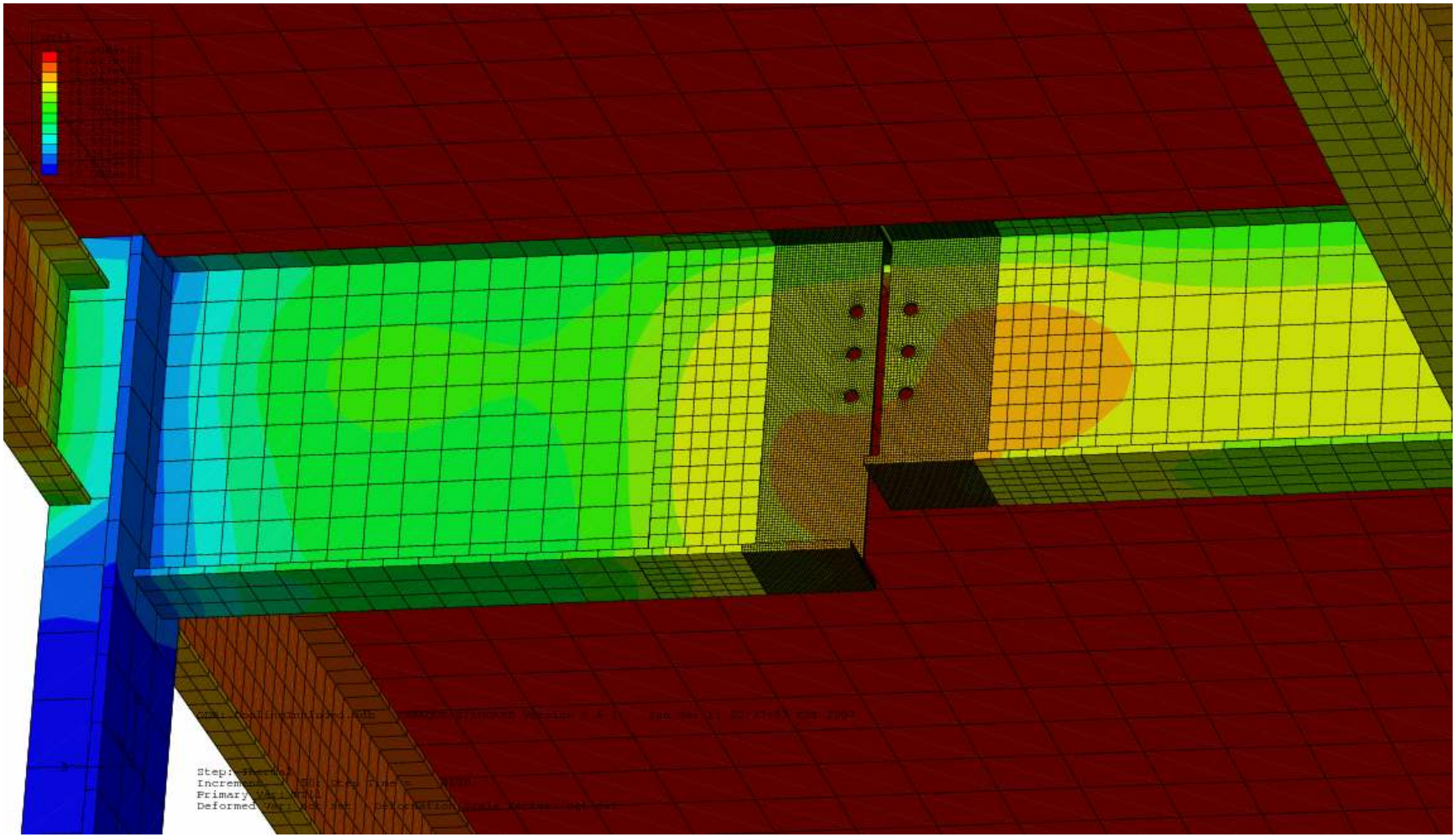

Figure 75: Steel Temperature Distribution (1 Hour of Fire Exposure)

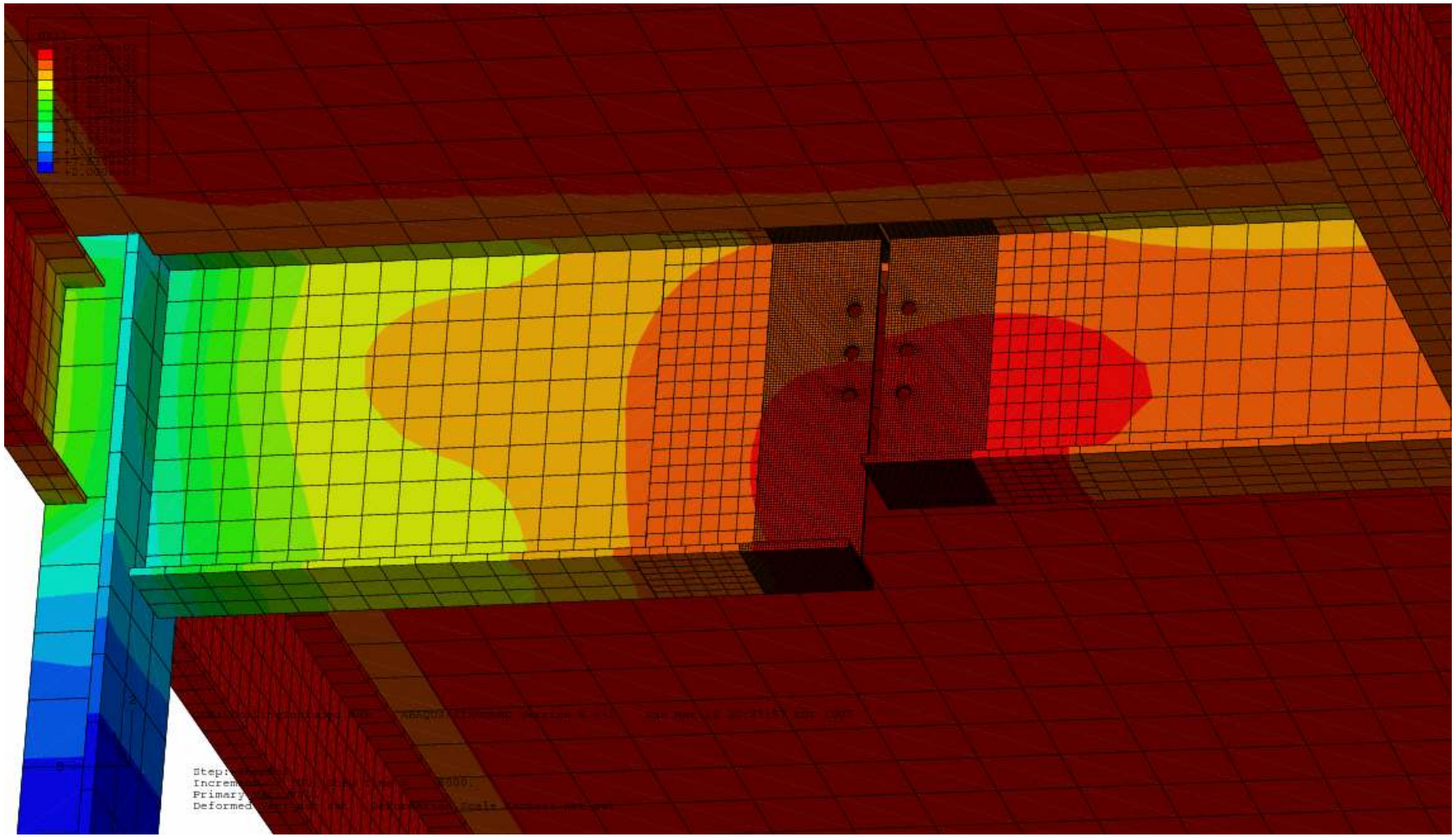

Figure 76: Steel Temperature Distribution (2 Hours of Fire Exposure)

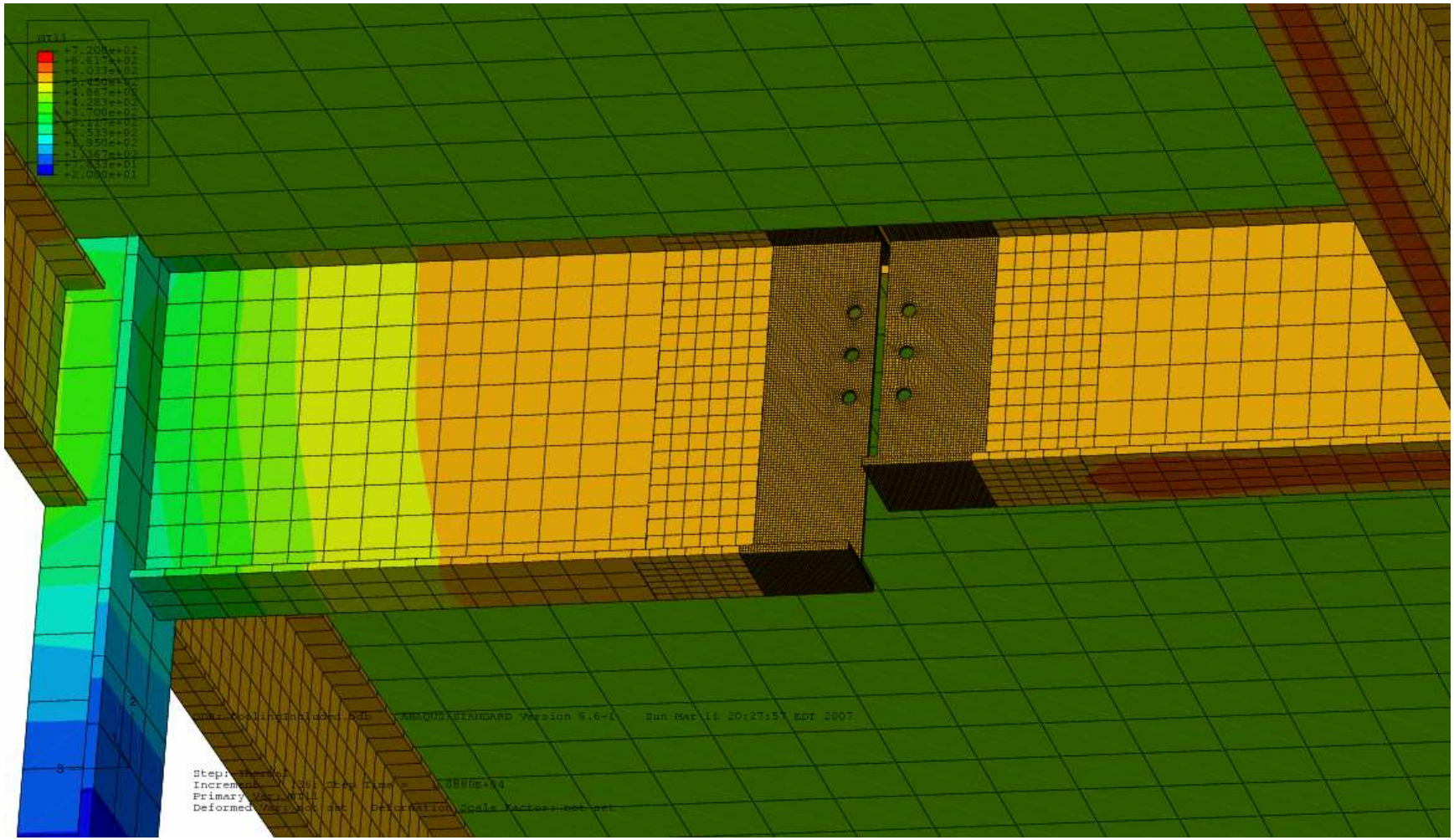

Figure 77: Steel Temperature Distribution (3 Hours of Fire Exposure)

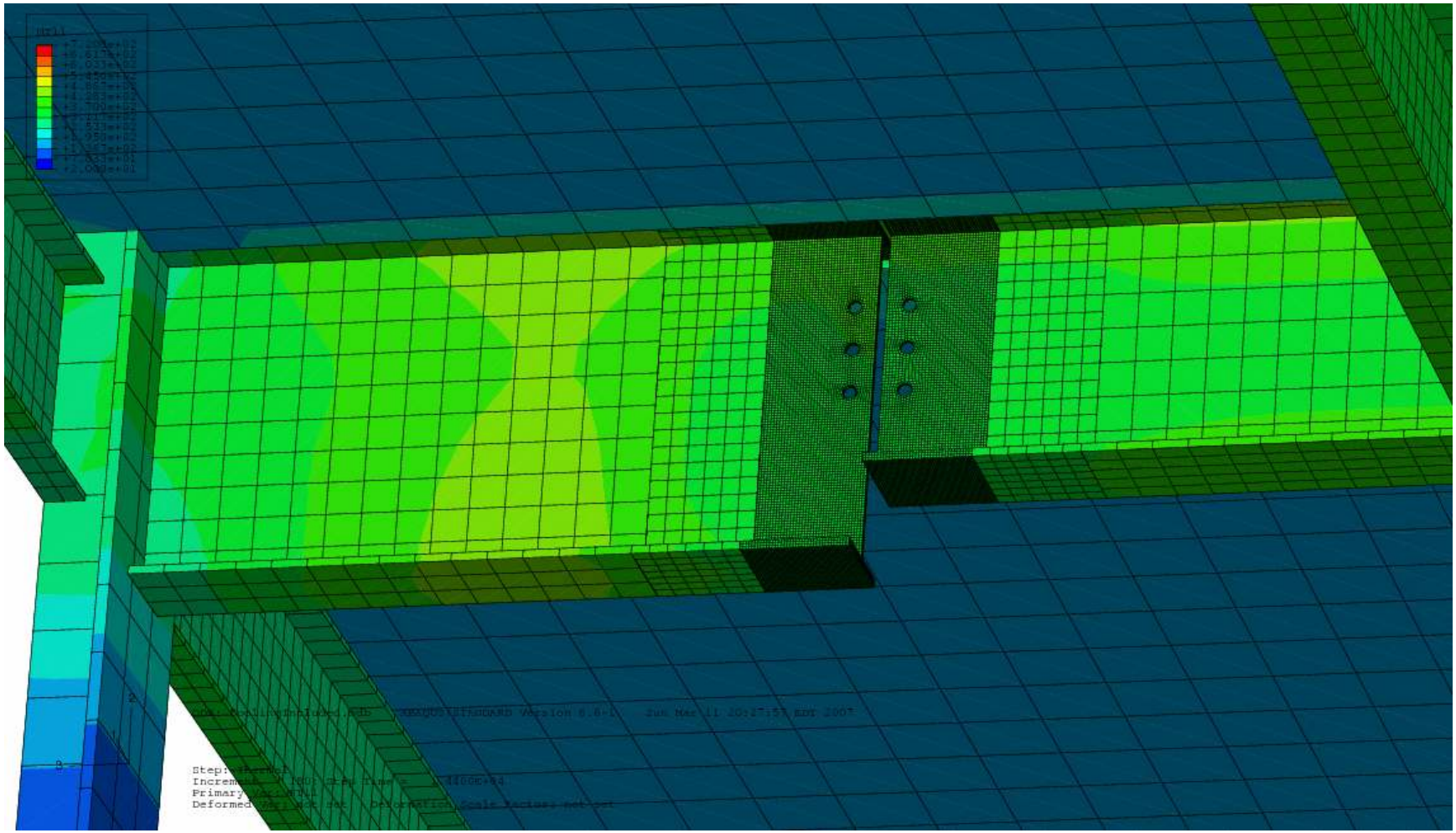

Figure 78: Steel Temperature Distribution (4 Hours of Fire Exposure)

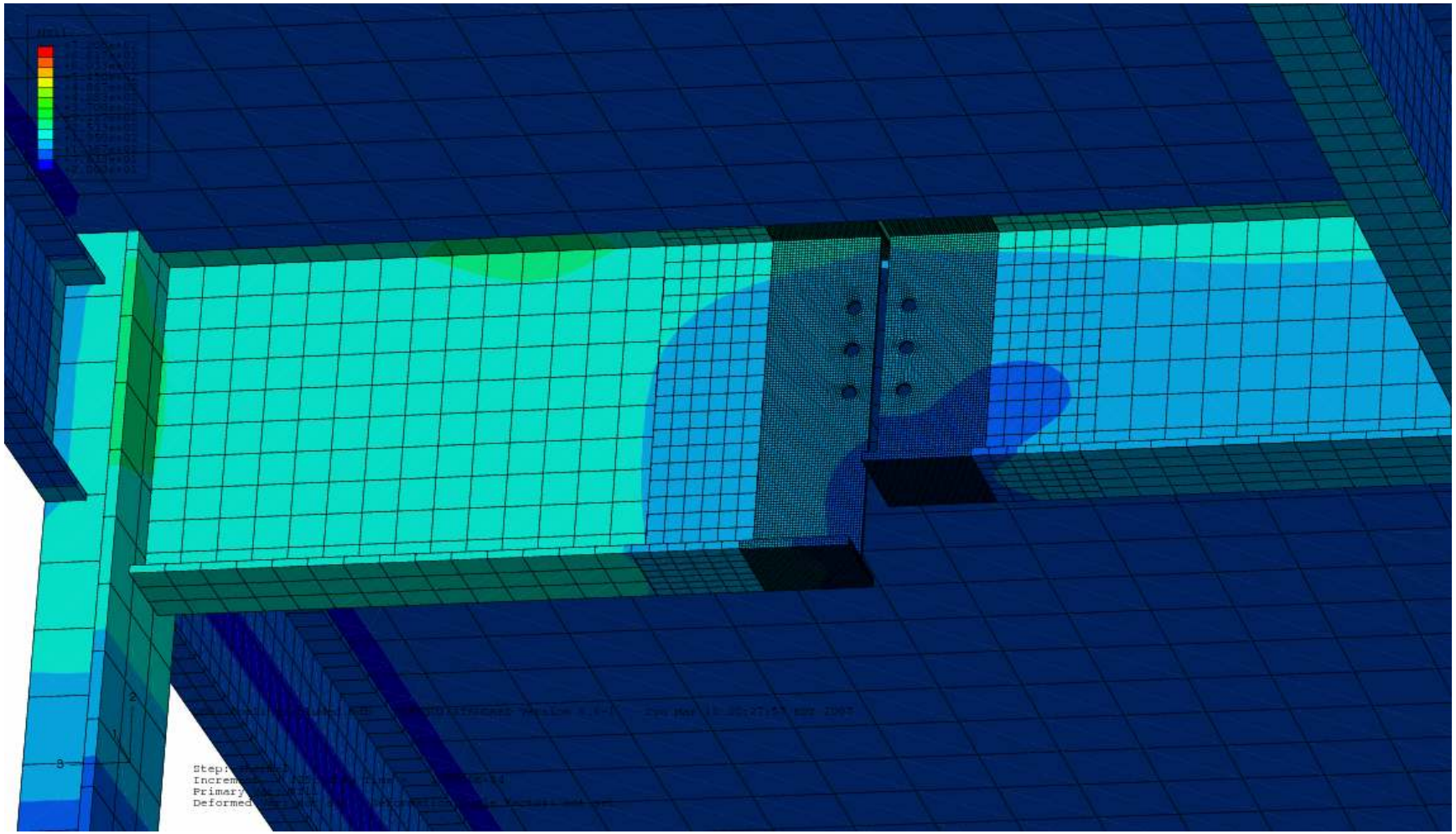

Figure 79: Steel Temperature Distribution (5 Hours of Fire Exposure)

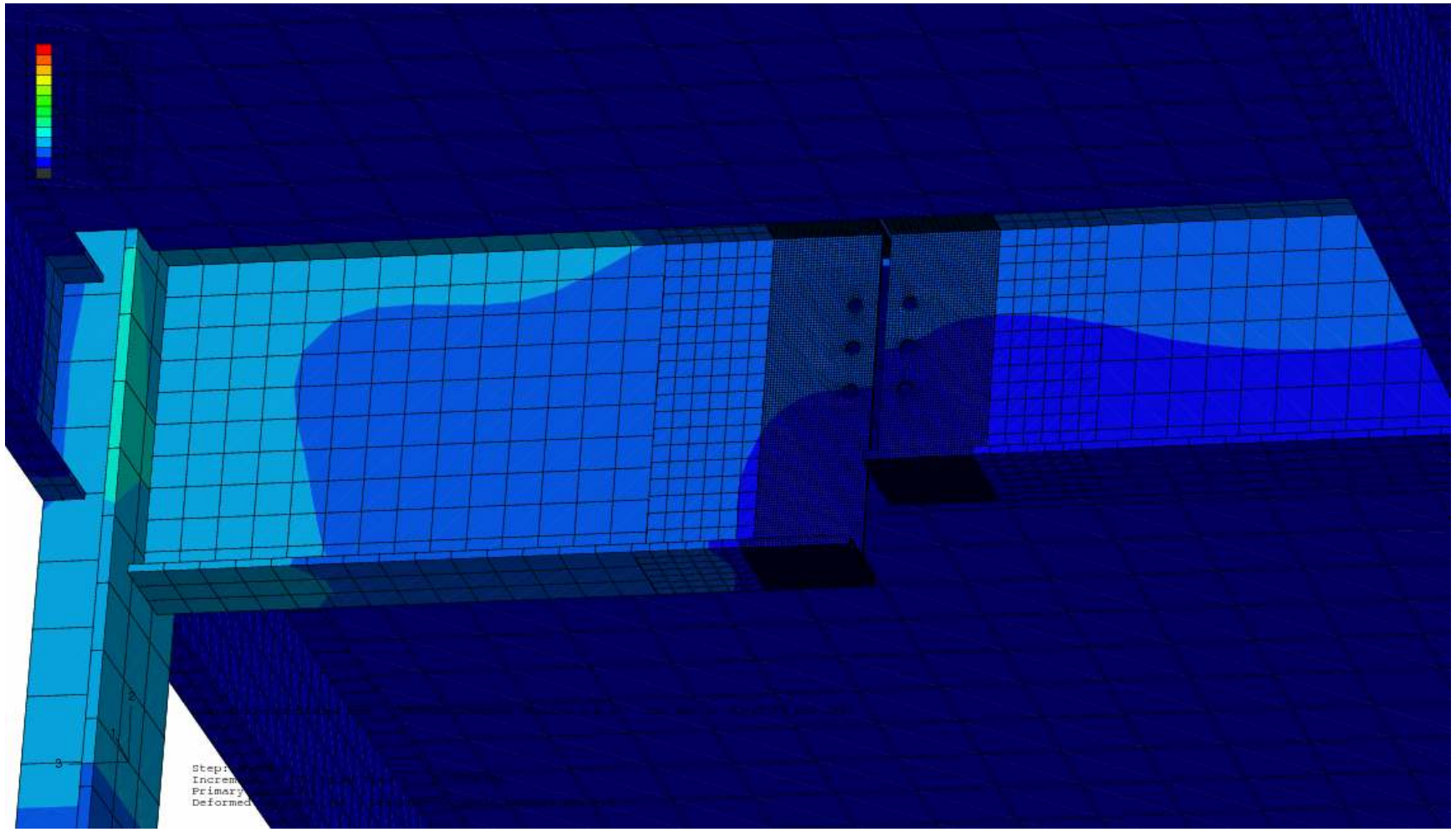

Figure 80: Steel Temperature Distribution (6 Hours of Fire Exposure)

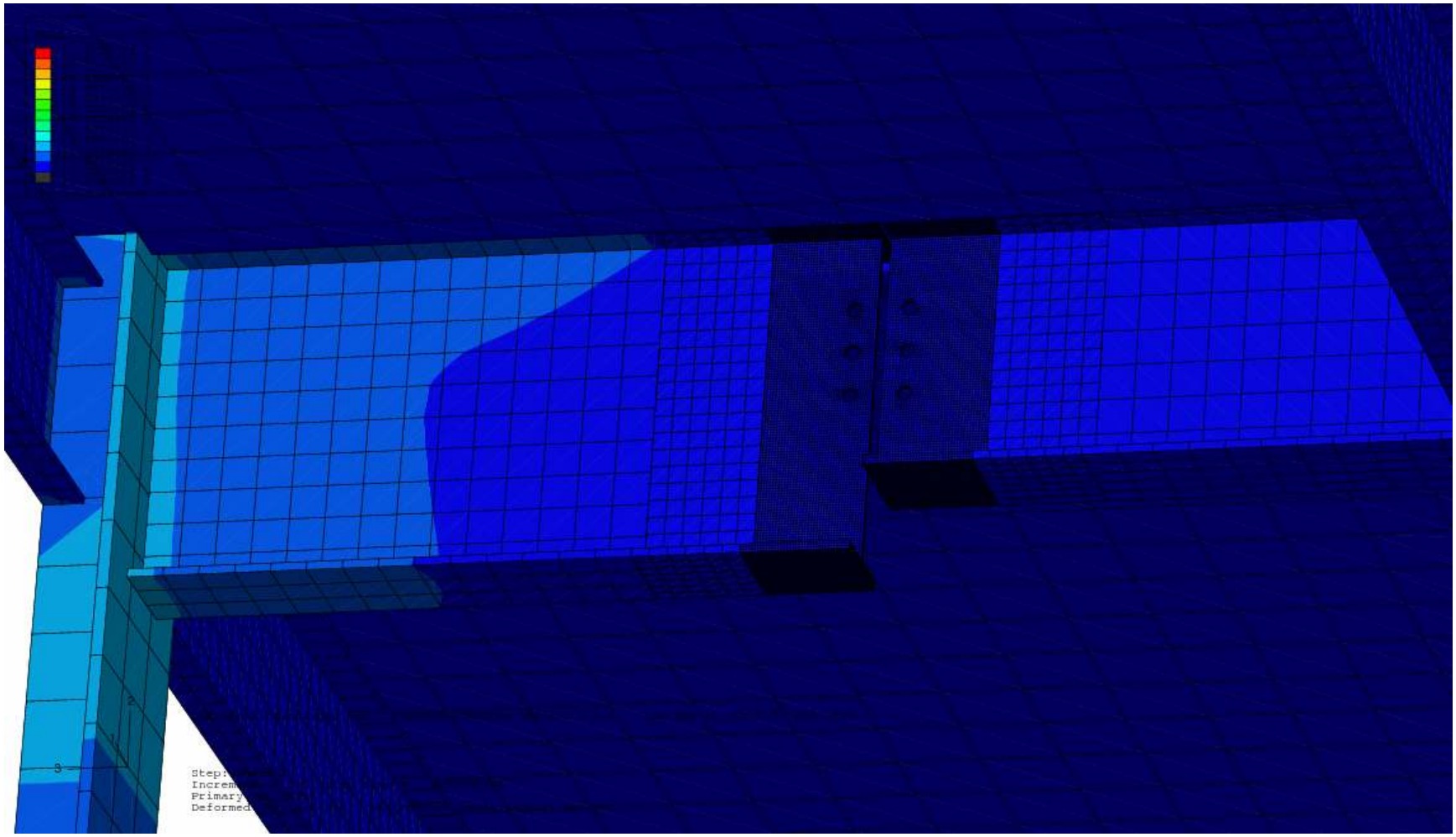

Figure 81: Steel Temperature Distribution (7 Hours of Fire Exposure)

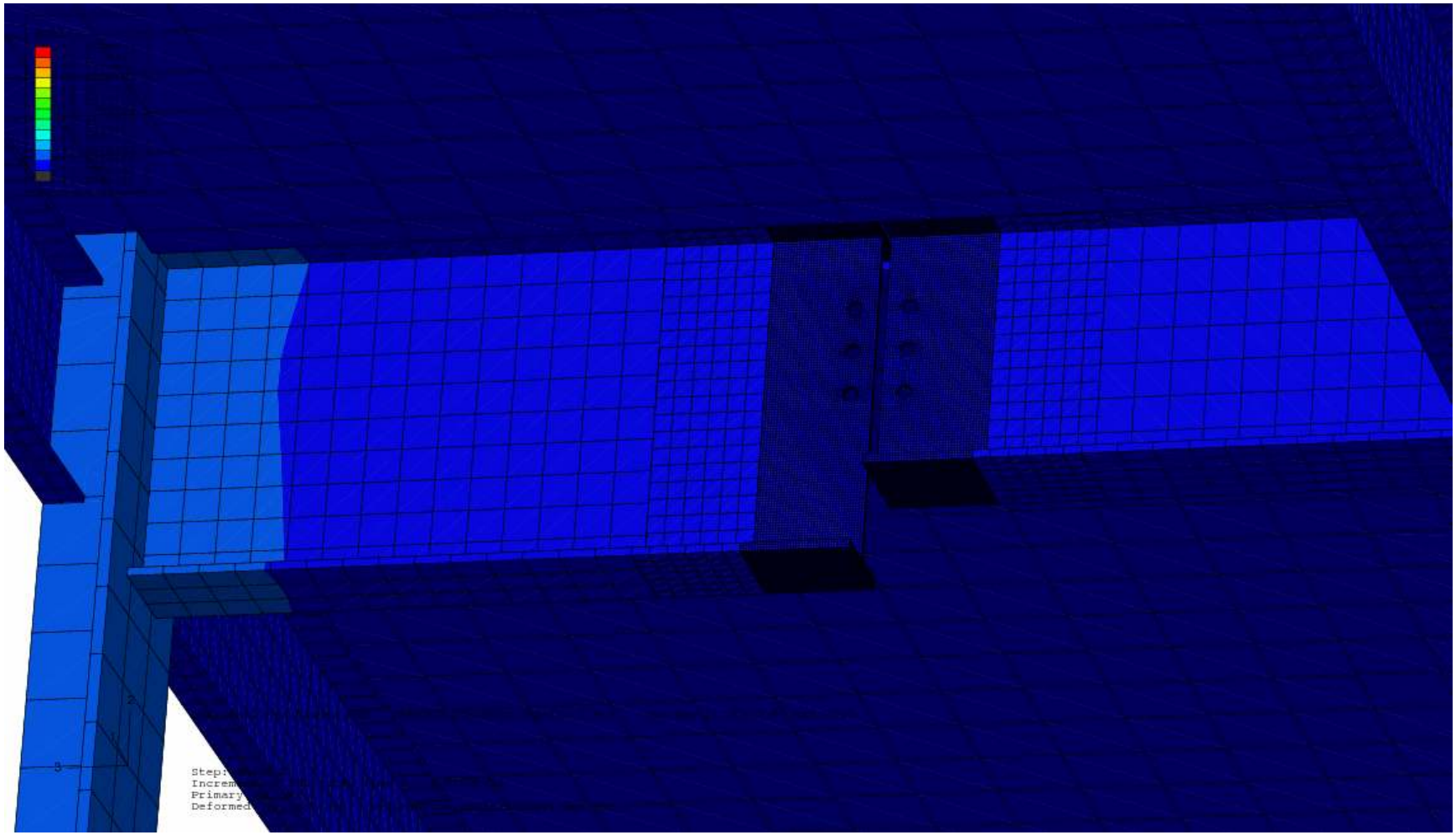

Figure 82: Steel Temperature Distribution (8 Hours of Fire Exposure)

Figure 83 below shows the beam stem and shear tab assembly after 1 hour of fire exposure with the insulation included in the rendering. It is observed that the insulation functions as predicted: it delays the transmission of heat to the steel during the fire exposure. Moreover, it can be observed that the top of the assembly remains relatively cool due to the heat sink effect of the concrete slab above it.

Figure 84 below is the same assembly as shown in Figure 83, but after 2 hours of fire exposure. This figure acts as a critical check of the thermal model. The ASTM E-119 test is used as a basis for the insulation requirements in the UL Fire Resistance Directory. Prior to its specification in the directory, a single beam with 1-in. of mineral fiber insulation was tested in a furnace. After about 2 hours, the temperature of the steel beam probably reached a specified "critical temperature" of around 600 ºC. Although, the real fire in WTC 5 was different from the furnace fire, Figure 84 below does provide a validation of the model because it is observed that the steel temperature is relatively close to 600 ºC after 2 hours of fire exposure.

Section 10.1.1 of this report presents an estimated thermal analysis of the steel girders located in WTC 5. It is interesting to compare the results of the sophisticated finite element thermal analysis as described in this section to those hand calculations performed in Section 10.1.1. Figure 85 below is the predicted temperature of the steel girder as a function of fire exposure time according to the hand calculations. These hand calculations assume a uniform temperature distribution through the steel at any given point in time. Figure 75 through Figure 82 above show that this assumption not always reasonable. As another baseline check on the thermal model, a rough estimation of the average steel temperature across the beam stem span was determined from the finite element model results. These values are compared to the temperatures predicted by hand calculations in Table 10 below.

Table 10: Comparison of Hand Calculations and FEM Analysis Results

Time [hours]	**Uniform Steel Temperature [ºC]** (Hand Calculations)	**Average Steel Temperature** (FEM Analysis)	**Steel Temperature at Bolt Holes** (FEM Analysis)
1	**291**	**300**	**600**
2	**483**	**450**	**660**
3	**522**	**500**	**600**
4	**410**	**400**	**350**

Table 10 above shows that hand calculations characterize the average steel temperature reasonable well. Yet, the hand calculations do not provide any information concerning the distribution of the temperature, which is very drastic and important in this case. Therefore, hand calculations alone may misguide a designer. In the case of the WTC 5 structural assembly, the hand calculations grossly under-predict the steel temperature in the vicinity of the shear connection during the heating phase of the fire.

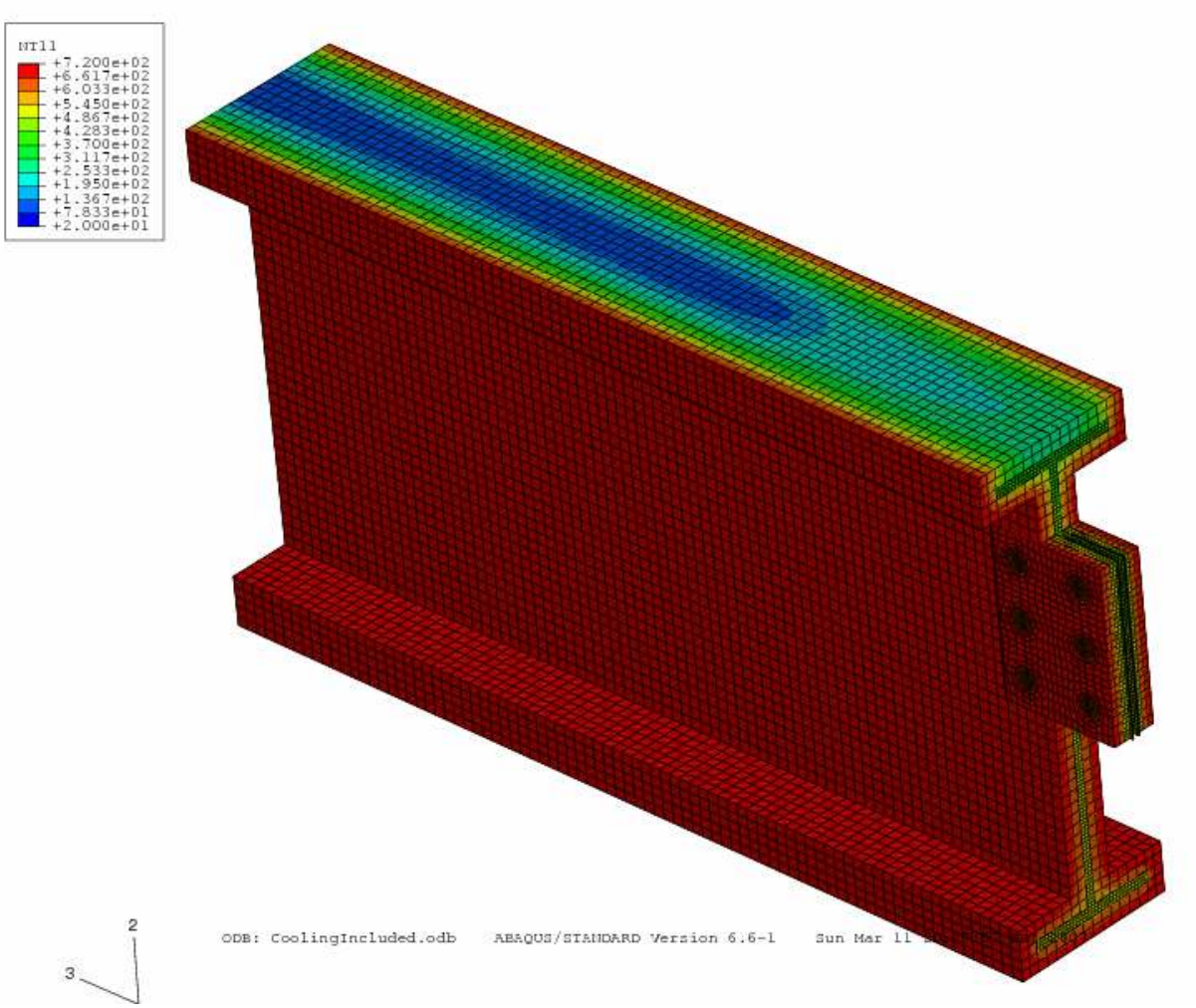

Figure 83: Beam Stem/Shear Tab Assembly with Insulation (1 Hour of Fire Exposure)

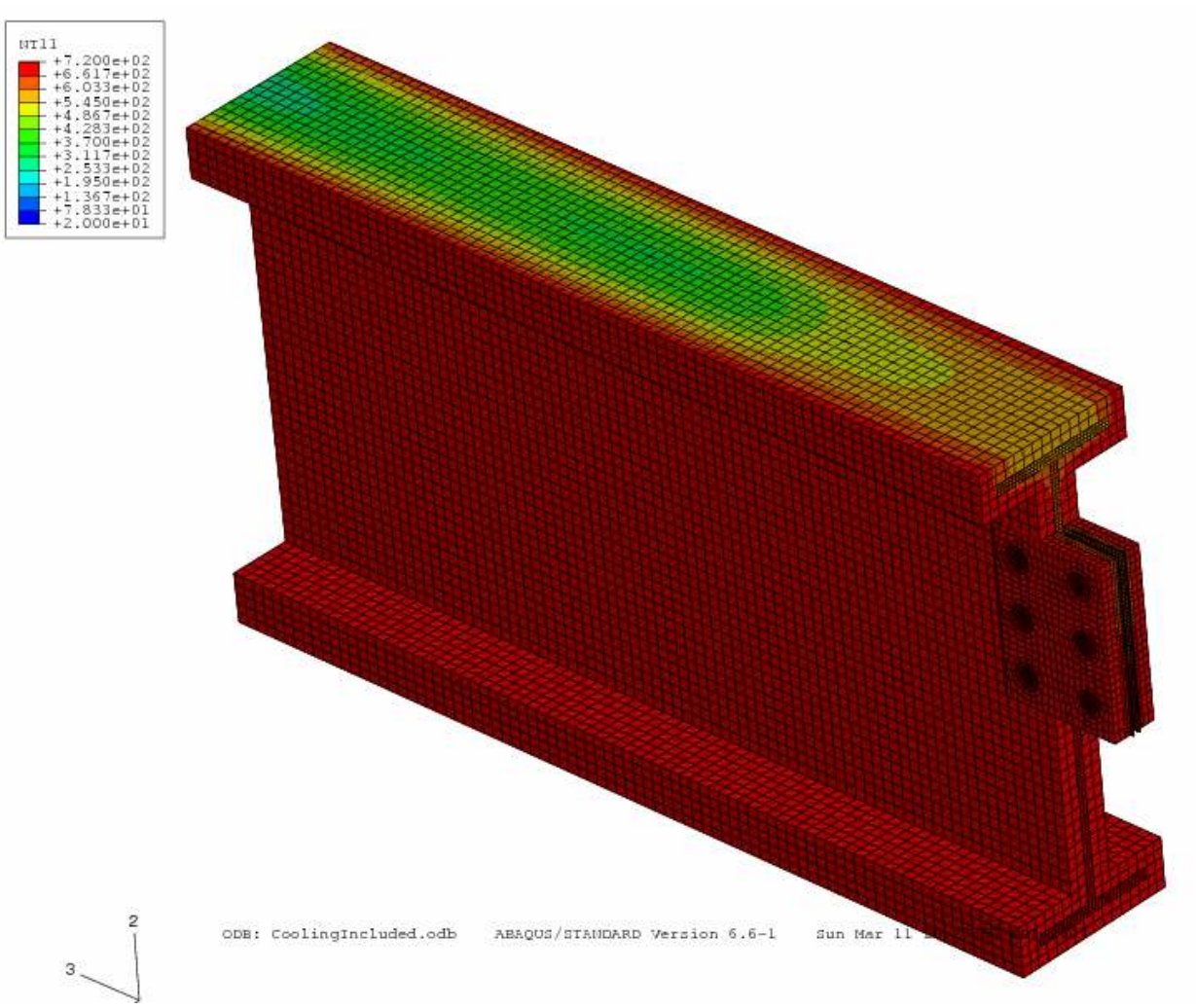

Figure 84: Beam Stem/Shear Tab Assembly with Insulation (2 Hours of Fire Exposure)

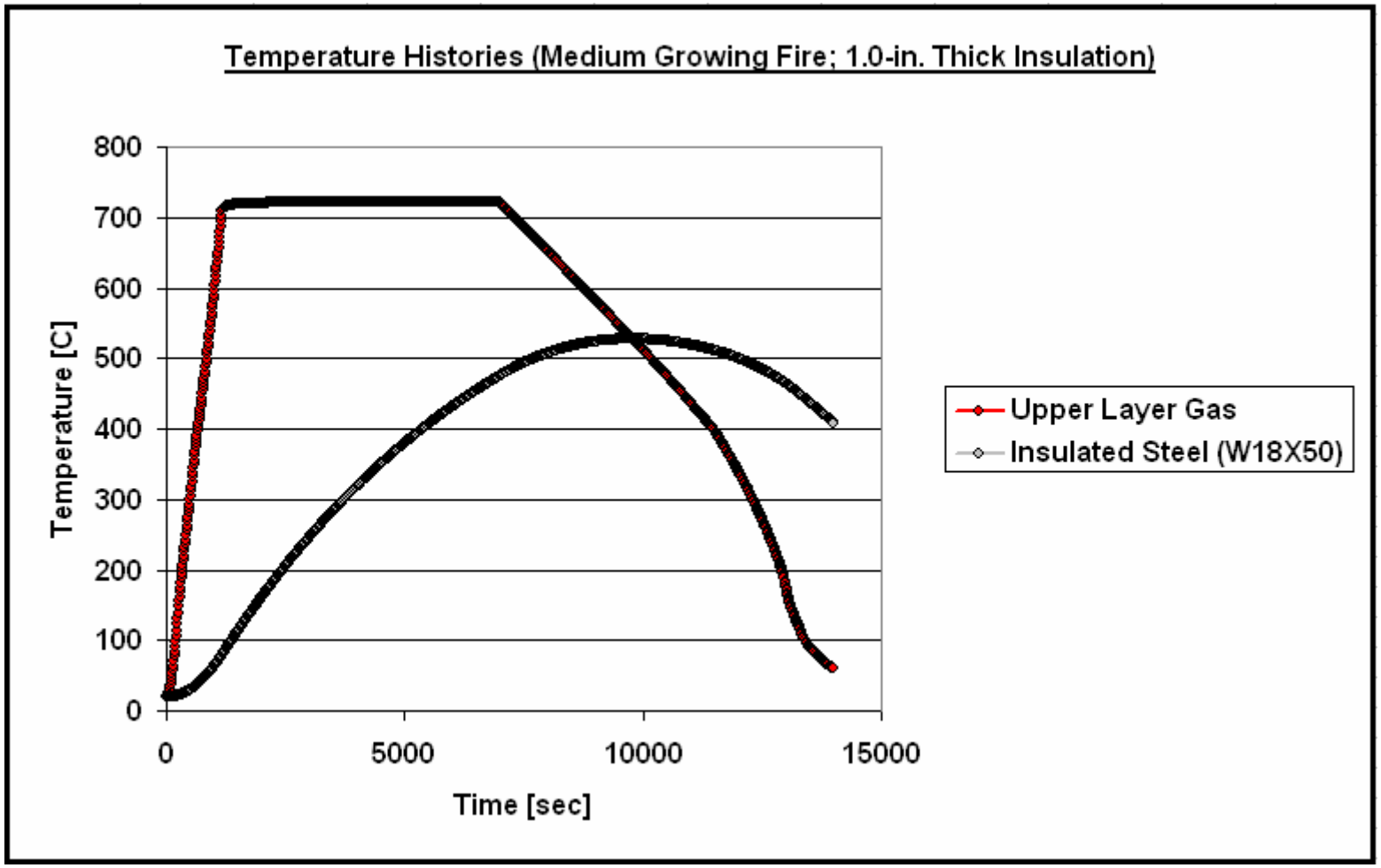

Figure 85: Predicted Steel Temperature History During Fire Exposure (Hand Calculations)

6.2 Results of the Thermal-Stress Analysis

ABAQUS was used to create a sequentially-coupled, thermal-stress model that encompasses the global behavior of the four structural bays of interest on the 8th floor of WTC 5 when exposed to the reconstructed fire. This model serves as an accurate reconstruction of the quasi-dynamic thermal-stress behaviors that occurred and led to progressive structural collapse. This model integrates a vast amount of research and is capable of representing highly-nonlinear thermal and mechanical behaviors.

The structural assembly is initially at ambient temperature (20 °C) carrying the specified gravity loads with minimal deflection. As the compartment heats up in the first hour of fire exposure, the steel assembly slowly increases in temperature (as described in Section 6.1). As the steel heats up, it undergoes thermal expansion which causes the floor girder to elongate significantly and close the gap between it and the beam stem. This elongation causes relatively harmless compressive stress concentrations to form on the strong side (i.e., toward the beam stem span) of the bolt holes (see Figure 86 below).

As the assembly continues to increase in temperature, the steel's rigidity decreases steadily and the floor girder begins to undergo significant deflection. Figure 87 below shows the stress distribution in the vicinity of the shear connection after one hour of fire exposure. It is apparent that the floor girder has deflected significantly. In fact, the floor girder has deflected enough for its lower flange to contact and penetrate the beam stem web. This phenomenon shall be referred to as the formation of a *fulcrum point*. At this time during the fire exposure, the top bolt continues to bear against the strong (left) side of the bolt hole due to the influence of thermal expansion of the floor girder. Forensic evidence suggests that the top bolt was bearing against the weak (right) side of the bolt hole at failure. It should be noted that the values of stress are not important at elevated temperatures as discussed in Section 5.2; Figure 87 simply serves as a convenient representation of where the stress concentrations exist.

Figure 88 shows the stress distribution in the vicinity of the shear connection after 2 hours of fire exposure. At this point in time during the fire exposure, the loss of rigidity in the steel has "outpaced" its thermal expansion. More precisely, the floor girder has deflected by a much greater margin than it is expanding. Recall from Figure 87 that the thermal expansion aids in the stability of the shear connection by holding the floor girder close to the beam stem across their entire cross-sections. Figure 88 shows that the top bolt has undergone a sudden stress reversal and is now bearing against the weak side of the bolt hole. This stress reversal can be attributed to the fulcrum mechanism which has fully formed at this point in time during the fire exposure. The fulcrum mechanism has fully formed because tensile stresses surrounding the lower flange's penetration into the beam stem web have arrested further penetration in this region. Therefore, the fulcrum point has been fully established because this point can now resist the movement of the floor girder's lower flange. This phenomenon is analogous to using the back end of a hammer to pry a nail out of a wall; the nail is analogous to the top bolt.

Plastic shear strain is the failure criterion that is used to assess when web tear out failure occurs at the shear connection as the forensic evidence suggests (see Section 5.2 for a detailed discussion of this failure criterion). Figure 89 below shows the plastic shear strain distribution in the vicinity of the bolt hole after 2 hours of fire exposure. The limits of the contour plot are set as -0.16 and 0.16; plastic shear strain exceeding these limits represents rupture failure according to the failure criterion determination model. In Figure 89, it can be observed that the regions in black and white are outside the failure limits. In fact, the maximum plastic shear strain at the top bolt hole is 0.33, which clearly represents that rupture has occurred by this point in the fire exposure. Figure 90 shows a close-up view of plastic shear strain at the top bolt hole.

The plastic shear strain actually demonstrates a "runaway" failure at this point in time. More precisely, the plastic shear strain reaches values that are triple and quadruple the failure limit over the course of only minutes in the model analysis. Figure 91 below shows the plastic shear stress distribution after 2 hours and 15 minutes of fire exposure. In reality, the shear connection would have undergone catastrophic failure prior to this point in the fire exposure. The shear planes are consistent with those observed from the forensic evidence. More precisely, the shear planes are about -15 degrees from the x-axis, in which the x-axis runs parallel to the span of the floor girder.

When the top bolt fails (i.e., pulls out of the beam stem web), there are only two bolts left to carry the largely deflecting floor girder. Although the bottom two bolts are bearing against the strong side of their bolt holes in Figure 88 and Figure 89 below, the failure of the top bolt would surely have caused a stress reversal. This stress reversal would cause the two remaining bolts to bear against the weak side of their respective bolt holes. These two bolts would then tear out from the beam stem in the same manner as the top bolt. Once the top bolt has failed, the failure of the remaining two bolts would happen almost instantaneously; this can be referred to as an "un-zipping" effect.

Figure 92 below presents a comparison between the model's results and forensic evidence. The left side of Figure 92 shows the equivalent strain in the vicinity of the three bolt holes in the beam stem web after 2 hours of fire exposure. The right side of Figure 92 shows a recovered beam stem sample from WTC 5 that serves as forensic evidence of the structural failure. It is observed that the failure in the finite element model is very similar to the failed structural specimen. More precisely, the angles at which the bolts pried against the bolt holes are similar. The top bolt bears against the weak side of its bolt hole at about 15 degree below the horizontal. The bottom bolt bears against the strong side of its bolt hole initially, but as a result of the failure of the top bolt hole, pulls outs from the beam stem web in the direction of the floor girder.

Figure 93 and Figure 94 below present photographic evidence that a fulcrum point mechanism formed prior to catastrophic failure. It is observed that penetrations were made toward the lower part of the beam stem webs. This is in the region that the thermal-stress model predicted the lower flange of the floor girder would penetrate into the beam stem web. These photographs represent more key articles of forensic evidence which help to validate the results of the thermal-stress model.

The sequentially-coupled, thermal-stress model has estimated that the time in which catastrophic structural collapse occurred within WTC 5 was approximately two hours. This model captures all the relevant properties of steel except for its thermal creep strain. In addition, radiation from the compartment was neglected; only radiation to the ambient was considered. Lastly, the steel decking which supported the concrete slab in WTC 5 was not explicitly modeled. Instead, it was assumed that the concrete slab was in uniform contact with the top flange of the members. In reality, the ribbed geometry of the decking would decrease the heat sink effect of the concrete, for a fraction of the top flanges' surface area would not be in contact with the floor assembly. The exclusion of creep strain, the rigorous treatment of radiation feedback, and the steel decking would suggest that the failure occurred slightly earlier than the thermal-stress model has predicted. This is because the steel temperatures in the vicinity of the shear connections would have been slightly higher than predicted at any given point in time during the heating phase of the fire.

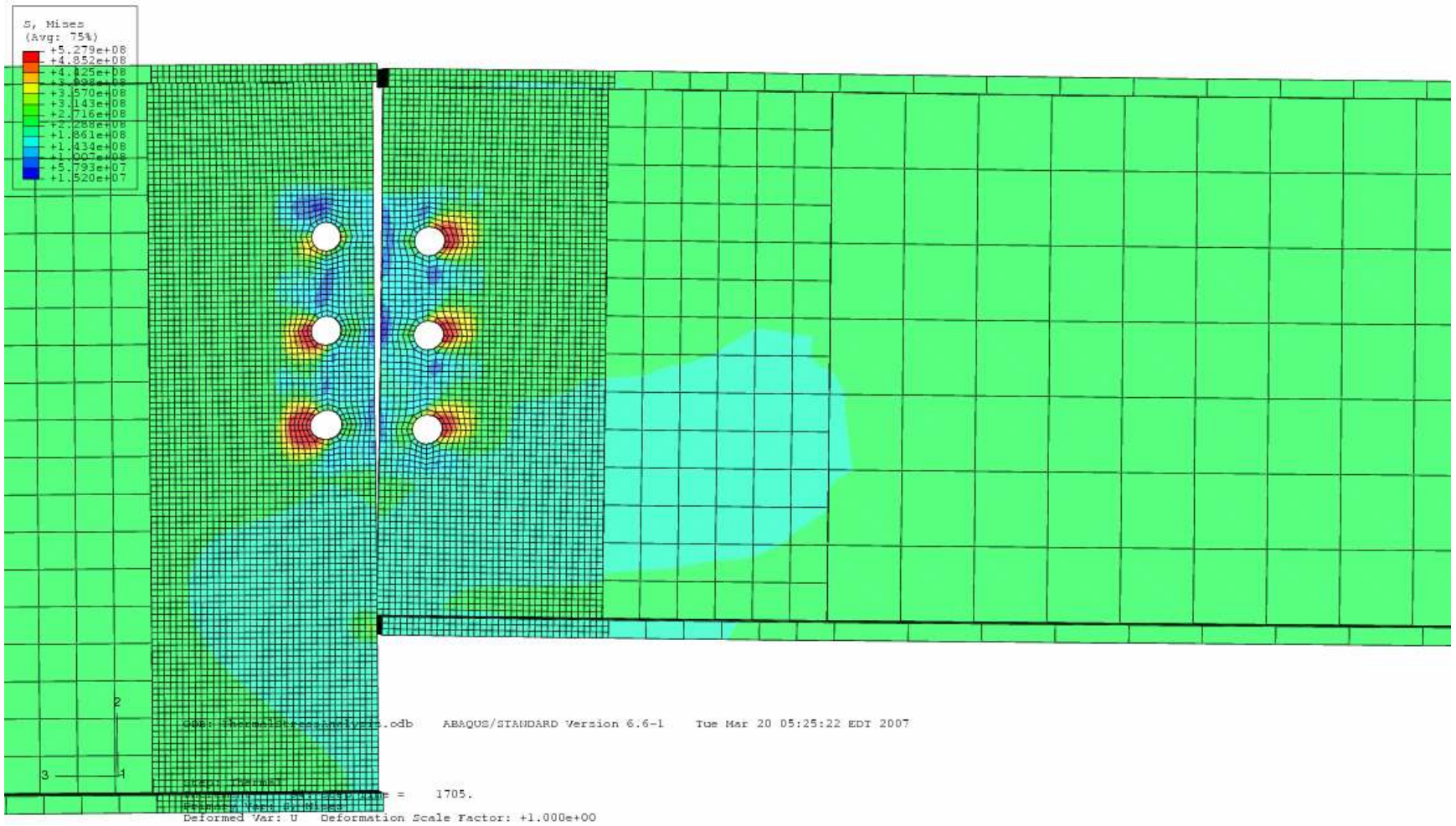

Figure 86: Stress Distribution (30 Minutes of Fire Exposure)

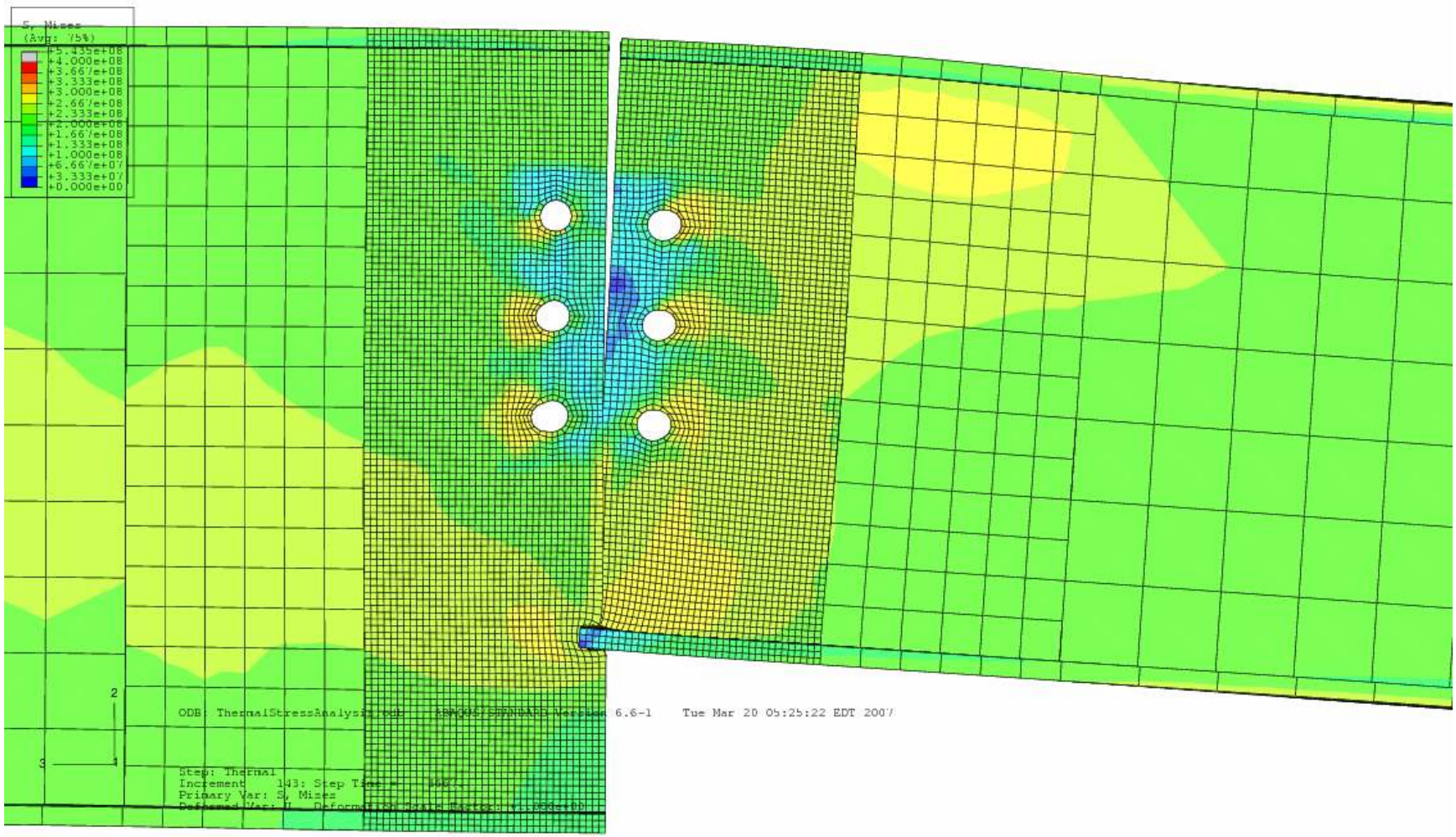

Figure 87: Stress Distribution (1 Hour of Fire Exposure)

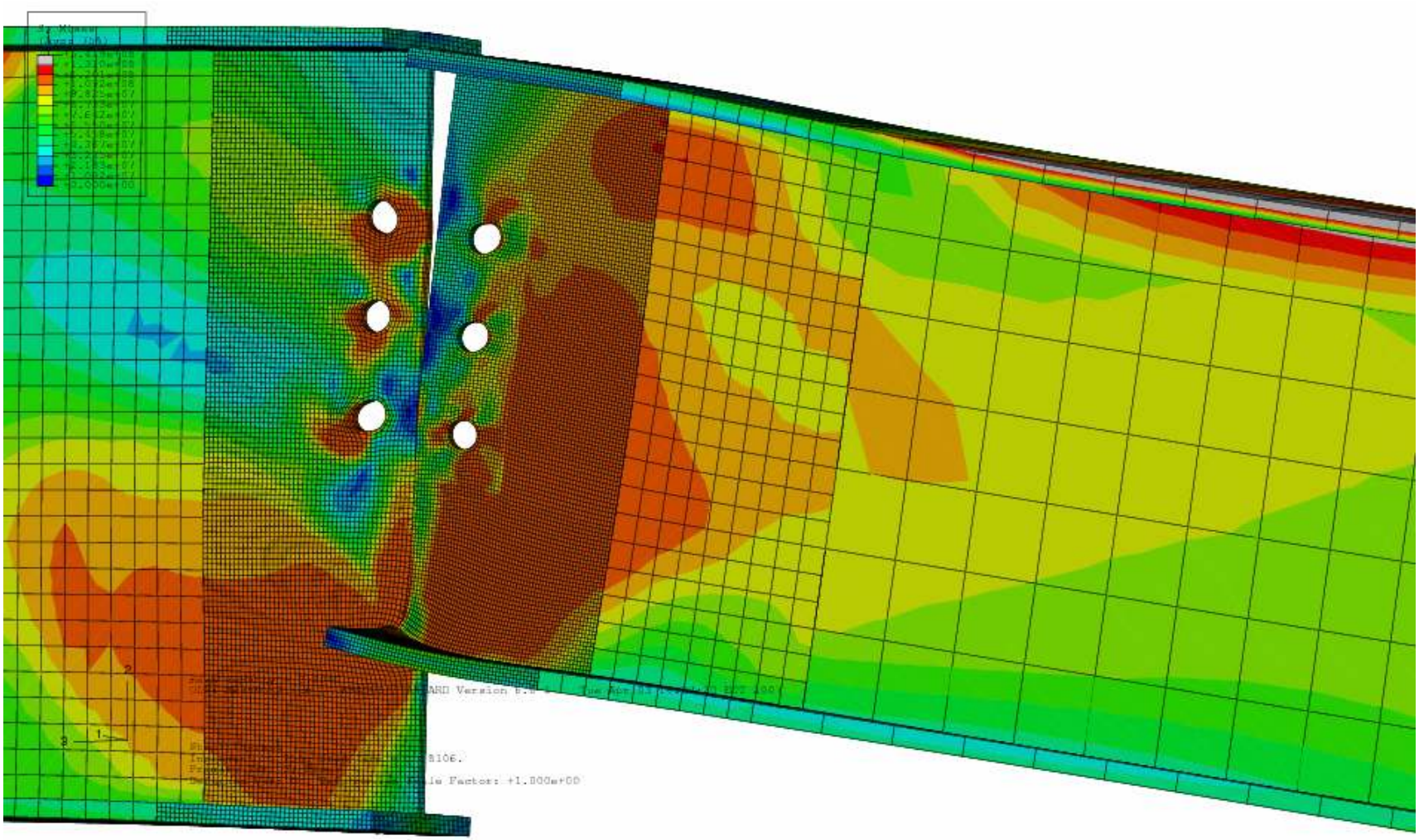

Figure 88: Stress Distribution (2 Hours of Fire Exposure)

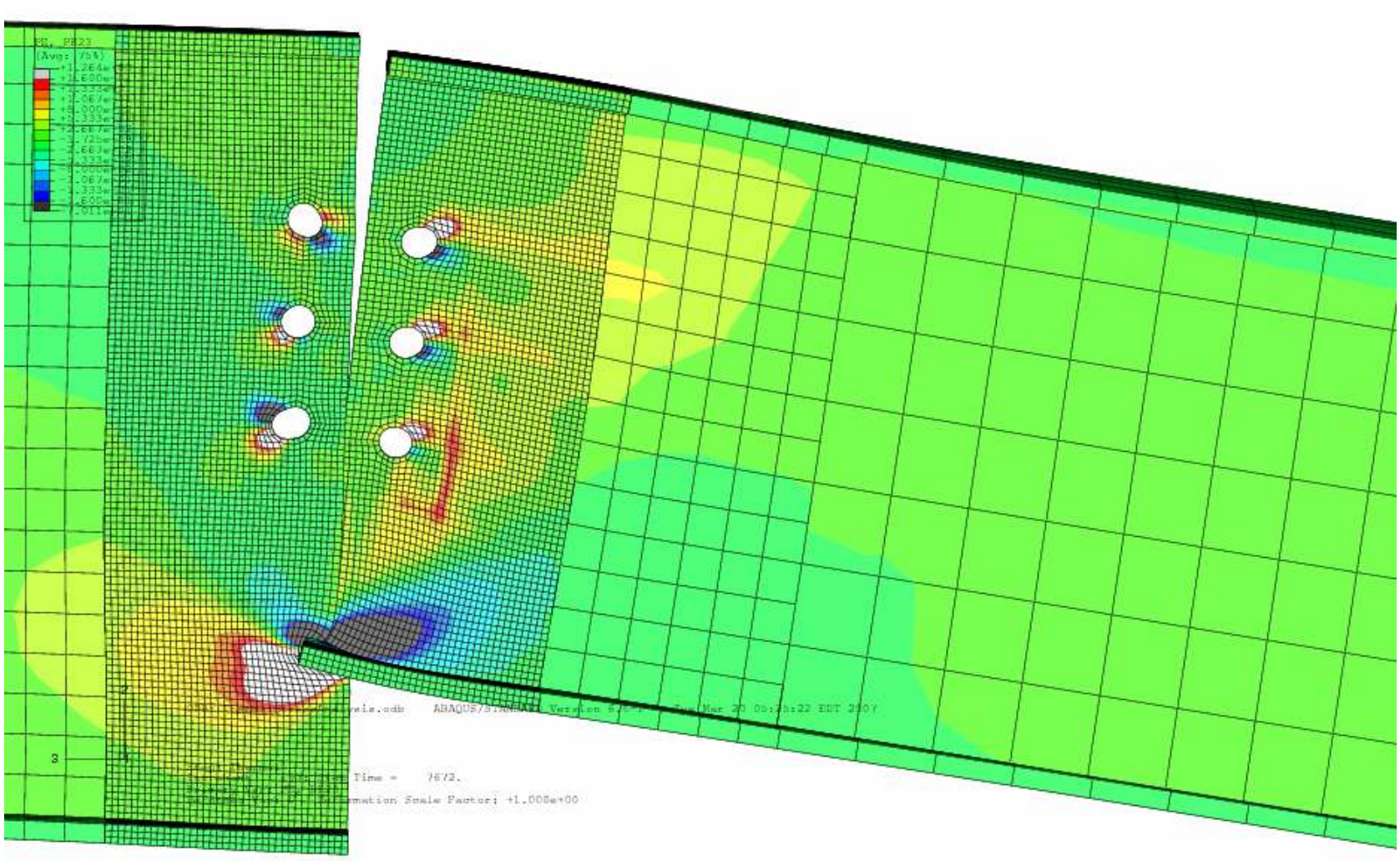

Figure 89: Plastic Shear Strain (2 Hours of Fire Exposure)

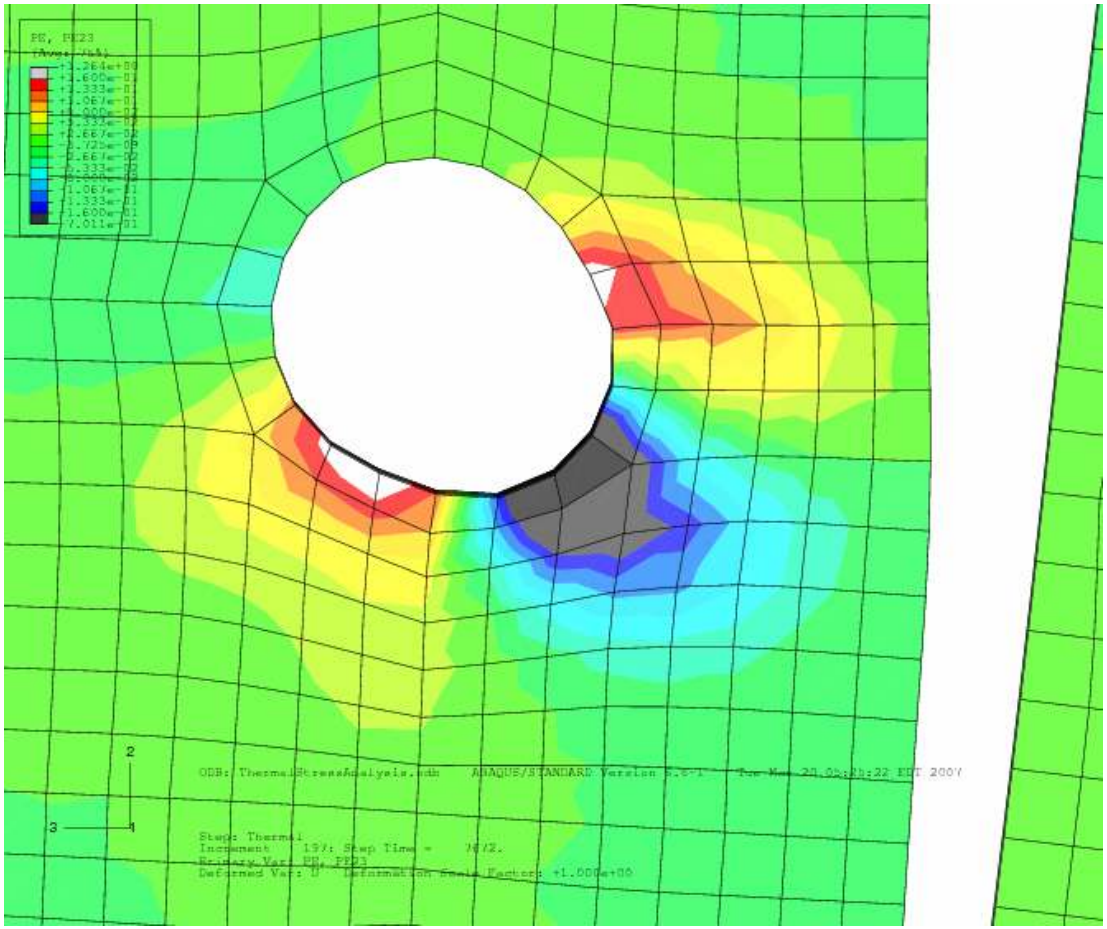

Figure 90: Plastic Shear Strain at the Top Bolt Hole (2 Hours of Fire Exposure)

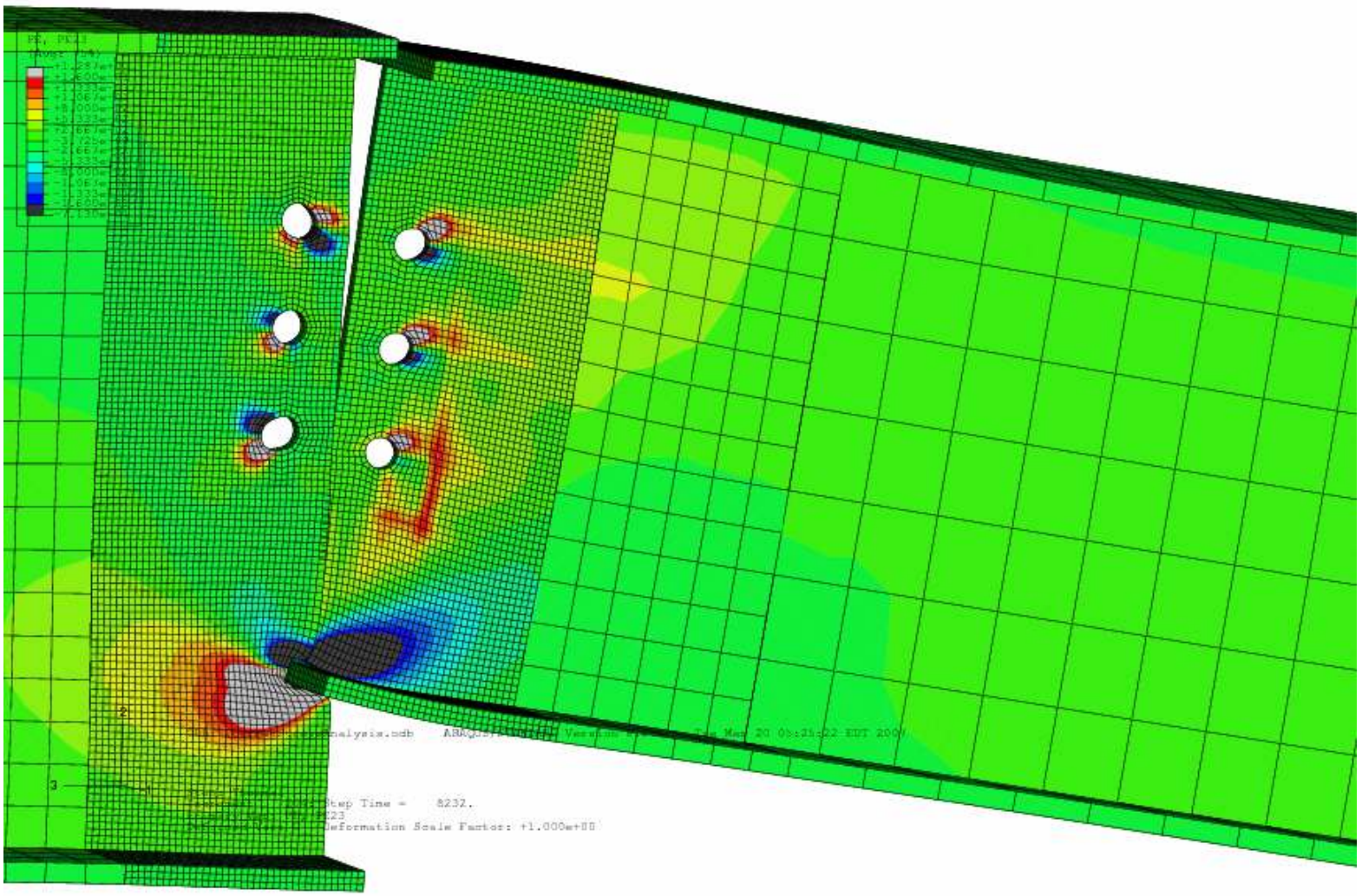

Figure 91: Plastic Shear Strain (2 Hours, 15 Minutes of Model Run Time)

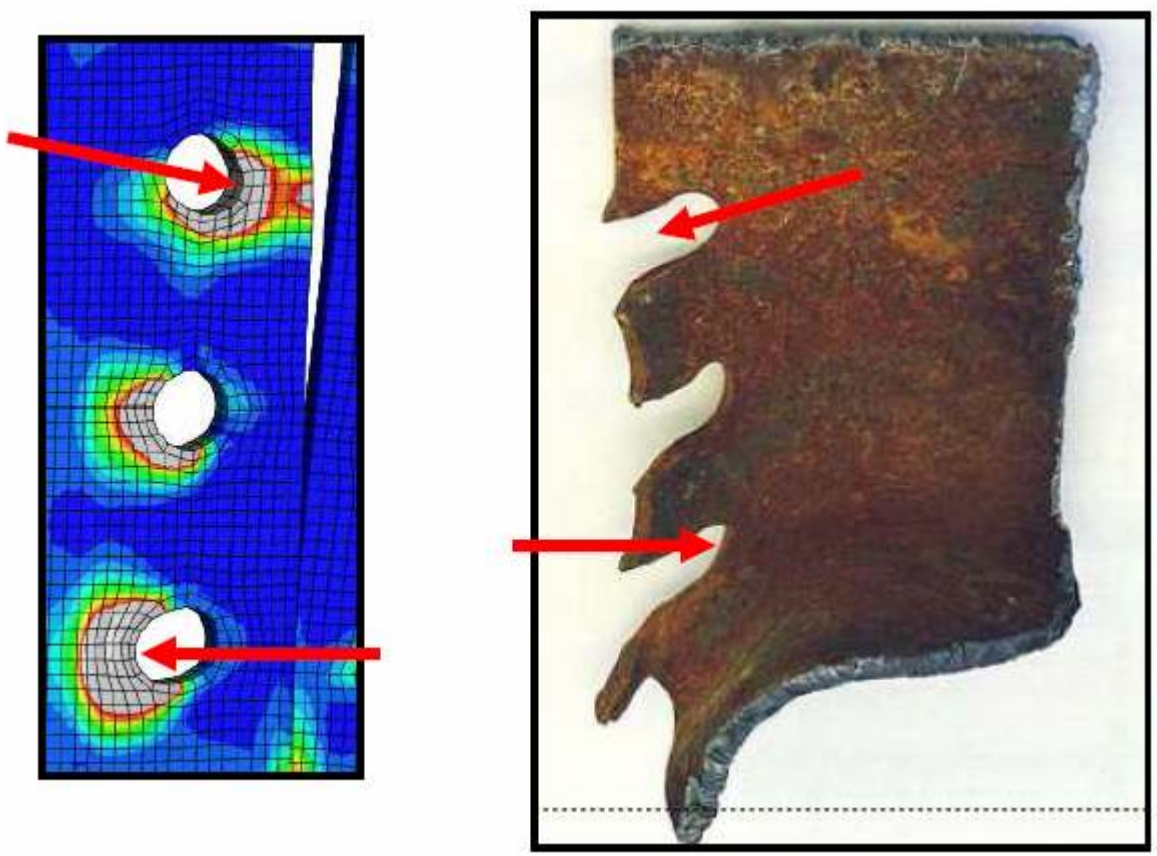

Figure 92: Comparison of FEM Results (Equivalent Strain After 2 Hours of Fire Exposure) Versus Forensic Evidence (Recovered Sample)

Figure 93: Evidence of the Formation of a Fulcrum Point (1 of 2)

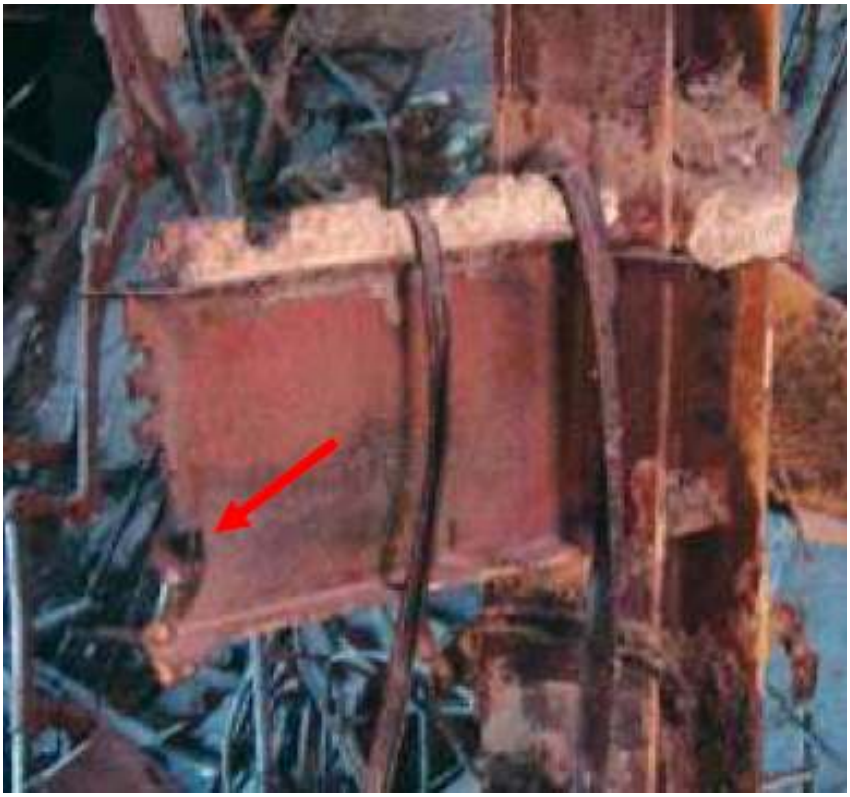

Figure 94: Evidence of the Formation of a Fulcrum Point (2 of 2)

7 Sensitivity Analyses

7.1 Mesh Refinement

According to the sequentially-coupled thermal-stress model, the catastrophic, progressive collapse within WTC 5 occurred at approximately 2 hours into the fire exposure. The meshes of this model were very fine in order to prevent overclosure errors in ABAQUS. For instance, the mesh in the vicinity of the bolt holes was defined so as to create smooth circular holes using hexahedral elements around their circumferences. Therefore, the results described in Section 6 are very accurate. The results may be very accurate, but it is still beneficial to further refine the meshes and determine if the results change by an appreciable margin. If the results do not change by an appreciable margin then it can be concluded that the results are mesh-independent.

Table 11 below compares the number of elements used for particular model parts in the original thermal-stress model (Section 5.5) to that in which the meshes are further refined. Only those model parts in the vicinity of the shear connection were refined. Moreover, the mesh of the floor girder (fine mesh section) was dramatically refined in order for its elements to have comparable sizes to that of the beam stem web (fine mesh section). This is important since the bottom flange of the floor girder penetrates the beam stem web in the formation of the fulcrum point mechanism. Figure 95 below illustrates the refinement of the meshes in the vicinity of the shear connection.

Table 11: Number of Elements Used for Each Model Part (Mesh Refinement)

Model Part	Original Model	Refined Model
Beam Stem (Fine Mesh Section)	16,626	37,611
Beam Stem (Intermediate Mesh Section)	198	423
Beam Stem (Coarse Mesh Section)	244	244
Bolt	964	4,296
Column	304	304
Shear Tab	2,688	8,232
Steel Shim	2,184	2,184
Floor Girder (Fine Mesh Section)	14,706	64,444
Floor Girder (Intermediate Mesh Section)	168	387
Floor Girder (Coarse Mesh Section)	800	800
Total:	**38,882**	**113,248**

A full analysis was performed on four parallel processors of a Sunfire X4100 (quad-core) machine with a FP rating of 117 and 4 GB of RAM (per processor). The memory policy of the job run was set to the maximum for fully devoted processing power. The job was only allowed to run to 3 hours of fire exposure since previous results have rendered the remainder of the analysis as meaningless (i.e., the cooling phase after failure has already occurred).

Figure 96 below shows the plastic shear strain distribution in the vicinity of the shear connection after about 2 hours of fire exposure. The limits of the contour plot are -0.16 to 0.16, which represents the failure limit; any regions of black or white are outside the failure limits for plastic shear strain. Using the "probe" function in ABAQUS, it was determined that the top bolt hole has a maximum plastic shear strain of 0.25. Similar to the original thermal-stress model, it can be concluded that the catastrophic, progressive failure occurred at about 2 hours into the fire exposure. As mentioned, the thermal-stress model experiences a "runaway" failure in which the plastic shear strain reaches values in excess of triple the failure point.

Figure 97 and Figure 98 below show the plastic shear distribution after 2 hours and 15 minutes of fire exposure. The maximum plastic shear strain at the top bolt hole is 0.47. Figure 99 shows the stress distribution in the vicinity of the shear connection. Similar to the previous thermal-stress model, an excessive stress concentration at the weak side of the top bolt hole is observed at this point in time during the fire exposure. This extended analysis has confirmed the results described in Section 6.2, for the intensive refinement of the meshes in the model did not result in any appreciable change in the observed results.

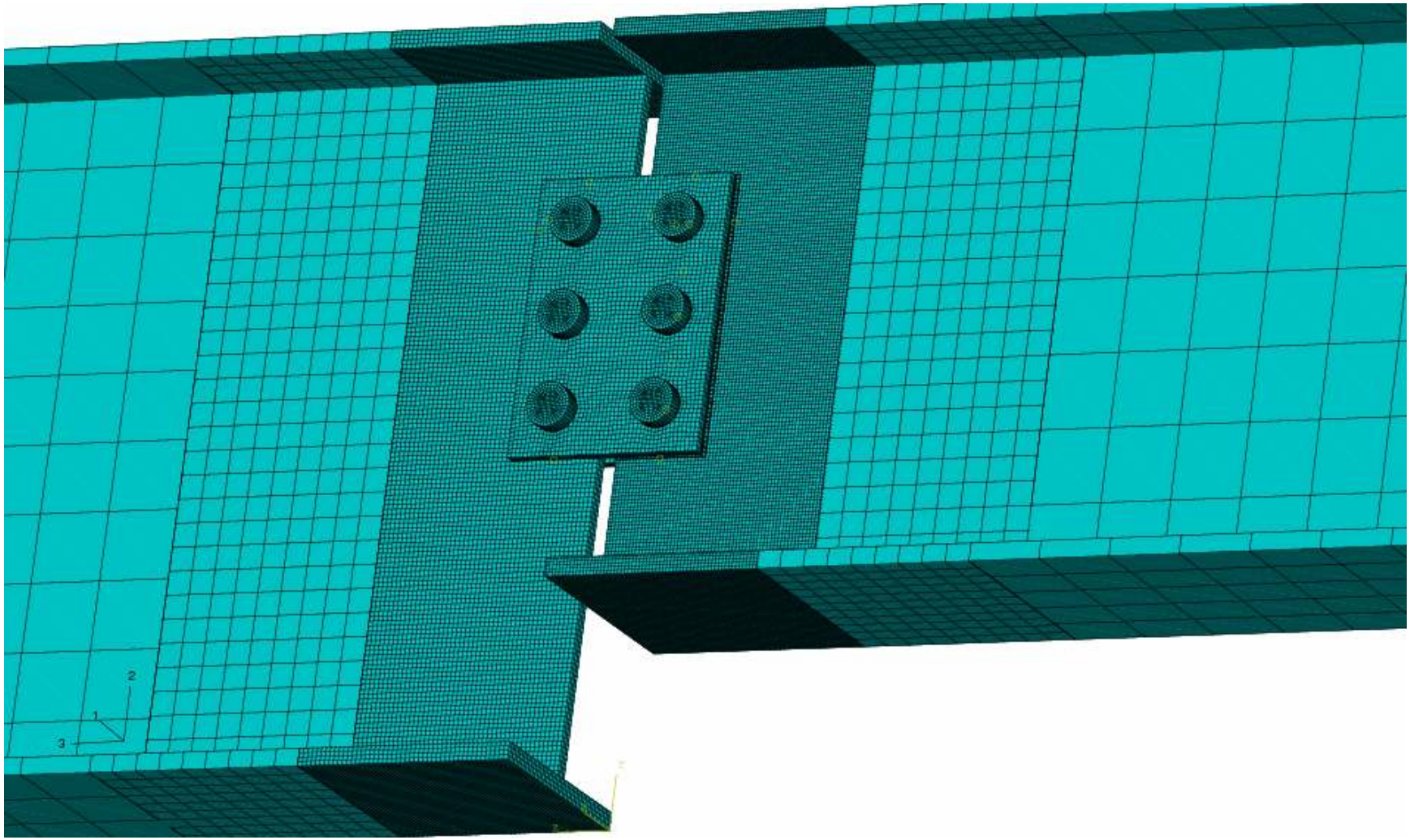

Figure 95: Refined Mesh at the Shear Connection

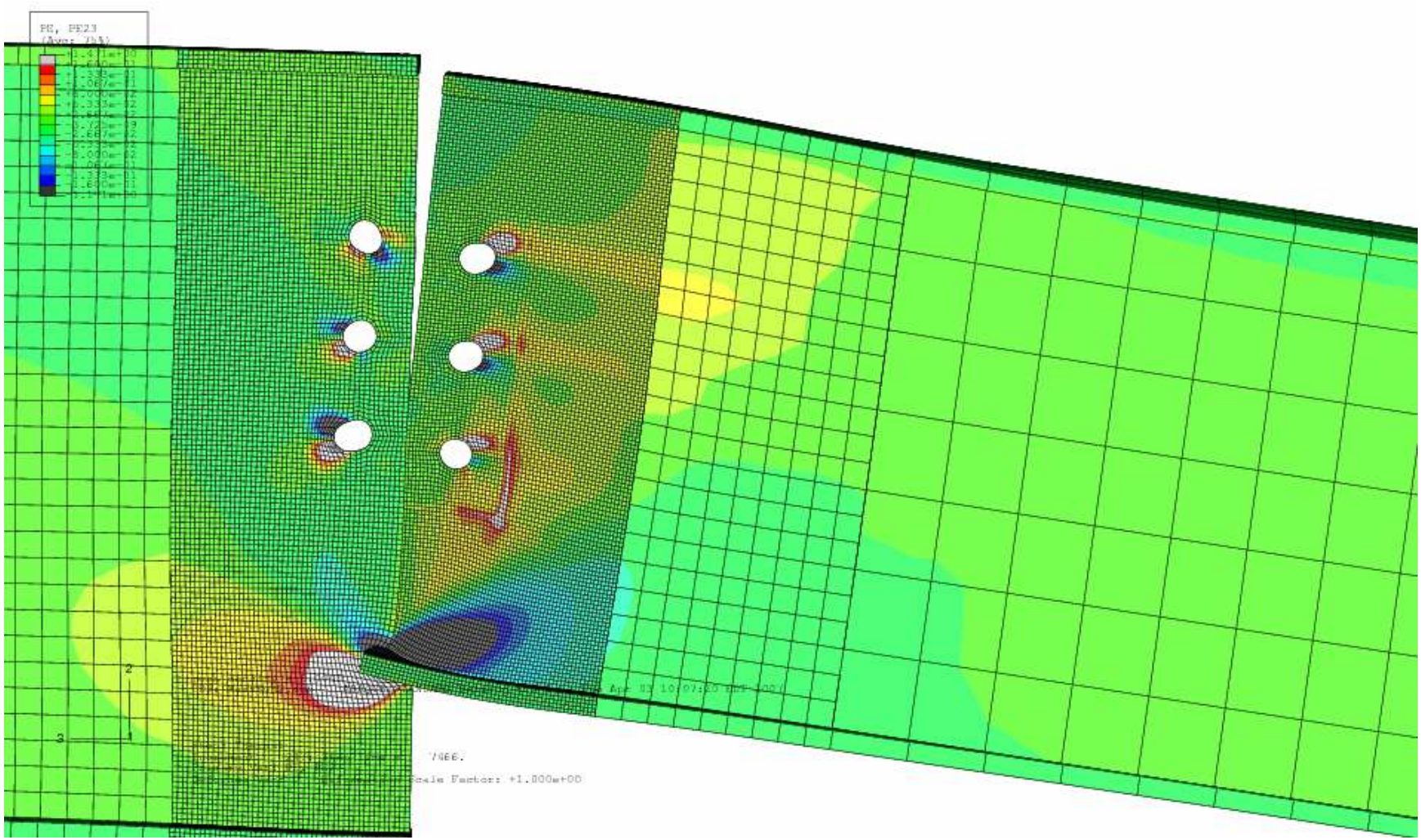

Figure 96: Plastic Shear Strain (2 Hours of Fire Exposure)

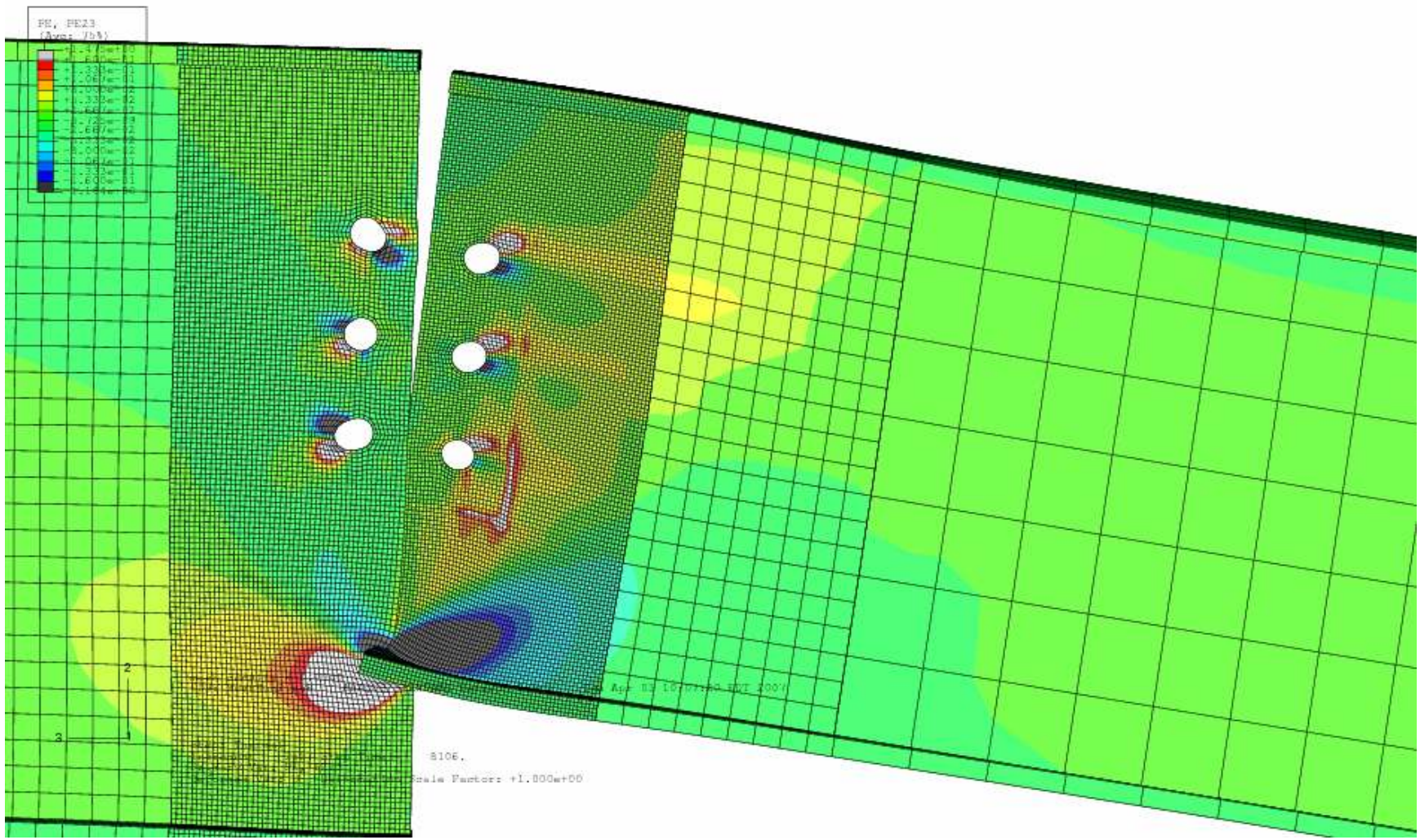

Figure 97: Plastic Shear Strain (2 Hours, 15 Minutes of Fire Exposure)

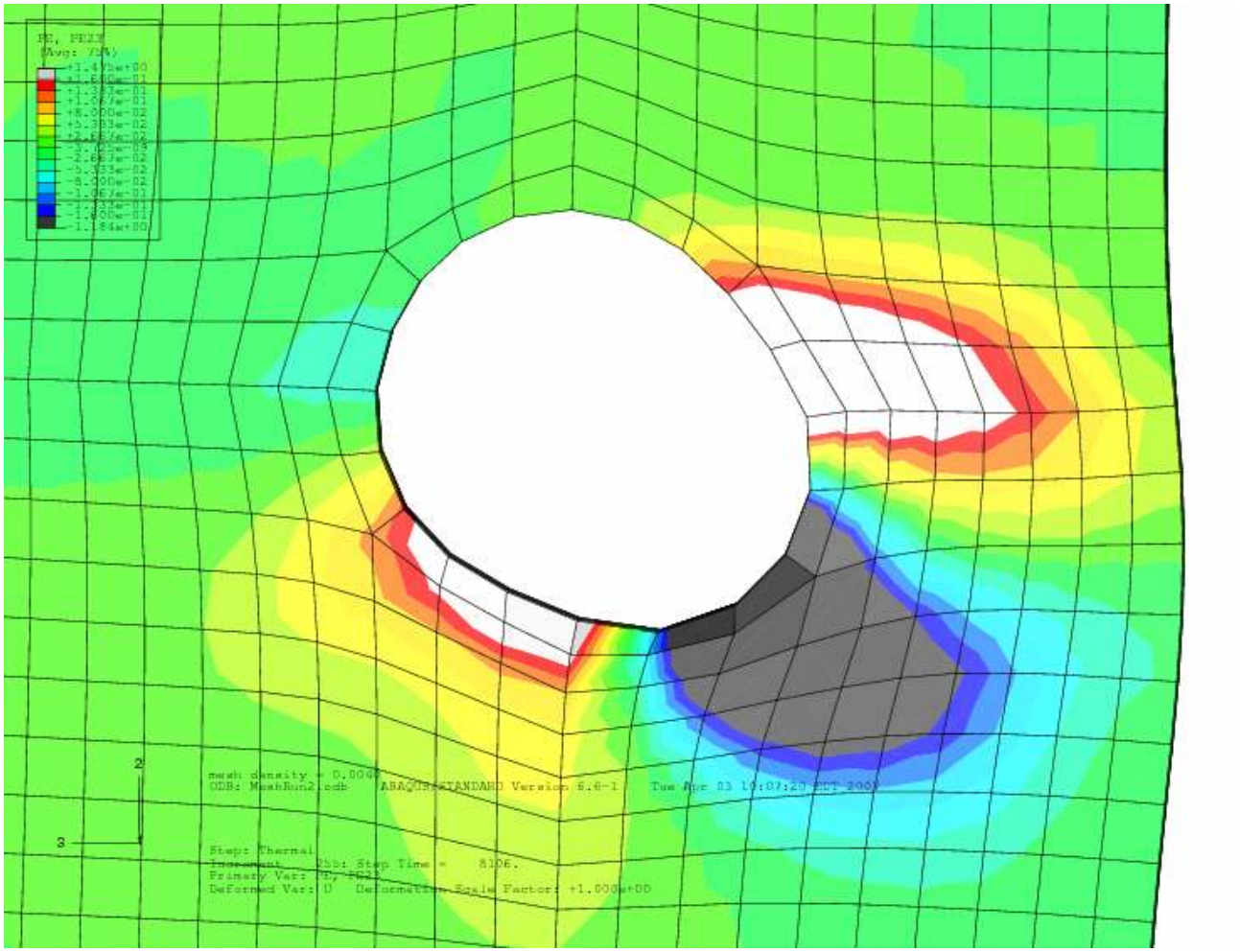

Figure 98: Plastic Shear Strain at the Top Bolt Hole (2 Hours, 15 Minutes of Fire Exposure)

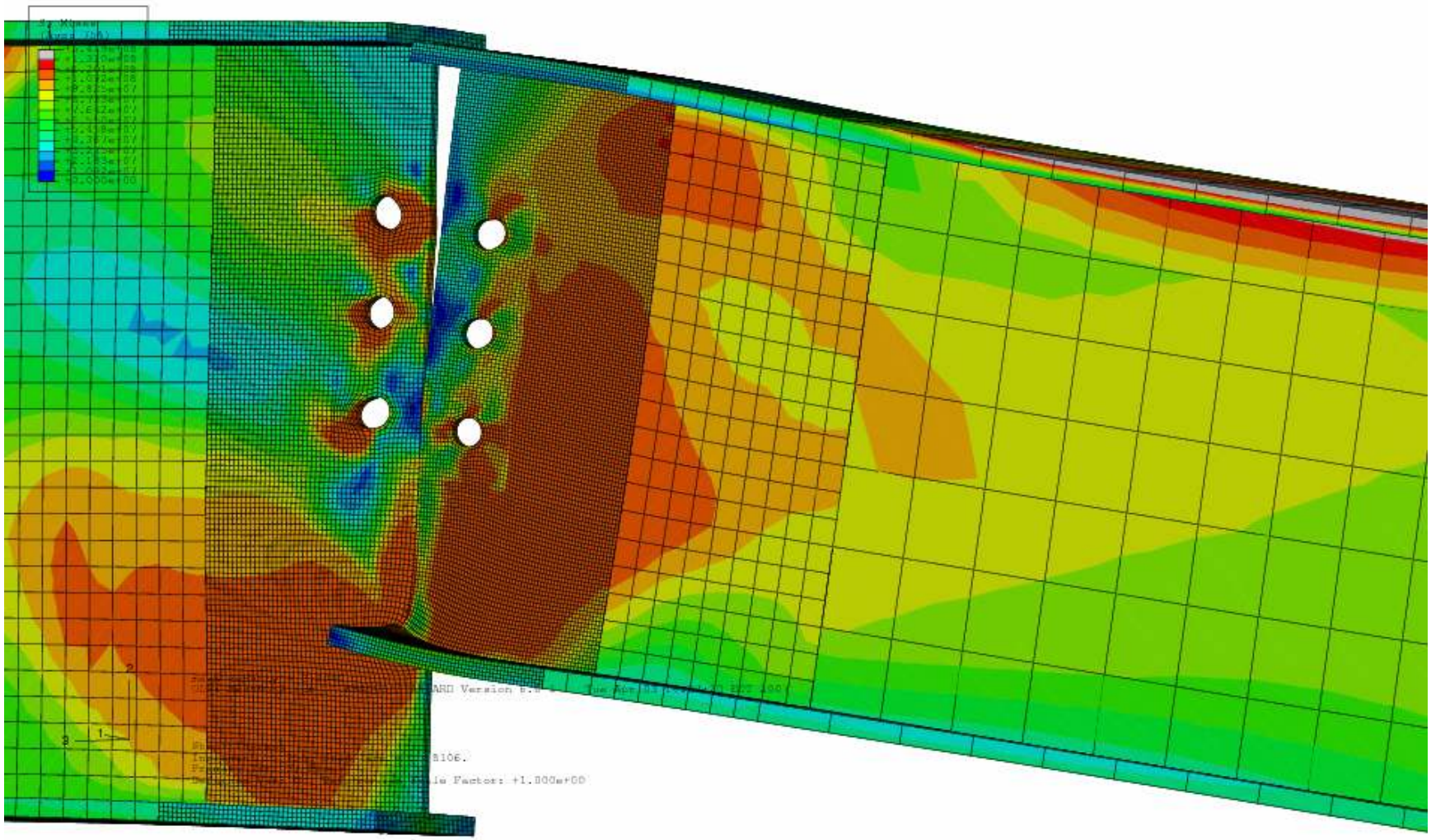

Figure 99: Stress Distribution (2 Hours, 15 Minutes of Fire Exposure)

7.2 Higher Temperature Fire Scenario

ABAQUS was used to derive the steel temperature distribution in three-dimensional space and time when the structural assembly is exposed to the reconstructed fire (see Section 6.1). Since WTC 5 allowed rapid heat venting during its fire exposure by means of impact holes in the roof of the western portion of the building, the peak temperature of the upper gas layer only reached about 720 °C. According to the 2005 NIST study, the peak temperature reached inside WTC 1 was approximately 1000 °C. The peak temperature of 720 °C is the most accurate estimate for the fire that occurred in WTC 5, but it is beneficial to test a higher peak temperature in order to ensure that the thermal model in ABAQUS is stable and follows a reasonable pattern of behavior.

Figure 100 below shows the upper layer gas temperature history derived from CFAST (see Section 4) that served as input into the thermal model described in Section 5.4. This figure also shows a modified temperature history that peaks at 1000 °C; this curve was manually derived using engineering judgment. This higher peak temperature curve was inputted into the thermal model and the results were derived. Figure 101 below shows the structural assembly after 1 hour of fire exposure; the upper limit of the contour plot is 1000 °C. The maximum temperature of the steel in the vicinity of the bolt holes is 600 °C. Figure 102 below shows the structural assembly after 1.5 hours of fire exposure. The maximum temperature of the steel in the vicinity of the bolt holes is 770 °C. Finally, Figure 103 below shows the structural assembly after 2 hours of fire exposure. This is approximately the time in which the steel has reached its peak temperature of 800 °C in the vicinity of the bolt holes for this case.

This sensitivity analysis proves that the thermal model is stable and the steel temperatures calculated in Section 6.1 were not a coincidence. Applying a higher peak temperature does not increase the speed at which the steel heats up or its peak temperature in any type of dramatic fashion (see Table 12 below). Instead, the thermal inertia of the insulation and the steel resists dramatic changes in steel temperature over the course of the fire exposure. The higher temperature fire scenario does produce a higher peak steel temperature, but it is physically reasonable and would be expected upon analyzing the results from Section 6.1.

Table 12: Steel Temperature in the Vicinity of the Bolt Holes

Fire Exposure Time	WTC 5 Fire Exposure	Elevated Fire Exposure
1 Hour	600 °C	600 °C
1.5 Hours	640 °C	770 °C
2 Hours	660 °C	800 °C

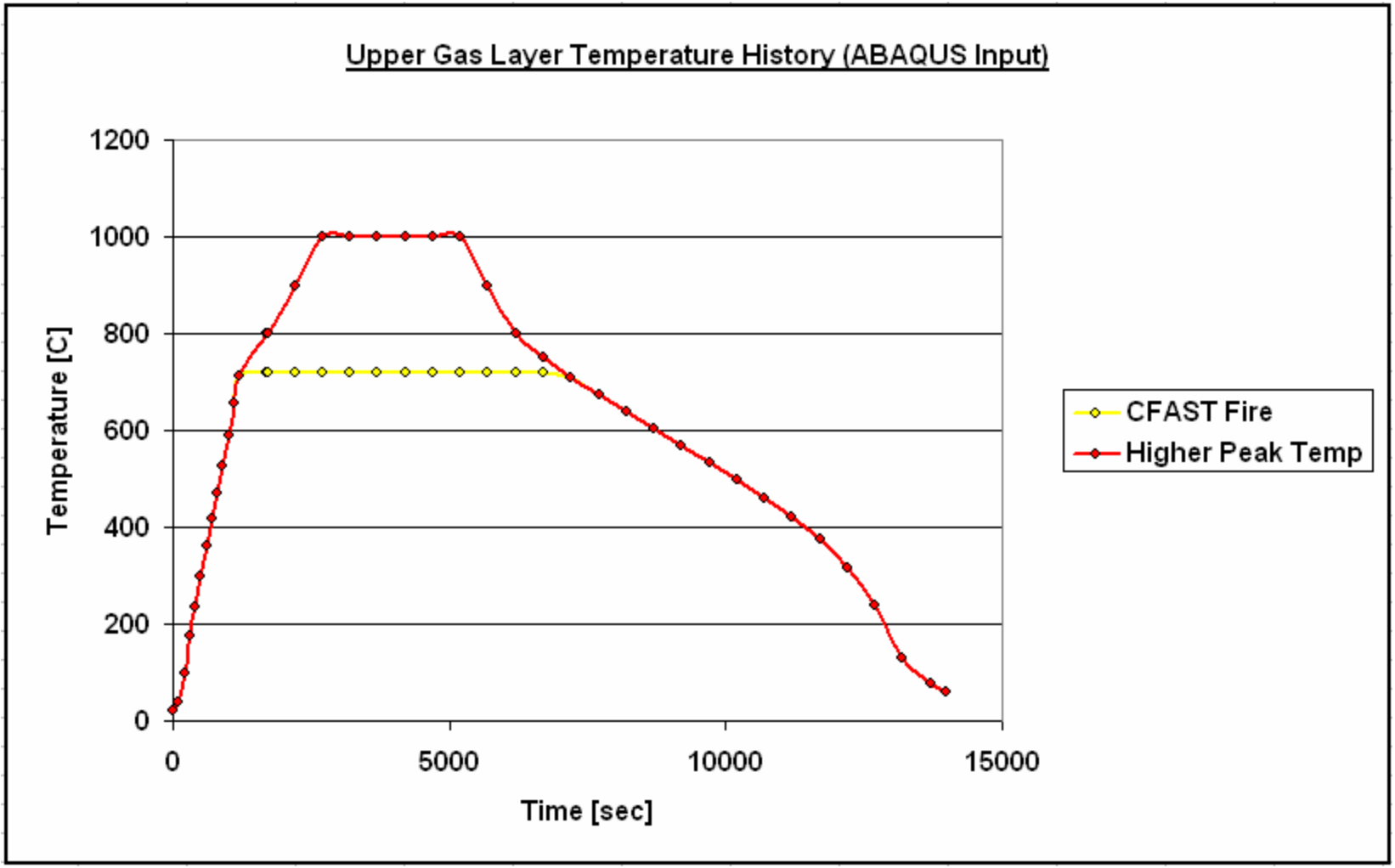

Figure 100: Comparison of Upper Gas Layer Temperature Histories (Greater Intensity Fire Scenario)

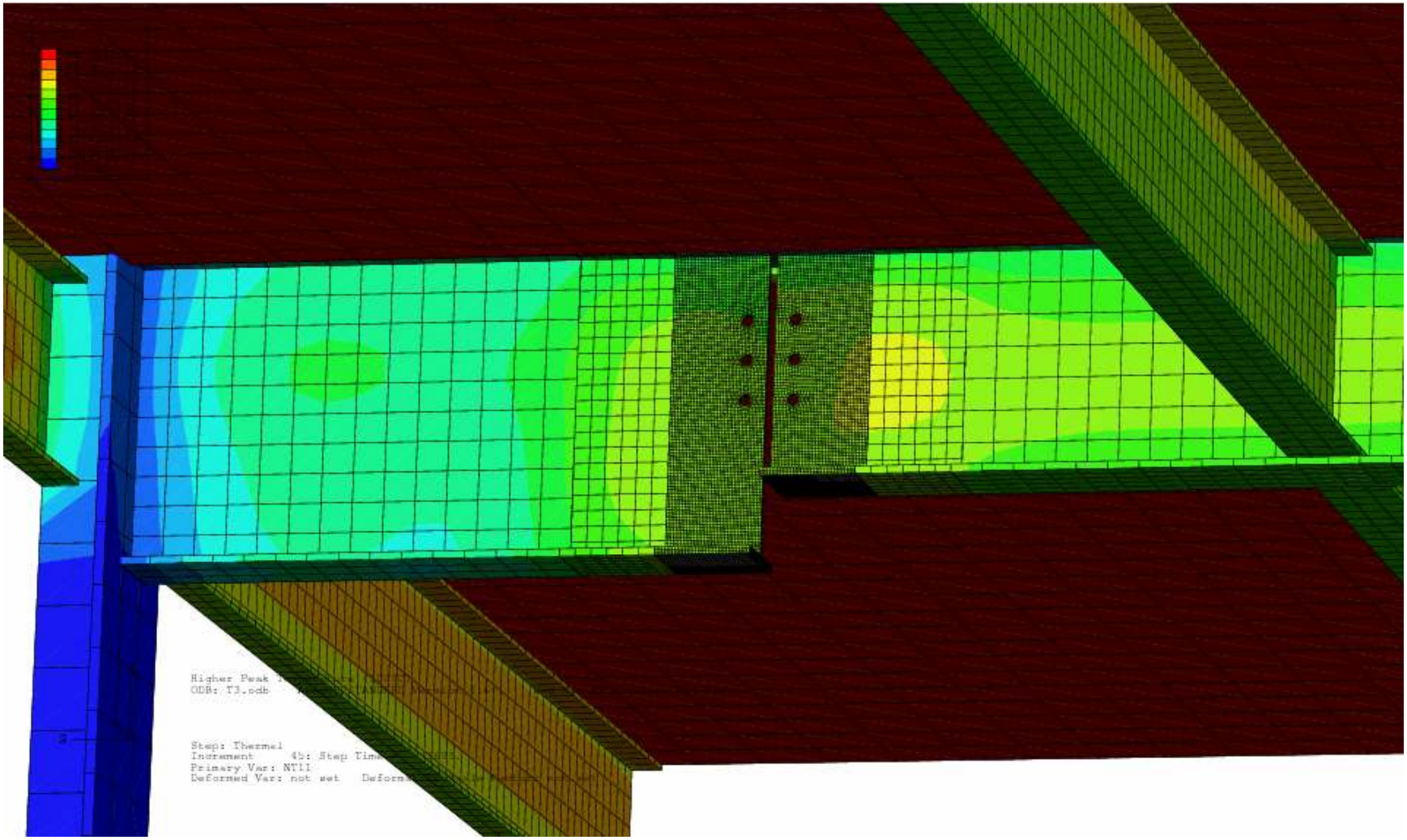

Figure 101: Temperature Distribution After 1 Hour of Exposure (Greater Intensity Fire Scenario)

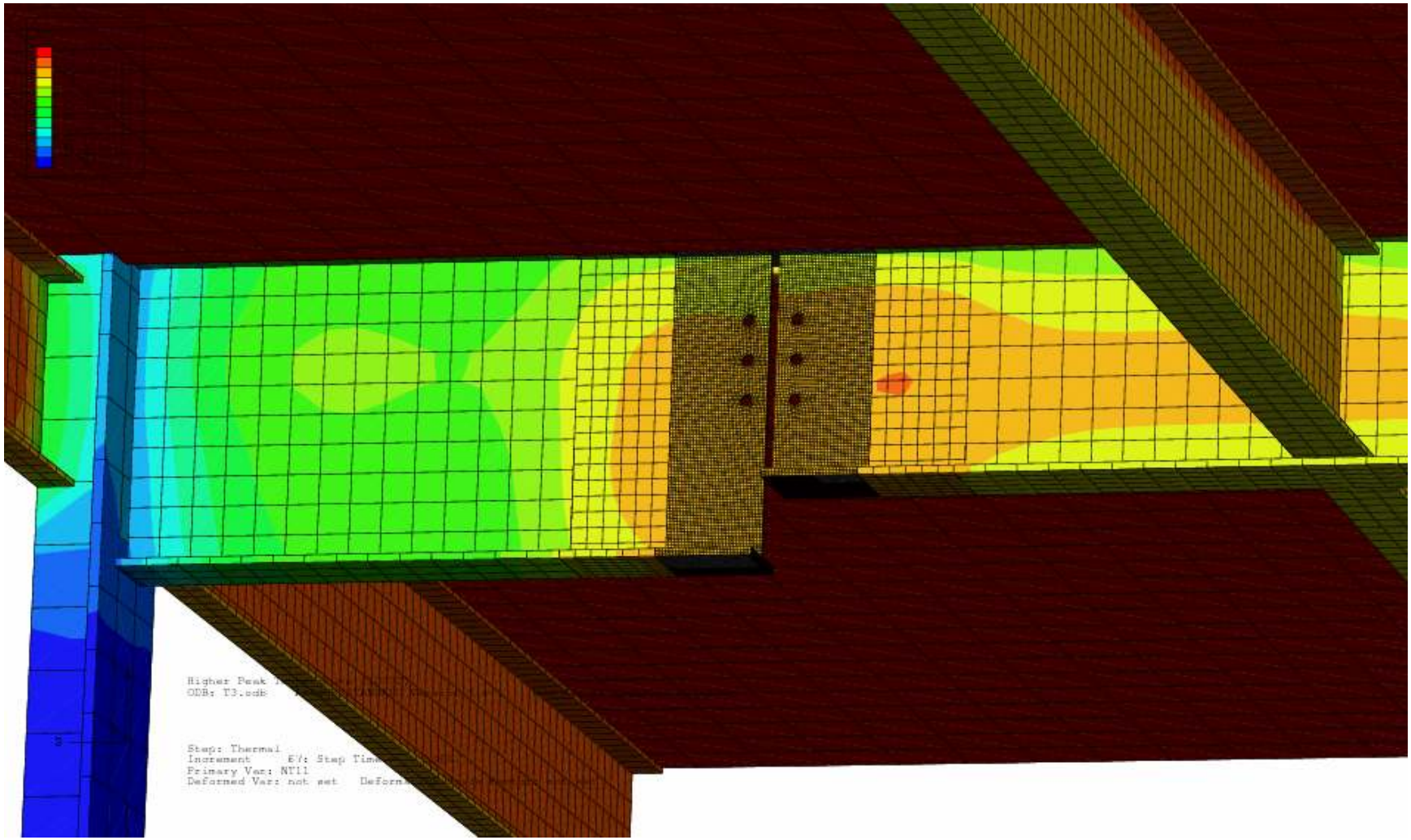

Figure 102: Temperature Distribution After 1.5 Hours of Exposure (Greater Intensity Fire Scenario)

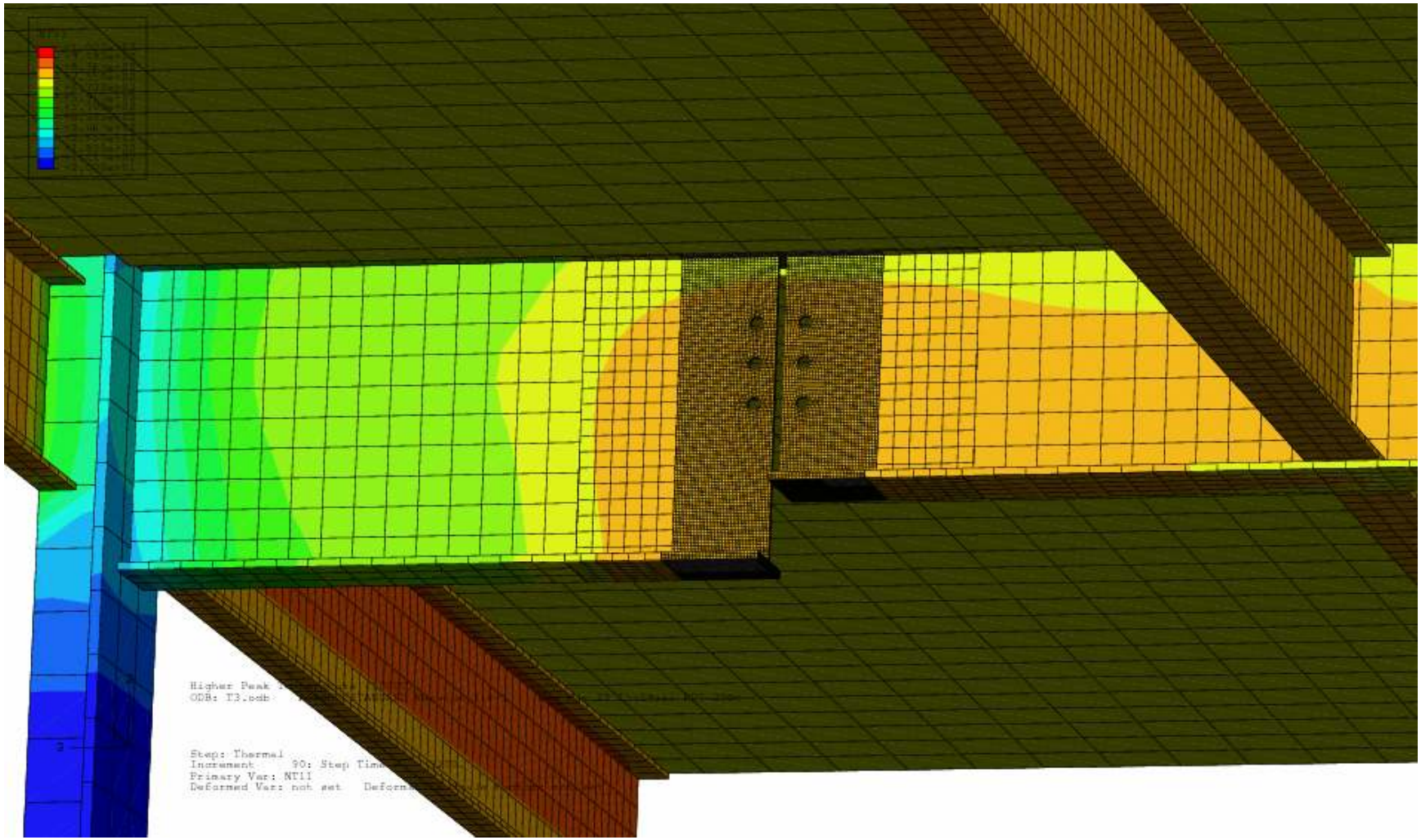

Figure 103: Temperature Distribution After 2 Hours of Exposure (Greater Intensity Fire Scenario)

7.3 Oversized Bolt Holes

According to the AISC Guide to Design Criteria for Bolted and Riveted Joints, bolt holes may be to be oversized for construction purposes. More precisely, larger bolt holes are sometimes used to meet tolerances during erection and to avoid rigid alignment conditions. For 7/8 in. diameter bolts, as were used for WTC 5 at the shear connections, the maximum hole size allowed is 1-1/16 in. diameter. It is valuable to test the use of oversized bolt holes in the WTC 5 thermal-stress model in hope of arresting the fulcrum point mechanism which leads to catastrophic failure.

The bolt holes in the WTC 5 thermal-stress model were changed from 15/16 in. to 1-1/16 in. diameter and the analysis was run. Figure 104 below is a contour plot of the plastic shear strain in the vicinity of the shear connection after 2 hours of exposure. The limits of the contour plot are set as -0.16 and 0.16; plastic shear strain exceeding these limits represents rupture failure according to the failure criterion model. Regions in black and white would be considered outside the failure limits. It is observed that after 2 hours, the top bolt has not reached its failure limit for rupture as of yet. Figure 105 below shows the same contour plot after 2 hours and 15 minutes of fire exposure. It is observed that the top bolt has reached its failure limit and would experience catastrophic failure.

It was hoped that using oversized bolt holes would arrest, or at least significantly delay, the formation of a fulcrum point mechanism by allowing for more translational freedom of the bolt shanks within their respective holes. Yet, the result of the thermal-stress analysis suggests that this provision would only slightly delay the onset of catastrophic failure. In reality, the failure would probably occur at the about the same time as for the smaller holes, for the clear distance is reduced when oversized holes are used. Perhaps the use of *slotted holes* may be beneficial, for they may allow for large rotation at the shear connection with limited bearing stress. The implementation of slotted holes represents the introduction of new geometry into the finite element model, as opposed to modifying existing geometry. Hence, the implementation of slotted holes into the thermal-stress model would require major modifications and is out of the scope of this research.

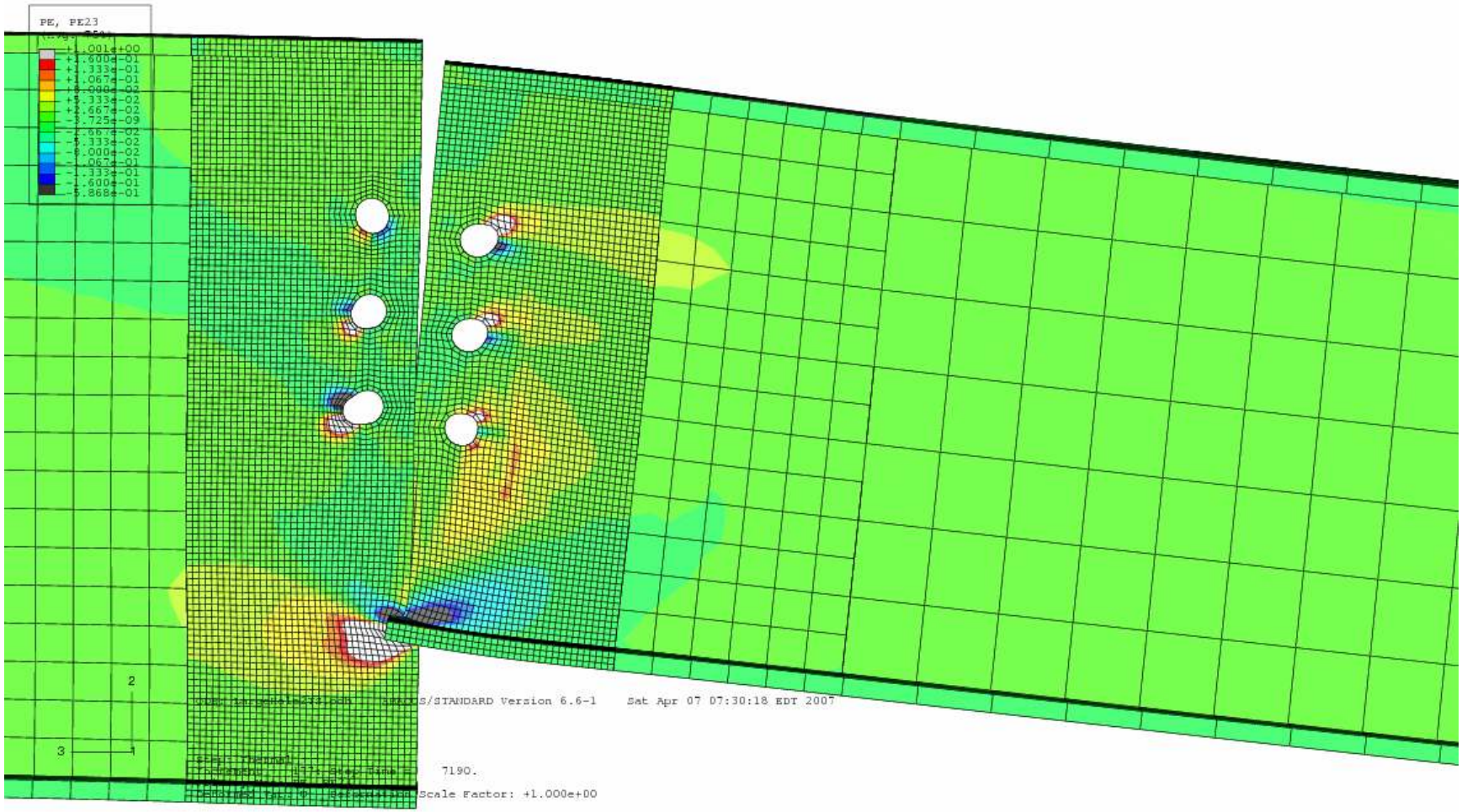

Figure 104: Plastic Shear Strain (2 Hours of Fire Exposure)

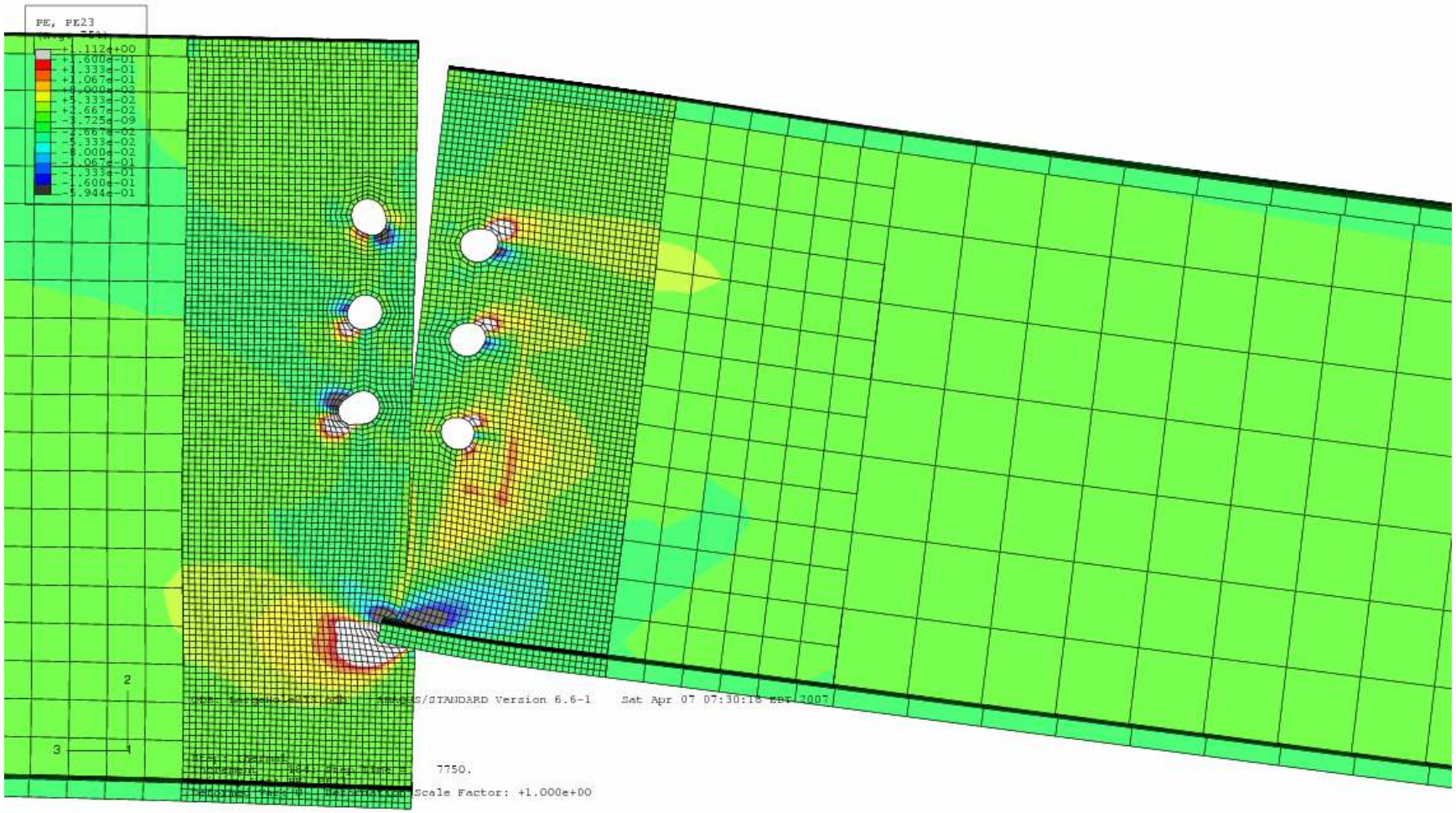

Figure 105: Plastic Shear Strain (2 Hours, 15 Minutes of Fire Exposure)

7.4 Thermal Creep Strain

Creep is the term used to describe the time-dependent deformation of materials under constant load. Under most conditions, creep is only a concern for structural members with very high permanent loads. Moreover, creep is negligible in structural steel at normal temperatures. However, creep becomes very significant at steel temperatures over 500 °C and is highly dependent on the stress level. At high temperatures, creep deformations in steel can accelerate rapidly, leading the plastic behavior and "runaway" failure (Buchanan 144-145).

Creep strain is not usually included explicitly in structural fire protection engineering calculations because of its complexity and the lack of sufficient input data. Any structural analysis computer program for elevated temperature is already very complex without having to explicitly include the effects of time-dependent behavior. The effects of creep are usually allowed for implicitly by using stress-strain relationships which include an allowance for the amount of creep that could be expected in a structural member exposed to fire (145).

Since the data available for thermal creep strain are extremely limited, the author chose to run the finite element models without this effect explicitly included. Yet, it is beneficial to perform a sensitivity study in which this phenomenon is explicitly included in the sequentially-coupled, thermal-stress model of the structural assembly in WTC 5. The deformation of steel at elevated temperatures is dependent upon three components of strain which are shown in Equation 11 (194).

$$\Delta\varepsilon = \varepsilon_{th}(T) + \varepsilon_{\sigma}(\sigma, T) + \varepsilon_{cr}(\sigma, T, t) \qquad (11)$$

$\varepsilon_{th}(T)$: Thermal expansion component

$\varepsilon_{\sigma}(\sigma, T)$: Stress-related strain

$\varepsilon_{\sigma}(\sigma, T, t)$: Thermal creep strain

The models described in this research have fully integrated the effects of thermal expansion and stress-related strain. For this sensitivity analysis, the third and least understood component of strain will be integrated. SGH has developed an algorithm for creep strain that is compatible with the finite element software ANSYS. This algorithm was adapted for use in ABAQUS and is shown below (Equation 12).

$$\frac{d\varepsilon}{dt} = C_1(T)\sigma^{C_2(T)}t^{C_3(T)} \qquad (12)$$

$T =$ Temperature [°C]

$\sigma =$ Von Mises equivalent stress [MPa]

$t =$ Time [sec]

$C_1(T)$, $C_2(T)$, and $C_3(T)$ are temperature-dependent parameters that can be expressed as follows:

$$C_1(T) = \frac{1}{100}a(T)b(T)\left(\frac{1}{60}\right)^{b(T)}\left(\frac{70.5}{\sigma_{uRT}}\right)^{c(T)}$$

$$C_1(T) = c(T)$$

$$C_3(T) = b(T) - 1$$

$$a(T) = 0 \quad \text{(for T < 350 °C)}$$
$$a(T) = 10^{-(6.1+0.00573T)} \quad \text{(for 350 °C < T < 500 °C)}$$
$$a(T) = 10^{-(13.25-0.00851T)} \quad \text{(for 500 °C < T < 725 °C)}$$

$$b(T) = -1.1 + 0.0035T \quad \text{(for T < 725 °C)}$$

$$c(T) = 2.1 + 0.0064T \quad \text{(for T < 725 °C)}$$

σ_{uRT} = Reference ultimate stress [MPa]

The expressions shown above were integrated into the thermal-stress model in ABAQUS. It was determined that the "runaway" failure described in Section 6.2 still occurs at approximately 2 hours into the fire exposure (see Figure 106 below). In other words, adding the effects of thermal creep strain does not change the results described in Section 6.2 as it pertains to catastrophic failure of the shear connection. This makes physical sense because creep is time-dependent; the stress reversal due to the formation of a

fulcrum point mechanism occurs very rapidly and leads to rupture failure within a few minutes following. Therefore, the effects of thermal creep strain would be minimal in this case granted the limited time in which it may occur. However, the effects of thermal creep strain are observed in another -less critical- aspect of the thermal-stress behavior. It is observed that the deformation of the bolt holes in the downward direction is more extensive as compared to the results described in Section 6.2 (see Figure 106 below). This is physically reasonable considering that gravity loads act upon the assembly over a prolonged period of time when the steel temperatures are high.

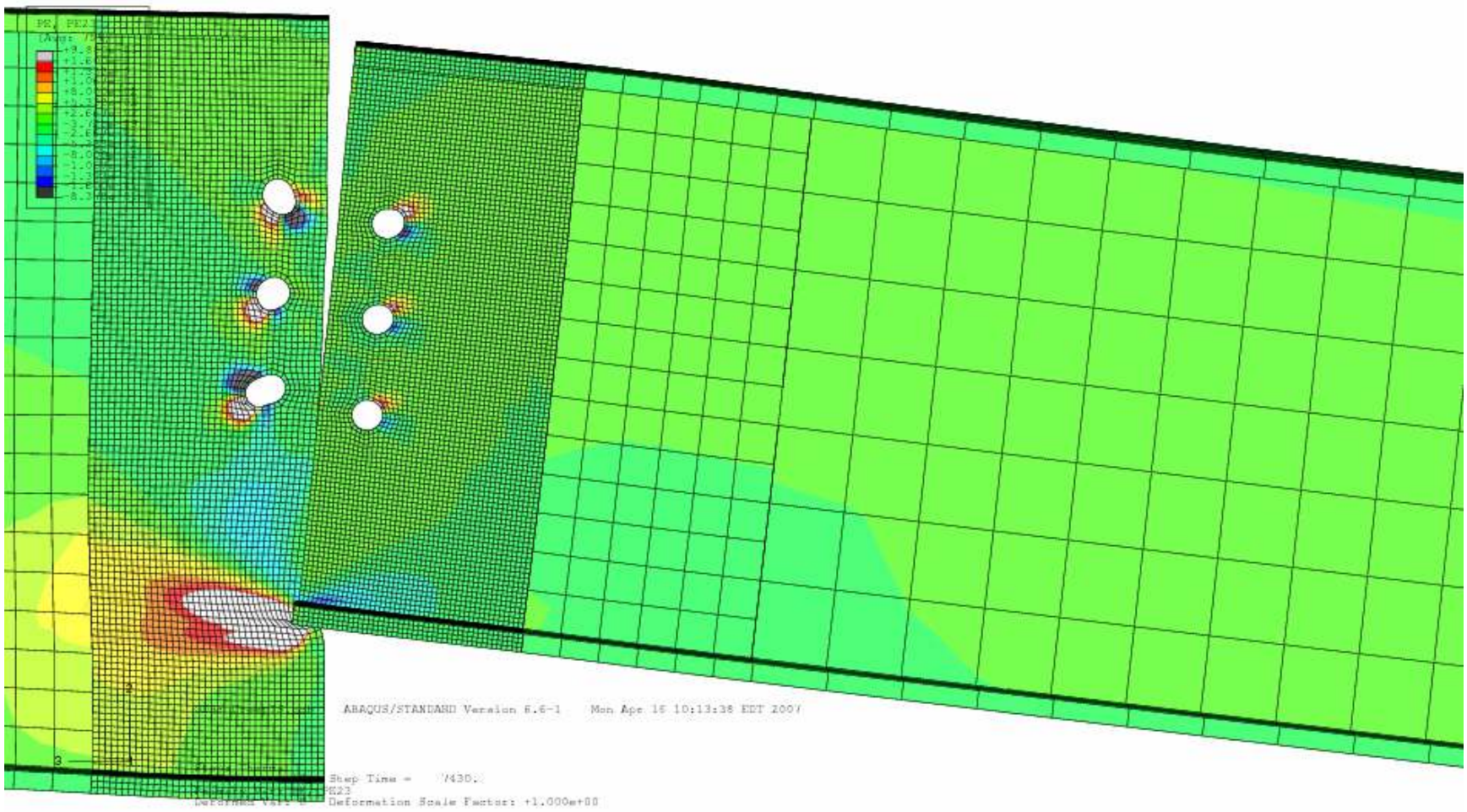

Figure 106: Plastic Shear Strain with Thermal Creep Strain Included (2 Hours of Fire Exposure)

8 Conclusions

8.1 Structural Fire Performance of WTC 5

The fire that occurred within WTC 5 has been estimated using relevant data and computer modeling. More precisely, the upper layer gas temperature history that engulfed the structural assembly on the 8th floor (the initial location of collapse) was approximated. The official construction documents of WTC 5 were referenced to determine the dimensions of the steel assembly accurately. Using this information, finite element models were created. These models included a thermal, mechanical, and a thermal-stress type. The thermal model captured the heating behavior of the insulated steel assembly when exposed to the reconstructed fire and its following cooling phase. The mechanical model captured the stress behavior of the steel when gravity loads are applied. Modifications were made to the mechanical model, and the output result from the thermal model was used to create a sequentially-coupled, thermal-stress model. This model was used to derive the structural fire performance of WTC 5 when exposed to the reconstructed fire.

Results of the thermal-stress model demonstrate that WTC 5 experienced a catastrophic, progressive structural collapse during the heating phase of its fire exposure. This model predicts a "runaway" bolt rupture failure at approximately 2 hours of fire exposure. It is not the precise time of failure which is paramount, but the fact that the structure failed during the heating phase, as opposed to the cooling phase, which would have been expected based upon current knowledge and experience of structural fire performance. In a general sense, this early failure is very surprising, but in view of the construction details of WTC 5, this failure is physically reasonable. More precisely, the Gerber beam design used for floors 5 through 8 of WTC 5 possesses certain details which make it inherently weak in terms of fire endurance.

The Gerber beam design isolates the shear connection from its heat sink to the rest of the "cooler" structure via the column. The results of the thermal model demonstrate how this isolation causes the shear connection to become 450 °C hotter than the interface at the column after one hour; this gradient reduces to 400 °C after two hours (see Figure 75 and Figure 76 above). It is apparent that locating the connections at the column interfaces would have kept the connections from reaching highly-elevated temperatures during the fire exposure, for they would have been able to dissipate heat efficiently. In the case of the Gerber beam design, the only way for a connection to dissipate its heat is to conduct it across the relatively-thin thermal mass (i.e., the beam stem) to eventually reach the heat sink. This heating phenomenon is exacerbated by the fact that the shear connection has a relatively-high surface area to volume ratio, which allows for efficient heating via turbulent convection from the hot upper layer gases. Moreover, the beam stem itself was heated by the fire exposure which reduces the thermal flow from the shear connection toward the column.

As the structural assembly on the 8th floor heats up in the first hour of the fire exposure, the floor girder undergoes thermal expansion, which causes relatively harmless

compressive stress concentrations to form on the strong side of the bolt holes (see Figure 86 above). As the fire exposure approaches the 2-hour mark, the decrease in the rigidity of the girder begins to "outpace" the thermal expansion and the girder deflects significantly. The deflection causes the lower flange of the floor girder to form a fulcrum point mechanism which leads to the top bolt rupture failure at approximately 2 hours of fire exposure (see Figure 88 and Figure 89 above). Once the top bolt experiences this "runaway" rupture failure, the two remaining bolts would undergo a stress reversal and rupture quickly in sequence ("unzipping" failure).

The initial structural collapse on the 8th floor of WTC 5 due to fire exposure alone led to the progressive collapse through the 5th floor below it. These collapses were due to the kinetic energy of the falling debris from the 8th floor and subsequent floors below. It is likely that this collapse would have progressed all of the way down to the ground level, if it had not been for a particular architectural feature of the building. In Figure 1 above, it is observed that the 4th floor cantilevers toward the adjacent streets. By observing the structural details of WTC 5, it was determined that moment-type connections were used on the 4th floor to accommodate this cantilever design (see Figure 39 above).

The moment-type connections on the 4th floor were most likely able to arrest the progressive collapse of the four floors above it. More precisely, the moment-type connections were probably able to prevent beam stem rupture, for the strong flange connections were capable of preventing a fulcrum point mechanism from occurring. Whereas large deflections due to fire exposure on the 8th floor caused rupture failure, floors 7 through 5 experienced rupture failure from the large girder deflections due to the impact of falling debris. The moment-type connections on the 4th floor most likely prevented these large deflections, for the entire beam stem and floor girder assembly would have effectively acted as a single fixed-ended span.

The 9th floor of the building experienced a similar fire exposure as the 8th floor, but it did not collapse. In fact, forensic evidence demonstrates that the beams reached the catenary phase and remained stable (see Figure 21 above). The only difference between the structural assembly on the 8th floor and that on the 9th floor is the location of the shear connections. On the 9th floor conventional-type construction was used in which the floor girders are connected directly to the columns. This design feature allows for efficient dissipation of heat at the connections during a fire exposure. The 8th floor utilized the Gerber beam design, which isolated the shear connections from their heat sinks and led to a rapid decrease in steel strength in the vicinity of the connections.

8.2 Critical Implications of Findings

It has been concluded that the catastrophic, progressive structural collapse that involved four floors of WTC 5 most probably occurred during the heating phase of the fire exposure, at about 2 hours from the time of ignition. WTC 5 utilized the Gerber beam design which is currently used for approximately 20,000 existing steel buildings in the U.S. and continues to be a popular design option.

The Gerber beam design has application to high-rise buildings. During a fire event in a high-rise building, only those occupants on the floors in the direct vicinity of the fire are instructed to evacuate via relatively narrow stairways. Other occupants are ordered to stay inside the building and wait to egress during this phased-type evacuation. In fact, those occupants on the floors near the fire are often merely relocated to another floor of the building. Phased evacuations are necessary since high-rise building egress systems are never designed for full evacuation of all the occupants at once; otherwise, the stairways would need to be extremely wide. Thus, occupants of a high-rise building may be required to stay inside the building many hours after a fire has started. In the 1993 bombing incident at WTC 1, it took approximately 6 hours to evacuate the entire building (Blossom 76).

The Gerber beam design has application to hospitals. During a fire event in a hospital, a "defend-in-place" strategy is utilized in which patients are kept inside the building. Moving patients out of the hospital would take an extended amount of time and may adversely affect the welfare of those patients (e.g., patients on life support). Thus, the fire alarm system in a hospital is most always set to private mode and patients not located on the fire floor are not moved. This "defend-in-place" strategy relies upon the fire department to extinguish the fire, and then patients are slowly evacuated. It should be noted that firefighters enter buildings during the heating phase of fires to attempt to extinguish them. Therefore, the conclusions of this research demonstrate a previously unappreciated risk to firefighters attempting to fight fires in buildings utilizing the Gerber beam design.

In general, sprinklers systems are reliable and efficient, but there are still concerns. During earthquakes, the water mains of a sprinkler system could easily rupture, for they are stiff and fragile elements without seismic dampers. Moreover, there may be a complete loss of city water supplies. In addition, the probability of ignition after an earthquake is high because of toppled furniture, electrical malfunction and movement of hot equipment. There are many examples of serious fires following earthquakes, including San Francisco in 1906 and 1989, Tokyo in 1923, and Napier, New Zealand in 1931 (Buchanan 26-27).

The possibility of a fire occurring during the construction process, or during alterations, is often overlooked, despite many serious losses. The fire hazard will usually be greater during construction than at any other time in the life of the building because of the increased number of ignition sources. For example, there are many recorded cases of ignition from cutting and welding during construction, some leading to massive fire losses. There are also documented cases of fires spreading through unprotected concealed

spaces which were created during alterations (28-30). During construction and alterations of a building, the structure itself is the only measure that can be relied upon to resist damage from a potential fire.

During normal conditions, a sprinkler system may not operate during a fire exposure for one of the following reasons: poor maintenance, inadequate design, shut valves, or poor water supply. In many cases, the sprinkler system within a building is not designed to extinguish the fire, but rather to control the spread of the fire. For example, the sprinkler system for a plastic commodity storage facility would only be designed to increase the time available to firefighters to extinguish the fire; the application of a hose stream is required for extinguishment.

Buildings are continually facing new hazards such as car bombs and arson. Sprinkler systems are only designed to extinguish small fires in their incipient phase. More precisely, the hydraulic calculations assume that only a small percentage of the sprinklers will actuate and they will be in only a single location. Therefore, an arsonist who ignites multiple, dispersed fires could overpower a given sprinkler system with ease. This is not to mention that an explosion could cause a large percentage of sprinklers to actuate at once.

The bottom line is that the structure itself is the last line of defense against fire and must be designed not a collapse due to a fire event. In terms of structural fire protection engineering, WTC 5 did not represent an engineering failure, but rather a failure to engineer (for fire exposure). The solutions to structural fire protection engineering problems do not necessarily need to be elaborate (e.g., designing a “fortress”), but rather well-engineered. Whereas structural design for seismic and wind considerations is performance-based, structural fire protection is still primarily prescriptive and/or proprietary. This fact has the unfortunate effect of preventing engineers from fully understanding and designing for building performance during fires.

8.3 Recommendations for Future Work

In general, there has been limited research into the fire performance of bolted connections in structural assemblies. It has been numerically demonstrated that the catastrophic, progressive collapse involving four floors of WTC 5 occurred during the heating phase of the fire exposure. It is recommended that full-scale experiments be conducted to verify these results. More precisely, a typical structural bay from the 8th floor of WTC 5 should be reconstructed and exposed to fire. One inch of mineral fiber insulation should be applied to the structural assembly to replicate the conditions as they were in WTC 5. Cameras could be directed at the shear connections to capture the hypothesized formation of a fulcrum point mechanism that acts as a precursor for failure. Currently, almost no structural test results are available for full burnout fires; this recommended testing could address this void in data.

If it is indeed confirmed that the Gerber beam design is susceptible to collapse during the heating phase of a fire, more research is required to ensure public safety in buildings of this type. It is not sufficient to merely identify the problem, but in addition, a solution should be sought. In the case of the Gerber beam design, certain hypersensitive structural details which contribute to the formation of a fulcrum point failure mechanism may be identified. The most apparent hypersensitive details include: the geometry of the bolt holes at the shear connection, the construction clearance distance between the beam stem and the floor girder at the shear connection, and the location of the shear connection itself with respect to its heat sink (i.e., the column).

Currently, the use of finite element software is primarily reserved for research purposes. Extended run times and the difficulty of using the software make finite element modeling uneconomical for routine structural designs. The finite element models created for this project could be further researched and used to devise pre-engineered solutions for the building codes. By addressing the influence of the hypersensitive structural details identified above, updated methods of using the Gerber beam design could be engineered.

It may be discovered that using slotted-type bolt holes significantly increases the fire endurance of the structural assembly by allowing for large rotations without high bearing stresses. If this is the case, then provisions may be made to the building code using this pre-engineered solution. Therefore, increased fire endurance may be incorporated into routine structural work that involves the Gerber beam design. In other words, structural engineers that do not necessarily possess knowledge of fire dynamics may create structural designs according to the updated code which are inherently resistant to collapse in a post-flashover fire. There may be other common structural designs that are prone to failure during fire exposure. More engineering research should be conducted to identify other opportunities to devise pre-engineered structural solutions for fire endurance.

It has been mentioned that approximately 20,000 existing steel structures in the U.S. utilize the Gerber beam design. Since it has been demonstrated that this type of design may be prone to failure during the heating phase of a fire, this information should be made available to incident commanders of fire departments. Certain incident commanders may chose to identify those buildings in their respective districts that utilize

construction similar to that identified in WTC 5 because of the increased risk they may pose to firefighters. Therefore, these incident commanders can make better informed decisions during a fire event, as compared to not having this knowledge.

9 References

ABAQUS User Manual (Version 6.6) ABAQUS Software, 2004

AISC Guide to Design Criteria for Bolted and Riveted Joints, 2nd ed., American Institute of Steel Construction (AISC): 1987

AISC Manual of Steel Construction, 7th ed., American Institute of Steel Construction (AISC): 1970

AISC Manual of Steel Construction: *Load and Resistance Factor Design*, 3rd ed., American Institute of Steel Construction (AISC): 2001

Blossom, David R. "High-Rise Safety: Have We Missed the Obvious?" *Fire Engineering*: January 2002

Bower, A.F. "Solving Solid Mechanics Problems Using the Finite Element Method," Brown University Division of Engineering, < http://www.engin.brown.edu/courses/En175/Notes/FEM_overview/FEM.htm >

Brannigan, Francis L. Building Construction for the Fire Service, National Fire Protection Association (NFPA): 1982

Buchanan, Andrew H. Structural Design for Fire Safety, John Wiley & Sons, New York: 2002

Caro, Tony C, et al. A Survey of Fuel Loads in Contemporary Office Buildings, NIST (1995), < http://www.fire.nist.gov/bfrlpubs/fire96/PDF/f96080.pdf >

Eurocode 1 (EC1): *Basis of Design and Design Actions on Structures*, European Committee for Standardization, Brussels, Belgium: 1994

Fire Resistance Directory, Vol. 1, Underwriters Laboratories (UL): 2004

Harmathy, T.Z. Fire Safety Design and Concrete, Longman Scientific and Technical, United Kingdom: 1993

Hemstad, Mechael Cantilever Beam Framing Systems, American Institute of Steel Construction (AISC) Engineering Journal (Third Quarter 1999)

Hibbeler, R.C. Mechanics of Materials, 5th ed., Prentice Hall, New Jersey: 2002

Incropera, Frank P., et al. Introduction to Heat Transfer, 4th ed. John Wiley & Sons, New York: 2002

McGrattan, Kevin B., et al. Computer Simulation of the Fires in the World Trade Center Towers, Federal Building and Fire Safety Investigation of the World Trade Center Disaster, NIST (2005), < http://wtc.nist.gov/pubs/NISTNCSTAR1-5FDraft.pdf >

New York City Building Code (1970)

Ohlemiller, Thomas J, et al. Fire Tests of Single Office Workstations, Federal Building and Fire Safety Investigation of the World Trade Center Disaster, National Institute of Standards and Technology (NIST), 2005, < http://wtc.nist.gov/NISTNCSTAR1-5C.pdf >

Peacock, Richard D., et al. Consolidated Model of Fire Growth and Smoke Transport (CFAST) User Manual, Version 6.0, NIST: 2005

Schierle, G G "Indeterminate Beams" < http://www.usc.edu/dept/architecture/mbs/struct/ >

Seely, Fred Advanced Mechanics of Materials, 1st ed. John Wiley & Sons, New York: 1946

SFPE Handbook of Fire Protection Engineering, 3rd ed. Society of Fire Protection Engineers (SFPE), National Fire Protection Association (NFPA), 2002

World Trade Center Building Performance Study: *Data Collection, Preliminary Observations, and Recommendations*, Federal Emergency Management Agency (FEMA), New York: 2002

10 Appendices

10.1 Thermal Analyses

10.1.1 Simplified Thermal Analysis of the Protected Steel

Figure 107 below is a schematic of the column-tree and floor girder assembly contained in WTC 5. This particular analysis shall focus on the W18X50 floor girder. The floor girders of WTC 5 had a 2-hour fire resistance rating. Design No. N715 of the 2004 UL Directory specifies that the spray-applied fire resistance must be 1-inch thick in order to achieve a 2-hour rating (see Figure 108 below).

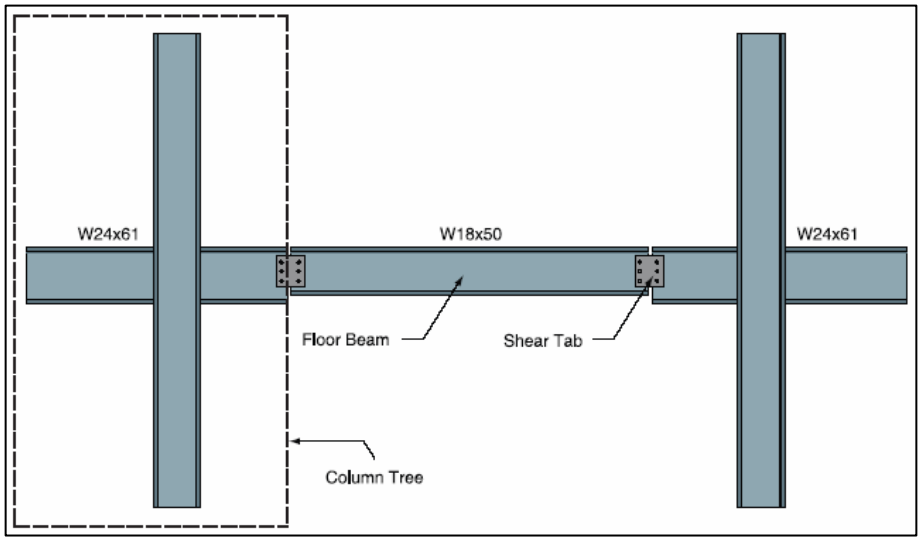

Figure 107: Column-Tree and Girder Assembly

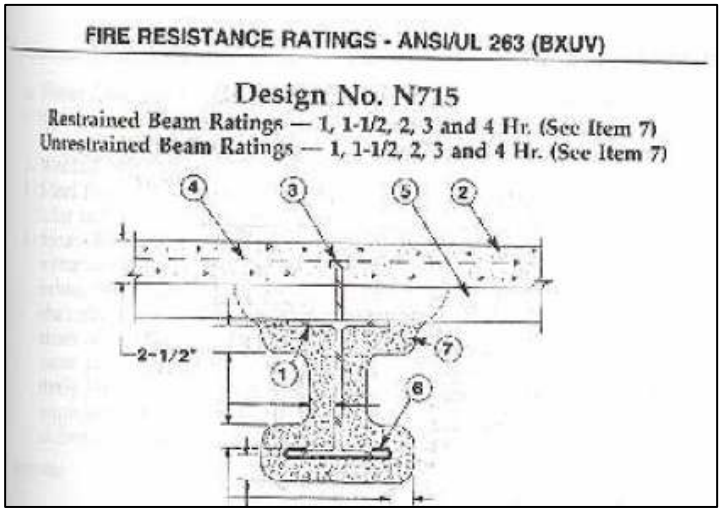

Figure 108: Design No. N715 (Spray-Applied Fire Resistance)

The SFPE Handbook provides an expression to predict the heat transfer within insulated steel members, in which the thermal capacity of the insulation is accounted for (Equation 13). The following criteria shall be assumed: the steel is thermally-thin; a lumped-mass approach is applicable; and the heat sink effect of the concrete slab will be neglected.

$$\Delta T_s = \frac{k_i / t_i}{C_{ps}\rho_s V_s + \frac{C_{pi}\rho_i t_i A_i}{2}} A_i \left(T_g - T_s\right)\Delta t \qquad (13)$$

$A_i = 2d + 4b_f - 2t_w$ (heated perimeter of the member)

$$\Delta t \le \frac{25000}{A_i / V_s} \text{ (time step)}$$

The following parameters were substituted into the expression shown above:

Insulation Properties

$\rho_i = 300\ kg/m^3$ (density)

$C_{pi} = 1200\ J/kgK$ (specific heat)

$k_i = 0.12\ W/mK$ (thermal conductivity)

A36 Steel Properties

$\rho_s = 7850\ kg/m^3$ (density)

$C_{ps} = 520\ J/kgK$ (specific heat)

The ASTM E-119 test exposes a steel member to a known gas temperature history. Using Equation 13, a spreadsheet was created to derive the change in steel temperature as a function of time, as the girder is exposed to the E-119 furnace test (see Figure 109 below). It is observed that there is a thermal lag in the temperature change of the steel over time. The medium, fast, and ultra-fast fire scenarios were also referenced to conduct similar analyses (see Figure 110, Figure 111, and Figure 112 below).

A sensitivity analysis was conducted for the insulation thickness of the steel girder for the medium growing design fire. It is observed that the peak temperature of the steel significantly increases as the thickness of the insulation decreases (see Figure 113 below).

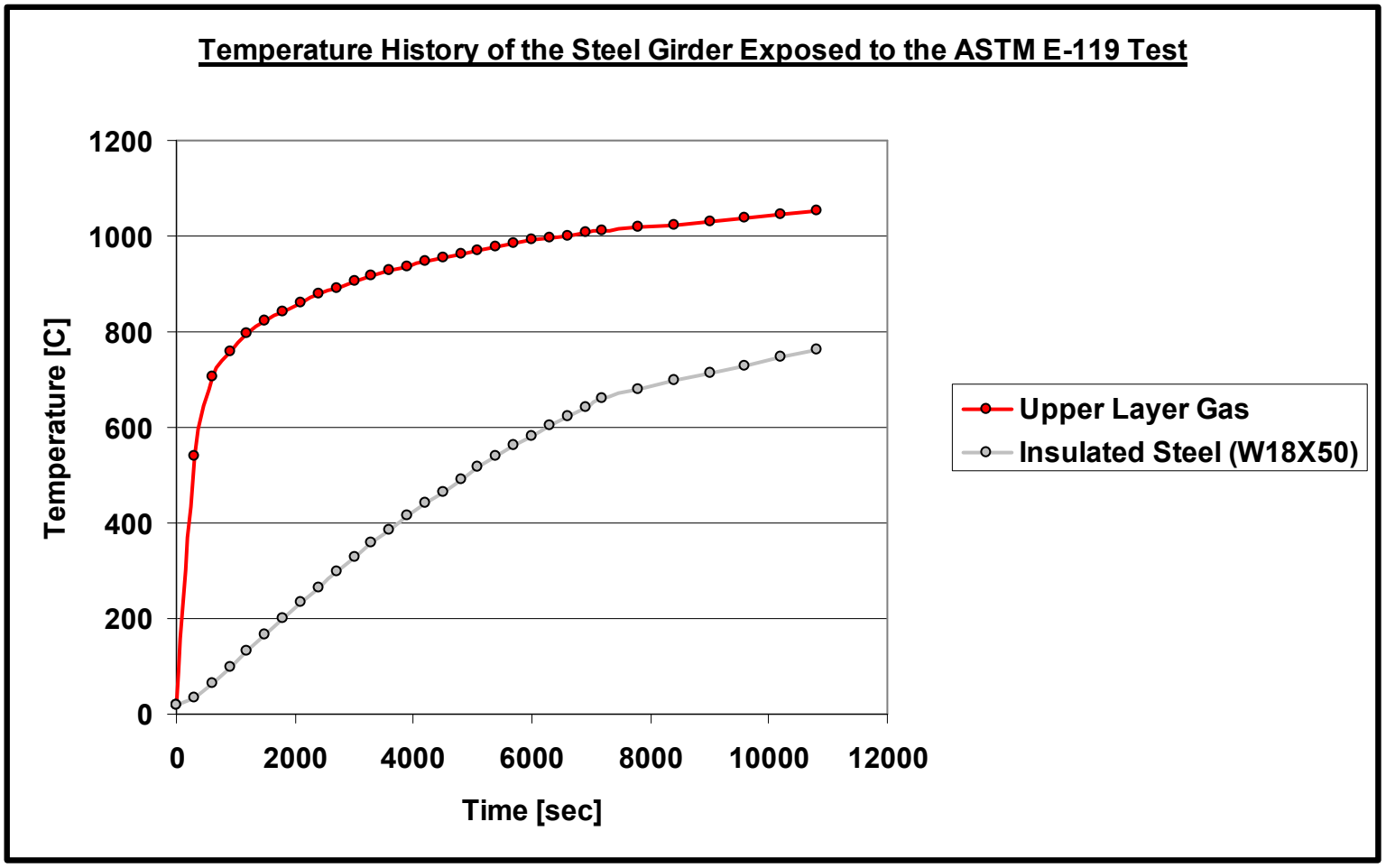

Figure 109: Temperature History of the Protected Steel Girder (ASTM E-119 Test)

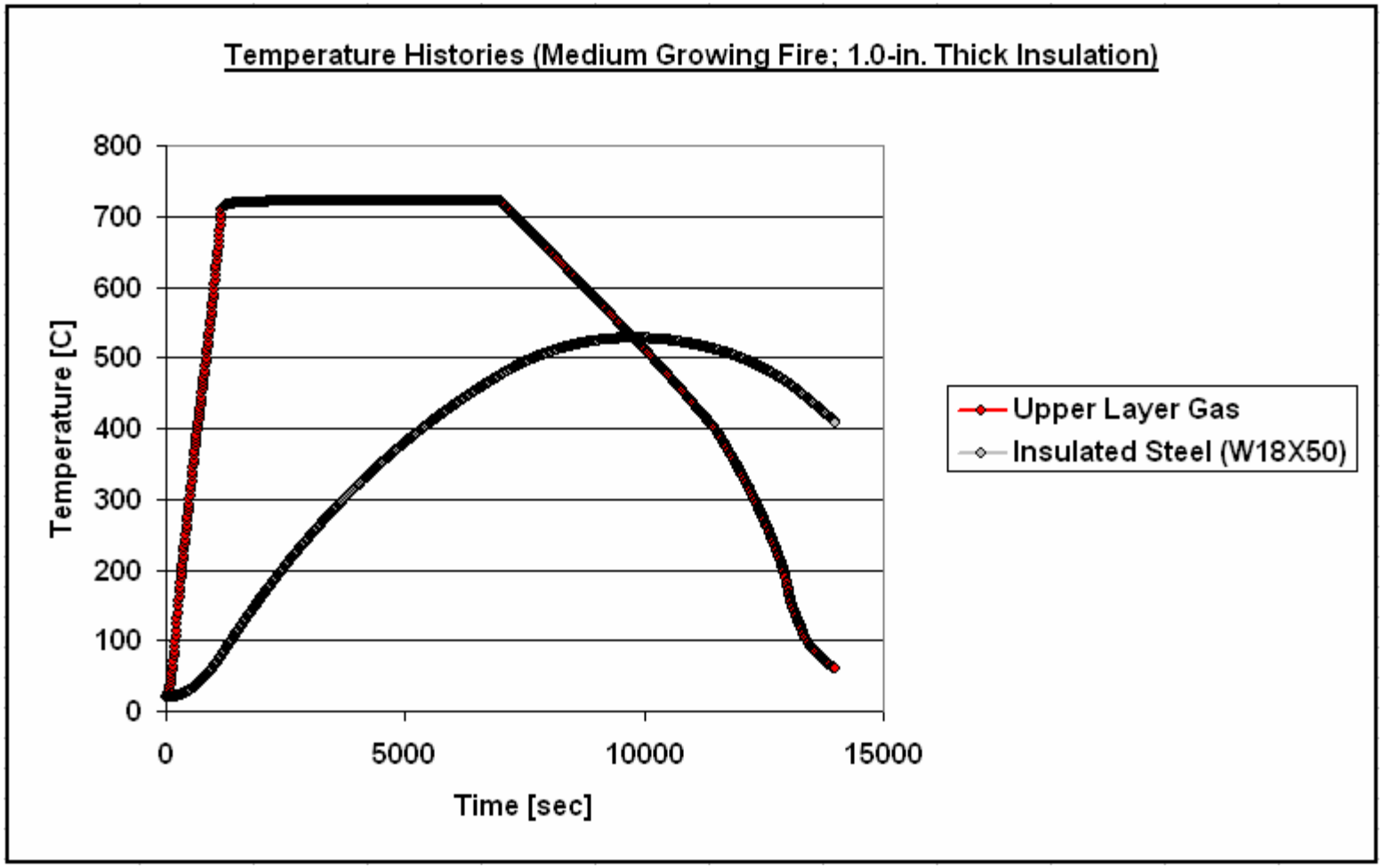

Figure 110: Temperature History of the Protected Steel Girder (Medium Growing Fire Scenario)

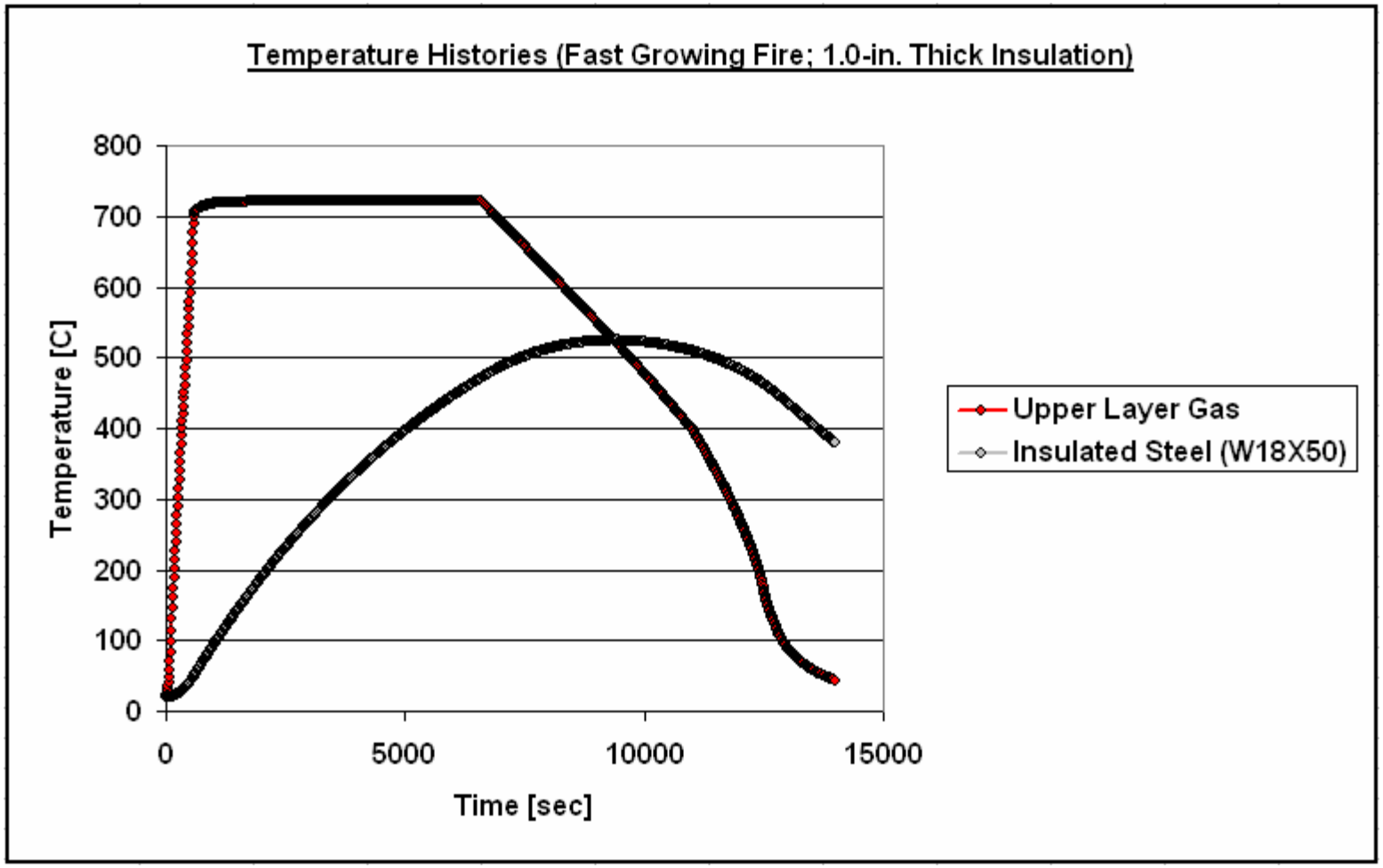

Figure 111: Temperature History of the Protected Steel Girder (Fast Growing Fire Scenario)

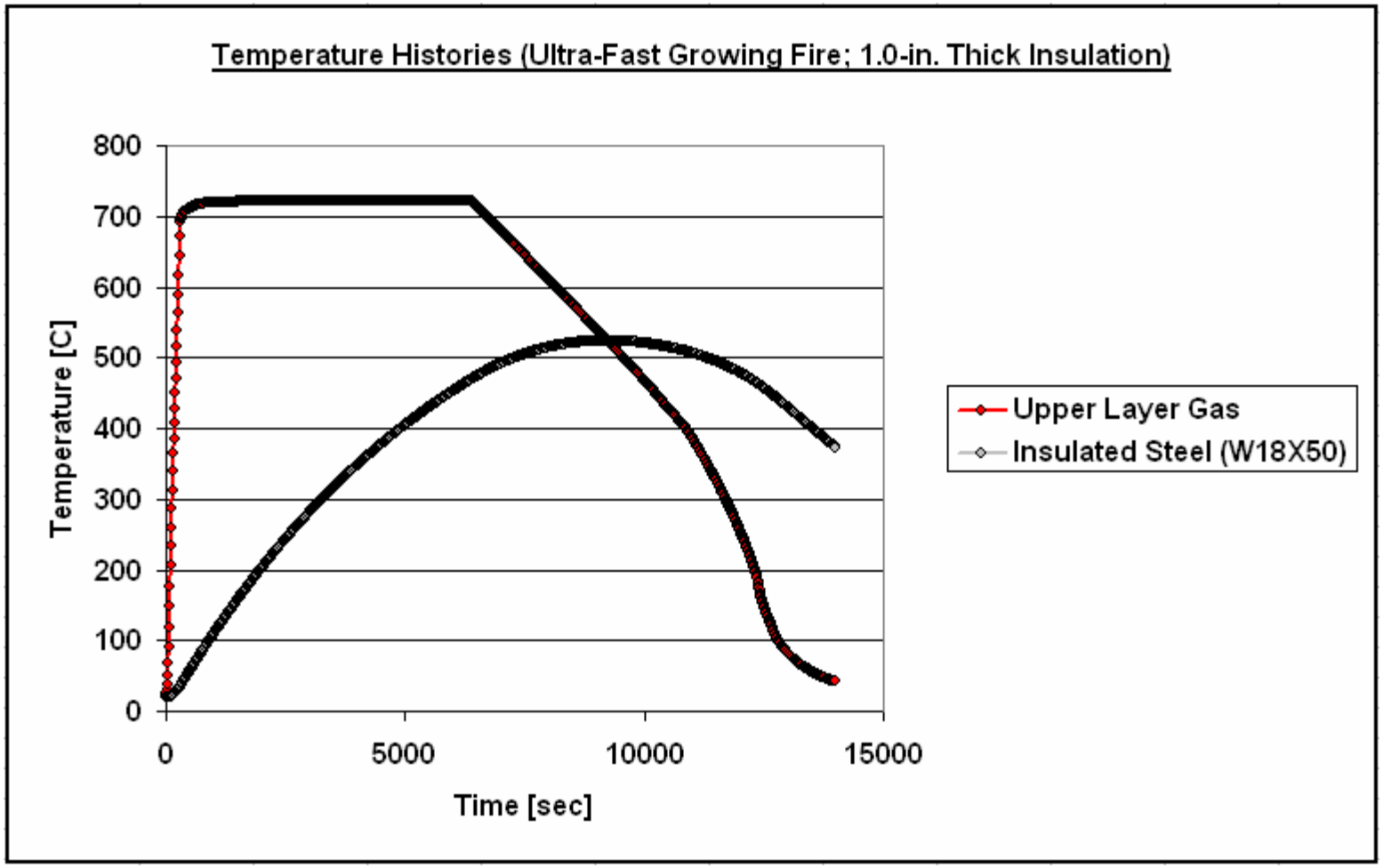

Figure 112: Temperature History of the Protected Steel Girder (Ultra-Fast Growing Fire Scenario)

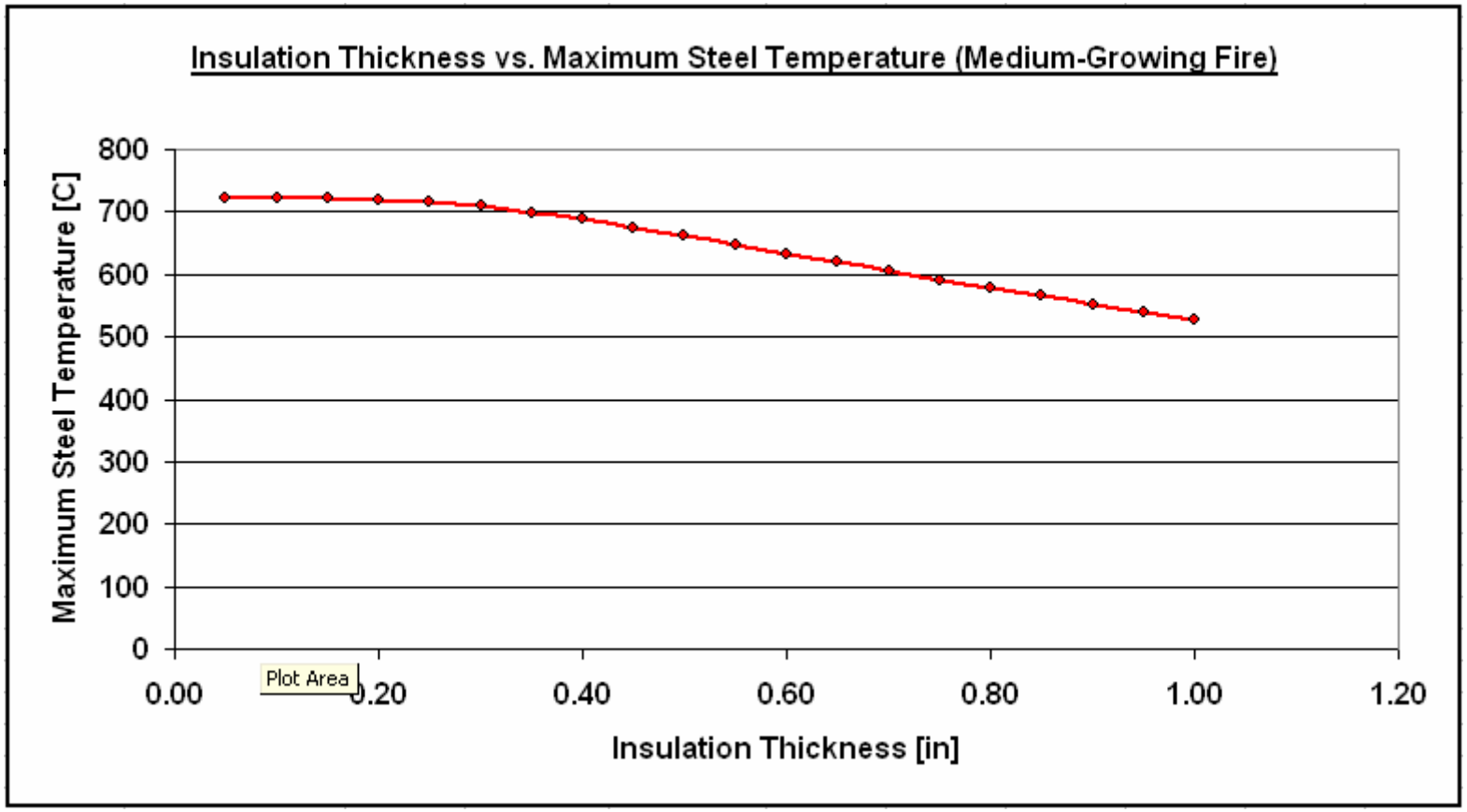

Figure 113: Insulation Thickness Versus Peak Steel Temperature (Medium Growing Fire Scenario)

The SFPE Handbook also provides expressions for determining the yield strength of structural steel members at elevated temperatures (Equations 14 and 15).

For $0^o C \le T \le 600^o C$:

$$F_y = \left[1.0 + \frac{T}{900 \ln\left(\frac{T}{1750}\right)} \right] F_{y0} \qquad (14)$$

For $600^{oC} \le T \le 1000^o C$:

$$F_y = \left(\frac{340 - 0.34T}{T - 240} \right) F_{y0} \qquad (15)$$

Using Equations 14 and 15, the yield strength for A36 steel was plotted as a function of steel temperature (see Figure 114 below).

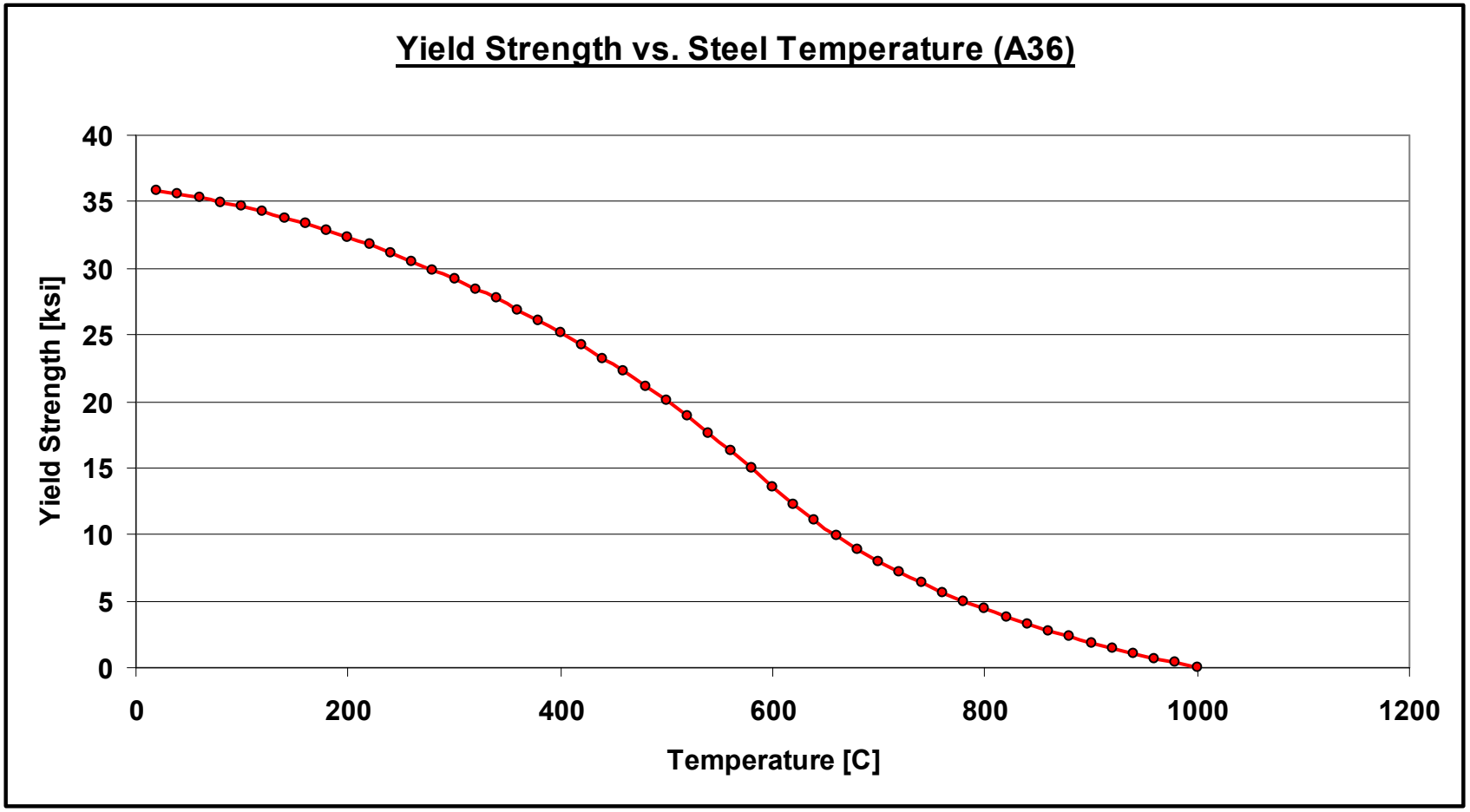

Figure 114: Yield Strength Versus Steel Temperature (A36 Steel)

10.1.2 Simplified Beam Stem Heat Transfer Analysis

Figure 107 above is a schematic of the column-tree and floor girder assembly contained in WTC 5. This particular analysis shall focus on the W24X61 beam stem. It is known the column that is shop-welded to the beam stem acts as a heat sink. More precisely, heat absorbed by the beam stem during fire exposure is transferred to the column, which is then transferred to the other members of the structure. It is valuable to estimate the temperature distribution across the length of the beam stem for this case.

Heat transfer involving fins has been thoroughly studied. For this analysis, the beam stem shall act as the "fin" of the column. To simply the analysis, the W24X61 beam stem will be assumed to have a rectangular cross-section (see Figure 115 below). The temperatures at the end of the beam stem and at its base are 600 °C and 400 °C, respectively. Moreover, the ambient temperature is 600 °C to represent fire exposure.

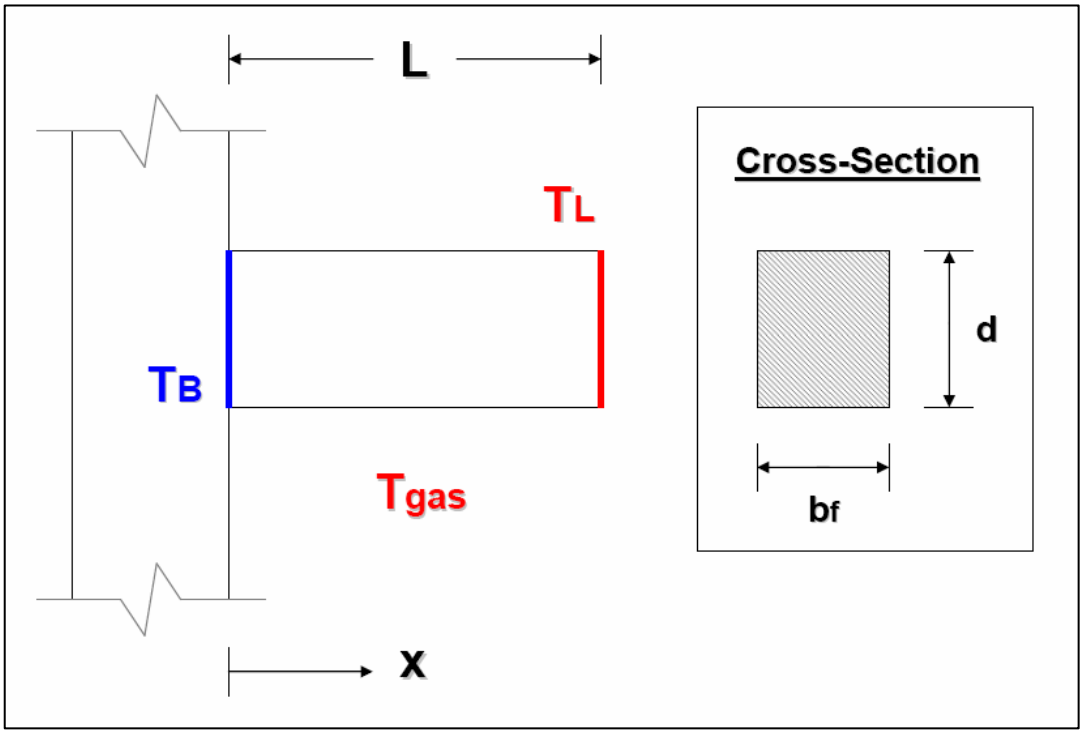

Figure 115: Schematic of the Fin Heat Transfer Problem

Since the temperature has been specified at the end of the beam stem, the temperature distribution may be derived using Equation 16:

$$\frac{\theta}{\theta_b} = \frac{\left(\theta_L / \theta_b\right)\sinh(mx) + \sinh\left(m(L-x)\right)}{\sinh(mL)} \qquad (16)$$

$$\theta = T - T_{gas}$$
$$\theta_b = T_b - T_{gas}$$
$$\theta_L = T_L - T_{gas}$$

$$m = \sqrt{\frac{hP}{kA}}$$

$$P = 2d + 2b_f$$
$$A = db_f$$

The parameters of this fin heat transfer problem are as follows:

$T_b = 400^o C$ (fixed temperature of the beam stem base)

$T_L = 600^o C$ (fixed temperature of the beam stem end)

$T_{gas} = 600^o C$ (fixed temperature of the ambient)

$k = 51.9 {}^{W}\!/_{mC}$ (thermal conductivity of A36 steel)

$L = 1.22m$ (length of the beam stem)

$d = 0.60m$ (depth of the beam stem cross-section)

$b_f = 0.178m$ (width of the beam stem cross-section)

$h = 25 {}^{W}\!/_{m^2 C}$ (heat transfer coefficient for natural convection with turbulent gas)

Using Equation 16, the temperature distribution across the length of the beam stem was derived (see Figure 116 below). Consider that the beam stem is divided across its length into four sections. It can be concluded that the quarter section at the end of the beam stem essentially has a uniform temperature distribution. Therefore, the temperature of the steel in the vicinity of the shear connection can be assumed to have a uniform temperature at any given time during fire exposure. Moreover, the temperature distribution drops sharply in the quarter section of the beam stem in contact with the column (heat sink).

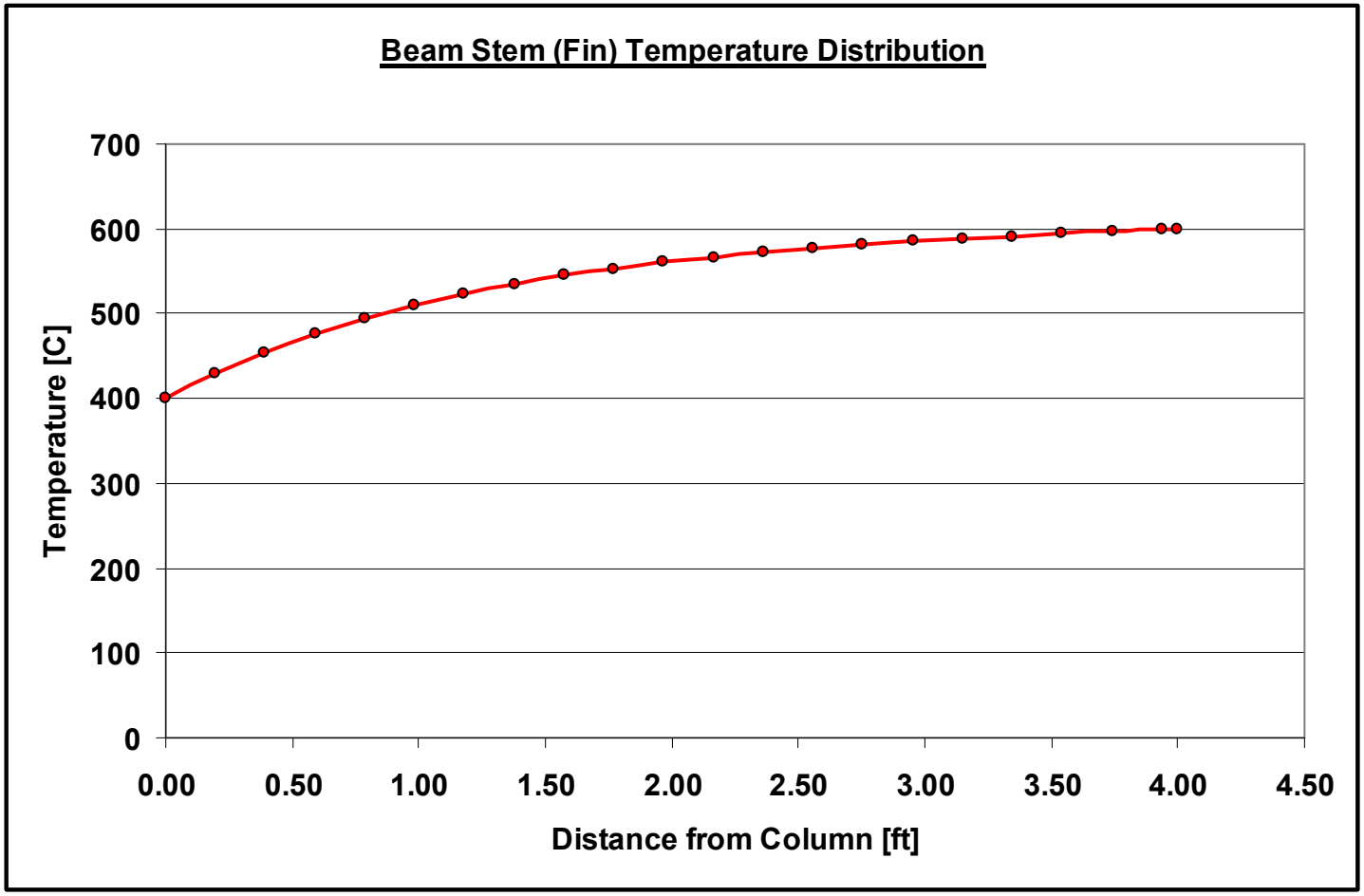

Figure 116: Beam Stem Temperature Distribution Across the Length

10.1.3 Estimation of the Post-Flashover Gas Temperature

In 1981, Vytenis Babrauskas published an approximate calculation method for determining the peak, post-flashover gas temperature in a compartment containing a single opening. Equation 17 contains five efficiency factors based upon the specific characteristics of the fire situation. This calculation method was used to estimate the post-flashover gas temperature within a compartment of WTC 5.

$$T_f = T_\infty + (1725 - T_\infty)\theta_1\theta_2\theta_3\theta_4\theta_5 \qquad (17)$$

Stoichiometric Factor (θ_1)

The model compartment used in CFAST has five horizontal flow vents that are 1m. wide by 3 m. tall. These five vents will be consolidated into a single vent to match the requirements of this calculation method. Therefore, the following boundary conditions apply:

$A = 15m^2$ (area of consolidated ventilation opening)
$h = 3m$ (height of ventilation opening)

The maximum fuel flow rate was derived for the medium growing design fire as follows:

$\dot{m}_f = 0.87\,{}^{kg}\!/_{s}$ (maximum fuel flow rate)

It shall be assumed that the fuel is 100% cellulose. Therefore, the chemical equation may be represented as follows:

$$C_{12}H_{16}O_8 + 16(O_2 + 3.76N_2) \rightarrow 8H_2 + 12CO_2 + 60.16N_2$$

Based upon the chemical equation shown above, the stoichiometric ratio r = 4.7. Therefore, the equivalence ratio may be calculated as follows:

$$\phi = \left(\frac{r}{0.5A\sqrt{h}}\right)\dot{m}_f = 0.315$$

Since the equivalence ratio is less then unity, the stoichiometric factor may be calculated as follows:

$$\theta_1 = 1.0 + 0.5\ln\phi = 0.422$$

Steady-State Wall Loss Factor (θ_2)

The second efficiency factor accounts for heat losses from the wall and ceiling surfaces. According to the CFAST model, the following parameters apply:

$$A_w = 206m^2 \text{ (total surface area of the walls/ceiling)}$$
$$L = 0.016m \text{ (wall thickness)}$$
$$k = 0.17 {}^{W}\!/_{mC} \text{ (thermal conductivity of gypsum wallboard)}$$

Using these parameters, the steady-state wall loss factor may be derived as follows:

$$\theta_2 = 1.0 - 0.94 \exp\left(-54 \left[\frac{A\sqrt{h}}{A_w} \right]^{2/3} \left[\frac{L}{k} \right]^{1/3} \right) = 0.998$$

Transient Wall Loss Factor (θ_3)

Since a steady-state solution is sought, the following value for the transient wall loss factor applies:

$$\theta_3 = 1.0$$

Opening (Vent) Height Factor (θ_4)

This fourth efficiency factor accounts for radiation losses from the vent opening and may be calculated as follows:

$$\theta_4 = 1.0 - 0.205h^{-0.3} = 0.853$$

Combustion Efficiency Factor (θ_5)

The fire compartment can be viewed as a well, but not perfectly stirred reactor. Thus, a certain "unmixedness" is present. A maximum combustion efficiency can be used to characterize the unmixedness as follows:

$$b_p = 0.9 \text{ (conservative value for unmixedness)}$$

Therefore, the combustion efficiency factor may be derived as follows:

$$\theta_5 = 1.0 + 0.5 \ln(b_p) = 0.947$$

The five efficiency factors may be used to calculate the peak post-flashover temperature as follows:

$$T_f = T_\infty + (1725 - T_\infty)\theta_1\theta_2\theta_3\theta_4\theta_5 \approx 600^o C$$

10.2 Structural Analyses

10.2.1 Beam Stem Web Rupture Analysis

Figure 107 above is a schematic of the column-tree and floor girder assembly contained in WTC 5. This particular analysis shall focus on the W24X61 beam stem. As the W18X50 girder deflects during fire exposure, it is expected to create an axial tensile force on the beam stems. It is valuable to estimate the tensile force required to cause beam web shear failure as a function of the temperature of the steel.

Figure 117: Recovered Beam Stem Sample from WTC 5

Figure 117 above shows a recovered beam stem sample from WTC 5. It is observed that failure was due to web shear. Therefore, other connection failure modes such as gross shear rupture may be ruled out. It is known that the beam stems are composed of A36 steel with yield and ultimate strengths of 36 and 58 ksi, respectively. Moreover, the W24X61 beam stems have a clear distance and web thickness of 1.03125 and 0.4375 inches, respectively. The nominal bolt and bolt hole diameter is 7/8 and 15/16 inches, respectively. Figure 118 below is a schematic showing the two shear tabs connected to the beam stem.

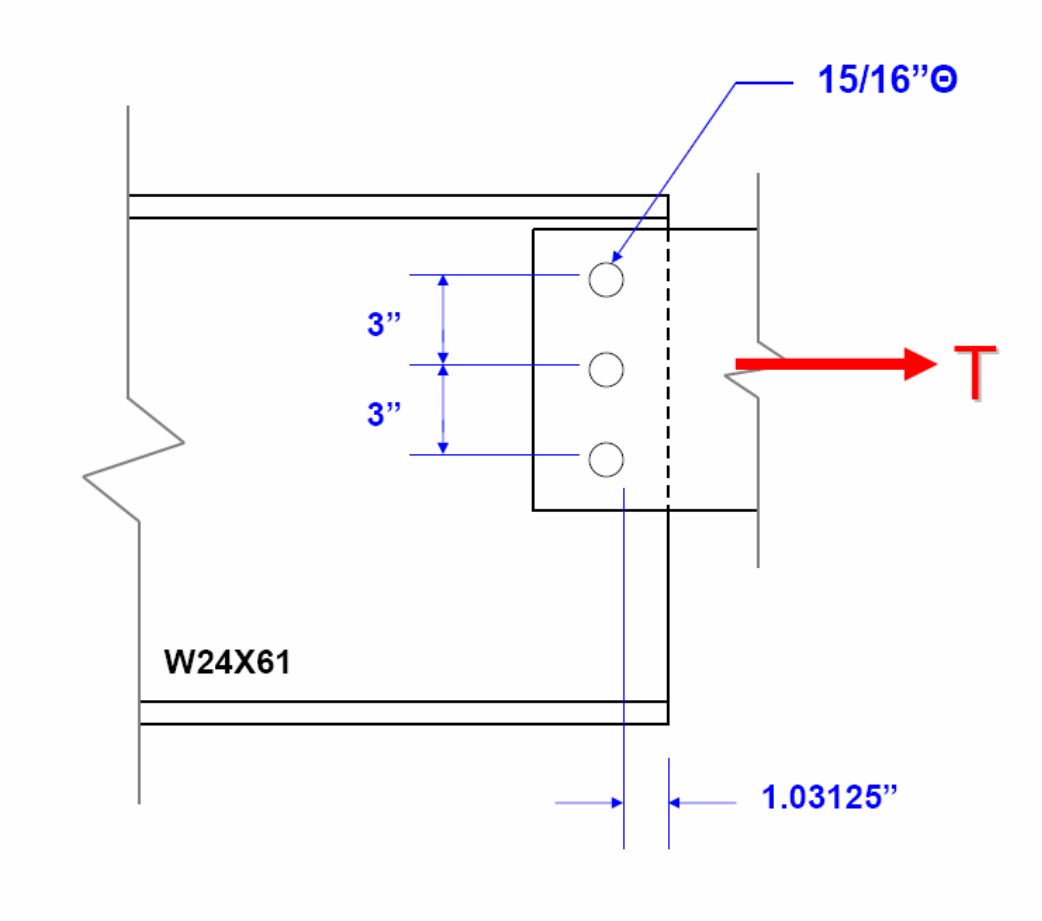

Figure 118: Elevation View of the Beam Stem

As shown in Figure 118 above, a tensile force is applied to the shear tabs. As a result, the high strength bolts each apply a bearing force on the weak (right) side of each bolt hole. As shown in Figure 119 below, this bearing force equals one-third of the tensile force applied to the shear tabs because there are three bolts contained at this connection.

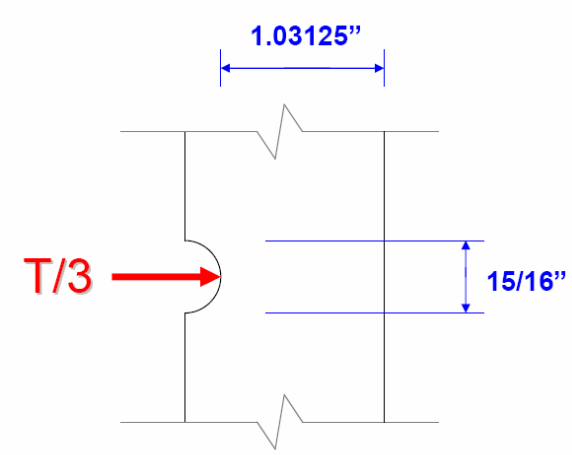

Figure 119: Schematic of the Bearing Force on the Bolt Hole in the Beam Web

The bearing capacity of the beam web is governed by Equation 18. Since the beam web has three bolts, the capacity is tripled (as represented in the expression).

$$R_n = (3)1.2L_c t_w F_u \geq (3)2.4 d_b t_w F_u \qquad (18)$$

L_c = web clear distance [in]

t_w = web thickness [in]

d_b = nominal bolt diameter [in]

F_u = ultimate strength of A36 steel [ksi] (function of temperature)

It should be noted that Equation 18 does not contain any safety factors and is based upon LRFD design. Therefore, the smaller of the two values calculated represents the ultimate capacity of the beam web. If this capacity is surpassed, rupture would be imminent.

The change in ultimate strength of the steel with temperature is known. It is also known that the thickness and clear distance of the beam stem web is 0.4375 inches and 1.03125 inches, respectively. Moreover, the nominal bolt diameter is 7/8 inches. Therefore, the maximum tensile force that can be applied to the shear tabs before web tear-out failure occurs can be plotted as a function of the steel temperature (see Figure 120 below). Referring to Figure 120 below, “Criterion A” refers to the shear plan capacity of the beam web (left side Equation 18) and “Criterion B” refers to the bearing strength of the web (right side of Equation 18). It is observed that increasing the steel temperature from 20 °C to 650 °C results in a 75% reduction in the connection’s ability to resist loading.

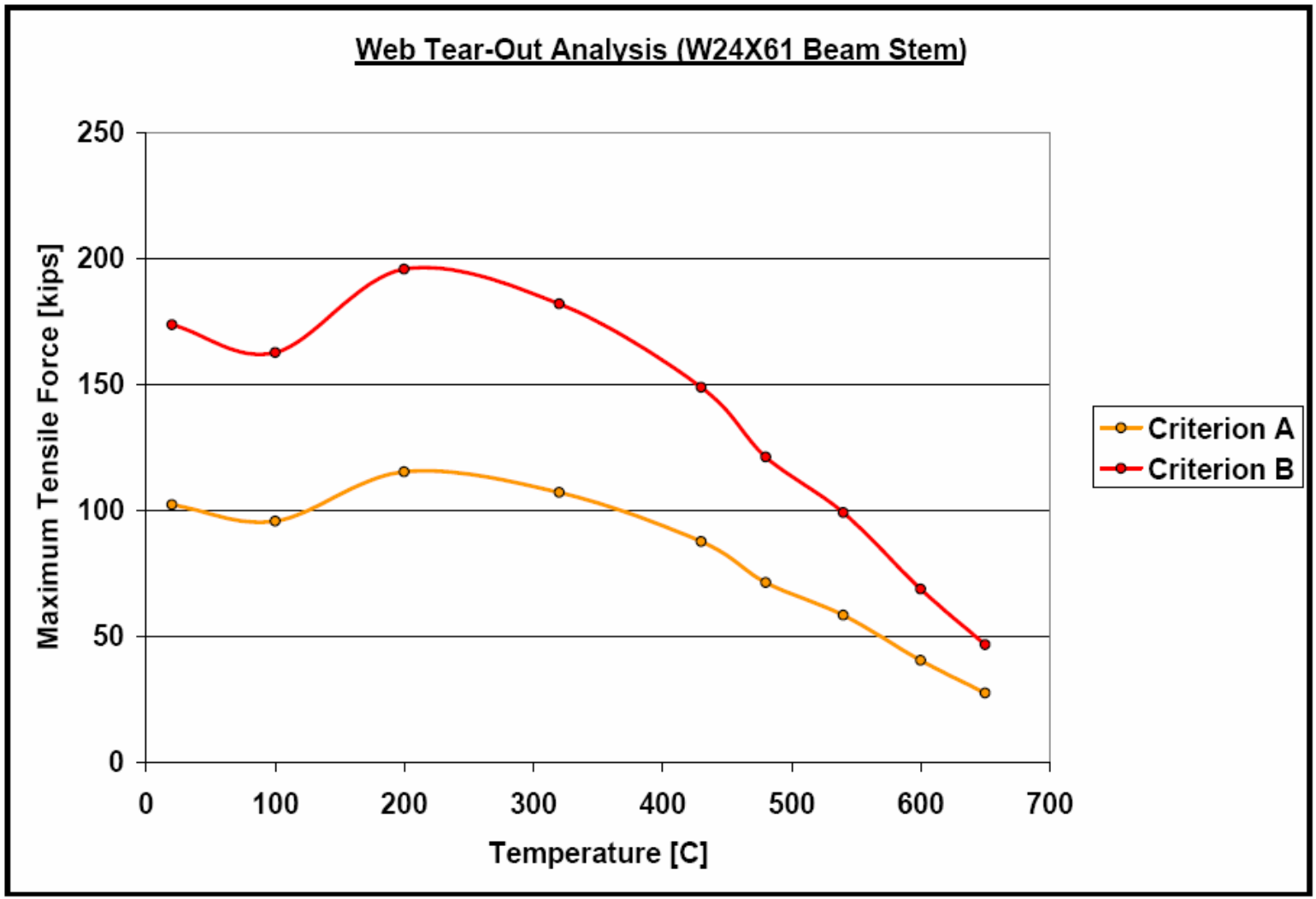

Figure 120: Maximum Tensile Force Versus Steel Temperature

10.2.2 Analysis of the Shear Tabs

It must be determined if shear tabs were on both sides of the beam stem web in WTC 5. This is a requisite to an accurately model of the shear connection assembly in ABAQUS. Figure 121 below is a photograph provided by NIST that presents forensic evidence that two shear plates were used at each connection. Since the clarity of this photograph is open to interpretation, a mock structural connection design must be used to confirm this fact.

Figure 121: Photograph of the Shear Tab Connection (WTC 5) (NIST)

Figure 122 below shows a schematic of the beam stems and floor girder assembly. A distributed design load of 3.2 kips per foot is applicable to the assembly. The shear force at the shear tab connection is determined to equal about 35 kips. It is known that the shear tabs are composed of A36 steel. The 1970 AISC Steel Manual was referenced for the mock connection design. Table I-A3 of the manual states that a double tab assembly that is ¼-in thick and has 7/8-in diameter bolt holes will provide about 54 kips of shear resistance. Thus, a single shear tab would only provide about 27 kips of shear resistance. Therefore, it can be concluded that the two tabs were used at each shear connection in WTC 5.

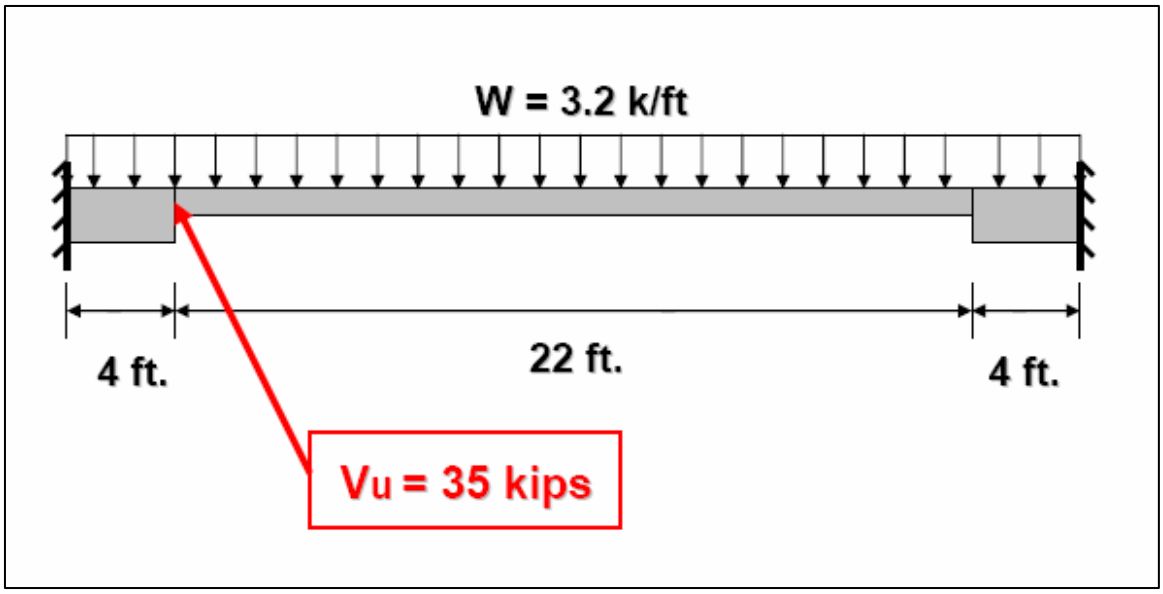

Figure 122: Beam Stem and Floor Girder Schematic

10.2.3 Structural Analysis of the Floor Girder

Figure 107 above is a schematic of the column-tree and floor girder assembly contained in WTC 5. This particular analysis shall focus on the W18X50 floor girder. The floor girders of WTC 5 had a 2-hour fire resistance rating. Design No. N715 of the 2004 UL Directory specifies that the spray-applied fire resistance must be 1-inch thick in order to achieve a 2-hour rating. A schematic of the floor girder is shown in Figure 123 below.

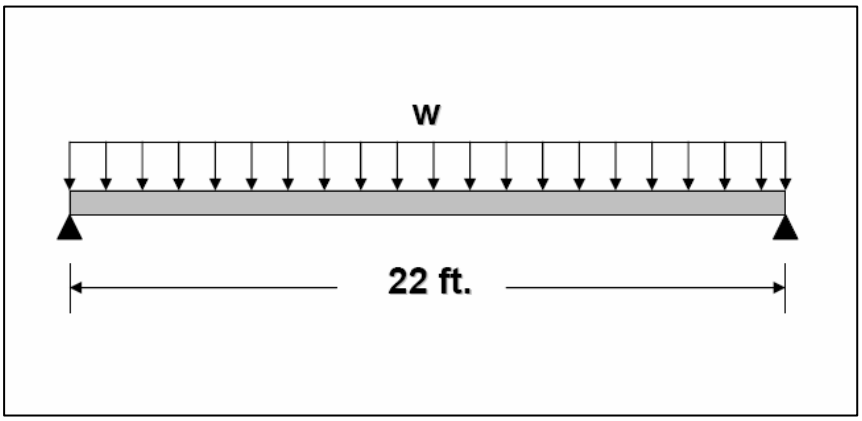

Figure 123: Schematic of the Girder

The 1970 New York City Building Code was referenced in order to derive design live loads for the girder. A summary of loads acting upon the girder are summarized below. It should be noted that loading factors were not used.

Dead Loads

4-inch lightweight concrete slab: $DL_{slab} = 38.3\,psf$

W18X50 girder: $DL_{girder} = 50\,plf$

Live Loads (Table 1607.1 of IBC 2006)

Office load: $LL_{office} = 50\,psf$

Partitions load: $LL_{partitions} = 15\,psf$

Since the tributary area of the girder is $660\,ft^2$, the distributed load was calculated to be:

$$w = 3.2\,{}^{k}\!/_{ft}$$

It is known that the nominal maximum moment is defined by Equation 19:

$$M_n = \frac{wL^2}{8} \qquad (19)$$

By substituting the known values, the maximum moment was calculated to be:

$$M_n = 194 \text{ k*ft}$$

The girders of WTC 5 were composed of A36 steel. The material behavior of A36 steel is represented in Figure 124 below.

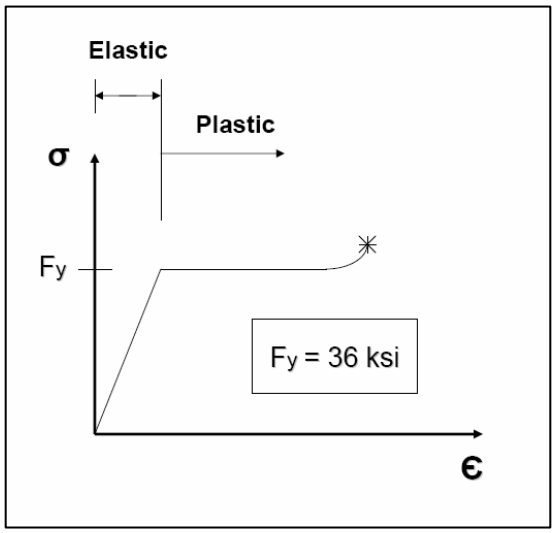

Figure 124: Stress/Strain Curve for A36 Steel

Three structural analyses were conducted for the girders of WTC 5: elastic, plastic yield, and plastic hinge. Figure 125 below summarizes the limit state of the steel for each of the three analyses conducted. For each of the structural analyses conducted, the minimum yield strength to maintain the limit state was derived.

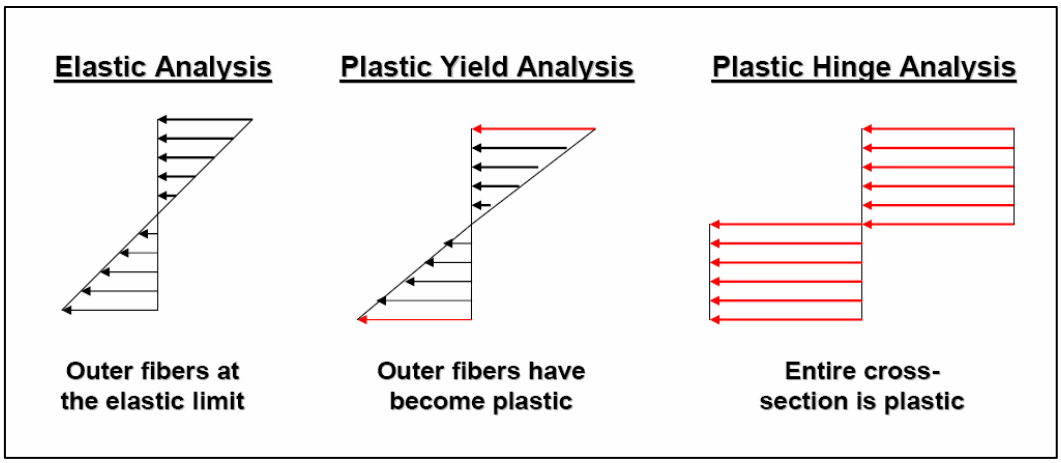

Figure 125: Summary of Limit States

Elastic Analysis

The elastic analysis involves the determination of the minimum yield strength required so that the outer fibers of the girder remain at the elastic limit (see Figure 124 above). Equation 20 represents the minimum required yield strength:

$$F_{y(\min)} = \frac{M_n}{S_x} \qquad (20)$$

$S_x = 88.9 in^3$ (section modulus (Table 1-1 of AISC Manual))

Therefore, the minimum required yield strength of the steel is as follows:

$$F_{y(\min)} = 26 ksi$$

Section 10.1.1 reveals that the yield strength of the steel will decrease to 26 ksi once the following temperature has been reached:

$$T = 380^o C$$

Furthermore, Section 10.1.1 demonstrates that the steel girder with 1-inch insulation reaches a temperature of 380 °C after the following time of exposure to the ASTM E-119 furnace test:

$$t = 1.0 \text{ hour}$$

Plastic Yield Analysis

The plastic yield analysis involves the determination of the minimum yield strength required so that the outer fibers of the girder are plastic and the inner fibers remain elastic. Equation 21 represents the minimum required yield strength:

$$F_{y(\min)} = \frac{M_n}{Z_x} \qquad (21)$$

$Z_x = 101 in^3$ (plastic modulus (Table 1-1 of AISC Manual))

Therefore, the minimum required steel strength is as follows:

$$F_{y(\min)} = 23 ksi$$

Section 10.1.1 reveals that the strength of the steel will decrease to 23 ksi once the following temperature has been reached:

$$T = 450^{o} C$$

Furthermore, Section 10.1.1 demonstrates that the steel girder with 1-inch insulation reaches a temperature of 450 °C after the following time of exposure to the ASTM E-119 furnace test:

$$t = 1.2 \text{ hours}$$

Plastic Hinge Analysis

The plastic hinge analysis involves the determination of the minimum yield strength required so that the entire cross-section of the girder becomes plastic. This is the point at which the girder is on the verge of rupture (excessive deflection), as defined by the standards of the ASTM E-119 test.

The nominal moment calculated above does not apply to this analysis. The method of virtual work was utilized in order to derive an expression for the fully-plastic moment. Figure 126 below provides a schematic of a plastic hinge formation.

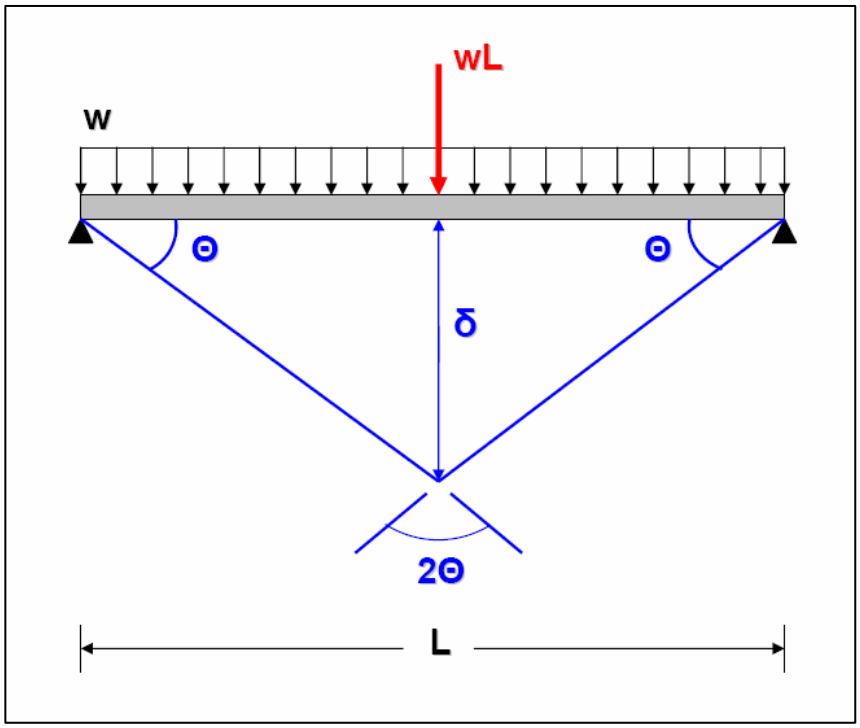

Figure 126: Schematic for Plastic Moment Derivation

The generalized virtual work equation is as follows:

$$W_{external} = W_{internal}$$

In general terms, the external work required to cause a given deformation equals the internal work required to cause a given stress in the material. This general equation above may be rewritten as follows (Equation 22):

$$\sum P_i \delta_i = \sum M_p \theta_j \qquad (22)$$

According to Figure 126 above, the following is true:

$$\tan\theta = \frac{\delta}{\left(L/2\right)} \Rightarrow \delta = \left(L/2\right)\tan\theta$$

For small deformation: $\tan\theta \approx \theta$

$$\delta = \left(L/2\right)\theta$$

Therefore, the virtual work equation may be represented as follows:

$$\left(wL\right)\left(\left(L/2\right)\theta\right) = \left(M_p\right)\left(2\theta\right)$$

The plastic moment can be solved for as follows:

$$M_p = \frac{wL^2}{4}$$

If the given parameters are substituted into the expression above, the moment required to cause a plastic hinge to form can be derived as follows:

$$M_p = 387k * ft$$

The ratio of M_p to M_n equals 2. More precisely, the shape factor equals 2; the girder has two times the reserve strength available. Therefore, the minimum steel strength required for this case is half of that calculated in the plastic yield analysis above.

$$F_{y(hinge)} = \frac{23ksi}{2} \approx 11ksi$$

Section 10.1.1 reveals that the strength of the steel will decrease to 11 ksi once the following temperature has been reached:

$$T = 640^{o} C$$

Furthermore, Section 10.1.1 demonstrates that the steel girder with 1-inch insulation reaches a temperature of 640 °C after the following time of exposure to the ASTM E-119 furnace test:

$$t = 1.9 \text{ hours}$$

This calculated time makes practical sense because the girder is 2-hour rated, as defined by the standards of the ASTM E-119 test. Moreover, the girder would resist failure for longer than 1.9 hours under experimental conditions because of strain hardening of the steel.

10.3 Finite Element Modeling

10.3.1 Overview of the Finite Element Analysis Method

The finite element method originated from the need for solving complex structural problems in civil and aeronautical engineering. In 1678, Robert Hooke established the basis for modern finite element stress analysis as Hooke's Law, which states that an elastic body stretches (strain) in proportion to the force (stress) on it. Development of the finite element method can be traced back to the work by A. Hrennikoff and R. Courant in the early 1940s and this method has been continually developed and improved since then (Bower).

Although the finite element method is a complex mathematical technique, the fundamental principles are relatively straightforward. The finite element method works by breaking a real object down into a large number of elements (e.g., 100,000 cubes). The behavior of each little element, which is simple in shape, is readily predicted by a set of mathematical equations. The summation of the behavior of each individual element produces the expected behavior of the actual object, which often has complex geometry (Bower).

As a typical example, consider a body in which the distribution of an unknown variable (e.g., temperature, displacement, etc.) is sought. The first step of any finite element analysis is to divide the actual geometry of the structure using a collection of discrete portions called finite elements. These elements are joined together by shared nodes. The collection of nodes and finite elements is known as the mesh (see Figure 127 below). After the problem has been divided into the discrete elements, the governing equations for each element are calculated and then assembled to yield a system of equations that describe the behavior of the body as a whole. In a stress analysis problem, the displacements of the nodes would be calculated, and from this information, the stresses and strains in the elements can be determined.

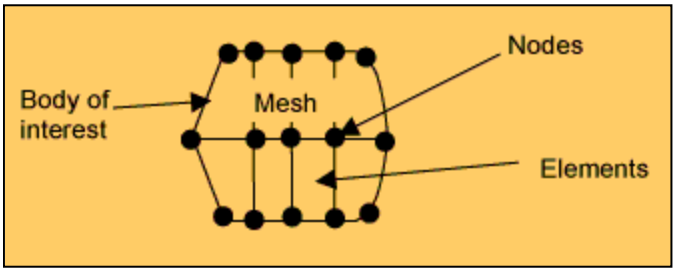

Figure 127: Example of a Finite Element Mesh

Prior to the development of finite element computer software, engineers employed integral and differential calculus techniques to solve these types of problems. Presently, the finite element method is commonly known as a computer technique for solving partial differential equations by partitioning a solid body into discrete regions. These

computer programs are used to predict the deformation and stress fields within solid bodies subjected to external forces. Additionally, most finite element software can be used to solve problems involving fluid flow, heat transfer, electromagnetic fields, diffusion, and many other phenomena (Bower).

For this project, the computer software ABAQUS is used for performing finite element analyses. ABAQUS consists of three core programs: ABAQUS/Standard, ABAQUS/Explicit and ABAQUS/CAE. ABAQUS/Standard can be used to solve traditional implicit finite element problems (e.g., static and thermal) with a wide range of contact and nonlinear material options. ABAQUS/CAE is a graphical user interface that supports both ABAQUS/Standard and ABAQUS/Explicit. ABAQUS/CAE allows the user to create, edit, monitor, diagnose, and visualize the problem. Moreover, ABAQUS/CAE integrates modeling, analysis, job management, and results visualization in a unified environment.

ABAQUS/Explicit was not used during this project because it focuses on transient dynamics and quasi-static analyses. This explicit approach is appropriate for applications such as manufacturing processes. In general, ABAQUS is known for its high performance and ability to solve a multitude of highly-nonlinear engineering problems.

10.3.2 Utilization of Advanced ABAQUS Features

In order to accurately model the structural bay system of WTC 5, as well as simulate the thermal conditions to which it was exposed, certain key features of ABAQUS were utilized. These advanced features are described in this section.

Contact Interactions

In ABAQUS, mere proximity of two bodies is not sufficient to model their contact with each other. Contact may be defined in terms of two surfaces that may interact with each other as a "contact pair." ABAQUS enforces contact conditions by forming equations involving groups of nearby nodes from the respective surfaces. Conditional constraints at various locations on each surface are applied to simulate contact conditions; the locations and conditions of these constraints depend on the contact discretization used in the overall contact formulation. ABAQUS offers two contact discretization options: a traditional "node-to-surface" and a "surface-to-surface."

With traditional node-to-surface discretization, the contact conditions are established such that each "slave" node on one side of a contact interface effectively interacts with a point of projection on the "master" surface on the opposite side of the contact interface. The slave nodes are constrained not to penetrate into the master surface; however, the nodes of the master surface are allowed to penetrate into the slave surface. The contact direction is based in the normal of the master surface.

ABAQUS also offers a "small-sliding" option which creates an invisible boundary between surfaces that are parallel to each other. This option prevents contact "chattering" in which nodes from the slave surface "fall" past the master surface. This option was used for the contact defined between the shear tabs and the steel members since translation in the vicinity of the bolt holes tends to cause contact "chattering" to occur.

When surfaces are in contact they usually transmit shear, as well as normal forces, across their interface. There is a relationship between these two-force components commonly referred to as friction. By default, ABAQUS assumes that the interaction between contacting bodies is frictionless. Friction may be included in the model if a contact property definition is established. Experimental data show that the friction coefficient that opposes the initiation of slipping is different from the friction coefficient that opposes established slipping. The former is referred to as the "static" friction coefficient, and the latter is referred to as the "kinetic" friction coefficient. The static friction coefficient is typically higher than the kinetic friction coefficient. These friction coefficients may be defined in ABAQUS and assigned to particular contact pairs of a given model assembly.

In the WTC 5 model, friction was defined for all surfaces in contact. In addition to mechanical contact, thermal contact is defined in the WTC 5 model. At interfaces such as that of the spray-applied insulation and the beams, thermal contact is defined to simulate the conduction heat transfer that occurs between the two bodies. The thermal contact between the beams and the concrete slab is particularly important because the concrete acts as an effective heat sink.

Heat Transfer Phenomena

ABAQUS has the capability to simulate conduction, convection, and radiation. Conduction is simulated by specifying the thermal conductivity of the materials that compose a given model. Heat transfer due to convection is modeled by creating surface film condition interactions at specific surfaces of a given model. Film condition interactions define heating or cooling due to convection by surrounding fluids. In this case, the convection heat transfer coefficient, as well as the sink temperature, must be specified. Radiation interactions may be utilized in a model to simulate the heat transfer to a nonreflecting environment due to radiation. In this case, the Stephen-Boltzmann constant must be specified.

In the WTC 5 model, all three modes of heat transfer are simulated. The upper layer gas from the fire interacts with the spray-applied insulation of the structural components via natural convection. Since the temperature of the compartment changes with time, the sink temperature varies over the duration of the simulation. Heat that is transferred to the insulation via convection is conducted through the insulation and to the steel via conduction through the insulation, as well as across the contact interface. Since the structural assembly reaches elevated temperatures during the simulation, it will radiate to the surroundings. This heat transfer process is inherently transient since the gas temperature is a function of time.

Nonlinear Temperature-Dependent Material Strength Properties

Most materials of engineering interest initially respond elastically to external forces. Elastic behavior means that the deformation is fully recoverable: when the load is removed, the material returns to its original shape. If the load exceeds the material's yield point, the deformation is no longer recoverable. Once the yield point of steel has been exceeded, it will permanently deform and begin to gain strength due to strain hardening. Strain hardening describes the phenomenon of the crystalline realignment at the atomic level of the steel material that occurs under high strains. It is apparent that once the yield strength of steel has been exceeded, the strength properties become highly nonlinear.

Stress-strain data representing the nonlinear steel strength properties can be inputted in ABAQUS. Plastic true stress and strain values, not total stress and strain, are used in defining hardening behavior. Furthermore, the first data pair must correspond with the onset of plasticity (the plastic value must be zero in the first pair). For the WTC 5 model, test data was referenced and inputted into ABAQUS to represent the nonlinear strength behavior of A36 steel. Furthermore, the data that is used for the model is temperature-dependent.

Sequentially-Coupled Thermal-Stress Analysis Method

A sequentially-coupled thermal-stress analysis is used when the stress/deformation field in a structure depends on the temperature field in that structure, but the temperature field can be found without knowledge of the stress/deformation response. A typical analysis of

this type consists of two ABAQUS runs: a heat transfer analysis and a subsequent stress analysis.

After a thermal analysis has been run, nodal temperatures can be stored as a function of time in the results file or output database. The nodal temperatures are then read into the stress analysis as a predefined field; the temperature varies with position and is usually time dependent. The field is predefined because it is not changed by the stress analysis solution. Predefined fields are always read at nodes and are then interpolated to the calculation points within elements as needed. This analysis method is utilized for the WTC 5 model because the structural response is highly dependent upon the steel temperature history, but there is not inverse dependency.

Geometric Large Deflection Theory

When a body undergoes large deflections, nonlinear effects result. Large deflection may result in geometric or boundary nonlinearity. Geometric nonlinearity can be attributed to the change in direction of a force resultant as the body deflects. For instance, a cantilever beam that is level will have a force resultant due to gravity loads which is vertical. Alternatively, a cantilever beam that has deflected significantly will have a force resultant due to gravity loads which is diagonal. Boundary nonlinearity occurs when a body was deflected so much that it contacts another body.

ABAQUS allows the user to specify whether geometric nonlinearity is accounted for in a given model. Use of the geometric nonlinearity option increases the computational cost, but results in a more accurate simulation. In the case of the WTC 5 model, accounting for geometric nonlinearity is important because it is expected that the beams deflected significantly under high thermal loading.

Tie Constraints

A surface-based tie constraint ties two surfaces together for the duration of a simulation. This type of constraint can be used to make the translational and rotational motion equal for a pair of surfaces. One surface is designated to be the slave surface, and the other surface is the master surface. In addition to modeling connected parts of an assembly, tie constraints are useful for mesh refinement purposes because they allow for rapid transitions in mesh density within a given model.

In the WTC 5 model, tie constraints are prevalently used. Simple connections away from the shear connection of interest are modeled using tie constraints: the beam section web is fused to the girder web in the thermal model. Moment connections are also modeled using tie constraints: the beam stem web and flange sections are fused to the flange of the column. Lastly, tie constraints are used to allow for rapid mesh density transitions in the vicinity of the shear connection of interest. If tie constraints are not used for these rapid transitions, a high degree of mesh distortion would occur, which could lead to model divergence or inaccurate results.

Symmetry Boundary Conditions

Symmetry boundary conditions are used to perform a mirrored analysis. It is computationally less expensive to model a small section of a symmetric body, as opposed to explicitly modeling its entirety. Moreover, symmetry boundary conditions can be applied to a symmetric portion of the body in order to simulate the behavior of its entirety.

In the case of the WTC 5 model, behavior of a 4-bay structural system is sought (the region of initial collapse solely due to fire on the 8^{th} floor). Only 1/8 of this structural assembly is modeled explicitly in ABAQUS. Symmetry boundary conditions are applied to the outer edges of this section in order to derive behavior of the entire 4-bay assembly. For instance, a floor girder is only modeled up to its mid-span. A symmetry boundary condition about the x-y plane is applied at the mid-span in order to derive the behavior of the entire span of the girder.

Bolt Pretension

The bolts in WTC 5 were installed with a specified pretension. Bolts loads are used to model the tightening forces in the bolts. The tension in the tightened bolts is modeled by applying a concentrated force across a user-defined pretension section of each bolt in the first step of the mechanical analysis. This force is self-equilibrating and acts in the direction normal to the pretension section of each bolt. In later steps, further length changes of the bolt is prevented to ensure that the bolts act as standard, deformable components which respond to externally-applied loadings. Otherwise, the force in the fastener will remain constant.

Automatic Stabilization of Rigid Body Motions in Contact Problems

Since the WTC 5 mechanical model is a "quasi-dynamic" analysis, stabilization capabilities of the software were used. Since the shank diameter of the bolts is smaller than the diameter of the bolt holes, the bolts are free to undergo rigid body motions prior to stable contact being established. This rigid body motion early in the analysis often leads to model divergence. To account for this initial rigid body motion, the software offers automatic control of rigid body motions prior to contact closure. This capability is specified for the contact step of the model.

The stabilization feature is meant to be used in cases in which it is clear that contact will be established, but the exact positioning of multiple bodies is difficult to predict. This is especially true for the configuration of the shear tab of the WTC 5 model. When this feature is used, the software activates viscous damping for relative motions of the contact pair at all slave nodes. During the step in which stabilization is activated, the applied loading should be restricted to that necessary to establish contact. In the case of the WTC 5 model, only 1% of the pretension force was activated; the remaining parts of the model were restrained.

By default, the damping coefficient is calculated automatically at each slave node based on the stiffness of the underlying elements and the step time. The damping coefficient is applied to all contact pairs equally in the normal and tangential directions and then is ramped down linearly over the step. It should be noted that the stabilization feature is only active when the distance between the contact surfaces is smaller than a characteristic surface dimension. Thus, this feature applies itself well to the bolt-hole gaps in the WTC 5 model. The use of stabilization via viscous damping does not affect the solution of the model, for the damping vanishes completely at the end of the contact step.

Restart Analysis

The WTC 5 mechanical and thermal models both contain numerous analysis steps. The initial steps of each model (the mechanical contact and pretension steps especially) can take an extended amount of time to complete. During the long troubleshooting phases of each model, changes to later steps were made and then needed to be tested. In order to analyze these changes efficiently, the restart analysis capability of the software was utilized.

When an analysis is run, the software can write "memory" files upon request. These files, collectively referred to as the restart files, allow an analysis to be completed up to a certain point in a particular run and then restarted and continued in a subsequent run. The user may control the amount of data written to the restart files by specifying a particular frequency at which the data is written to file. Restart files can be very large if the user does not control this frequency. For the WTC models, only one increment per step was retained for later reference, thus minimizing the size of the files.

The user may restart (continue) an analysis by specifying that the restart or state, analysis database, and part files created by the original analysis be read into the new analysis. Moreover, the user specifies the point (step, increment, and iteration) in the previous analysis from which to restart. The use of restart analysis was particularly useful for troubleshooting the loading step of the model. In this case, the contact and pretension steps were not required to run every time, but rather the load step alone.